2011-01-01

The Combined Otto and Stirling Cycle Prime-Mover-Based Power Plant

Barry Cullen
Technological University Dublin, barry.cullen@tudublin.ie

The Combined Otto and Stirling Cycle Prime-Mover-Based Power Plant

Barry Cullen BE

Doctor of Philosophy (PhD)

Dublin Institute of Technology

Supervisor: Professor Jim McGovern

School of Mechanical and Transport Engineering

January 2011

Dedicated to my parents, Albert and Ann Cullen

ABSTRACT

An exploratory study of the combined Otto and Stirling cycle prime mover is presented. The Stirling cycle acts as the bottoming cycle on the Otto cycle exhaust, the aim being the generation of additional mechanical power which may subsequently be converted to electrical power. It is postulated that the increases in brake power and efficiency afforded by the addition of the Stirling cycle are of sufficient magnitude to offset the inherent increase in plant cost and complexity. The analysis necessitated the development of thermodynamic models for both the Otto cycle and Stirling cycle engines and relationships to link the two together through the Stirling cycle hot-side heat exchanger. The models are derived using the principles of Finite Time Thermodynamics (FTT), a field which is considered to offer reasonably good simulation capability for a comparably low level of model complexity. The Otto cycle FTT model is developed from an existing model available in the literature. The Stirling cycle FTT model represents a new contribution to the literature. Both models are validated as part of the present work. They are subsequently combined using expressions derived for the Stirling cycle hot-end heat exchanger and the combined performance is simulated. Finally a techno-economic analysis is performed to compare the economic performance of the combined system with a base-case single cycle system; this is done for mono-generation and poly-generation scenarios. It is seen from the analysis that the combined cycle system offers an economically attractive investment when analysed for Net Present Value, Internal Rate of Return and Simple Payback Period.

ACKNOWLEDGMENTS

First and foremost I would like to thank my supervisor, Prof. Jim McGovern for his expert guidance and, above all, patience during this research project. This work would not have been possible without his interest in the concept from the start and his constant assistance throughout.

I am also hugely indebted to my international collaborators Prof. Michel Feidt of University "Henri Poincare" of Nancy, France, and Prof. Stoian Petrescu of Politehnica Bucharest, Romania for all their help and support. Their guidance and assistance throughout the project was absolutely invaluable, and I feel honoured to have worked with such esteemed colleagues.

Special thanks must also be given to Dr. Marek Rebow, without whose unbounded energy, enthusiasm and drive this work would not have been possible. Marek's commitment to helping my fellow post-graduate researchers and I was unparalleled, and I owe a huge debt of gratitude to him for his efforts throughout my time as a post-graduate.

Thanks to Prof. Roy Douglas of Queens University, Belfast for help and advice regarding the Otto cycle simulation and in particular the Ricardo Wave package.

Thanks also to Dr. Abdul Ghani Olabi of Dublin City University for his input during the confirmation examination and thereafter.

Thanks to all of my colleagues and students in the College of Engineering and the Dublin Energy Lab for all of their support throughout. Thanks to Dr. David Kennedy for his guidance and support as head of the department; to Mr. James

Mahon for his assistance in the Thermodynamics Lab; to Mr. James Egan and Mr. James Breen for their help with the development of the (later abandoned!) test rig. Thanks to Dr. Fergal Boyle for his help with the final drafting of the thesis. Thanks also to all of my fellow post-graduate researchers – it was always good to know that I wasn't the only one going through the pains of research!

Finally, it is not possible to state my unbounded thanks to my partner Mary for her support and devotion throughout the work, and to all my family and friends for their tolerance of protracted absences, anti-social working hours and the generally elevated stress levels (particularly in the closing stages!) of this researcher. Although this work bears my name, it is woven intricately around the latticework of their love, patience and support. I am eternally grateful.

This work was funded under the Dublin Institute of Technology ABBEST Scholarship.

DECLARATION

I certify that this thesis, which I now submit for examination for the award of Doctor of Philosophy (PhD), is entirely my own work and has not been taken from the work of others, save and to the extent that such work has been cited and acknowledged within the text of my work.

This thesis was prepared according to the regulations for postgraduate study by research of the Dublin Institute of Technology and has not been submitted in whole or in part for another award in any institute.

The work reported on in this thesis conforms to the principles and requirements of the Institute's guidelines for ethics in research.

The Institute has permission to keep, lend or copy this thesis in whole or in part, on condition that any such use of the material of the thesis be duly acknowledged.

Signature _____ Date_____

Candidate

LIST OF ABBREVIATIONS AND SYMBOLS

A	Area
A_{T}	Throat area
A_{w}	Wetted area
ACC	Anthropogenic climate change
AD	Anaerobic digester
AR	Annual revenue
$\mathrm{AR}_{\mathrm{NG}}$	Net annual revenue, novel gas applications
A_{ff}	Free flow area
A_{fr}	Frontal area of individual heater tube
A_{vol}	Heat transfer per unit volume
A_{p}	Piston face area
A_{R}	Regenerator cross sectional area
b	Regenerator mesh wire gap
B	Exergy or exergy transfer rate, cylinder bore
BMEP	Brake mean effective pressure
BMS	Building managment system
C_{D}	Coefficient of discharge
C_{E}	Electrical tariff
$C_{E,fixed}$	Fixed overhead costs associated with connection electrical grid
C_{F}	Fuel cost per unit of fuel energy
C_{f}	Friction factor
C_{G}	Gas tariff
$C_{\mathrm{G,fixed}}$	Fixed overhead costs associated with connection to fuel gas grid

C_{m}	Maintenance cost
C_{R}	Electricity tariff to producers generating from renewable energy sources
C_{r}	Ratio of heat capacitance rates
$\dot{C}$	Heat capacity rate
$\dot{C}_{\mathrm{min}}$	Minimum heat capacity rate
$\dot{C}_{\mathrm{max}}$	Maximum heat capacity rate
c_p	Specific heat at constant pressure
c_v	Specific heat at constant volume
CCHP	Combined Cooling, Heat and Power generation
CHP	Combined Heat and Power generation
CI	Compression Ignition
d	Bore, diameter
d_{h}	Hydraulic radius of tube bank passages
d_{i}	Internal diameter
d_{o}	Outer diameter
d_{regen}	Regenerator diameter
$d_{\mathrm{t,h}}$	Outer diameter of heater tube
DG	DG
EC	Equivalant power cost
ECE	External combustion engine
EGR	Exhaust gas recirculation
F	Empirical factor in an expression for brake power
f	Frequency
FST	Finite Speed Thermodynamics

FTT	Finite Time Thermodynamics
G	Mass velocity
g	Dimensionless mass
H	Enthalpy
h	Heat transfer coefficient
I_{R}	Irreversibility parameter or ratio
i	Interest rate
ICE	Internal Combustion Engine
IPCC	The Intergovernmental Panel on Climate Change
IRR	Internal Rate of Return
j_{H}	Colburn j-factor
k	Thermal conductivity
k_f	Thermal conductivity of working gas
$\mathrm{kW_m}$	Kilowatts of mechanical power
L_{H}	Heat transfer length
LPG	Liquefied Petroleum Gas
m	Mass
$\dot{m}$	Mass flow rate
MN	Methane number
N	Operating frequency, Rpm
N_{cond}	Ratio of conduction losses to total heat input
N_{H}	Number of operating hours per year
N_{HUF}	Heat Usage Factor
N_{ex}	Ratio of Stirling exhaust heat losses to total heat input
N_{L}	Loss ratio

N_m	Mass ratio
N_{ml}	Empirical constant for mechanical losses
n	Number of years
n_v	Number of valves
NPV	Net Present Value
NTU	Number of transfer units
Nu	Nusselt number
P, p	Pressure
$\bar{p}$	Dimensionless pressure
P	Power
P_{brake}	Brake power
P_{e}	Electrical power
P_{f}	Fuel power
P_{I}	Power output of cycle, taking irreversibility within the gas processes into consideration
P_{irrev}	Irreversible power output
P_{m}	Mechanical power
P_{p}	Pumping power
P_{rev}	reversible power output
P_{μ}	Cycle power lost through global friction effects
p_{m}	Mean pressure
p_0	Stagnation pressure
PES	Primary Energy Savings
PV	Present Value
Pr	Prandtl number

R_{g}	Specific gas constant
R_{HEX}	Radius of heater heat exchanger
R_{mass}	Mass ratio
RC	Running cost
Re	Reynolds number
R_v	Compression ratio, Stirling cycle
R_Q	Ratio of maximum heat transfer to heat available in source
R_{total}	Total thermal resistance
$R_{\mathrm{t,cond}}$	Conductive resistance
R_{H}	Hydraulic radius
RC_{NG}	Net running costs associated with operation, novel gas applications
r_v	Compression ratio, Otto cycle
rpm	Revolutions per minute
Q	Heat transfer, rate of heat transfer, volume flow rate
$\dot{Q}$	Rate of heat transfer, CHP engine recoverable thermal power
Q_{cond}	Conduction loss
Q_{L}	Heat transfer loss to Otto cycle cylinder walls
Q_{ex}	Exhaust loss
Q_{in}	Heat input
Q_{out}	Heat rejection
$Q_{\mathrm{isothermal}}$	Isothermal heat transfer
$Q_{\mathrm{isochoric}}$	Isochoric heat transfer
s	Specific entropy
S	Otto cycle stroke
SI	Spark Ignition

SPP	Simple Payback Period
T	Temperature
T_0	Stagnation temperature
T_∞	Free stream temperature
t	Time interval
t_{th}	Thermodynamic cycle period
U	Overall heat transfer coefficient, U-value
V	Volume
V_{c}	Volume of compression space
V_{C}	Compression space swept volume (Stirling cycle)
V_{E}	Expansion space swept volume (Stirling cycle)
V_{e}	Volume of expansion space
V_{dead}	Dead volume
V_{h}	Stirling heat volume
V_{k}	Stirling cooler volume
V_0	Clearance volume
V_p	Swept volume of power piston
$\bar{v}$	Mean velocity
W	Work
W_{f}	Friction work
W_{I}	Work output of an irreversible cycle
W_{rev}	Reversible work
WTE	Waste to energy
X_{CC}	Specific capital cost of combined cycle plant
X_{Otto}^{1}	Specific cost of Otto cycle engine 1

X^2_{Otto}	Specific cost of Otto cycle engine 2
$X_{\text{Otto,E}}$	Specific cost of Otto cycle engine based on unit electrical power output
$X_{\text{Otto,F}}$	Specific cost of Otto cycle engine based on unit fuel power input
X_{Stirling}	Specific cost of Stirling cycle engine
$X_{\text{capital,chp}}$	Specific cost of CHP unit
$X_{\text{capital,NG}}$	Specific cost of novel gas fired unit
x_D	Clearance depth
x_s	Stroke of piston in Stirling cycle
$x_{s,eff}$	Effective stroke of Stirling cycle

Greek

α	Phase angle, Pumping loss coefficient
Γ	Temperature ratio
γ	Ratio of specific heats
ε	Phenomenological constant to quantify lost work
ε	Effectiveness
ε_{R}	Regenerator effectiveness
ε_{H}	Effectiveness of hot side heat exchanger
μ	Friction coefficient
η	Efficiency
η_{alt}	Alternator efficiency
η_{C}	Carnot efficiency
$\eta_{\text{C,fr}}$	Carnot efficiency for reservoirs of finite thermal capacity
η_e	Engine efficiency
κ	Swept volume ratio

ρ	Density
σ	Area ratio
τ	Temperature ratio
τ	Cycle period (Stirling)
ϕ	Mesh porosity, Stirling cycle crank angle
χ	Dead volume ratio
ψ	Density ratio
θ	Crank angle

Subscripts

amb	Ambient
avg	Average
bd	Blowdown
C	Carnot
c	Cooler
CC	Combined Cycle
chp	Combined Heat and Power
comb	Combustion
disp	Displacement
e	Electrical
eff	Effective
ex	Exhaust
f	Friction
f	Based on fuel input
ff	Free flow
fr	Frontal

fr	Finite reservoir
g	Gas
H	Heater
HUF	Heat Usage Factor
II	Second law
irrev	Irreversible
m	Mechanical
m	Maintenance
NG	Associated novel gas applications
O	Otto cycle
rev	Reversible
St	Stirling cycle
w	Wall

TABLE OF CONTENTS

TABLE OF FIGURES

TABLE OF TABLES

PUBLICATIONS

1. **Cullen, Barry** and Jim McGovern, '*Development of a theoretical decoupled Stirling cycle engine*', Simulation Modelling Practice and Theory, 2010, 8 pp., in press, doi:10.1016/j.simpat.2010.06.011.
2. **Cullen, Barry**, Michel Feidt, Jim McGovern and Stoian Petrescu, '*Thermodynamic Optimisation of the Otto / Stirling Combined Cycle*', Proceedings of ECOS 2010, 23rd International Conference on Efficiency, Cost, Optimization Simulation and Environmental Impact of Energy Systems, Lausanne, Switzerland, June 14–17, 2010, Paper 387, 9 pp. http://arrow.dit.ie/dubencon2/6/
3. McGovern, Jim, **Barry Cullen**, Michel Feidt and Stoian Petrescu, '*Validation of a simulation model for a combined Otto and Stirling cycle power plant*', Proceedings of ASME 2010 4th International Conference on Energy Sustainability (ES2010), May 17–22, 2010, Phoenix, Arizona USA, Paper no. ES2010-90220, 9 pp. http://arrow.dit.ie/dubencon2/7/
4. **Cullen, Barry** and Jim McGovern, '*Energy system feasibility study of an Otto cycle/Stirling cycle hybrid automotive engine*', Energy, 2010, vol. 35, issue 2, Feb., pp. 1017–1023.
5. **Cullen, Barry**, Jim McGovern, Stoian Petrescu and Michel Feidt, '*Preliminary Modelling Results for an Otto Cycle / Stirling Cycle Hybrid-Engine-Based Power Generation System*', Proceedings of ECOS 2009, 22nd International Conference on Efficiency, Cost, Optimization Simulation and Environmental Impact of Energy Systems, August 31 – September 3, 2009, Foz do Iguaçu, Paraná, Brazil, pp. 2091–2099. http://arrow.dit.ie/dubencon2/1/

6. **Cullen, Barry** and Jim McGovern, '*The Quest for More Efficient Industrial Engines—a Review of Current Industrial Engine Development and Applications*', ASME Journal of Energy Resources Technology, 2009 131(2), 9 pp.

7. **Cullen, Barry** and Jim McGovern, '*Development of a theoretical decoupled Stirling engine*', in Sustainable Energy Beyond 2020: *Proceedings of the 3rd International Conference on Sustainable Energy & Environmental Protection—Part 2*, Ed. Abdul Ghani Olabi, Sumsun Naher and Michele Dassisti, 2009, Dublin, Ireland 12–15 August, pp. 244-250. http://arrow.dit.ie/dubencon2/2

8. **Cullen, Barry** and Jim McGovern, '*Proposed Otto Cycle / Stirling Cycle Hybrid Engine Based Power Generation System*', in *Proceedings of the 2008 ASME Power Conference (POWER2008)*, Orlando, Florida, USA, July 22–24, 2008, Paper ref. POWER2008-60039, 6 pp.

9. **Cullen, Barry** and Jim McGovern, '*Energy System Feasibility Study of an Otto Cycle / Stirling Cycle Hybrid Automotive Engine*', in ECOS 2008, *Proceedings of the 21st International Conference on Efficiency, Cost, Optimization, Simulation and Environmental Impact of Energy Systems*, Cracow-Gliwice, Poland, June 24–27, 2008, pp. 483–490, Ed. Andrzej Ziebik, Zygmunt Kolenda and Wojciech Stanek.

10. **Cullen, Barry** and Jim McGovern, '*The Stirling Engine as a Prime Mover*', in *ESAT 2008, Proceedings of the 23rd European Symposium on Applied Thermodynamics*, Cannes, France, May 29 – June 1, 2008, pp. 899-904, Ed. Jean-Noël Jaubert.

11. **Cullen, Barry** and Jim McGovern, '*The Quest for More Efficient Industrial Engines—a Review of Current Industrial Engine Development and Applications*', *Proceedings of the 2007 ASME Power Conference (POWER2007)*, Paper no. POWER2007-22078, 17–19 July 2007, San Antonio, Texas.

1 INTRODUCTION

1.1 Motivation for the Research

As with a broad range of current academic work, the motivating factors for this research are the related issues of global climate destabilisation and security of energy supply. Anthropogenic climate change (ACC) is acknowledged as fact by the scientific community. Mitigating its effects is also seen as an issue of critical importance for the survival of modern developed societies and for the advancement of developing societies. Similarly, it is not easy to overstate the importance of energy security in the development of a nation and a society. In a world of increasing population (with increasing standard-of-living expectations) and dwindling stocks of finite fuel resources, it is reasonable to foresee a potential descent into political instability and tension over restricted supplies. Therefore it is incumbent upon the current generation of global citizens to think and act to avert such an undesirable future.

1.2 Future Projections for Anthropogenic Climate Change

The major source of data concerning ACC is the work of the Intergovernmental Panel on Climate Change (IPCC). The most recent report from the panel is the IPCC Fourth Assessment report [1]. Though a subject of some controversy recently, its major findings have not been disputed, and it makes for rather grim reading. Among its predictions are increased average global temperatures of between 0.6°C and 6°C by the year 2100, giving rise to increased frequency of high intensity weather events such as hurricanes, heat waves, heavy precipitation and flooding. In addition, a rise in sea level brought about through thermal expansion and the thawing of ice cover in the polar caps is anticipated.

Interestingly, the potential for increased crop productivity exists for moderate temperature increases; however this is balanced in some regards by the social and economic consequences of destruction of lands and settlements in coastal locations due to sea level changes and increases in flooding events, as well as the population disturbances due to high intensity weather events. It is also expected that health services will be further stressed in vulnerable regions due to an increased propensity among the populations for malnutrition, diarrhoeal diseases and cardio-respiratory diseases arising due to increased ground – level ozone in urban areas. Rather worryingly, a recent paper by Giannantoni and Zoli [2] has raised the possibility that the mathematical modelling methods used in the IPCC studies to predict the global temperature changes in the future are, even in the most undesirable extremes, too conservative by a considerable margin. Whilst they are careful to qualify their results, the authors indicate the possibility that the actual temperature rise could be as much as 150% higher than the predictions made in the IPCC report. Considering the environmental, social and economic upheavals predicted in the IPCC report, this possibility is somewhat alarming.

1.3 Security of Supply

In addition to these problems are the political and economic unrest brought about through insecurity in the global energy supply chain. Currently, the world economy, led by the western civilisations, is based on the availability of cheap, relatively reliable supplies of fossil fuels, in particular oil. Being finite reserves, they are by definition depleting. The 'peak oil' scenario, the predicted situation in which global oil production finally reaches a maximum before beginning to decline, cannot be ignored. Recent figures from the International Energy

Agency's World Energy Outlook report indicates that 70.2 million barrels per day (Mb/d) of crude oil were produced by the oil fields in operation in 2007 [3]. The report projects output to reach 84.3 Mb/d in 2030. An alternative study of the same data by Aleklett et al [4] suggest however that a more plausible estimate would be 75.8 Mb/d. The differences in estimates illustrates the inherent difficulties in forecasting production—the depletion of existing reserves, the discovery of new reserves and the ability to economically exploit previously uneconomical resources, for example oil shales or the tar sands of Canada, are all factors that necessarily include uncertainty in their projectable futures. There is huge uncertainty inherent in the peak oil estimation process, and as a result predictions for global maximum production range from about 2004 to anywhere after 2020 [5]. This is not a new dilemma. Projections for peak oil have historically been difficult for a variety of reasons [6], however what remains an unalterable fact is that in the long term, reliance on fossil fuel reserves is not possible, and substitutes must be found. Future scenarios in which peak oil is assumed to have occurred in the absence of an alternative backbone resource for industrial society have been analysed by Friederichs [7]. The outlook is not particularly inspiring. Societal instability, declines in living standards and increased social stratification, military interventionism and the rise of totalitarianism in already unstable regions are some of the possible outcomes predicted.

Alternatives must be found. However, this search for alternatives in itself gives rise to further unrest. Nuclear (fission) power is often touted as a carbon neutral alternative for the short and medium terms; however this might be seen as at best a stop-gap solution, as it depends on a finite fuel resource in itself.

The undesirable nature of the waste matter is a critical issue too of course. In addition, there is evidence that the waste heat from thermal power plant plays a significant role in the Global Warming effect [8], so that warming would continue even with the widespread adoption of nuclear fission power, albeit at a slower pace. The parallel complication of possible weapons production is a politically sensitive one too, such that widespread deployment of the technology in developing or politically unstable regions is unlikely [9].

Whilst it has become common to discuss the need for research and development of new novel power generation systems in terms of these pragmatic concerns, it might be contended that central to these twin aims is the ethical responsibility of the engineer to ensure maximum effective use of finite resources for the maximum benefit of the global population. The ethical responsibility of the engineer has always been a central tenet of the profession and it would seem that now more than ever, in light of the growing uncertainty around energy supplies and the complications of ACC, the social responsibility of the engineer is paramount. Progress on these issues cannot occur in a vacuum though, and the willingness of the wider society to embrace change is key to the success of the best intentions of the engineering profession.

1.4 Society, Energy and the Engineer

It is perhaps pertinent to the discussion and the content of this work to broach the issue of public understanding of the two problems outlined above—ACC and Security of Supply—as a means of contextualising the work and of taking a 'snapshot' of the attitudes that form the social environment in which the

engineer must work. The ethics of efficiency that the engineer subscribes to must then find expression within this context.

The facts of ACC are not in serious dispute and do not need complete reiteration here. A full disclosure is detailed in the IPCC Fourth Assessment Report. Rather, the paths by which the engineers of today and tomorrow will provide the solutions to these problems are of concern, as are the modes of resistance that are likely to be encountered. One such mode of resistance can be described as the partial or complete non-engagement with the problem at hand by the people who will be directly affected by it. Public misunderstanding of the problem of ACC is a crucial stumbling block to the development and introduction of new technologies aimed at averting it. Representation in the media has been problematic in certain quarters, with the machinations of the "climate sceptic" movement often giving rise to a false claim of controversy or dispute among the scientific community. Boykoff and Boykoff [10] and Antilla [11] provide insights into the coverage of ACC in the United States mass media. Doulton and Brown [12] provide a similar analysis for the UK, as do Sampei and Aoyagi-Usui [13] for Japan. Conclusions include, among other things, that lobbying on behalf of vested interests, poor understanding of the subject matter on behalf of the journalists and poor application of core journalistic professional practices lead to a situation of confusion among the general public, and an appeal to an ill informed, pseudo-sceptic mindset that serves only to further the narrow interests of a small but economically powerful group. This appeal to scepticism might be regarded as a cynical play on one of the corner-stones of the scientific method. Scepticism can be regarded as the foundation on which all scientific inquiry is built—the objective appraisal of evidence and formation of

conclusions based on this evidence is the key to proper scientific and technological progress. Misrepresenting it therefore, might be considered an attack on the very concept of scientific endeavour and rational thinking. An excellent discussion of the role of scepticism in science is provided by Winstanley [14], in which the requirement for properly informed debate is elucidated as vital to the progress of scientific understanding and the threat of what may only be termed zealotry both within and without the scientific circle is discussed.

The net effect of a culture of misinformation on the topic of ACC is a society that at best suffers from a diversion of talent away from the sciences and engineering and at worst is catastrophically underprepared for the challenges and responsibilities inherent in the changing environmental situation. A civilisation that distrusts its scientists and is short of engineers is surely not likely to progress very far. Similarly, a shortage of the necessary skills places the emphasis on the existing body to maximise performance and efficiency.

This presents another issue at this point in the debate; quite apart from the technological and economic arguments of whether it is more harmful to do something or not do something—arguments presented by some climate sceptics—is it really acceptable from a philosophical stance as engineers in the modern age to continue with policies and attitudes that espouse waste and inefficiency? Regardless of threat to the environment or the instability of supply structures, is it permissible to knowingly squander resources? The answer, I think most will agree, is a resounding 'No.'

Engineers are ethically bound to work for the benefit of society. For example, article 2.1 of the Engineers Ireland Code of Ethics [15] stipulates the requirement that

> *'Members shall at all times be conscious of the effects of their work on the health and safety of individuals and on the welfare of society. While acting as designers, operators or managers on projects, Members shall strive to eliminate risks to health and safety during all project stages.'*

Furthermore, the requirement to act without adverse effect on the natural environment is specified in the same article:

> *'Members shall also undertake to minimise or eliminate any adverse impact on the natural environment arising from the design and execution of all project work that they are engaged in.'*

Similar provisions are made in the Code of Ethics of other internationally recognised professional organisations such as the ASME [16] and the IEEE [17]. By implication, it is not ethically permissible to allow the wasting of finite resources. The atmosphere of distrust and apathy that appears to be growing every day towards the issues of ACC and supply security means that now more than ever the responsibilities of the engineer to society are crucial, and the failure to sustain a critical mass of expertise can mean only that the responsibility falls to fewer people, not that it disappears entirely. It is therefore a professional and ethical obligation that engineers strive always to minimise waste, in all guises, in order to ensure a sustainable relationship with the

natural environment and, by extension, to strive for efficiency and economy in all aspects of the profession and of society.

Central among these aspects are the requirement for highly efficient, clean and economical power plant. This is certainly not a new viewpoint; however it would seem to be relevant now more than ever. Now more than ever it is essential that engineers factor emissions and efficiency into all economic evaluations. However, 'efficiency' can be a nebulous concept in different scenarios, particularly when dealing with power generation plant. How best to define plant efficiency is discussed in the following section.

1.5 The First and Second Laws of Thermodynamics as Bases for Technology Assessment

Efficiency and economy have been central principles in the field of engineering thermodynamics since the beginning of modern scientific treatment of the subject by Carnot. This is evident in the laws of thermodynamics when applied to heat engines such as those used for power generation and as automotive prime-movers. The fist law of thermodynamics informs us of the immutable conservation requirement of energy; energy can neither be created nor destroyed but may only be converted from one form to another. In a practical heat engine this translates as the conversion of chemical energy in the fuel to the thermal internal energy of the combustion products, a portion of which is subsequently converted to work. The overall balance of energy remains the same; merely the forms in which it exists change.

First law efficiency therefore indicates what proportion of the total energy input to the system is recovered as work, but it tells nothing of the maximum possible

work output that might be done by the system. High first law efficiency indicates that a high proportion of the energy admitted to the system is converted to useful work. But what can be classified as a 'high' efficiency? In the absence of a definitive, physically meaningful basis of comparison, comparing efficiencies of different engines based on the first law is not particularly informative. Considering the myriad permutations of possible cycles, configurations and operating regimes, simple metrics such as the first law efficiency are only partially useful. The first law does not tell us anything about the 'quality' of the energy admitted to the system. For this, the second law is required.

The second law of thermodynamics tells us, among other things, that there must always be a heat rejection from a heat engine. This is not an accident of bad design but rather an unavoidable trait of the universe. Certain engines will reject less heat than others, implying better thermodynamic design; however there must always be a proportion discarded. Minimising the heat loss requires knowledge of the second law and familiarity with the concept that energy has quality as well as quantity. Higher temperature heat, for instance, can more easily be converted to work than lower temperature heat. Also, because work can be easily converted to different forms, it is considered the highest quality of energy. A full discourse on the many facets of the second law can be found in any standard textbook on engineering thermodynamics [18, 19], but of importance to this discussion is the implication that there exist for all thermodynamic cycles a maximum possible output for the given heat reservoir conditions. Comparing the actual performance to this maximum possible performance gives the second law efficiency.

The second law efficiency indicates what proportion of the maximum possible work output is done by a given heat engine. By comparing different engines based on their second law efficiency, a more meaningful picture of the quality of the design is generated. It can therefore be suggested that, in order to pursue energy efficiency goals in a more meaningful fashion, the second law efficiency must become the primary focus for assessing emerging technologies.

1.6 Economics of Deployment

Inextricably linked to the issue of maximising the efficiency is that the problem faced by any new technology is essentially one of economics. This is particularly relevant to the power generation industry. Because the product, electricity, is so fundamental to the structure of modern society and so interwoven into every product and service that we consume, fluctuations in the basic unit cost of the electrical power can have resounding economic effects. New power generation technologies, whether they are renewable or of conventional stock, must therefore compete with an existing industry that supplies cheap, reliable power on demand. This has come to be one of the defining features of modern society; the expectation of cheap power on demand. The onus is therefore on scientists and engineers to develop clean, reliable and cost effective alternative technologies, and on politicians to create an economic environment in which these new technologies can compete fairly with conventional ones. The requirement is not just for completely new energy convertors capable of exploiting renewable sources of energy—there is also the need for high efficiency conventional power plant which would enable the maximisation of existing supplies. This is a crucial and often overlooked corollary of the 'green energy' movement. All renewable energy technologies are currently reliant on a

fossil fuel system. The manufacture of the plant is energy intensive, as are the logistical issues faced in putting large, low-power-density converters in remote and often poorly accessible locations. Operation of the systems is also still heavily dependant on the back up capability of a fossil fuel supplied grid network. For the foreseeable future therefore, fossil fuel technology will be a significant part of the generation mix. In order that a reasonably smooth and stable transition to a green energy society be realised, the 'teething' period associated with the development and integration of truly renewable energy technologies will require the parallel development of high efficiency conventional generation plant.

1.7 Rationale for the Research

The current work presents an exploratory research project aimed at investigating a novel combined cycle engine system suitable for use as a prime mover in the small and medium scale power generation sector. It is anticipated that such an engine would benefit from significantly higher first and second law efficiencies than those possible from the single cycle engines currently used. Central to this though, is not whether higher efficiency is attainable—simple calculations indicate the validity of the concept, as does the existence of such systems in the large scale power generation sector—but crucially whether the combination can be realised in an economically attractive manner. As will be seen in the next chapter, Combined Heat and Power (CHP) is a power generation technology that is currently the subject of considerable interest due to its high primary energy efficiency. It therefore offers considerable emissions and energy security benefits. However, its application is limited for situations that do not have significant heat demand in addition to their electrical demand.

A combined cycle system such as that proposed in the present study might feasibly offer the benefit of reducing the heat output and increasing the electrical power output of a CHP unit. Tipping the production balance of the unit in favour of electrical output could therefore allow the deployment of such CHP systems in market sectors that have traditionally not been suitable, such as office and residential blocks where heat demand is not as high as would be the case in industrial or hotel applications. This concept is detailed further in the next chapter.

The two engines involved in the proposed combined cycle, the Otto cycle internal combustion engine (ICE) and the Stirling cycle external combustion engine (ECE) are both technologically established. The Otto cycle engine is ubiquitous as an automotive power plant as well as a prime mover for small scale distributed power generation. The Stirling cycle engine, though long established, is only now coming to the fore as a prime mover in various novel power generation scenarios. These include solar thermal generation, micro-CHP and even use as a power converter for space applications. Examples of such works include [20–25].

1.8 Aims and Objectives

1.8.1 Aims

To investigate the Otto / Stirling combined cycle as a prime mover for use in the Distributed Generation (DG) industry. To assess the techno-economic performance of the proposed combined cycle plant through thermodynamic simulation and established economic appraisal techniques. To draw

conclusions regarding the suitability of the plant for use as both a mono-generation and a poly-generation prime mover.

1.8.2 Objectives

The objectives to be reached in order to achieve the above mentioned aims are:

- Conduct a literature survey to establish the current market and technology status in the DG industry. The prime mover technologies of interest are the Otto cycle engine, typically used for Natural Gas fired CHP applications and WTE power generation systems, and the Stirling cycle engine typically used for micro-CHP and solar thermal generation. Also of interest are the thermodynamic modelling and simulation methods applicable to both cycles, necessitating a comprehensive review of the relevant scientific literature.

- Generate a thermodynamic simulation model for the Otto cycle engine capable of accounting for the energy balance of the three main energy sinks; mechanical power output, heat transfer to the cylinder walls that ultimately arrives in the coolant water circuit and heat loss to the exhaust stream.

- Verification of the Otto cycle thermodynamic simulation model using a commercially available virtual engine simulation software package.

- Generation of a thermodynamic simulation model for the Stirling cycle engine. Similar to the Otto cycle, it is required to model and simulate the heat loss to the energy sinks. As with the Otto engine the sinks in question are the mechanical power output, the coolant heat loss and the exhaust heat loss.

- Validation of this thermodynamic model against technical specifications and experimental data available in the literature.

- Simulation of the combined cycle system and a full techno-economic appraisal of the potential of the system to perform as a prime mover for the DG scenarios mentioned previously. Technical appraisal comprising of first and second law analysis and economic appraisal through standard economic modelling techniques of Simple Payback Period (SPP), Net Present Value (NPV) and Internal Rate of Return (IRR) of the proposed investment. The economic performance of the combined cycle system is compared against that of the Otto cycle system acting alone and against the case of a high efficiency Otto cycle unit acting alone. This latter step is important so as to gauge any advantage over the best-in-class of the existing single cycle engines used in these circumstances.

- Draw conclusions as to the viability of the proposed combined cycle plant as a prime mover for stationary power generation. Provide discussion on these results and detail proposed future work on the concept.

1.9 Organisation of the Thesis

This thesis is presented in nine chapters. Chapter 2 comprises a complete literature review and state of the art assessment of the two engine types involved, the DG industry and the industrial heat engines used in it.

Chapter 3 presents the thermodynamic model of the Otto cycle engine that has been developed from models available in the literature. The model is developed

in the framework of FTT. Central to the development of the model is the inclusion of the exhaust sensible thermal energy content and temperature.

Chapter 4 details a validation of the Otto cycle thermodynamic model. Validation is completed by comparing the model against a virtual engine simulation created using a commercially available software package.

Chapter 5 presents an FTT model of the Stirling cycle engine. This model represents a new addition to the literature. It draws upon modelling techniques used previously for reciprocating internal combustion cycles such as the Diesel, Otto and Atkinson cycles. This model is validated in Chapter 6 using technical and experimental data for the General Motors GPU-3 Stirling engine. It is seen that the thermodynamic model represents a reasonable approximation to the actual engine performance, with percentage difference values within 10%. This is considered reasonable for the level of complexity in the model. The model is comparable in terms of its accuracy to other models of similar complexity, such as models based on the traditional second order de-coupled methods used in the literature.

Chapter 7 details the simulation of the combined cycle. Linking the two thermodynamic cycles developed in the previous chapters is done through the development of gas temperature relationships to link the working gas temperature within the engine to the temperature of the source, in this case the Otto cycle exhaust gas. A full technical appraisal of the hybrid arrangement is conducted, both from first law and from second law perspectives. An exergy analysis is completed to gauge the level of exergy destruction inherent in the combined cycle over that of the Otto cycle operating alone.

Chapter 8 details the economic analysis of the combined cycle plant. This is conducted so as to investigate whether the combined cycle system would offer any investment advantage over that of the single cycle Otto engine generation plant. The analysis is done for a series of scenarios, including the use of the combined cycle plant as a CHP engine and as a mono-generation engine as would be used on WTE sites. It is seen that the combined cycle plant represents a more-profitable investment relative to the Otto cycle engine plant, even when the additional capital cost is taken into account.

Chapter 9 details the conclusions drawn from the analysis of the plant, both from a technical and from an economic perspective. The major contributions of the thesis are presented also.

2 LITERATURE SURVEY

2.1 Introduction

The present work concerns the investigation of the use of the Stirling cycle engine as a bottoming cycle for the Otto cycle industrial engine. The industrial Otto cycle engine commonly finds use in DG scenarios such as CHP generation, typically using Natural Gas as the fuel; and WTE applications whereby gases such as Landfill Gas, Mine Gas and Syngas are used as the fuel source for the engines. Renewable gases such as Anaerobic Digester (AD) Gas are used also and are particularly useful on agricultural sites and in food-production plants, where process waste products can be used as feedstock for gas production. The central hypothesis is that this novel combined cycle system may have distinct performance advantages over the Otto cycle engine working on its own.

With regard to forming a complete picture of the relevant engine technologies and their place in the current mix of power generation technologies, this chapter presents a review of the literature concerning the different aspects of the research work; The Otto cycle engine, The Stirling cycle engine, the thermodynamic modelling and simulation methods usually used when considering the cycles and their practical realisation, as well as the status of the DG energy market both in Ireland and in the wider international context.

2.2 The Otto Cycle Engine

The Otto cycle engine is probably most widely recognisable through its ubiquity in the automotive sector. Petrol / gasoline fuelled engines, almost exclusively the power plant of choice in the automotive sector worldwide, operate on the

Otto cycle or a very close variant such as the Miller or Atkinson cycles. The engine is also extremely common in the industrial sector. The industrial Otto cycle engine is a robust, versatile and relatively efficient technology. It typically sees use as a prime mover for small industrial scale CHP systems or in situations where use of Compression Ignition (CI) Diesel cycle engines is not feasible, such as emission sensitive areas. It is also used in DG situations that have alternative gas supplies, such as mine gas, biogas and landfill gas.

As will be seen in the following section, the theoretical Otto cycle is conceptually simple, relying on basic thermodynamic relationships. Practically, however, the engine based on the cycle is a relatively complex arrangement, relying on valves, cams, spark plugs and numerous associated gears to work effectively. In comparison to other engines though, specific power is relatively high and transient response characteristics favourable, resulting in an extremely flexible prime mover. The industrial heat engine is discussed in a more general sense later in the present chapter, with the key historical, technical and economic drivers for successful deployment considered. In the following section, the underlying thermodynamic theory and issues pertaining to its practical realisation are discussed.

2.2.1 The Otto Cycle - Thermodynamic Theory

The Otto thermodynamic cycle is represented on the Pressure – Volume diagram shown in Figure 2.1. The ideal air standard cycle comprises of the following four processes [19]:

1-2 Adiabatic compression of the working gas

2-3 Isochoric heat addition to the working gas from external source

3-4 Adiabatic expansion of the gas

4-1 Isochoric heat rejection from the gas to the external sink

The cycle is usually realised in practice as a four – stroke, spark-ignition (SI)

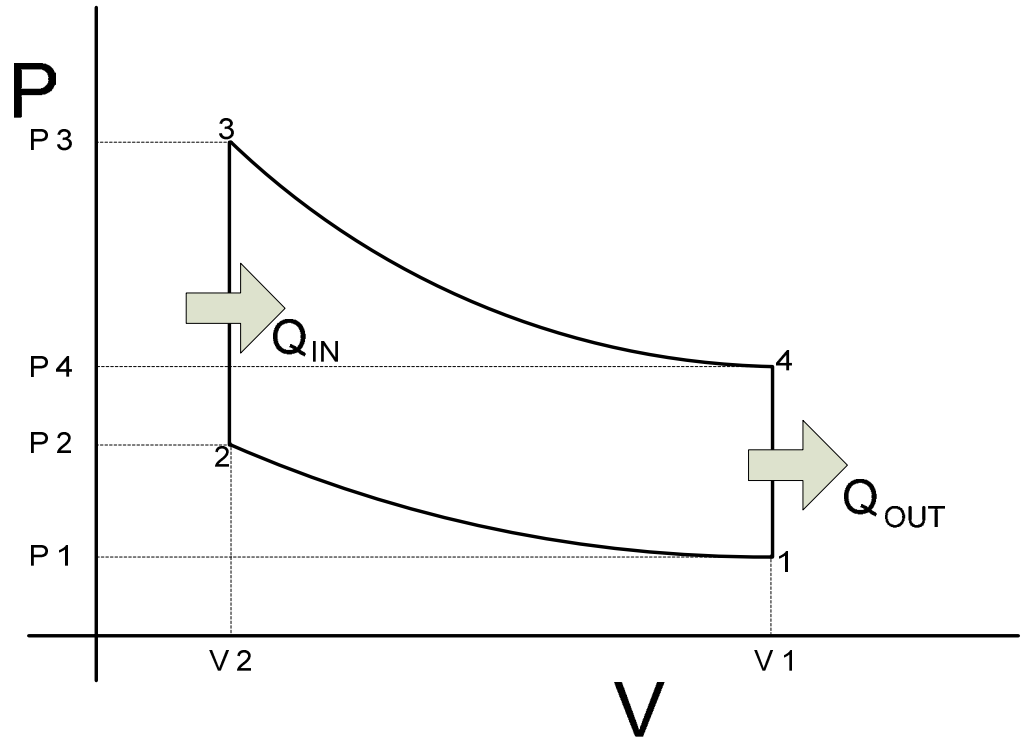

Figure 2.1 The ideal air standard Otto cycle

reciprocating piston engine cycle [26, 27]. The necessary consequence of using any continuous motion crank linkage such as that required in the practical engine is the rounding of the process branches on the *P*-*V* diagram. This is represented in Figure 2.2. It is immediately apparent therefore that the practical implication for this and other thermodynamic cycles is that the use of continuous motion crank mechanisms leads to a compromise in the work performed by the cycle for the same temperatures and compression ratio.

The four strokes occur over two complete revolutions of the crank, and can be summarised as follows [28].

Intake: The charge gas is drawn into the working cylinder through the open intake valve by the downward motion of the piston, which causes a negative pressure in the cylinder. In supercharged and turbocharged engines, which are common in the industrial engine field, a positive pressure is created in the intake manifold by the compression of the gas using a rotary compressor. This leads to the distinction between 'naturally aspirated' engines which use the negative pressure manifold, and 'forced induction' types of engines which operate with positive pressure manifolds created by the supercharger. Thermodynamically, the advantage of this is an increase in the charge air density within the cycle, allowing the combustion of a greater mass of fuel. This increases the specific power output of the given engine and can increase efficiency also. This intake stroke is missing from the ideal air standard cycle however, and instead is present as a technological necessity to allow internal combustion in the cycle.

Compression: as per the ideal air standard cycle, the compression stroke acts to increase gas temperature and pressure within the cycle and bring the gas to a state suitable for effective combustion of the fuel.

Power Stroke: This is the working stroke of the cycle. It involves the ignition of the fuel-air mixture and expansion of the combustion products against the piston face, causing work to be done on the crank shaft. With respect to the ideal air standard cycle, the power stroke usually occupies a crossover between the isochoric heat addition process and the adiabatic expansion process.

Exhaust: Also missing from the classical thermodynamic description of the cycle, the exhaust stroke occurs after the expansion of the gas on the power stroke. The exhaust valve opens and the spent combustion products are evacuated from the cylinder by the upward stroke of the piston. The spent gases exit the system at high temperature and are rejected to the external sink, the atmosphere.

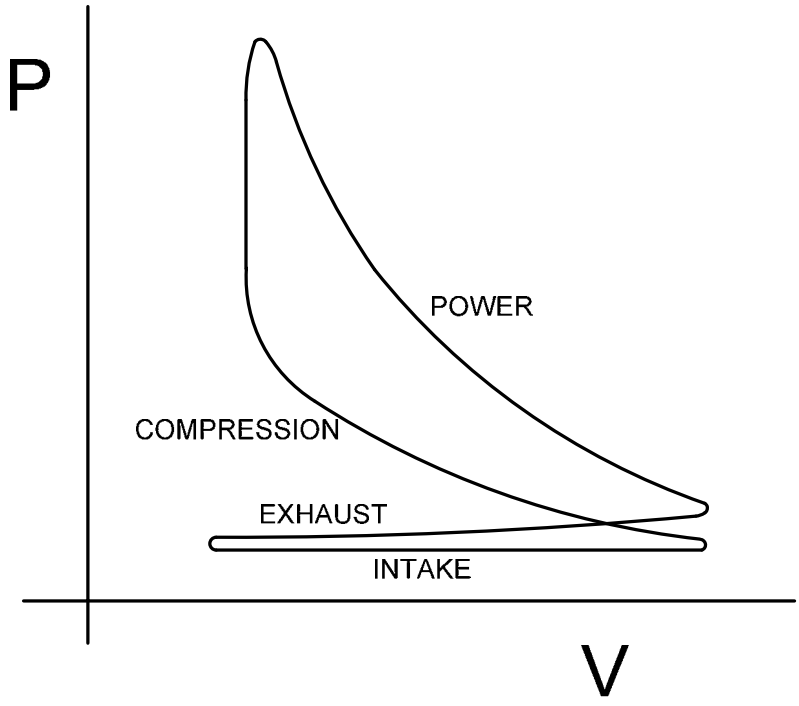

Figure 2.2 The practical 4-stroke Otto cycle

2.2.2 The Industrial Internal Combustion Heat Engine

Industrial engines can be defined as those prime movers which are used in a fashion other than for propulsion. Typically they are characterised by robust construction and heavy loading environments. Generally, they are understood to be those engines used to drive machines such as electrical generators, pumps and compressors; however the designation also includes engines used to drive industrial plant such as excavators, dumpers and loaders as well as those in agricultural use. Whilst the term may technically include gas and steam turbine

plant, the area of interest of this study is the reciprocating ICE. The present work addresses the requirement for and the subsequent pursuit of higher efficiencies in these engines.

The modern industrial ICE, commonly operating on Otto or Diesel type thermodynamic cycles, owes its inception in no small part to the steam engine, an external combustion engine (ECE). Steam engines first appeared in the early eighteenth century and found favour as prime movers in the burgeoning industrial revolution. The motive power of steam was eventually harnessed to drive machinery such as pumps, locomotives, steam ships and traction engines. When the ICE as we know it today began to be developed in the late nineteenth century at the hands of inventors such as Otto, Benz, Daimler and Diesel, its technological manifestation was based heavily on that of the steam engine [26]. The ICE eventually surpassed the steam engine as the prime mover of choice in the world at large. This eclipse is attributable to the ICEs relative simplicity, ruggedness, favourable transient response characteristics and high power to weight ratio as well as the increasing availability of the liquid fuels utilised in such engines [28, 29].

In the century since its inception, the ICE has enjoyed constant development. Whilst the operating principles of such engines have changed little in this time, the technology used to realise these principles has improved radically, with consequent increases in efficiency and power-to-volume outputs. Incremental improvements in design and simulation methods, the materials used for construction, manufacturing processes, fuels and fuel quality, ignition systems and superchargers, as well as different lubricants and the advent of sophisticated electronic control systems saw the rise of the ICE to become the

dominant prime mover technology of the twentieth century for transport and small scale power generation. A notable indicator is the increase in engine primary energy efficiency. Whereas the first engines produced by Otto et al operated with efficiencies of about 10 percent, modern engines can reach figures above 40 percent.

The relevant literature examines the development of the ICE almost exclusively from the perspective of the quest for self propelled vehicles, however the industrial engine can be said to have been the forebear of this development. The industrial ICE was borne of a need of small business owners and craftsmen for cheap, reliable stationary power generators other than steam powered engines. Steam engines were costly and subject to strict regulation and were therefore primarily owned by large companies with the resources to buy and operate them[27]. The Otto engine, and indeed its sister ICE the Diesel engine, found favour due to a high power/weight ratio, the increasing availability of the liquid petrochemical fuel and inherent reliability. Thus, the ICE established itself early on as an economic alternative for onsite power generation.

Industrial ICEs do owe much of their own development to the automotive ICE—the two engines are virtually identical in principle and share many of the same features and consequently research and development efforts for the two have tended to coincide. The fundamental difference in these engines is their application. Automotive engines operate in a widely varying loading regime dictated by the local conditions encountered by the operator. Power demand is met through the relative interplay of torque and engine speed. In general, such engines operate at varying speeds and partial load for the larger proportion of their operation.

Industrial engines generally operate in low or constant speed, high load regimes. One area of industrial engine application is that of stationary electrical power generation. In such cases, a constant speed requirement is imposed on the engines as they are required to drive electrical alternators and thereby produce power at a constant frequency. Depending on alternator construction and desired frequency, engine rotational speed can be specified. In the European market, an engine operating at 1500rpm delivering electrical power at 50Hz would be typical. Fluctuating load is accommodated by an engine governing system, which controls engine output by regulating the fuel air mixture admitted to the engine cylinders. Constant speed is maintained by allowing engine torque to vary. An exception to the constant speed design is recent work carried out in Italy by Badami et al [30], in which a novel CHP system is described that operates on an Otto cycle that incorporates variable speed operation to increase part load efficiency and reduce emissions. Power electronics are incorporated to ensure constant electrical frequency.

2.2.3 Engine Efficiency

The efficiency of an industrial engine operating in such scenarios is discussed in terms of the useful power produced per unit fuel power utilised in the conversion. Typically, the electrical power is of importance and therefore is used as the reference as opposed to the mechanical power of the engine. The engine efficiency η_e is given by Equation (2-1)

$$\eta_e = \frac{P_e}{P_f} \tag{2-1}$$

where

$$P_e = \eta_{alt} P_m \tag{2-2}$$

and P_e, P_f and P_m are the electrical, fuel and mechanical power respectively and η_{alt} is the alternator efficiency. The benefits of efficiency gains in such engines are readily apparent; increased work output per unit fuel energy utilised results in a fuel cost saving to the operator. All else kept equal, greater efficiency also implies a higher power density, which results in a reduction in overall engine size per given output. Production and transport costs could reasonably be assumed to be positively affected as a result. However, increases in efficiency may be accompanied by increased plant complexity, with due regard having to be paid to the manufacturing cost and time, as well as the required maintenance schedules. Some methods of increasing engine efficiency for such engines are discussed later. These centre on the optimization of the combustion process and include areas such as piston bowl shape, valve timing and supercharging. These are all methods of manipulating the dynamics of the charge flow to enhance combustion and minimise heat losses, the desired result being maximum energy conversion with minimum toxic by-products such as Nitrogen Oxides (NO_x), Carbon Dioxide (CO_2) and Carbon Monoxide (CO).

2.2.4 Knock

It is also important at this juncture to note the implication of fuel quality on the efficient operation of the engine. Knock is a destructive phenomenon in the operation of the SI engine that is related to fuel quality. It is a combustion phenomenon that arises when uncontrolled ignition of the mixture occurs in pockets of heated gas in isolation of the flame front instigated by the spark plug. Mixture gas is compressed by the movement of the flame front through the cylinder. This can cause some regions of the mixture to auto-ignite, in effect creating sub-zones of combustion activity in the cylinder. This effect is

undesirable as it is unpredictable and has detrimental effects on component life within the cylinder [28].

Similar to the octane rating of gasoline used in the automotive sector, the propensity of a given gaseous fuel to knocking is represented by the *methane number* (MN). An MN of 100 represents anti knocking and is defined for methane (CH_4); 0 represents high knocking tendency and is defined for hydrogen (H_2) [31]. All MNs in between represent different equivalent fuel mixtures of the two components and their consequent knock resistance. The scale is not a percentage scale though, and MN values in excess of 100 exist, as for biogas (MN > 120) and mine gas (MN ~ 105). This is due to the presence of other components, such as inert N_2 and CO_2 which do not take part in combustion. Biogas plant can have poorer fuel conversion efficiencies than conventional fuel plant, resulting in lower operational efficiencies being obtained than with equivalent conventionally fuelled plant. Roubaud and Favrat [32] indicate this is due to high $C0_2$ content of the gas causing reduced laminar flame speed.

Elimination of knock is not an uncomplicated process though, and knock control can have a detrimental effect on engine efficiency. In order to prevent knocking, corrective measures such as exhaust gas recirculation (EGR), charge pressure reduction and ignition time advancement are utilised. Such measures affect specific fuel consumption adversely [27, 33].

Knock is also a function of the compression ratio of the engine and, as such, places a limit on the achievable compression ratios of engines. For the ideal

Otto cycle, thermal efficiency is directly related to the compression ratio by the Equation (2-3) [19]:

$$\eta = 1 - \frac{1}{r_v^{\gamma-1}} \tag{2-3}$$

where r_v is the compression ratio and γ is the specific heat ratio c_p/c_v. It can therefore be seen that the known occurrence of knock inhibits the achievable efficiency at the design stage of the engine through the limiting of the compression ratio. However, the development of fuel additives for knock reduction has contributed to the increase in practical compression ratios. Today, industrial SI engines have compression ratios in the region of 12: 1, with some units having ratios in excess of 15: 1.

In the case of biogas fuelled engine operation, although the fuel is of a higher MN and is therefore less prone to knocking then other conventional fuels, it is common practice for manufacturers to request a full gas component analysis at the planning stage to assess fuel quality. This is due to the non-standard composition of the fuel.

2.2.5 Ongoing Research and Development

The desired engine brake-thermal efficiency improvement mentioned above is pursued in a number of ways. It should be noted that essentially all areas of the ICE are constantly subject to research and development to improve not only power and efficiency performance but also component durability, size and manufacturing efficiency. As efficiency gains are the subject of this thesis, discussion will be limited to aspects of this that are currently active areas of research. These areas include piston design, valve timing and supercharging.

2.2.5.1 Piston Design

Piston design is a broad area of research in itself in the wider field of ICE design. The piston functions as a movable wall that transfers power from the combustion of the charge mixture to the crankshaft via the wrist pin and connecting rod [27]. The piston also serves, in conjunction with the piston rings, to seal the combustion chamber and prohibit the escape of combustion gases and passing of lubrication oil. Increasing power output of the engine can lead to the temperature and pressures experienced by the piston increasing. This increase in temperature and pressure can incur penalties on the piston that must be properly combated so that piston failure does not occur.

Damage mechanisms to pistons include wear and fatigue. Wear is defined as progressive material loss from the surface of a solid body caused by mechanical effects i.e. the contact and relative movement against a solid, liquid or gaseous counterpart [27]. It impedes function and shortens the service life of the component. Methods for detection and analysis of wear of pistons and piston rings are therefore of utmost importance. These include radiotracing; Schneider and Blossfeld [34] describe a novel radiotracing method that allows higher accuracy in determining wear rates of the components, information vital for correct hardware design. With the correct statistical data available, design of piston components may be optimised in terms of lubrication, geometry, gas mixing and combustion dynamics. Examples of current developments in these related fields can be seen in [35–38].

In conjunction with wear, fatigue is among the most prominent damage mechanisms for engine pistons. Fatigue is the failure of a component at a level

below the ultimate tensile stress of the material due to fluctuating, repeated or reversed stresses [39]. Silva [40] presents case studies of piston failure due to fatigue. A number of corrective measures, divided into the five areas of materials, local reinforcements, surface coating, design and piston cooling are ultimately suggested.

Geometry of the piston crown is an area of interest as it has implications in the combustion behaviour of the engine and can ultimately affect engine efficiency. Flow conditions of the charge mixture are manipulated by careful design of the crown shape. Myriad bowl designs are in use in both the industrial and automotive sector. A comprehensive list of different piston designs is collated by van Basshuysen and Schafer [27]. Kajiwara et al [41] also demonstrate the correlation between piston bowl/combustion chamber dimensions and emissions in Diesel engines manufactured by a Japanese concern.

2.2.5.2 Valve Timing

Manipulation of valve timing to increase engine performance is generally the preserve of the automotive engine sector. It does, however, have analogues in the industrial sector. Of particular note is the use of the Miller cycle as an enhancement. The Miller cycle is a thermodynamic cycle akin to the Otto cycle that is used to yield higher specific power output [42, 43]. This is done by having a shorter compression stroke than expansion stroke. Realisation of this concept is achieved by either an early or late closing of the intake valve on the induction stroke of the cycle. Supercharging is utilised for charge pressure boosting—the Miller cycle is a modern modified version of the older Atkinson

cycle which utilises the modified valve timing regime without supercharging [42].

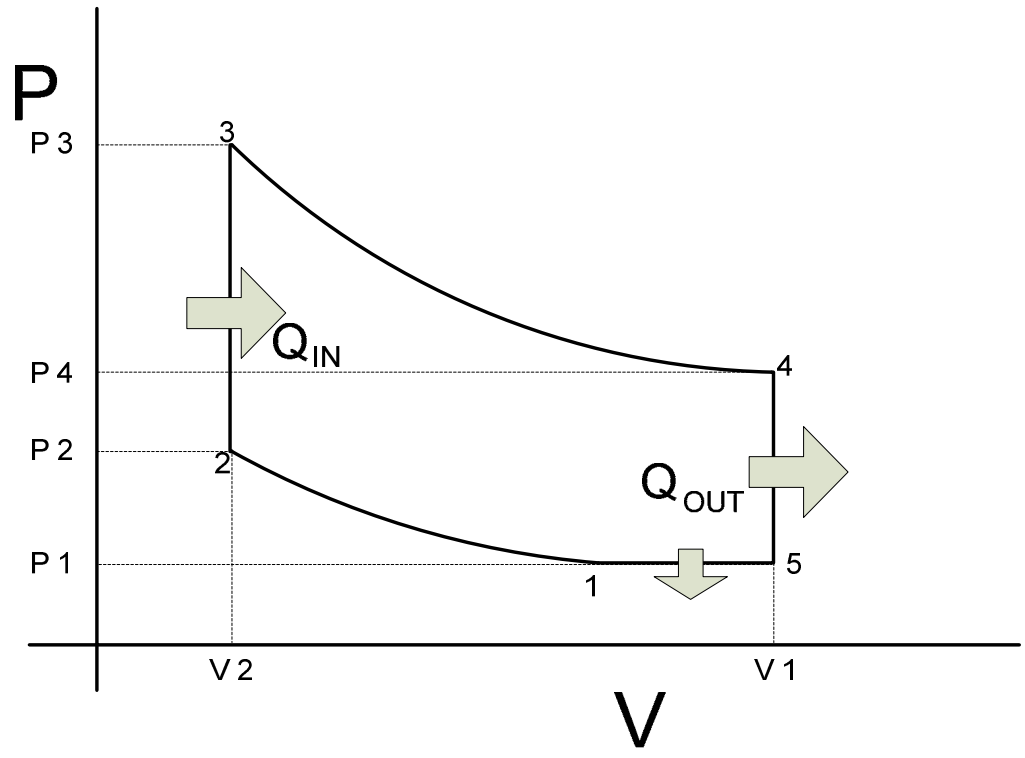

Figure 2.3 The ideal air standard Miller cycle

Although gaining attention in the automotive sector currently, the Miller cycle has been utilised in the industrial and marine sector for a time [43]. Currently, manufacturers of large stationary generators are utilising the technology for performance gains. Table 2.1 shows a segment of a complete product range for a typical Natural Gas engine manufacturer operating in the European market. Models 1 and 2 are Otto cycle engines with mechanical power outputs of 525 kW and 700 kW respectively. Models 3 and 4 are the same models adapted to operate on the Miller cycle.

Table 2.1 Comparison of Otto and Miller cycle versions of Natural Gas CHP engines

Model	$\mathbf{P_{fuel}}$ kW	$\mathbf{P_m}$ kW	$\boldsymbol{\eta_m}$	$\mathbf{B_{MEP}}$ bar
1	1346	525	39.00%	16
2	1795	700	38.99%	16
3	1422	600	42.20%	18.3
4	1882	800	42.50%	18.3

As can be seen from the table, the engine models operating on the Miller cycle have a higher Brake Mean Effective Pressure (BMEP), representing a higher specific power output over their Otto cycle counterparts. Higher fuel consumption is noted also, although this is accompanied by higher brake efficiencies. Wu et al [44] indicate that there is no inherent efficiency gain in the ideal Miller cycle over the ideal Otto cycle but a higher net work output is achieved with reduced propensity to knock. The reduced proportion of cycle work attributed to overcoming frictional effects may offer an explanation to the increased brake efficiency. Wang et al [45] and Wang et al [46] have analysed the use of the Miller cycle for a petrol fired engine for reduction of NOx emissions. A positive effect on the NOx emissions is noted. Mikalsen et al [47] have investigated the Miller cycle as an alternative to the Otto cycle engine for small scale CHP applications, concluding that while fuel efficiency improvement is possible, this may come at the expense of power density. Further validation of the simulation techniques used is required before definitive conclusions are drawn though.

The Miller cycle has been adopted on Diesel cycle engines also. Wang et al [48] describe an experimental investigation of this, with key results indicating a reduction in NOx emissions for the Diesel engine under examination.

2.2.5.3 Supercharging

Supercharging is the act of increasing the air (or mixture) density by increasing its pressure prior to entering the engine cylinder [28]. This creates a condition in which a greater quantity of fuel can be burned efficiently in the engine and thereby increases specific power of the plant. Different methods exist for the performance of this compression. These are mechanical supercharging, turbine-driven supercharging (turbocharging) and pressure wave supercharging. By far the most common type associated with stationary engines, both SI and CI is the turbocharger; therefore it is advances in this sector which are of interest here.

Turbocharging involves two primary components: a turbine that is placed in the exhaust stream of the engine and a compressor placed in the intake stream of the engine. The two are mechanically linked via a shaft. The operation of the unit involves the turbine extracting energy from the exhaust stream and driving the compressor via the shaft; the compressor, in turn, compresses the intake air/mixture, increasing the charge density admitted to the cylinder.

Turbocharging of ICEs, its effect on performance and the parameters affecting optimal performance are detailed extensively in the available literature [26–28]. Kesgin [49] analyses the particular case of a turbocharging system on the performance of a Natural Gas engine. The importance of factors such as the exhaust manifold geometry, the location of the turbocharger and its efficiency

are all highlighted. The latter is of particular note—an increase in turbocharger efficiency of 1% was found to increase engine efficiency by approximately 0.08%. Galindo et al [50] investigate different architectures for two-stage turbochargers and the effect on pumping losses in the system. Nakonieczny [51] develops a second law model to investigate the entropy generation within a Diesel engine turbocharging system. Dynamic response of turbocharged engine alternating current (AC) gensets is addressed by Katrasnik et al [52]. In the study it is held that the dynamic response of turbocharged Diesel engines can be improved by incorporation of electric assisting systems such as an integrated starter-generator-booster (ISG), which is a method of direct energy contribution to the engine flywheel, or an electrically assisted turbocharger. The relative merits of each with different limiting factors, such as transient frequency deviation (TFD) and frequency recovery time (FRT) are detailed.

A related area is that of turbo-compounding. This involves the use of an exhaust-gas-driven turbine to recover kinetic energy from the exhaust stream; the kinetic energy is then contributed directly to the mechanical drive through a gearing and transmission system, or else converted to electrical power and stored as part of a hybrid electric configuration. The idea is receiving considerable attention at the moment in the Diesel engine market for trucks and power generation, as is evidenced by the considerable number of recent patents, for example [53] and [54]. Vuk [55] provides some general information on the technology, indicating that the major advantages of the technology are the comparative simplicity of the architecture, the reasonable cost and the availability of cheap sophisticated electronic control systems that would be required. Also, he suggests that a 10% increase in fuel economy and a 20%

increase in power density are possible. The disadvantages associated with turbo-compounding are the possible requirement for a relatively complex gear / transmission system and possible adverse affects on the turbocharger and the engine.

This technology is related in principle to the combined cycle system under investigation and is part of a wide body of work concerning waste energy recovery from engine exhaust systems. Future work would involve cost/benefit comparisons of the two technologies; however this is beyond the scope of the present work.

2.2.6 Energy Balance of the Otto Cycle Engine

The energy balance of the Otto cycle engine is a function of the loading of the engine in service. The three main energy sinks – brake power, heat transfer to the coolant and heat loss to the exhaust - all accept differing proportions of the fuel energy under different load conditions. As mentioned previously, automotive engines typically operate in varying loading regimes. This ultimately results in fluctuations in the quantities of energy transferred to each sink, making generalisations of the energy balance difficult. Industrial engines on the other hand are typically required to operate at constant, full-load. Under these conditions, brake thermal efficiency is higher than at part load, and energy loss to the exhaust is generally considerable. It is this regime that is of interest in the present study.

2.3 The Stirling Engine

Although pre-dating the invention of the ICE by some half century, the Stirling cycle engine has traditionally struggled to gain a foothold in the market when placed in competition with its ICE counterparts such as Otto and Diesel cycle engines. Among the reasons typically conceded are that although theoretically more efficient than the ICEs, the Stirling cycle engine, as an ECE, suffers from relatively sluggish performance due to its reliance on comparatively slow heat transfer processes through heat exchanger walls. It also possesses a relatively complicated thermodynamic circuit requiring a fixed mass of gaseous working fluid to be continually cycled from a hot space to a cold space via a regenerative matrix [56–59]. The net result is a prime mover that has struggled to keep pace with its competition.

2.3.1 The Stirling Cycle - Thermodynamic Theory

Figure 2.5 shows the ideal air standard Stirling cycle. The cycle comprises the following four processes:

1–2 Isothermal compression, heat rejection to external sink

2–3 Isochoric regeneration, internal heat transfer from the working fluid to the regenerator

3–4 Isothermal expansion, heat addition from external source

4–1 Isochoric regeneration, internal heat transfer from the regenerator to the working fluid

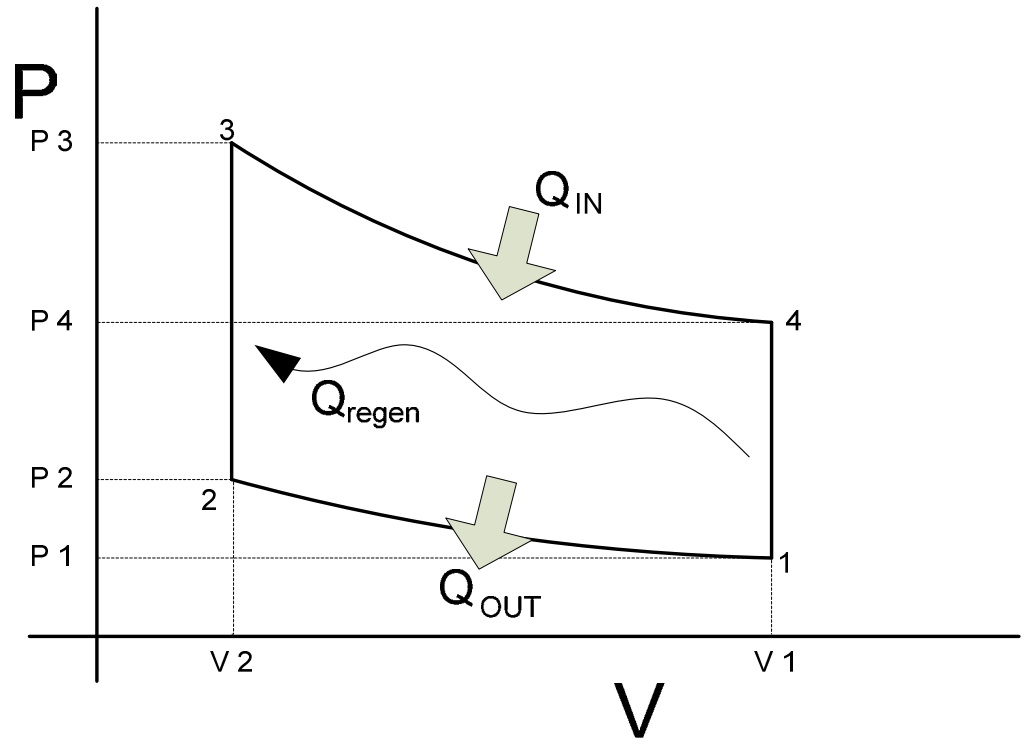

Figure 2.4 The ideal air standard Stirling cycle

The Stirling cycle is realised as a closed cycle external combustion engine with regenerative heat exchange for part of the cycle. It utilises two working spaces, each held at a constant temperature. One space is maintained at the temperature of the thermal source, typically a gas burner although any heat source is possible. The other space is maintained at the thermal sink temperature, generally an air cooled heat exchanger or cooling water circuit. In the ideal cycle, gas is heated in the hot space, causing expansion and work on the piston. It is cycled to the cool side via the regenerator matrix, generally a fine wire mesh with high thermal capacity. The regenerator stores a quantity of the heat from the passing gas. The remaining heat is rejected from the gas in the cool side heat exchanger. The gas is then cycled to the hot side, again via the regenerator. It collects heat from the matrix as it passes, emerging in the hot side, where it is heated further. In the practical engine though, gas may be in

both working spaces at any instant, causing a departure from the ideal cycle and making analysis considerably more complex [56]. This is a result of the kinematic linkages that are necessary to realise the system.

2.3.2 Stirling Engine Kinematic Linkages

2.3.2.1 Alpha configuration

The alpha configuration comprises two pistons in separate working chambers. Conceptually it is the simplest embodiment of the engine, with one cylinder acting as the heated side, the other as the cooled side. The working fluid is cycled to each space continuously, with the resulting expansion and contraction of the gas generating work which is transmitted to the crank shaft via the pistons.

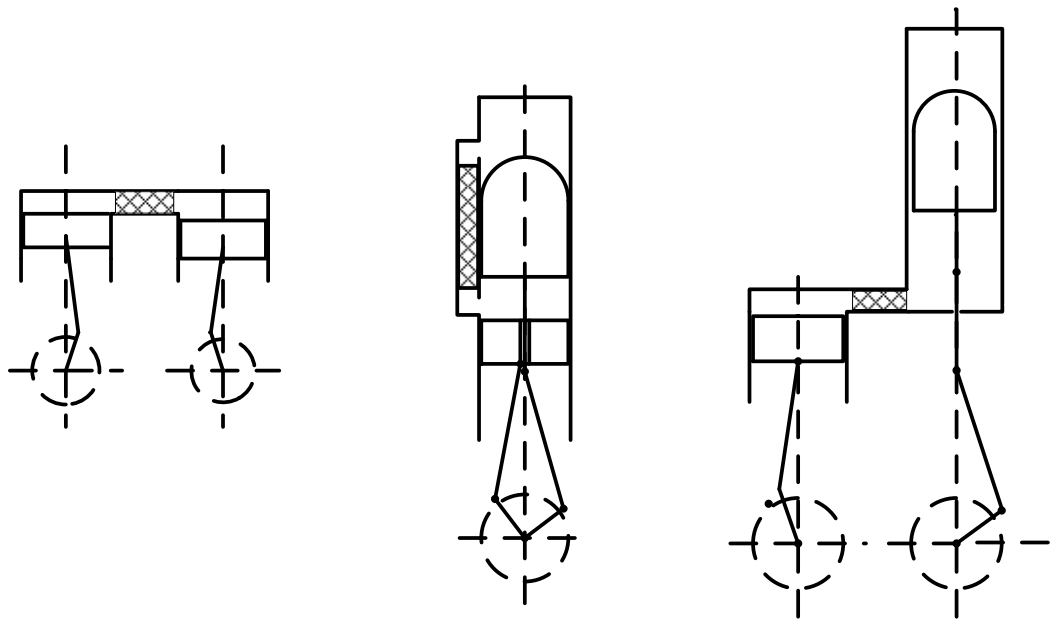

(a) (b) (c)

Figure 2.5 Kinematic configurations of the Stirling engine—(a) alpha, (b) beta and (c) gamma

2.3.2.2 Beta Configuration

The beta form of the engine is manifest as a single cylinder arrangement. The working fluid is moved between the working spaces by a displacer. Gas is heated at the hot end, causing it to expand through the cylinder and regenerator and doing work on the power piston. The displacer is used to shuttle the gas between the hot and cold working spaces and in this manner permits the continuous cyclic operation on the gas.

2.3.2.3 Gamma Configuration

The gamma configuration, like the beta configuration employs a displacer-piston set up to move the gas and transmit work. However, where the beta engine employs only a single cylinder, the gamma engine is arranged in two separate cylinders. The gamma configuration has a lower specific power potential than the beta configuration due to a higher proportion of dead space effectively diluting the compression ratio [56].

The three configurations offer different advantages under different conditions, making the Stirling cycle engine a versatile technology. The alpha engine was adapted for automotive use due to its high specific power capability [60]. The beta engine was the first type used historically. It offers a reasonably high specific power output and a compact design, being a single cylinder arrangement. Also, a crankcase of minimum size and weight is possible, giving it an advantage over multi-cylinder arrangements. The gamma arrangement offers a compromise between ease of construction and performance and is usually favoured where engineering production concerns are of primary importance [57].

2.3.3 Comparison to Other Cycles

The ideal air standard Stirling cycle is presented in Figure 2.4 above. It differs significantly from the Otto cycle in that it incorporates heat transfer to and from the system under isothermal conditions, thereby permitting, in theory at least, the attainment of the Carnot efficiency for the given source and sink temperatures. This is a significant advantage over similar cycles such as the Otto cycle and the Diesel cycle. However, the practical realisation of the cycle is problematic and the promise of efficiency figures in excess of those from its internal combustion counterparts is rarely realised [56, 57, 59]. Mechanical linkages that allow the nearest approximations to the ideal processes are difficult to implement and the correct specification of heat exchangers is a sophisticated study requiring considerable art and skill [61]. This practical consideration of engineering design is the key issue in the application of all thermodynamic cycles. This is apparent also with the Otto and Diesel cycles. Although the Otto cycle has a higher theoretical thermal efficiency than its Diesel counterpart, it is limited in actuality by its compression ratio and the occurrence of engine knock. The CI Diesel engine, on the other hand, is capable of significantly higher compression ratios and as a result attains higher thermal efficiencies in the real world [19]. It would seem on inspection therefore, that although the ideal Stirling cycle has significant advantages over its internal combustion counterparts, until the challenge of its complicated design and construction has been overcome, the ICEs will continue to win out over them.

2.3.4 Applications of the Stirling Engine

Due to its nature as an external combustion engine, the Stirling cycle engine can operate with a variety of heat sources, meaning that it is an extremely versatile

technology. Although it has suffered set-backs on its path to widespread deployment throughout its history, it is currently undergoing something of a rich streak of development.

Historically, the Stirling has seen development for a number of applications, including portable power units for military deployment, locomotive engines, bus and truck engines and automotive engines. Most of this work stemmed from that done by the Philips BV company in Eindhoven, Holland from the 1930s right through to the 1970s. Details of the Philips development programs are given by Hargreaves [62]. Philips, working with partners such as General Motors, Ford Motor Company and United Stirling were responsible for much of the modern development of the Stirling above that of its 19th century incarnations. These developments, though successful in their own right, were never pursued beyond a limited number of test engines and prototypes, and mass commercial deployment of the engine was never realised at the time.

Interest in the Stirling engine did not completely die off, though, and there is something of a momentum starting to gather behind the technology in more recent times, particularly as a 'green' power converter. Current commercial developments of the engine have primarily diverged into two separate areas; solar thermal power generation and micro CHP generation. In solar thermal generation, the engine is placed at the focal point of a large parabolic mirror, used to focus solar radiation onto the heater of the engine, which then drives an electrical generator. This concept can be seen in Figure 2.6. Although gaining prominence now, these solar Stirling systems have been under investigation for some time, with a number of manufacturers active in the area [63]. Currently, companies such as Infinia Inc. and Stirling Energy Systems (SES) are actively

developing these systems for grid scale power generation. SES has recently attracted significant investment and is working towards an installed capacity of 800 MW in partnership with San Diego Gas & Electric and Southern California Edison [64]. Infinia is preparing for commercial launch of its PowerDish system in September 2010 [65].

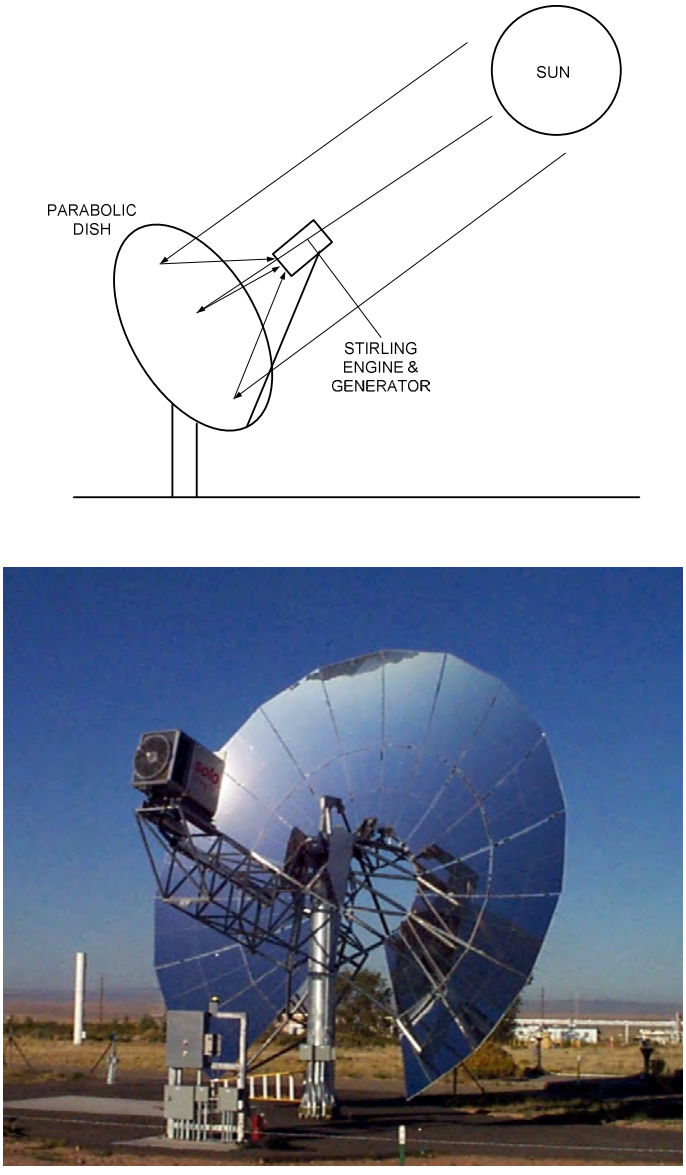

Figure 2.6 Solar Dish / Stirling system [66]

Use of the Stirling engine in micro-CHP systems is currently being pioneered by WhisperTech of New Zealand with their Whispergen system [67]. This is a natural-gas-fired Stirling engine system with heat recovery for domestic heating

and power. The company have recently partnered with Mondragon Corporacion Coopertiva of Spain to form Efficient Home Energy, a company aimed at manufacturing and distributing the Whispergen CHP unit for the EU market.

2.4 Distributed Generation—Mono-generation and Poly-generation

DG is the generation of electrical power at the demand centre by the end user. Historically, DG was the first system of electrical power generation actually used, with small industrialists generating their power requirement onsite for supply to plant and machinery. Only later did large scale central generation, transmission and distribution become the dominant power supply system.

DG can be divided approximately into two categories: mono-generation and poly-generation. Mono-generation describes systems whereby the electrical power output of the plant is the only economic consideration. Poly-generation describes systems whereby, in addition to the electrical power, the waste heat produced by the plant is recovered for diversion to space or process heating (CHP) and for heating and cooling (Combined Cooling, Heat and Power—CCHP or tri-generation). Of these scenarios, CHP is the most common.

DG has numerous advantages over centralised generation, particularly relating to a reduction of power losses from the transmission and distribution system, deferral of grid capacity investments and emissions reduction [68].

2.4.1 Mono-generation Applications of the Industrial ICE

The use of reciprocating ICEs for DG applications is well established. There are two modes typically associated with these DG applications: 1) Standby and 2)

Continuous generation. Whilst the majority of DG units sold are intended for standby generation, an increasing emphasis is being placed on continuous operation [69]. Standby power is emergency power supply in the instance of a failure of the main grid supply. Backup generators are therefore the norm in many industries where reliability of power supply is of importance. The sector is almost exclusively the preserve of CI engines, i.e. Diesel engines. This is for several reasons. CI engines are of robust construction and, crucially, have excellent load acceptance characteristics in comparison to an equivalently sized Spark Ignition (SI) engine. A CI engine can accept a larger proportion of its maximum rated load on start-up than the equivalent SI engine. This is vital in standby generation systems where fast reaction to grid failure is paramount. Efficiency, although still important, is less of a concern for machines operating in such a manner, as the transient nature of operation, the sudden heavy loading and the relatively short operational period require a unit based more on durability than economy.

Continuous operation on the other hand is more the preserve of the SI engine, typically operating on fuels such as Natural Gas (NG) and Liquefied Petroleum Gas (LPG), but with increasing emphasis being placed on special gases such as sewage gas, landfill gas, biogas and mine gas. Continuous operation is the relatively steady-state operation of the unit at a non- or near non-fluctuating load regime. Such mono-generation scenarios have inherent advantages in that the use of the SI engine over the CI engine in this regard offers improvements in factors such as emissions, fuel costs and fuel storage issues. Also, the true benefits of engine efficiency are more strongly felt over long steady-state operational periods, meaning that, by definition, engines experiencing sporadic

heavy loading are less prone to efficient operation than those designed to operate over long steady-state operational periods.

DG allows elimination of transmission and distribution costs, thereby increasing energy cost savings to the customer. An example of a DG system operating on a continuous load would be an SI engine operating as a Waste to Energy (WTE) gas converter. This is a mono-generation mode, possible due to the methane-rich gas produced at former landfill sites. In such an instance, it is possible to combust the gas using an SI engine operating on the Otto cycle, or similar. The power generated is converted to electrical power and transmitted to the grid, or else to a local user. Such setups are established worldwide. Themelis and Ulloa [70] report that in 2001, there were some 955 landfill sites recovering gas worldwide. The country with the most sites was the US, with Germany and the UK in second and third place respectively. Of the gas recovered, some 70% was utilised for power generation. The market for the technology is expected to grow considerably as market awareness increases and uptake at pre-existing landfill sites increases. Installed capacity in Ireland is expected to grow to approximately 305 MW_e by 2020 [71].

When discussing DG, perhaps the most important sector is that of CHP. This is a subject of much current research and is acknowledged to be a key technology in the energy sector of the twenty-first century [72, 73]. It therefore warrants separate treatment.

2.4.2 Poly-generation Applications of the Industrial ICE - Combined Heat and Power Generation

CHP Generation is a thermal process that produces electricity and heat simultaneously from a single source of fuel [74]. There are numerous plant in existence and being developed that are capable of realising this conversion; however, the ones most relevant to this study are those which are based on reciprocating spark-ignition ICEs. Other technologies include turbine-based plant, Stirling cycle plant and fuel cells.

The principal of operation is thus: fuel, typically Natural Gas or similar, is combusted in the engine cylinders, doing work on the pistons. The subsequent mechanical power is used to drive an alternator that converts it to electrical power. The nature of operation of such plant necessitates the production of heat as a by product. In CHP generation, this heat is of sufficient grade to be recovered from the engine cooling systems and utilised as space or process heat elsewhere. In a typical reciprocating SI-engine-based CHP plant, heat would be recovered via the engine jacket water cooler, oil cooler, turbocharger after-cooler and from the exhaust gases via a water circuit.

Unit efficiency is paramount in the selection and operation of a CHP unit. As is to be expected, there are three efficiency values used as a measure when examining such plant; electrical efficiency—the quantity of power available in the fuel that is ultimately converted to electrical power; recoverable thermal efficiency - the quantity of power available in the fuel that is converted to recoverable heat; and overall efficiency—the sum of the electrical and recoverable thermal efficiencies and therefore the quantity of power in the fuel that is converted to usable energy.

Currently, state-of-the-art CHP plant operating on the Otto cycle or similar are reaching electrical efficiencies in the region of 44%. Such plant have recoverable thermal efficiencies in the region of 44% also, with consequent total plant efficiency of approximately 88%. Smaller plant may have efficiencies of c. 35% electrical and c. 50% recoverable thermal. The first law efficiency of the whole plant is still evidently high. As such a high proportion of the primary energy is utilised, CHP generation is considered a key energy-efficient technology and is already the subject of governmental encouragement on a local and international level. In Ireland, a target of 800 MW_e installed capacity by the year 2020 has been set, although deployment has been somewhat sporadic and interim targets have not been met [72]. However, considering that the Irish government has committed to 500 MW installed capacity of ocean-based (tidal and wave) power generation by 2020 [75], considered to be a significant potential generator for the country in the future, the commitment to CHP is significant. Barriers to deployment remain, however, and must be overcome. These include Ireland's historically sparse industrial base, a low population density and limited familiarity with, or requirement for, district heating schemes [72].

These issues illustrate the problems, inherent in the correct specification of CHP generating plant, that render them more difficult to put into practice than other DG plant. Of importance when considering the implementation of CHP is the consideration of the demand characteristics of the prospective site. This is dealt with in the following section.

2.4.3 Demand Profiles

The energy demand of a building or facility can be readily displayed as a plot of instantaneous demand against time. Separate plots for electrical and thermal demand can be obtained. These profiles offer significant information regarding the facility's energy requirements. In the optimum application, information is available at regular intervals for both electrical and thermal requirements through metering systems, perhaps incorporated into a building management system (BMS). Where the respective demands are specified in non standardised terms, such as thermal demand being recorded as litres of oil purchased per year for example, it is possible to homogenise the terms and express each of the quantities in kW by accounting for the calorific value of the fuel and the rate of consumption. Such profiles can be compiled for any period of interest; however, the most useful are generally the daily and annual profiles. Figure 2.7 to Figure 2.9 display examples of such profiles for a faculty building in a large academic institution based in Ireland [76]. Daily profiles are displayed in (a) and (b) and a yearly profile in (c). A yearly profile is shown in Figure 2.7. Daily profiles are displayed in Figure 2.8 and Figure 2.9. Daily profiles are offered for a summer day and a winter day to illustrate the difference in seasonal demand for these periods. Data was acquired via a data logging system in the BMS. Data points were logged at fifteen minute intervals for the daily profiles. The annual profile utilised mean daily load information.

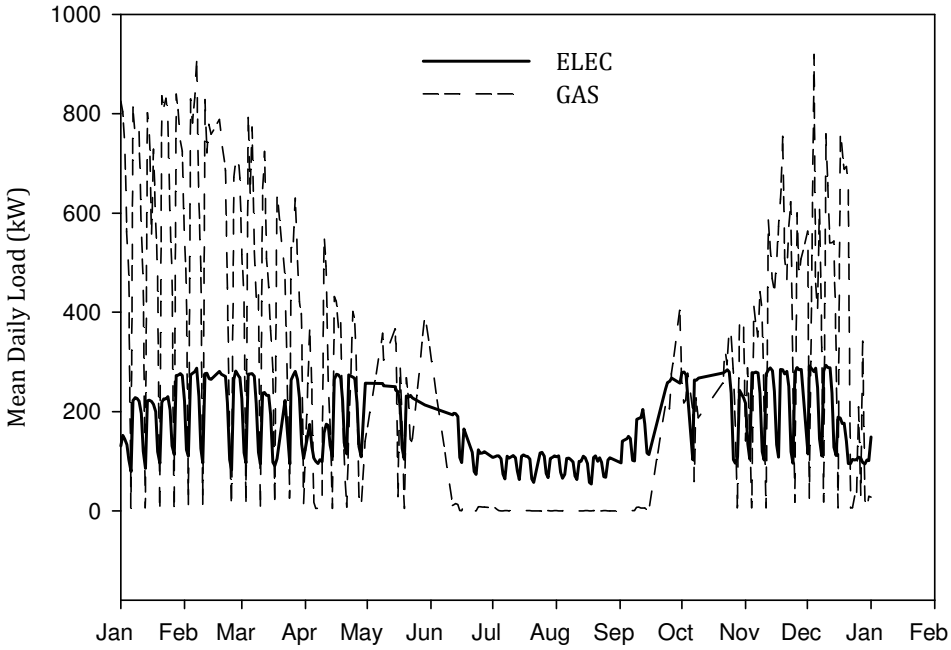

Figure 2.7 Annual mean daily electrical and thermal demand profile

1/1/2007 – 1/1/2008

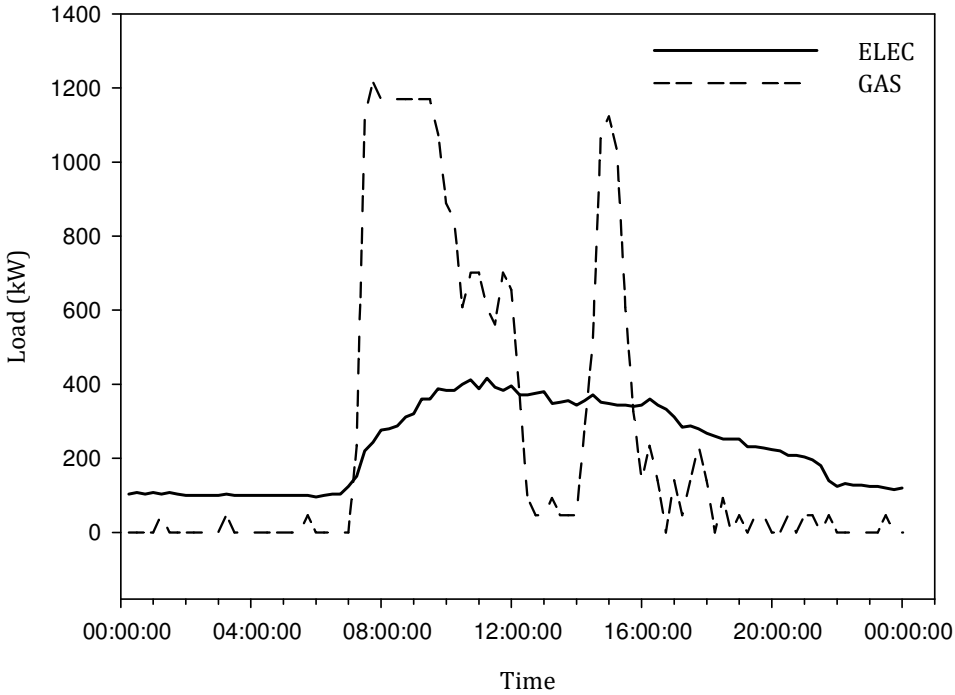

Figure 2.8 Daily electrical and thermal demand profile

21/5/2007

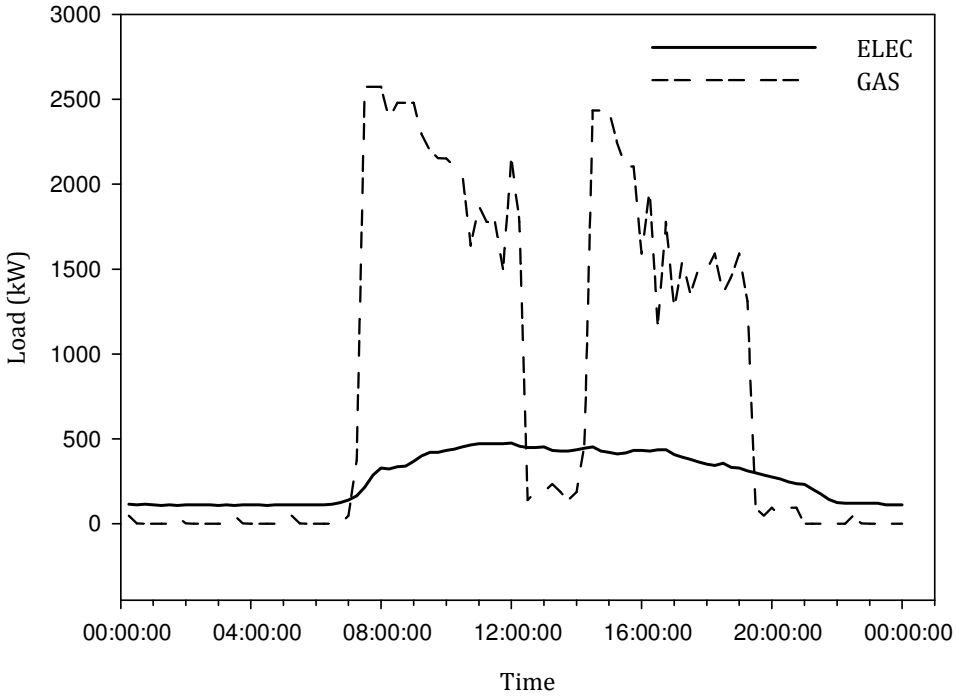

Figure 2.9 Daily electrical and thermal demand profiles

29/1/2007 (winter)

It is evident that in all cases, thermal and electrical demands differ significantly at different times throughout the measurement period. Electrical demand varies between 472 kW and 108 kW on the winter day. The summer day fluctuation is similar, varying between 344 kW and 92 kW. In both cases the peak is reached at late morning / noon, declining steadily until approximately late evening time before levelling out at the base load overnight. Thermal loads in each case exceed the electrical loads significantly for large parts of the day. Peak thermal requirement is 2,574 kW for the winter day and 1,216 kW for the summer day. Total thermal requirement for the winter day is significantly higher though at 20,147 kWh versus 6,423 kWh for the summer day. The importance of the energy demand profiles can be inferred from these examples, as they give an insight into the energy consumption behaviour of the site.

Typically, in order to accommodate any shortfalls in heat output of the CHP plant, secondary boilers are included in the installation, whilst electrical grid connection is maintained to likewise cope with electrical production shortfall. Also, the CHP unit can shut down during off-peak hours when power is cheaper to purchase from the utility. However, generally the economy-of-operation associated with use of a CHP plant requires that total yearly operating hours are maximised and full load operation is maintained. Therefore, applications such as that above, which have wide disparities between electrical and thermal demand over the daily and yearly profiles are generally less suited to CHP application as the fluctuating demand would require a generation plant to operate at part loads for significant periods. Thus, applications that have a closer coincidence of demand are more likely to benefit from CHP. This situation is analysed more closely in the following section.

2.4.4 Applications

To fully discuss the concept of CHP and its correct integration and grid connection is beyond the scope of this work. For a full feasibility analysis and detail of economic considerations of CHP plant use, readers are referred to [74] and [77]. Oh et al [74] concluded that CHP generation was feasible for a particular hotel under analysis, but was unsuited to an office block that was examined, by virtue of the unsuitable year-round energy demand profile. Panno et al [77] indicated the energy-saving and environmental benefits of CHP generation at a factory with a near-constant energy demand profile year-round. This data supports the experience in the industry at large whereby office and residential premises are held to be less suited to CHP generation than certain industrial concerns and the hotel sector. Considerable work has been

completed in this regard to fully assess the limits of these applications. The US EPA [78] conducted a study on the deployment of CHP in the hotel and casino sector in the United States. The conclusions reached indicated that deployment of the technology was more suited to the larger resort hotels and casinos, especially those in excess of 1000 rooms, again due to more favourable energy demand profiles. These more favourable profiles stemmed from the typical association of the resorts with casino gaming, large restaurants, spas and other entertainment facilities that had coincident electrical and thermal demand over longer periods. An economic cut-off point of 100 rooms was indicated. However, it was possible to economically utilise CHP in certain hotels below this size. Of the 98 existing CHP systems deployed in the hotel sector at the time of reporting (December 2005), some 20% were in hotels below 100 rooms. Madrano et al [79] presented information regarding the suitability of certain buildings to CHP or similar technology. Office buildings, educational buildings and hospitals were examined in terms of their electric-to-thermal demand ratios. Office blocks, with average electrical/thermal demand ratios in the U.S. of 2.3 were considered less suitable than hospitals (0.9) and educational buildings (0.67) for deployment of CHP or CCHP (combined cooling, heating and power). The reason behind this was the production imbalance of the CHP units themselves; the electrical power/thermal power production ratio was generally below unity, often as low as 0.66 for smaller reciprocating-engine-based plant. Gas turbine units had ratios below this again [73]. This created the issue whereby heat-dumping sectors that generally had large thermal sinks in conjunction with electrical loads were better positioned to benefit from combined generation than those without. Factories with considerable process

heat requirement and hotels with leisure/spa facilities were typical examples of suitable applications. In all cases, full analysis of the energy demand profile was the accepted protocol where an operation strategy was to be decided on.

While the ideal case for cogeneration is that electrical and thermal demand is coincident and all power produced can be accepted by the load site, the more common real case is different. Seasonal weather variations give rise to variation in space heating demand. Therefore, at design stage it is common to recommend that the site load be capable of accepting a certain proportion of the heat produced by the CHP unit, for example 60%. This Heat Usage Factor, N_{HUF}, is a common tool used in the specification of CHP plant. Inability to accept at least this proportion may lead to uneconomical plant operation as heat may need to be dumped or other control measures exercised. CHP unit controllers routinely incorporate power modulation capability whereby priority can be given to either thermal power or electrical power production or both, with the unit adjusting output accordingly. An example is a unit monitoring heat usage by way of the heating water loop return temperature. If the return temperature exceeds a set point, the unit recognises that thermal demand is insufficient and ramps down its output. The necessary consequence is that the complimentary power output, in this case electrical power, is reduced also, regardless of electrical demand. Excess electrical power could be purchased from the utility, a more expensive prospect. The converse case is true of electrical power modulation, with excess thermal demand, being met by peak boilers. A significant disadvantage of this is that the unit is placed into a part load operation regime, which is less efficient.

Combined cooling, heat and power generation (CCHP), or trigeneration, is an established generation technique. In this case, heat from the generator is supplied to an absorption chiller to produce chilled water. The chiller can supply air conditioning loads or other chilling requirements. This presents an alternative use for the CHP unit thermal output during times of reduced heat demand in residential and office situations, such as warm summer months. Although this method involves increased plant outlay, maintenance and comparative complexity as well as sophisticated control measures, if implemented correctly it can be very effective. Its market penetration is limited though in comparatively temperate climates due to less reliance on air conditioning during summer months. Absorption chillers offer the advantage of providing a thermal sink for the CHP unit during mild climatic conditions such as summer time. In doing so, they permit the CHP unit a year round thermal sink [79]. Madrano et al also indicate the advantage of Absorption chillers in allowing cooling to be transferred from an electrical to a thermal load. This shift can be cost effective for facilities subject to time of day electrical rates.

2.4.5 Discussion

Thus it can be appreciated that CHP systems are currently most easily deployed in situations where there is a coincident demand for heat and electrical power and the demand ratio corresponds approximately to the production ratio of the CHP generation plant. It is possible therefore to suggest that there exists a market for CHP plant that have production ratios that favour electrical power output. This is already evident in the market where concerted efforts are consistently being made to boost electrical efficiency. As has been seen, large CHP units already have electrical / thermal production ratios approaching unity.

Smaller units have not reached this point yet. A small scale CHP prime mover with a production ratio in excess of unity would feasibly find use in applications that have traditionally been ruled out as potential client sites, such as offices or residential blocks, as these typically do not have the high thermal demand.

Economic modelling of the power plant is crucial for decision making with regard to CHP and CCHP plant. With regard to the present work, an economic model is presented in Chapter 8 for the case of the combined cycle system being used as a prime mover for both mono-generation and poly-generation. The ultimate economic indicators used in analysis are the SPP, the NPV and the IRR of the investment represented by the plant.

2.5 Thermodynamic Modelling and Simulation Techniques for Engine Cycles

2.5.1 Finite Time Thermodynamics

Thermodynamic modelling and simulation is used in the present work to study the combined cycle system under investigation. Thermodynamic modelling holds the advantage of allowing relatively powerful simulation with limited complexity. The models developed in the present work are done so under the framework of what is traditionally called FTT. The concept of FTT can be said to offer a theoretical development of Classical Thermodynamics (CT) through the imposition of a finite time constraint on heat transfer to and from the system. Generally, the assumption of endo-reversibility within the engine is made, so that all irreversibility generation associated with the cycle is restricted to the system heat transfer boundaries [80]. This is central tenet of FTT, however its

validity has been disputed in different quarters [81, 82]. Despite this though, the technique retains widespread appeal.

Inception of the FTT method is generally attributed to the independent works of Novikov and Chambadal [80, 83, 84], although a paper by Curzon and Ahlborn [85] is often credited as the original work. The technique has seen considerable development in the intervening years, particularly in relation to thermodynamic cycles. However, although the FTT name is often used, it is apparent that the concept has broadened from the original study of the time parameter to include other constraints typical of such applications. In a recent work, Feidt [84] has proposed use of the term Finite Dimensional Optimization Thermodynamics (FDOT or FDT) as an umbrella term to include optimization procedures that might usually be ascribed to the literature of FTT – for example finite speed, finite area, finite volume, finite conductance and finite cost – even though their essential contribution might not specifically target analysis or optimization in terms of time. The issue is a semantic one, though, as the optimization of these parameters is implicit in the core principles of FTT. It does however represent an opportunity to provide a unifying title for a wide body of disparate works.

FTT is a versatile field and has been widely used to describe and optimize different thermodynamic systems and cycles. Bejan [86] describes the theory in terms of entropy generation minimization (EGM) and details its utility for the optimisation of devices of finite dimension. Similarly, Chen et al [87] provide a historical perspective of the technique as a tool for analysis of energy systems. Qin et al [88] use the method to analyse the universal power and efficiency characteristics of the Diesel, Atkinson, Brayton and Otto cycles. Lingen et al [89]

consider the case of power density optimization of the endo-reversible Brayton cycle.

The central advantage of the FTT framework is that of providing good magnitude and trend agreement with known operating characteristics of real engines using comparatively uncomplicated models.

2.5.2 Thermodynamic Modelling of the Stirling Cycle Engine

Thermodynamic modelling and simulation of the Stirling cycle engine has traditionally been approached in a hierarchical process incorporating what are typically referred to as zero, first and second order models. As the names suggest, the three represent an increasing level of complexity, starting with the most rudimentary and proceeding to the most sophisticated. A brief description of these methods is offered in the following sections.

2.5.2.1 Zero Order

The term zero order modelling was first used to describe the rudimentary 'back of the envelope' type calculations that were first popularised by William Beale of Sunpower Inc in Athens, Ohio [57]. Its genesis lies in empirical observation and experience more than mathematical and scientific principles. As a result, its use is traditionally considered difficult to justify [57, 58].

The equation originally derived by Beale has been expressed in a number of forms. The form adopted for this study was that developed by Walker, West and Senft as indicated by Kontragool and Wongwises [90]:

$$P = p_{\mathrm{m}} V_{\mathrm{p}} f F \left(\frac{1-\tau}{1+\tau}\right) \tag{2-4}$$

Equation (2-4) offers an expression for the brake power output of the Stirling engine P, as a function of the mean pressure within the engine, p_m, the swept volume of the power piston, V_p the frequency at which it operates, f, and the ratio of the source and sink temperatures, τ. The term F is an empirical factor. For the ideal cycle, F is 2. A value in the range 0.25–0.35 is offered as being representative of real engines. The equation can be easily manipulated to allow basic investigation of system parameters that describe the engine size (V_p), the thermodynamic regime (p_m, τ) and the operating frequency (f). The method is limited in its scope but nonetheless provides some analytical capability.

2.5.2.2 First Order

First order modelling is a term that describes a level of analytical study of the ideal Stirling cycle that was originally developed in the nineteenth century by the German mathematician Gustav Schmidt [91]. The term 'first order' has been generally adopted to signify its priority over other 'zero order' methods in terms of mathematical rigour and approach. Although it still relies on highly idealised assumptions and therefore generates profoundly optimistic performance predictions, it nonetheless is a useful tool for analysis and understanding of the cycle. The assumptions made in the model are described at length elsewhere [57, 91].

A number of treatments similar to the type developed initially by Schmidt exist. Organ presents a summary of the numerous different models available, along with useful information on the merits and limits of each [92]. Urieli and Berchowitz [91], Thombare [60], Reader [93] and Hargreaves [62] among others all provide isothermal models similar to Schmidt's original work. Carlson

et al [94] develop an ideal model with non isothermal heat exchange. Models of this type suggest an improvement on the isothermal model as they eliminate the necessity for infinite heat transfer and impractically slow engine speed associated with isothermal working spaces. Finkelstein [95] presents an alternative isothermal model that aims to avoid some of the technical pitfalls of Schmidt style analysis. Kontragool and Wongwises [96] offer an isothermal model with emphasis on system dead volume and imperfect regeneration. Walker [58] develops a similar model in terms of four dimensionless ratios pertaining to the engine geometry. The advantage of this method is the removing of geometric design of engine components to a secondary design phase, however its usefulness is disputed by some [91]. In all cases, Schmidt style models are highly idealised and therefore unsuitable for use as sole design aids. The engine efficiency predicted by the Schmidt model for instance is equivalent to the Carnot efficiency for the given source and sink temperatures, an impossibility in any real engine. It is possible to correlate the actual performance of an engine to the Schmidt style analysis prediction for that engine. This is done by using a correction factor to align the ideal model with realistic performance expectations. This treatment is advocated in the literature as an acceptable initial design step. Walker suggests a correction factor of between 0.3 and 0.6 as suitable to align with real operating limits, with 0.5 being suggested as representative of a reasonably well designed engine.

2.5.2.3 Second Order

Second order analysis is a further step in complexity for modelling of the engine. Whilst the first order method is an improvement in terms of mathematical complexity and rigour over the zero order methods, it is nonetheless a highly

idealised representation of the engine and its performance. Use of empirical factors such as the correction factor described above is a way of overcoming the optimism of the model outputs; however it is not necessary to elaborate on the shortcomings of this method. Implicit in the correction factor used are losses associated with real engine operation. Second order analysis attempts to quantify these losses. The term generally refers to the de-coupled methods of analysis that offer a refinement of the first order method by subtracting the various power loss mechanisms that occur in the engine from the ideal cycle power computed using the first order methods. These can be generally defined as Heat Transfer losses and Flow Power losses [97]. Martini presents a comprehensive study of some typical methods used in the analysis [98]. Inherent in this method is the requirement for engine component specification, implying either access to a fully described engine or a complete ground-upwards design process. A wealth of analyses exist that offer design schemes for components such as heat exchangers, regenerators, seals, pistons, displacers and all associated components. Readers are referred to [92, 99, 100, 101, 102, 103] for more detailed descriptions.

The methods apply equally to the use of the Stirling in heat pumping situations. For instance, Domingo details a solution method for a second order method applied to Stirling heat pumps [104].

2.5.3 Finite Time Thermodynamics Modelling of the Stirling Cycle

Other methods exist for analysing the Stirling cycle engine. FTT has proven particularly useful in the analysis of the cycle and its real-world limitations. Although analyses based on the ideal cycle have typically been considered as zero order methods [57], the imposition of the finite dimension constraints

within the model can have significant effects with regard to creating realistic simulations of the engine operation, such that delineation as a zero order method is not fully appropriate. For the current work, the FTT treatment of the cycle is considered separately to the traditional methods for this reason.

Petrescu et al [105, 106, 107] have applied the Direct Method for processes with finite speed to the Stirling cycle to account for the irreversibilities present in the non-ideal situation. Analysis centers on the endo-irreversible Stirling engine. Losses within the engine are quantified specifically in relation to the speed of the piston. The loss mechanisms are identified as those through friction, gas throttling in the regenerator and pressure drops within the gas circuit. Erbay and Yavuz [108, 109] provide analyses concerning the optimisation of the engine with respect to the power and power density of the system, as well as for the case of polytropic processes in the power and displacer volumes. Work by Feidt et al [101, 102] has focused on the dimensional optimisation of heat exchanger geometry. Other work by Feidt et al [110] developed a model based on the ideal cycle and a generalized form of the heat transfer law at the source and sink. Account is also taken of the effect of various irreversibility's in the system. Senft [111] provides an analysis of the Stirling engine to include heat transfer irreversibility in the heat exchangers as well as mechanical losses. Tlili et al [112] develop a model based on the ideal cycle but include for irreversibility in the engine and imperfect regeneration.

2.5.4 Modelling and Simulation of the Otto Cycle Engine

Unlike the Stirling cycle engine, the Otto cycle engine has benefitted from a protracted period of development since its first conception. However, similar to the Stirling cycle engine, a central facet to its incremental improvement has

been the requirement for powerful modelling and simulation tools to allow predictive analysis before costly manufacture or prototyping. Heywood's seminal work [28] remains the standard text for study of the ICE and provides insight into the different simulation methods available for engines of this type.

Similar to the techniques used for the Stirling cycle engine, the modelling methods used for the Otto cycle, and other ICEs, generally can be divided according to their relative complexity and the degree to which they describe actual processes inherent in the engine cycle under investigation. Although the text is by now somewhat dated, Heywood indicates the necessary theoretical division for study of such engines to be between *thermodynamic* models and those based on *fluid dynamic* principles. The distinction arises from the manner in which the general structure of the model is generated: through reliance on energy conservation or through full analysis of fluid motion.

Thermodynamic models of engine systems are generally limited to preliminary evaluation of upper performance limits and as such are typically described as zero-dimensional or quasi-dimensional, according to the level to which they incorporate (still simplified) geometric relationships and dependencies into the energy conservation equation. Recent examples of this work include [113] and [114].

Fluid dynamic modelling incorporates the study of the fluid behaviour through the engine cycle and necessarily includes solution of the mass, energy and momentum conservation equations for the particular engine geometry under investigation, up to and including modelling of complex flow phenomena encountered in the compressible flow regimes throughout the gas processes.

The term includes the quasi-steady, filling and emptying and gas dynamic models that are described in detail in the literature [28].

In practice, all of the above methods have been developed and included in a host of virtual engine simulation packages. The growth in computing power seen in the last decades has led to the current situation whereby virtual engine packages offer simulation capability on a par with real engine performance. They have therefore become an industry standard for research and development efforts. Examples include the Ricardo Wave platform and the Gamma Technologies GT Power platform. A body of in-house technical publications for both software suites are available at the company's websites [115, 116] and may be useful for appraising the capabilities of the virtual engine concept.

With such powerful and comparably inexpensive simulation capabilities available, the role of thermodynamic modelling has arguably been restricted to its original role as a preliminary design aid. This has not precipitated a decline in the activity level in the field though. In particular, developments in the field of FDOT modelling have allowed considerable advances in the accuracy of such preliminary simulations. An overview of these methods is given in the following section.

2.5.5 Finite Time Thermodynamics Modelling of the Otto Cycle

The Otto cycle is well represented in the literature of FTT. Angulo-Brown et al [117] provide an irreversible model that encompasses global friction losses within the cycle. The work is expanded in a subsequent work to include an irreversibility parameter within the cycle [118]. This work is the foundation for

a body of work. Calvo Hernandez et al [119] further develop this model to account for non-instantaneous adiabatic strokes. Ge et al [120] perform thermodynamic simulation of an Otto cycle with the inclusion of heat transfer in the system and variable specific heats of the working fluid. Chen et al [121] present information on the optimization of the Otto cycle with regard to maximum efficiency and maximum power. Curto-Risso et al [122, 123, 124] develop a finite time model that includes engine speed-related irreversibility parameters. The model is validated against numerical simulations and is demonstrated to offer good correlation.

2.5.6 Thermodynamic Modelling of Combined Cycle Engine Systems

Combined cycle power generation systems are an established method for increasing primary generation efficiency. Combined cycle gas turbines were first installed in the United States in 1949 [18]. Since then a wealth of different systems have been developed and installed, almost exclusively for large scale centralised generation systems. Such a coupling offers significant increases in total plant efficiency. Maximum net efficiency of such systems can reach 60% [125, 126]. Typical single cycle power plant generally operate at efficiencies under 40%.

Traditionally limited to large scale turbine plant, combined cycle systems involving reciprocating engines such as Otto cycle or Diesel cycle engines are less common but exist. Review of the literature reveals a number of patents and other publications concerning waste heat recovery from the exhaust system of Otto engines for the express purpose of additional mechanical power generation. This is done using a Rankine cycle turbine [127, 128], or in other cases a Stirling cycle engine [129, 130, 131]. Similar systems for Diesel cycle

engines also appear [132]. Otto cycle engines are routinely used as prime movers for small scale (< 5 MW) power systems such as light industrial cogeneration systems and stand-by power generation. Electrical power efficiencies for such systems generally increase with rated output, with the largest units typically capable of efficiencies above 40%.

Current thinking favours development towards DG networks in an effort to increase energy efficiency for both environmental and security reasons [75, 133, 134, 135, 136]. Although typically associated with large scale centralised power generation, there is an increasing interest in small-scale combined cycle systems involving reciprocating engines such as gas fired Otto cycle and Diesel cycle engines. These engines traditionally dominate this smaller scale (< 4MW) power systems market as CHP generators, renewable gas prime movers and standby generators [69]. Some recent work has focused on use of the Rankine cycle as a heat recovery device on a reciprocating ICE. Gambarotta and Vaja [137] investigated the organic Rankine cycle (ORC) as a bottoming cycle on an Otto cycle SI engine. Badami et al [128] investigated the standard Rankine cycle bottoming an Otto cycle for use as a CHP generator. Endo et al [138] have investigated the exergy gains possible from utilising a Rankine cycle as a bottoming cycle on an automotive ICE. Similar work has been conducted by Chammas and Clodic [139].

Use of the Stirling cycle as a bottoming cycle has been studied also by several different parties, as is evidenced by a number of international patents from leading automotive manufacturers [130, 132, 140, 131]. Use of the Stirling cycle as a bottoming cycle is of interest due to the high theoretical output and

efficiency that could be attained, in addition to potentially smaller plant footprint and quiet operation.

2.6 Conclusions

A literature review is presented in which the current status of the Otto cycle industrial engine and the Stirling cycle engine is described. The operating principles are discussed along with some of the technological issues affecting the practical realisation of the thermodynamic cycles.

The modern industrial engine is seen to be the subject of much research and development in all areas, particularly those aimed at increasing the brake-thermal-efficiency of the unit. The benefits to operators of non-combined-generation DG plants are readily appreciable—any increase in brake thermal efficiency, i.e. that proportion of the energy available in the fuel that is ultimately converted to mechanical shaft power, yields lower fuel costs to the operator as well as a reduction in the plant size for a given output. The special case of CHP generation generation is slightly different, as the successful application of the plant is highly sensitive to its matching to its energy sinks. The importance of areas of research such as piston design, valve timing and supercharging to the efficient operation of the engine is also examined.

The concept of DG is assessed briefly as a generation capacity mode. DG is seen to have inherent advantages over the traditional centralised generation structure that is the paradigm for modern electrical generation networks. The primary advantage is the reduction in transmission and distribution losses that arise in centralised generation systems due to long-distance power transmission through inefficient power lines and substations. The special case

of CHP generation is afforded separate treatment; the importance of the electrical/thermal production ratio of the plant is introduced, and the suitability of demand sites such as hospitals, office spaces and hotels are summarily assessed. The importance of the building energy demand profiles is illustrated and their role in correct simulation and implementation of combined generators is described. The possibility is introduced that a CHP prime mover, based on a combined cycle such as that proposed in the present work, might allow CHP to access markets that traditionally were not feasible due to the demand ratio of the site being unfavourably biased towards electrical demand. The combined cycle system may allow the 'tipping' of the production balance of the generator in favour of electrical power, thereby making it an option for such sites.

Finally, the thermodynamic modelling and simulation methods that are used in the analysis of the two thermodynamic cycles concerned are detailed. The traditional modelling steps are given in each case. For the Stirling cycle engine these are the zero, first and second order methods. For the Otto cycle engine these are methods such as the zero-dimensional thermodynamic models as well as the filling and emptying models and the complete gas dynamic models. The role of virtual engine simulation software in the development of the modern ICE is discussed also, with some of the current market competitors mentioned.

The concept of FTT is presented and a survey of the most relevant publications on the subject provided. Both the Stirling cycle engine and the Otto cycle engine are prominent in the literature of FTT and a brief review of the key publications concerning each is given. FTT is the study of thermodynamic systems under the constraint of finite heat transfer time and, consequently, finite heat transfer inventory. It therefore is a powerful tool for the study and optimisation of

thermodynamic systems and has been applied in various instances to the study of a variety of thermodynamic cycles and systems. In the next chapter, an FTT model of the Otto cycle engine is developed.

3 DEVELOPMENT OF A FINITE TIME THERMODYNAMICS MODEL OF THE OTTO CYCLE ENGINE

3.1 Introduction

The Otto cycle model proposed in the current study is based in the FTT model developed recently by Curto-Rizzo et al [122, 123, 124, 141]. This model is perceived to have an advantage over other models in its inclusion of a greater number of system variables, particularly relating to system geometry. The model adheres to a typical form of the irreversible thermodynamics analysis method, which involves the specification of the reversible thermodynamic work of the cycle and its subsequent degradation through irreversibility mechanisms.

3.2 The Otto Cycle Model

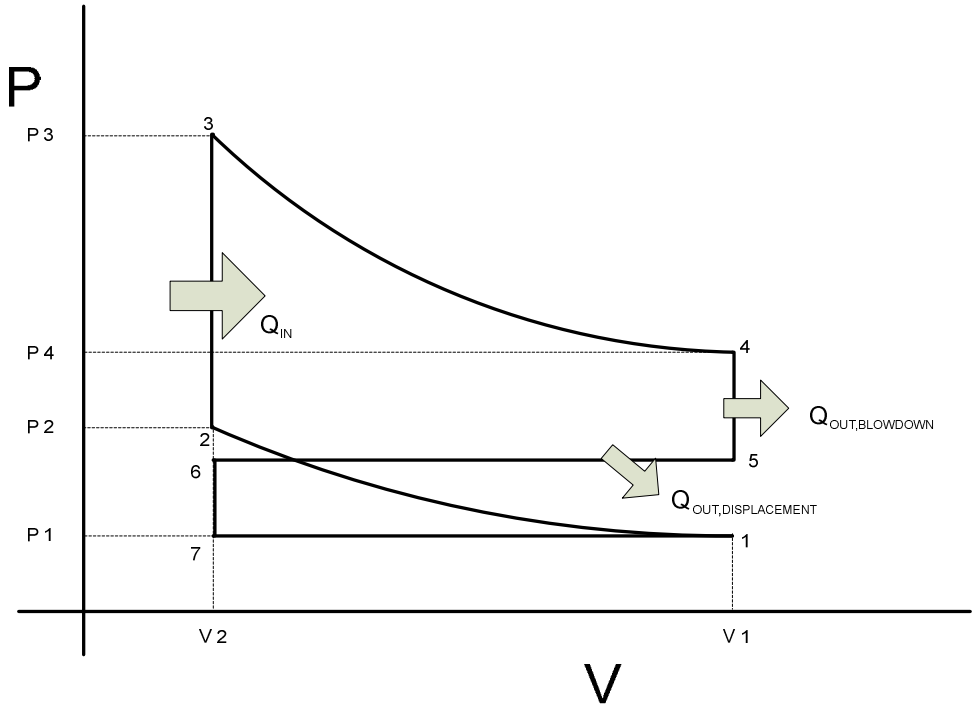

Figure 3.1 The ideal Otto cycle with intake and exhaust strokes

3.2.1 Outline of the Theoretical Model

For the Otto cycle, Figure 3.1, the reversible power of the cycle is:

$$P_{\text{rev}} = \frac{m}{t_{\text{th}}}\left[c_{v,23}(T_3 - T_2) - c_{v,41}(T_4 - T_1)\right] \tag{3-1}$$

where m is the cycle mass, t_{th} is the thermodynamic cycle period, $c_{v,23}$ is the averaged specific heat capacity at constant volume for the isochoric heat addition process, $c_{v,41}$ is the averaged specific heat capacity at constant volume for the isochoric heat rejection process and T represents the temperature at each cycle point. In comparison, the irreversible cycle power is calculated as [122]:

$$P_{\text{irrev}} = \frac{W_{\text{I}}}{t_{\text{th}}} - \frac{W_{\text{Q}}}{t_{\text{th}}} - P_{\mu} \tag{3-2}$$

where W_{I} is the work output of the thermodynamic cycle after accounting for irreversibilities within the cycle, W_{Q} is the work loss due to heat transfer from the cycle to the cylinder walls and P_{μ} is the cycle power lost through global frictional effects. It is important in the present analysis to differentiate between the thermodynamic cycle period and the mechanical cycle period. The full thermodynamic cycle requires two full revolutions of the crank shaft and therefore is equal to twice the mechanical cycle period. Also, the work terms all relate to one individual cylinder, and must therefore be multiplied by the number of cylinders to determine the total power output of the engine. This offers the benefit of allowing a scalable analysis of the engine. Calculation of the terms is as follows:

$$W_{\text{I}} = m\left[c_{v,23}(T_3 - T_2) - I_{\text{R}}c_{v,41}(T_4 - T_1)\right] \tag{3-3}$$

The irreversibility parameter, I_{R}, is a dimensionless parameter used to account for all irreversibilities generated within the system due to gas processes such as

gas throttling, pumping frictional losses, imperfect combustion etc. Estimates of the value or I_R are available in the literature. Curto-Risso et al indicate that a value of $I_R = 1.4$ is a good starting approximation [122]; however, it will vary with different engines and different operating regimes. It is possible, with knowledge of the actual brake power output of the engine to calculate the value of I_{R} at each operating point. This can be done by rearranging Equation (3-2) and substituting Equation (3-3) into it to give:

$$I_{\mathrm{R}} = \frac{1}{c_{v,41}(T_4 - T_1)}\left\{c_{v,23}(T_3 - T_2) - \frac{t_{\mathrm{th}}}{m}\left(P_{\mathrm{irrev}} + \frac{W_Q}{t_{\mathrm{th}}} + P_{\mu}\right)\right\} \tag{3-4}$$

Therefore, if the actual power output of the engine is known, it can be used as P_{irrev} in the above equation and the corresponding value of I_{R} calculated. As will be seen in the following chapter, for a full range of engine operating frequencies, P_{irrev} can be specified as a fitted polynomial expression, and the full range of I_{R} values calculated.

To calculate the maximum in-cylinder temperature after combustion within the cycle, T_3, Curto-Risso et al and previous sources [142] utilized the internal energy values of reactants and products of the chemical reaction during combustion of the fuel for calculating the combustion temperature T_3. In this thesis we use the simpler heat equation method with calculation of cycle temperatures from the isentropic compression and expansion relationships:

$$T_2 = T_1 r_{\mathrm{v}}^{\gamma - 1} \tag{3-4}$$

$$T_3 = \frac{Q_{23}}{m c_{\mathrm{v},23}} + T_2 \tag{3-5}$$

where r_{v} is the cycle compression ratio, γ is the ratio of specific heat capacities and Q_{23} is the heat added to the cycle during the isochoric heating process. The temperature at the end of the power stroke, T_4, is important for analysis of the

exhaust process. The method for this is elaborated later. To calculate the specific heat terms we assume air as the working fluid, thereby allowing us to use the polynomial offered by Abu-Nada et al [143] for the temperature-dependant specific heat at constant pressure of the working fluid:

$$\begin{aligned} c_p = {} & 2.506 \times 10^{-11} T^2 + 1.454 \times 10^{-7} T^{1.5} \\ & -4.246 \times 10^{-7} T + 3.162 \times 10^{-5} T^{0.5} + 1.3303 \\ & -1.512 \times 10^{4} T^{-1.5} + 3.063 \times 10^{5} T^{-2} \\ & -2.212 \times 10^{7} T^{-3} \end{aligned} \tag{3-6}$$

The specific heat at constant volume is:

$$c_{\mathrm{v}} = c_{\mathrm{p}} - R_{\mathrm{g}} \tag{3-7}$$

where R_{g} is the specific gas constant of the working fluid, approximated as air in this case. The averaged constant-volume specific heat terms for the heat addition and rejection processes are determined as:

$$c_{\mathrm{v},23} = \frac{1}{2}[c_{\mathrm{v}}(T_2) + c_{\mathrm{v}}(T_3)] \tag{3-8}$$

$$c_{\mathrm{v},41} = \frac{1}{2}[c_{\mathrm{v}}(T_4) + c_{\mathrm{v}}(T_1)] \tag{3-9}$$

However, as $c_{\mathrm{v},23}$ is required to calculate T_3, $\mathrm{c_v}(T_2)$ is used as an approximation in Equation (3-2) and Equation (3-5).

The heat-loss work is determined from the relationship:

$$W_{\mathrm{Q}} = \frac{\pi \varepsilon h B t_{th} T_3}{16} \left[B + \frac{V_0}{A_{\mathrm{p}}} (1 + r_{\mathrm{v}}) \right] \left[1 + {r_{\mathrm{v}}}^{1-\gamma} - 2 \frac{T_{\mathrm{w}}}{T_3} \right] \tag{3-10}$$

where ε is a phenomenological constant, h is the averaged convective heat transfer coefficient, B is the cylinder bore, A_{p} is the piston face area, V_0 is the clearance volume in the cylinder and T_{w} is the locally averaged cylinder wall temperature. The heat loss from the system through the cylinder walls is

assumed to occur exclusively in the power stroke, and is determined from Equation (3-11) [122]:

$$\bar{Q}_{\mathrm{L}} = \frac{W_{\mathrm{Q}}}{\varepsilon} = \pi h B \left[\frac{B}{2} + \bar{x}_{34}\right][\bar{T}_{34} - T_{\mathrm{w}}]t_{34} \tag{3-11}$$

where $\bar{\mathrm{x}}_{34}$ is a mean piston position term given by:

$$\bar{x}_{34} = 0.5(S) + x_0 \tag{3-12}$$

S is the piston stroke, $\bar{T}_{34}$ is the average temperature of the gas in the power stroke and t_{34} is the duration of the power stroke. The temperature at the end of the power stroke, and therefore immediately before the exhaust stroke, T_4, requires knowledge of the heat transfer from the cylinder on the power stroke. If we assume the mean temperature $\bar{T}_{34}$ to be:

$$\bar{T}_{34} = \left(\frac{T_3 + T_4}{2}\right) \tag{3-13}$$

Then, by substituting Equation (3-10) and Equation (3-13) into Equation (3-11), we can eliminate ε and, by rearranging the expression, determine T_4 as:

$$T_4 = \frac{\frac{T_3 t_{th}}{8}\left[B + \frac{V_0}{A_{\mathrm{p}}}(1 + r_{\mathrm{v}})\right]\left[1 + {r_{\mathrm{v}}}^{1-\gamma} - 2\frac{T_{\mathrm{w}}}{T_3}\right]}{\left[\frac{B}{2} + \bar{x}_{34}\right] t_{34}} + 2T_{\mathrm{w}} - T_3 \tag{3-14}$$

The friction loss power term is calculated as per the usual method in FTT [85]:

$$P_{\mu} = \mu \bar{v}^2 \tag{3-15}$$

where the friction coefficient μ is calculated as:

$$\mu = \frac{2W_{\mathrm{f}} t_{\mathrm{th}}}{\pi^2 S^2} \tag{3-16}$$

and W_{f} is the friction work loss. Mozurkewich and Berry [144] indicate that for an Otto cycle type engine $W_{\mathrm{f}} = 0.15\, W_{\mathrm{rev}} = 0.15\, P_{\mathrm{rev}} t_{\mathrm{th}}$. The mean piston velocity $\bar{v}$ is calculated as:

$$\bar{v} = 2Sf \tag{3-17}$$

The power output of the engine is therefore calculated from Equation (3-2) and the efficiency of the engine is therefore:

$$\eta_{\text{otto}} = \frac{P_{\text{irrev}}}{Q_{23}} \tag{3-18}$$

where the heat added per cylinder is:

$$Q_{23} = \frac{m}{t_{\text{th}}} c_{\text{v},23}(T_3 - T_2) \tag{3-19}$$

In the current analysis though, the heat addition to the cycle is usually an imposed parameter made available from manufacturer specifications through a fuel consumption parameter, expressed as kW or otherwise. This may be considered typical for stationary engines such as those used for CHP generation. Unit efficiency is paramount, translating directly to cost savings for the operator. Therefore either the efficiency of the unit or the fuel consumption, or both, is made available for engineers considering the systems.

3.2.2 Analytical Study of Exhaust Heat

The sensible thermal energy available in the exhaust stream of the Otto cycle engine can be calculated as the heat remaining after combustion once heat transfer losses to the cylinder wall have been accounted for. This necessitates an accurate evaluation of the mass of combustion products as well as the temperature. Continuing on the assumption of air as the working fluid, we can approximate the specific heat of the fluid as that of air at the appropriate temperature. The exhaust process can be approximated as a constant volume blowdown process, process 4–5 in Figure 3.1, followed by a constant pressure cylinder evacuation process completed by the displacement of the piston, process 5–6 in Figure 3.1. We can estimate the quantity of heat remaining in the spent charge gases after the power stroke using a first law balance of the

system. The exhaust thermal power can be considered as the difference between the heat added to the cycle and the sum of the brake work and the heat loss in the cylinder computed previously in Equation (3-2) and Equation (3-11):

$$\dot{Q}_{\text{ex}} = \dot{Q}_{23} - \left(P_{\text{irrev}} + \bar{\dot{Q}}_{\text{L}}\right) \tag{3-20}$$

It is necessary to compute the exhaust gas temperature during the gas displacement process. Equation (3-14) yields a value for T_4, the temperature of the gas at the end of the of the power stroke. Upon opening of the exhaust port valve, a blowdown process occurs as the gas pressure within the cylinder attempts to equalize with the surroundings. This process occurs immediately prior to the displacement of the gas by movement of the piston and causes a sudden cooling of the gas within the cylinder. The peak temperature during the blowdown process is understood to be T_4. In order to estimate the temperature of the gas remaining in the cylinder at the end of the blowdown process, we use an approximation for the mass of gas leaving the cylinder during the blowdown process. If we assume that the process happens sufficiently fast so as to be adiabatic, we can therefore posit that the energy leaving the cylinder during this time is limited to the enthalpy transported from the system with the mass flow of the gas. The mass flow at the blowdown step is assumed to be choked, and can therefore be calculated from Equation (3-21) [28]:

$$\dot{m}_{\text{bd}} = \frac{n_{\text{v}} C_{\text{D}} A_{\text{T}} p_0}{\sqrt{R_{\text{g}} T_0}} \gamma^{0.5} \left(\frac{2}{\gamma + 1}\right)^{\frac{\gamma+1}{2(\gamma-1)}} \tag{3-21}$$

where n_{v} is the number of valves, C_{D} is the discharge coefficient, A_{T} is the throat area, p_0 is the stagnation pressure and T_0 is the stagnation temperature. Selection of C_{D} and A_{T} is detailed in [28]. Once we estimate the blowdown

period, t_{bd}, the mass remaining in the cycle to be displaced by the piston motion is:

$$m_{\mathrm{disp}} = m - \dot{m}_{\mathrm{bd}} t_{\mathrm{bd}} \tag{3-22}$$

The blowdown period, t_{bd}, is estimated from data provided in the literature, for example [28, 144]. Stas suggests that exhaust blowdown usually takes approximately 40°–60° of crank angle to complete. This equates to approximately 7% of the total cycle duration. The proportion of energy rejected from the cycle during the blowdown process and that of the remaining energy within the cylinder can be represented simply as the ratios of the mass expelled during blowdown and that remaining in the cylinder respectively, to the total mass in the cycle:

$$R_{\mathrm{mass,bd}} = \frac{\dot{m}_{\mathrm{bd}} t_{\mathrm{bd}}}{m} \tag{3-23}$$

$$R_{\mathrm{mass,cyl}} = \frac{m_{\mathrm{disp}}}{m} \tag{3-24}$$

It is then possible to compute an estimate of the temperature of the remaining gas within the cylinder through the relationship:

$$T_5 = T_4 - \left(\frac{R_{\mathrm{mass,cyl}} Q_{\mathrm{ex}} t_{\mathrm{th}}}{m_{\mathrm{disp}} c_{p,\mathrm{ex}}} \right) \tag{3-25}$$

$c_{p,\mathrm{ex}}$ can be estimated as an average using the relationship in Equations (3-8) and (3-9) for temperatures T_4 and T_5. The total cycle mass, m, is used to calculate the temperature in this case as the full cycle mass is under consideration during the blowdown phase, not just that proportion that evacuates the cylinder.

In order to calculate the average value of the exhaust flow temperature it is necessary to consider an enthalpy averaged relationship as suggested by Heywood [28]. This is more favorable than using a time averaged value as it accounts for the thermal capacity of the mass flow in the different zones of flow—exhaust blowdown and piston-displacement gas expulsion. As we are considering the system immediately after blowdown, on the piston displacement stroke, we consider the system as operating at constant pressure. The total enthalpy of the gas after blowdown therefore is:

$$H_{\text{total}} = \dot{m}_{\text{bd}} t_{\text{bd}} c_p(T_4) T_4 + m_{\text{disp}} c_p(T_5) T_5 \tag{3-26}$$

and therefore the temperature corresponding to this enthalpy is:

$$T_{\text{ex,avg}} = \frac{2H_{\text{total}}}{m\left[c_p(T_4) + c_{\text{p}}(T_5)\right]} \tag{3-27}$$

Equation (3-27) provides an expression for the enthalpy averaged exhaust gas temperature of the Otto cycle engine immediately on exit from the cylinder.

3.3 Conclusions

This chapter has presented an FTT model for the Otto cycle engine. The model is based on an existing model available in the literature; however, it is expanded to include a quantification of the exhaust gas sensible thermal energy and the enthalpy-averaged exhaust gas temperature. A validation procedure for the model presented above is provided in the following chapter.

4 VERIFICATION OF THE OTTO CYCLE FINITE TIME THERMODYNAMICS MODEL

4.1 Introduction

In this chapter the FTT model developed in Chapter 3 is verified against data from a commercial virtual-engine simulation software package, Ricardo Wave. The effectiveness of the FTT modelling method for prediction of basic performance parameters such as brake power and brake thermal efficiency as well as the ability of the model to accurately predict cycle performance parameters such as peak in-cylinder temperature and exhaust port temperature is assessed.

4.2 Methodology

The methodology adopted for the verification comprises the modelling of a 4-cylinder, naturally aspirated, SI petrol (gasoline) fired Otto cycle engine using the FTT model described previously. This engine is taken from the suite of sample engines available from the Ricardo Wave support files. The engine is then simulated in the Ricardo Wave environment and the two models compared for similarity afterwards. The performance of the FTT model against the simulation is measured using a root mean squared (RMS) percentage difference calculation. The results of the percentage difference assessment are plotted and presented in the results section with the performance plots.

The criteria for comparison of the model and simulation include brake power, brake efficiency, exhaust heat, convective heat loss to engine coolant, inducted

mass, cycle temperatures, exhaust port temperature and energy balance over the full operating speed range.

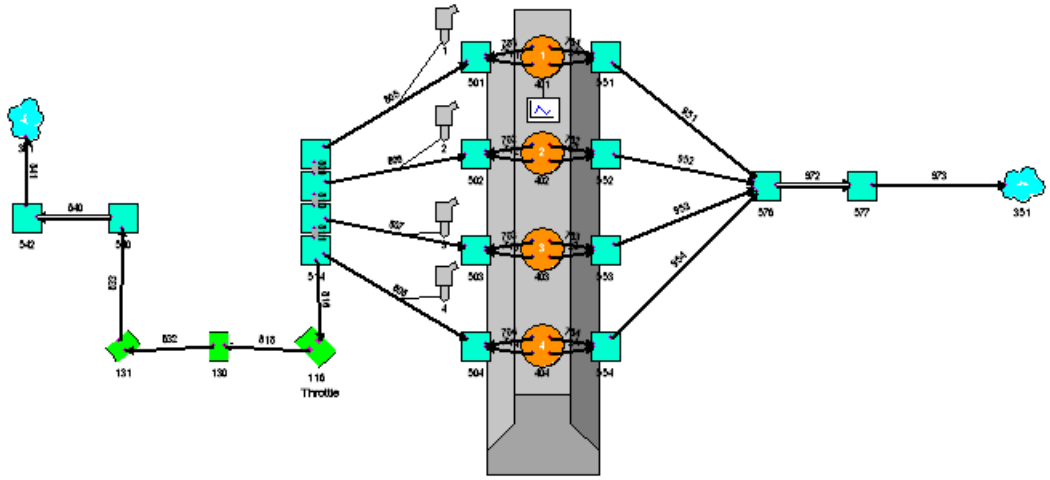

Figure 4.1 Ricardo Wave 4-cylinder naturally aspirated gasoline engine simulation model

4.3 The Simulated Otto Engine—Specifications

The engine under investigation is a 4-cylinder, naturally aspirated, SI, petrol (gasoline) fired Otto cycle engine. The system specifications are available as a sample engine from the Ricardo Wave support files. A schematic of the system in the Ricardo Wave environment is shown in Figure 4.1. The primary engine specifications are summarised in Table 4.1.

4.4 Thermodynamic Model—Specified Parameters

Aside from the geometric specifications of the engine, the inputs to the FTT model are:

- Operating frequency range (rpm)
- Heat input, $\dot{Q}_{\text{in}}$ (kW)

- Averaged in-cylinder heat transfer coefficient, h, $\left(\frac{\mathrm{W}}{\mathrm{m^2K}}\right)$
- Induced working mass flowrate through the engine, $\dot{m}$, $(\frac{\mathrm{kg}}{s})$
- To help determine experimentally the value of the irreversibility parameter, I_{R}, a polynomial curve fit of the simulated brake power output, P_{brake} is used (kW)

Table 4.1 Otto test engine specifications

Specification	**Value**
Fuel	Gasoline
Strokes	4
Engine type	I4
Displacement	2.0 L
Injection system	PFI
Induction system	Naturally aspirated
Valves/cylinder	4
Bore	85.0 mm
Stroke	88.0 mm
Connecting rod length	150.0 mm
Compression ratio	9.0 mm
Intake valve max. lift	8.5 mm
Exhaust valve max. lift	7.5 mm
Intake valve diameter	31.0 mm
Exhaust valve diameter	27.0 mm
Intake duration	240° CA
Exhaust duration	232° CA
RPM range	1000 to 6000

Peak power	90 kW @ 5000 rpm
Peak torque	174 N*m @ 4500 rpm
BSFC at peak eff.	296 g/kW/h

As the full range of engine operating speeds is analysed, a corresponding range for each of the above inputs is required. To facilitate ease of execution, these parameters can be specified as fitted polynomials taken from the simulation data. The polynomials used in this analysis are detailed in the following section. The exception is the heat transfer coefficient. Sensitivity analysis performed during the programming of the model indicated that the output parameters are somewhat insensitive to this coefficient across the full operating speed range. It is therefore possible to proceed with a single, averaged value. This is detailed in following section also.

The heat input and the mass flowrate through the engine can be justified as imposed parameters as they are routinely available from engine specifications. As detailed in the previous chapter, it is common in the analysis of CHP–type industrial engines to be provided with an energy balance of the system, which would include heat input specified in kW. Heat input is calculated from the simulation data by determining the ratio of brake power output to brake thermal efficiency. The resulting data plot can be fitted with a polynomial and the corresponding equation used to specify the heat input in the analytical model. This method is limited however in that it effectively assumes perfect heat release from the fuel to the working system. It does not account for the chemical reactions and combustion mechanics inherent in the heat release process. Consequently factors affecting optimisation of the heat delivery to the

system, such as air-fuel ratio, spark advance etc are not included within the model.

4.5 Polynomial Expressions for Imposed Parameters

4.5.1 Experimental Brake Power Polynomial for Calculation of I_R Parameter

A method for calculating the value of I_R at each operating point within the cycle is presented in the previous chapter. It was suggested that with knowledge of the actual brake power performance of the engine, I_R could be calculated by using a rearrangement of the FTT expression for the irreversible power and by substituting in the value of the measured brake power. For the full range of operating frequencies of the engine, it is possible to specify the brake power as a fitted polynomial in terms of the operating speed. This is evident in Figure 4.2, in which the simulated engine brake power output is presented, along with the fitted polynomial curve.

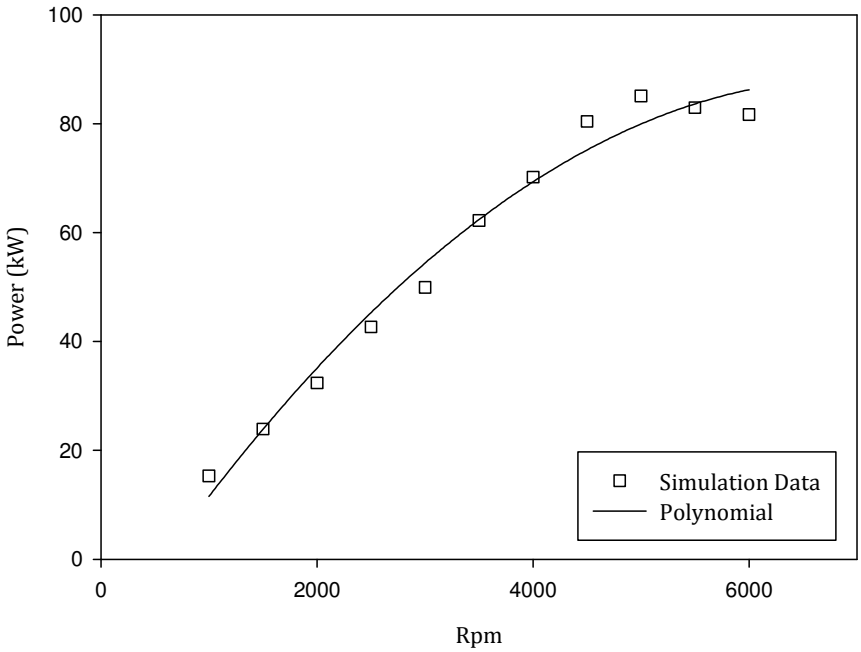

Figure 4.2 Simulated engine brake power output with fitted polynomial curve

The polynomial expression for this case is:

$$P_{b,exp} = [(-2 \times 10^{-6})N^2 + 0.0302N - 16.368] \times 10^3 \qquad (4\text{-}1)$$

where $P_{\mathrm{b,exp}}$ is the experimentally measured brake power in kW and N is the operating frequency of the engine in rpm. This expression can then be used in Equation (4-2) as the value of P_{irrev} and the real value of I_{R} calculated from this. The results of this are presented later in the present chapter.

4.5.2 Heat Input Polynomial Expression

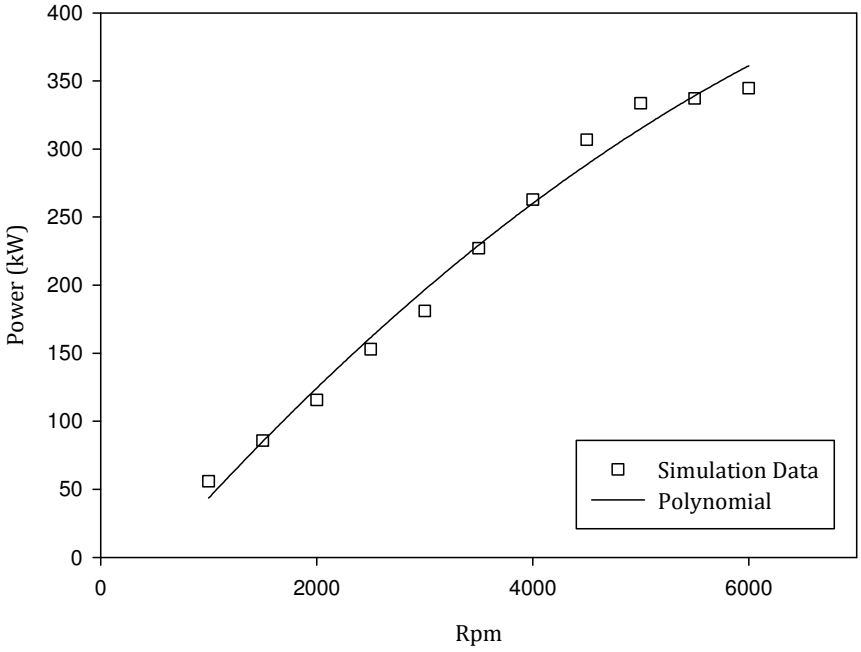

Figure 4.3 Simulated engine heat addition with fitted polynomial curve

The heat addition to the cycle is an imposed parameter also. In the case of a constant speed, steady state operational mode, the heat input can be simply specified as a single value from knowledge of the fuel consumption for the engine. Such data is routinely available, particularly for the industrial engines that are of interest to the present work. For the sake of completeness, it is desirable to analyse the performance of the FTT model over the full operational speed regime of the engine under investigation. This serves to test the fidelity of the model in the different operating states. To this end, the Ricardo Wave simulation was run for the specified engine and the heat input to the cycle calculated as the ratio of brake power output to brake thermal efficiency. The fitted polynomial for the heat input in this case is:

$$\dot{Q}_{IN} = \dot{Q}_{23} = [(-4 \times 10^{-6})N^2 + 0.0938N - 45.978] \times 10^3 \qquad (4\text{-}2)$$

In each of the above polynomials, the 10^3 term is used to convert from kW to W. This polynomial can then be used as an analytical input for the model to provide an expression for heat input over the whole operating speed range.

4.5.3 Engine Mass Flowrate Polynomial Expression

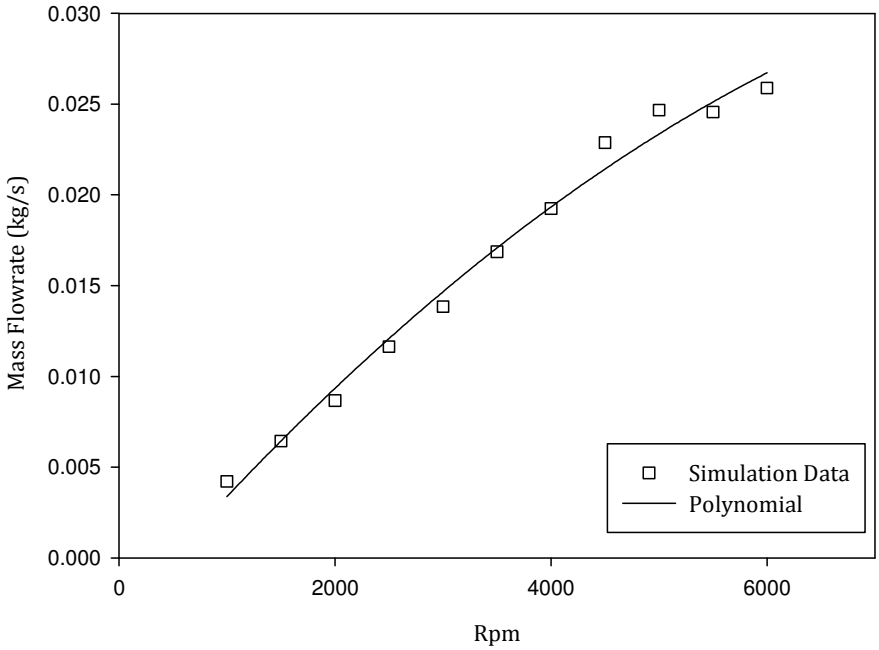

Figure 4.4 Simulated engine induced mass flowrate with fitted polynomial curve

A polynomial expression is also used to specify the inducted mass flowrate through the engine at each operating point. This is important, as frictional effects in the intake and exhaust systems as well as choking effects in the intake and exhaust-port valves have a restrictive effect on the mass entering the system. This effect becomes more pronounced at higher speeds. The net effect is a reduction in specific work, or BMEP at higher speed. This will be demonstrated in a later section. The fitted polynomial for the inducted mass flowrate through one cylinder is:

$$\dot{m} = (-3 \times 10^{-10})N^2 + (7 \times 10^{-6})N - 0.0032 \qquad (4\text{-}3)$$

The mass flowrate through a single cylinder is required. An assumption is made that in the 4-cylinder engine, two cylinders are aspirating at any one time; one inducing, one exhausting. These processes represent two of the four strokes of the practical cycle. The other two cylinders are assumed to be performing the other two processes from the cycle. Therefore, in the FTT model, the total instantaneous mass flowrate through the engine is twice the individual cylinder mass flowrate.

4.6 Results of Simulation

4.6.1 Pressure–Volume Indicator Diagram

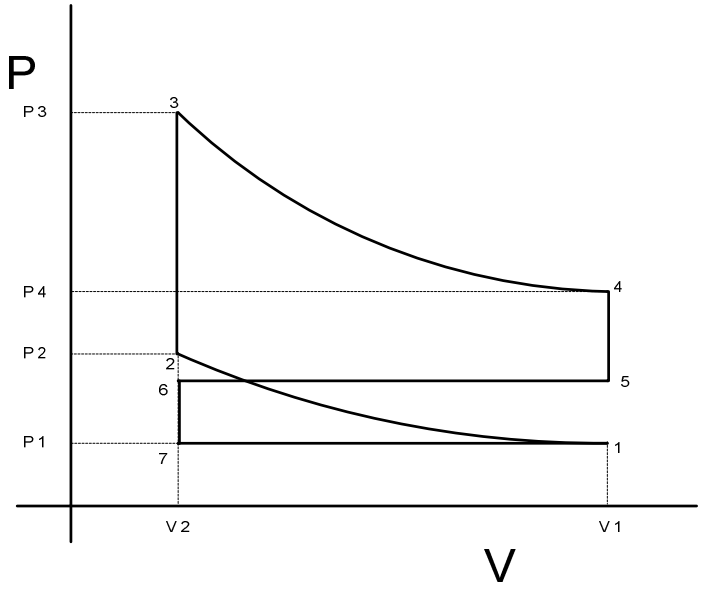

Figure 4.5 FTT model pressure–volume indicator diagram

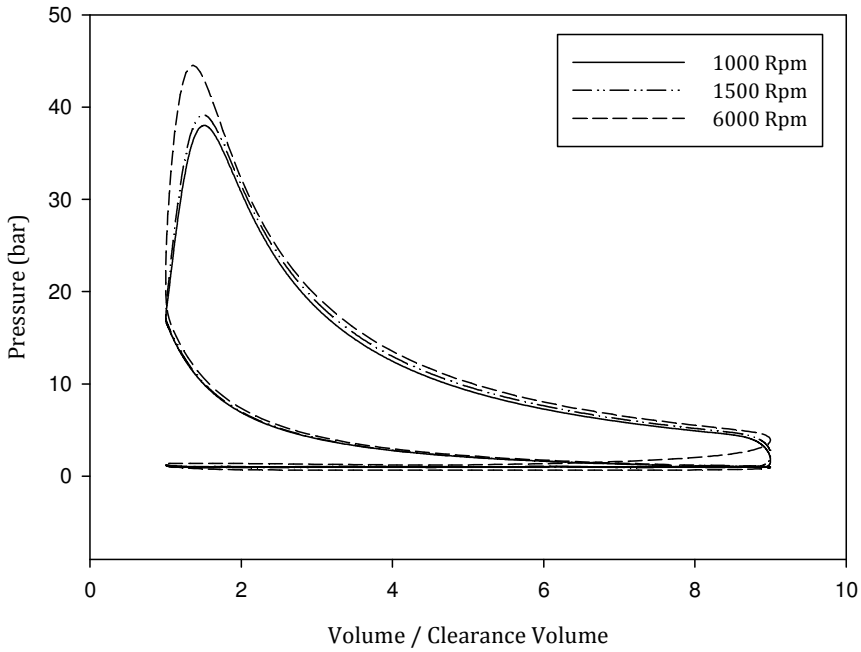

Figure 4.6 Simulated engine pressure–volume indicator diagram

Figure 4.5 shows the modified ideal air standard Otto cycle, on which the FTT model development is based. Figure 4.6 shows a *P*–*V* indicator diagram for the simulated Otto engine. This plot is retrieved from the Ricardo Wave post-processor analysis software. Three operating frequencies are represented; the maximum frequency, 6000 rpm; the minimum frequency, 1000 rpm; and an intermediary frequency, 1500 rpm. This frequency is of interest as it is typically used for industrial engines operating as decentralised power generators.

The plot is useful as it demonstrates the peak pressures reached in the cylinder. Also, the increasing cycle work with increasing operating frequency can be readily recognised. The FTT model does not include for in-cylinder plots such as that presented here, so that a direct comparison is not possible. However, the behaviour may be indirectly inferred from the operating temperatures that are calculated as part of the FTT model. These will be compared in later sections.

The *P–V* diagram presented in Figure 4.6 may also act as a qualitative aid for assessing the simulation performance.

4.6.2 In-Cylinder Heat Transfer Coefficient

The heat transfer coefficient is required for the FTT analysis of the Otto engine as it allows calculation of the convective heat transfer loss within the cycle and subsequently the heat transfer to the engine coolant. This is important for assessment of the overall energy balance of the engine. Figure 4.6 shows a plot of the in-cylinder heat transfer coefficient against engine crank angle taken from the engine simulation in the Wave software. It is evident from the plot that the heat transfer coefficient varies considerably over the full engine cycle as well as with operating frequency. This data is required to estimate the averaged heat transfer coefficient required in the FTT model.

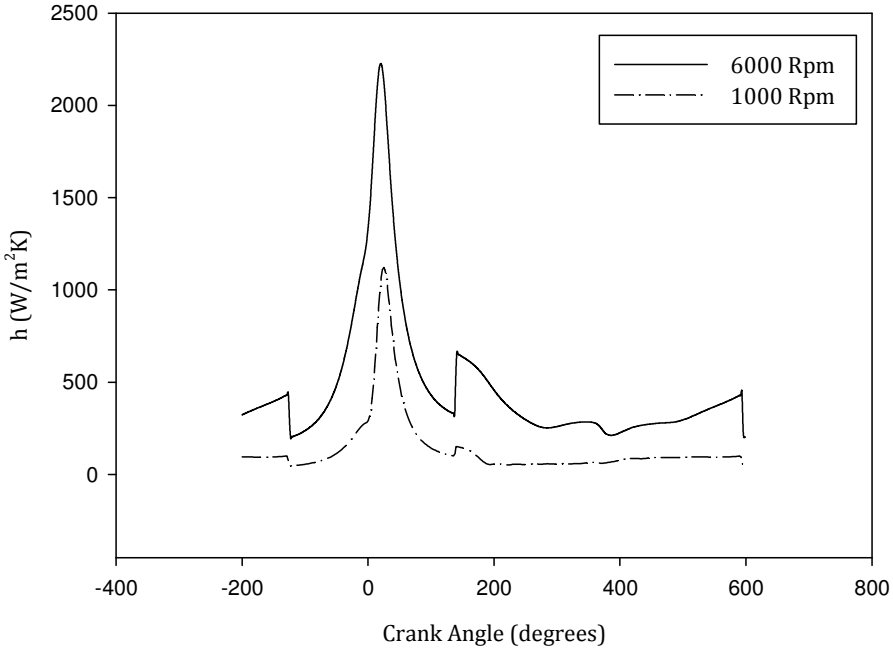

Figure 4.7 Simulated engine in-cylinder heat transfer coefficient vs. engine crank angle

The assumption made in the FTT model is that all heat transfer from the gas to the coolant by convective heat transfer is completed exclusively on the power stroke, 0° to 180° in the plot in Figure 4.7. This appears to be a justifiable assumption when considering Figure 4.7. It can be seen from the plot that for both operating frequencies analysed, there is a considerable peak in the value of the coefficient between these points, indicating that the majority of heat transfer occurs at this point. In order to estimate the averaged coefficient for use in the thermodynamic model, the values of h between these points are averaged. When this is done for the two frequencies presented above, the values are 330 W/m^2K and 882 W/m^2K for the cases of 1000 rpm and 6000 rpm respectively. These cases can be considered the extreme examples as they are the extreme operating frequencies of the engine. Actual operation will likely be within these limits.

Sensitivity analysis of the thermodynamic model to the heat transfer coefficient however indicates that the desired output performance parameters are only minimally affected by variation of the coefficient. It was therefore decided that for efficient analysis the intermediate value of 606 W/m^2K could be utilised with little loss in fidelity of the model.

4.6.3 Calculation of the Irreversibility Parameter, I_R

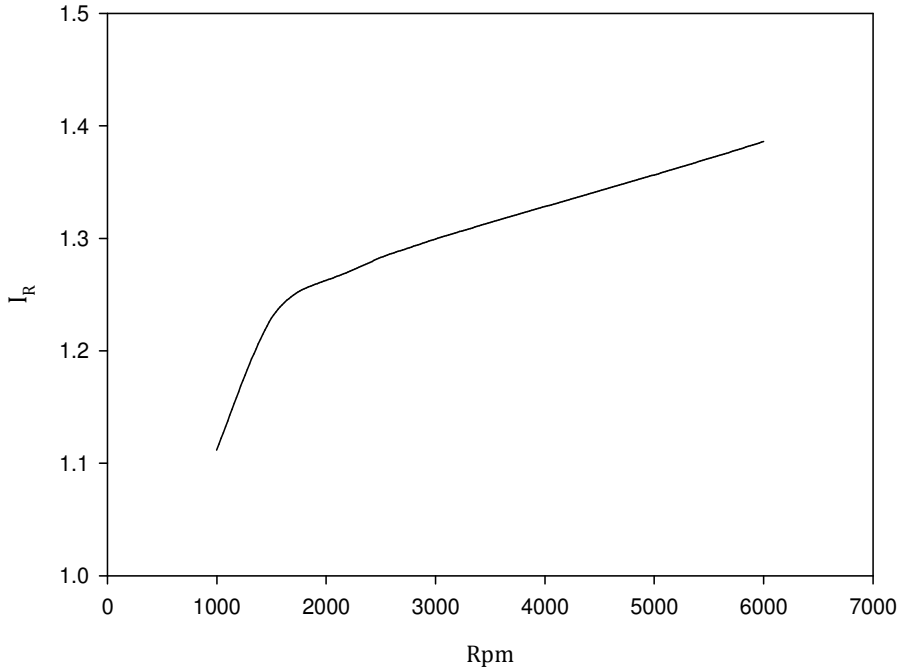

Figure 4.8 Irreversibility parameter, I_R, against engine rpm

The irreversibility parameter is presented against the engine rpm in Figure 4.8. It can be seen from the plot that the parameter exhibits a minimum at the lowest operating speed, approximately 1000 rpm, indicating that at this speed the internal irreversibilities in the gas processes of the engine are least pronounced. The parameter increases steadily after this value from a minimum of approximately 1.1 to an eventual maximum of approximately 1.39 at 6000 rpm.

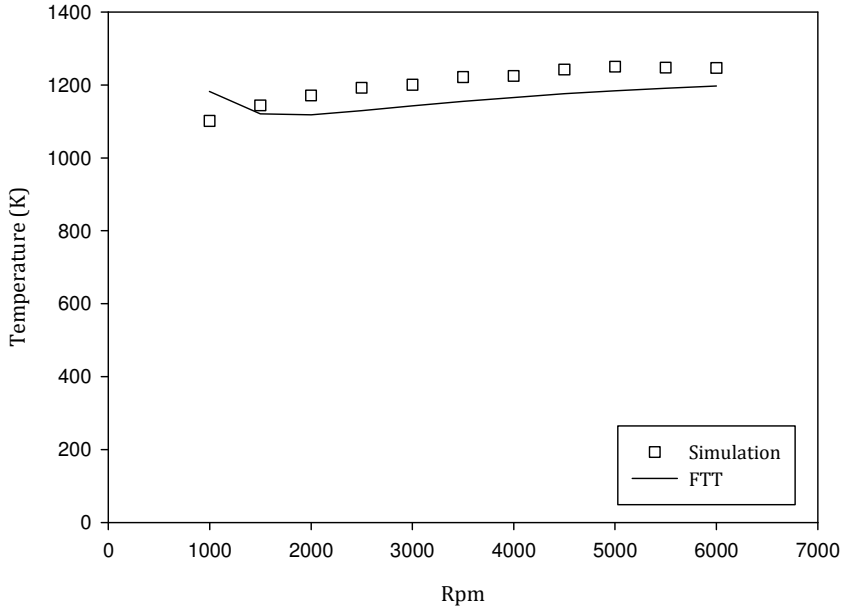

Figure 4.9 Engine exhaust gas temperature against engine rpm

4.6.4 Exhaust Temperature

Calculation of the exhaust gas temperature for the engine is of particular interest to the present study, as this will directly affect the analysis of the combined cycle system. The FTT model includes a simplified method for doing this by calculating the enthalpy averaged temperature for the working mass immediately after blowdown and immediately prior to displacement of remaining gas from the cylinder by the movement of the piston. The results of this are represented in Figure 4.9, along with the results of the temperature calculation done with the engine simulation in Ricardo Wave. It can be seen from the plot that the enthalpy averaged temperature used in the FTT model offers a good approximation to the actual values as given by the simulation results. A minor discrepancy is noticed at the lower extreme value of 1000 rpm, where the computed value is noticeably higher than the simulation value. An explanation for this can be inferred from Figure 4.10. The exhaust gas

temperature is computed as a ratio of the enthalpy of the exhaust gas to the total heat capacitance, as per Equation (3-27) . Figure 4.10 shows both these terms plotted against the engine operating speed. It can be seen from the plot that at the lowermost extreme, the heat capacitance term is below unity, implying that when used in the denominator the ratio will be caused to increase in magnitude. At 2000 rpm, the heat capacitance term is above unity, and the ratio is seen to drop below that calculated at the lower speed. The two curves are convex however, such that the ratio increases with increasing rpm, giving the overall trend seen in the exhaust temperature calculation in Figure 4.9.

4.6.5 Engine Working Mass

The working mass per cycle of the engine can be readily inferred from the polynomial expression for the mass flowrate through the engine. The mass per

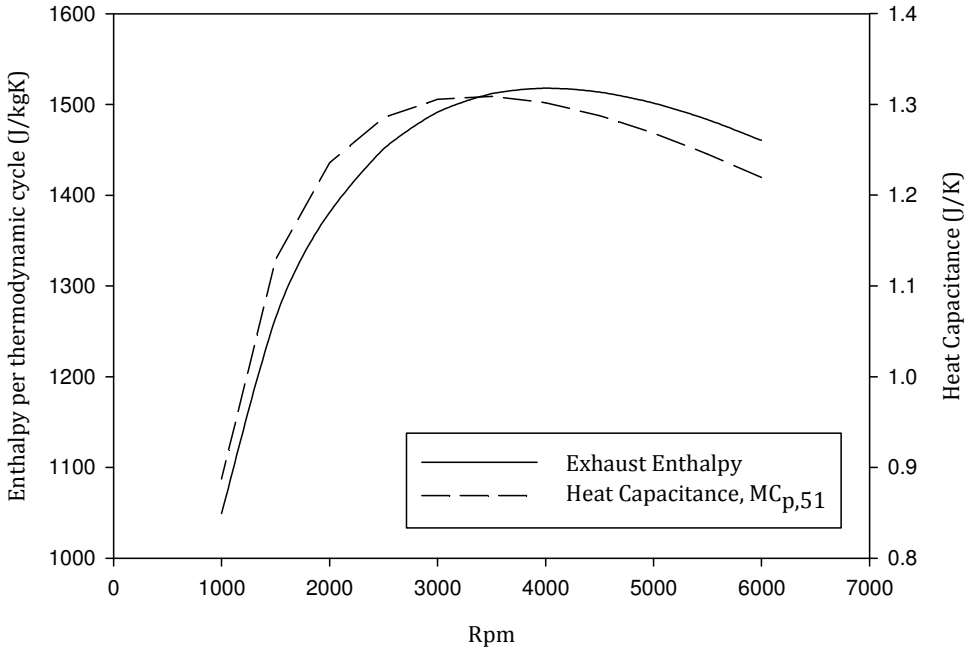

Figure 4.10 Engine exhaust gas enthalpy and heat capacitance against engine rpm

cylinder per operating cycle can be calculated using the expression:

$$m = \dot{m} t_{\text{th}} \tag{4-4}$$

where t_{th} is the thermodynamic cycle period. This expression has units of kg/cycle. In Figure 4.11, the resulting mass per cycle per operating cylinder is shown for each rpm operating point of the engine. Shown also is the blowdown mass, which is the quantity of the working mass which evacuates the cylinder on the blowdown phase of the exhaust stroke for each cycle, as well as the remaining mass, which is the mass left in the cylinder after blowdown has occurred. It can be seen that the quantity of mass exiting at blowdown reduces with increasing rpm. This may be due to an assumption made in the model that the crank angle duration for blowdown is constant through the full operating speed range; however, this is an assumption made merely to accommodate analysis. In actuality, the crank duration varies slightly with increasing operating frequency [28, 145]. What is notable is that this simplification appears to be justifiable, as the exhaust gas temperature detailed previously follows closely the magnitude and trend of the Ricardo Wave simulation results. This exhaust gas temperature calculation relies on the enthalpies of both the blowdown mass and that remaining in the cylinder. The simplified working mass trends displayed here therefore appear to be representative of the actual situation.

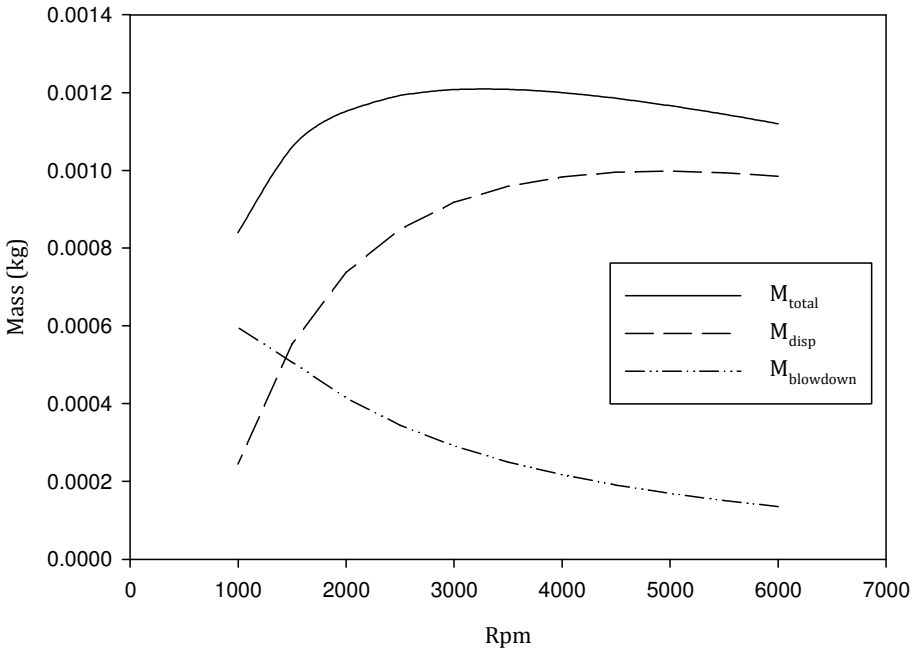

Figure 4.11 Engine cycle mass, blowdown mass and mass displaced by piston

4.6.6 Brake Cycle Work

As mentioned in Section 4.5.3, frictional effects in the engine intake and exhaust system as well as choking effects in the valves act to limit the mass inducted to the system, the effect becoming more pronounced at higher rpm. This is also readily visible in Figure 4.12. The effect of this reduction of working mass in the cycle is a drop in the specific work output of the engine; that is the work performed per individual thermodynamic cycle:

$$W_{\text{cycle}} = P_{\text{irrev}} t_{\text{th}} \tag{4-5}$$

An optimal point for the specific work output of the engine is presented clearly in Figure 4.12. In the figure, the theoretical specific work calculated using the above expression for both the FTT model and the simulation can be seen plotted against engine rpm. It is noticeable that the theoretical maximum point and the simulation maximum point are not coincident; the theoretical maximum occurs

approximately 2000 rpm earlier than that calculated for the simulation case. However, the existence of a maxima is clearly visible in each case. The disparity between the model and the simulation may be due to approximations made in the FTT scenario which ultimately led to the calculated brake power being slightly higher than the actual brake power for a brief period at low and medium rpm values. This in turn is visible in Figure 4.13 and Figure 4.14. Figure 4.13 shows the brake power output of the engine plotted against rpm. Figure 4.14 shows the brake efficiency for the engine against rpm. It can be seen from Figure 4.13 that the FTT model slightly over-predicts the engine brake power in the range 2000 rpm to 4000 rpm approximately. Similarly in Figure 4.14 the brake efficiency can be seen to be slightly higher over the full rpm range in the FTT model case, with the largest disparity being evident in the range 1,500 rpm to 2,500 rpm. These disparities appear to explain the cycle work maximum seen in Figure 4.12.

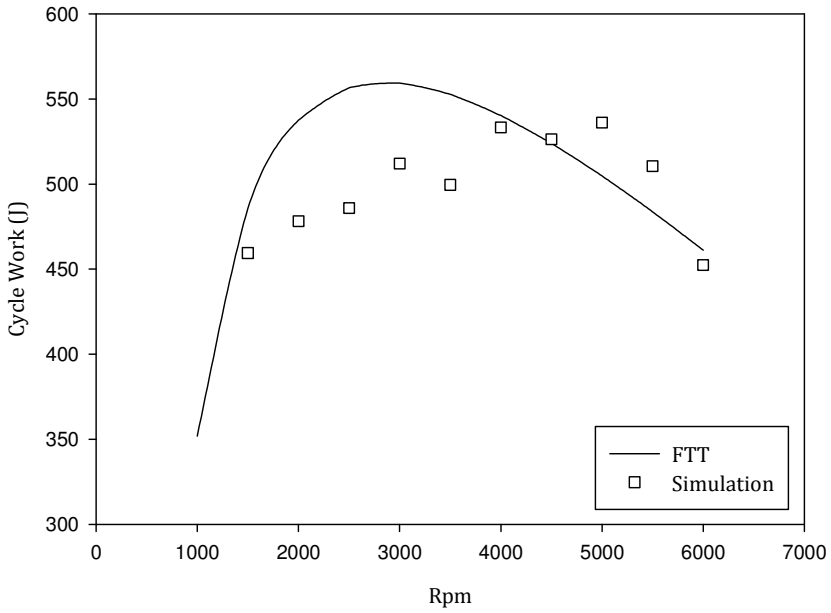

Figure 4.12 Engine cycle work against rpm

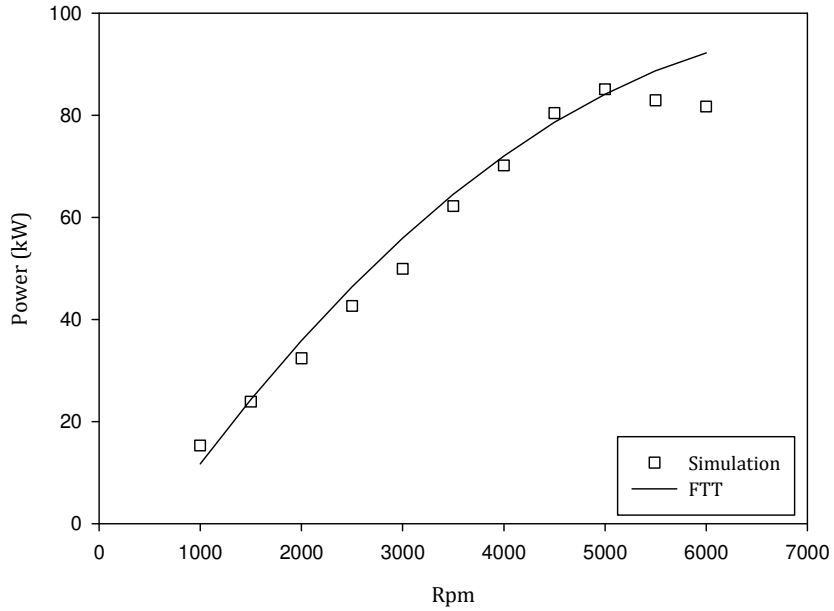

Figure 4.13 Engine brake power against rpm

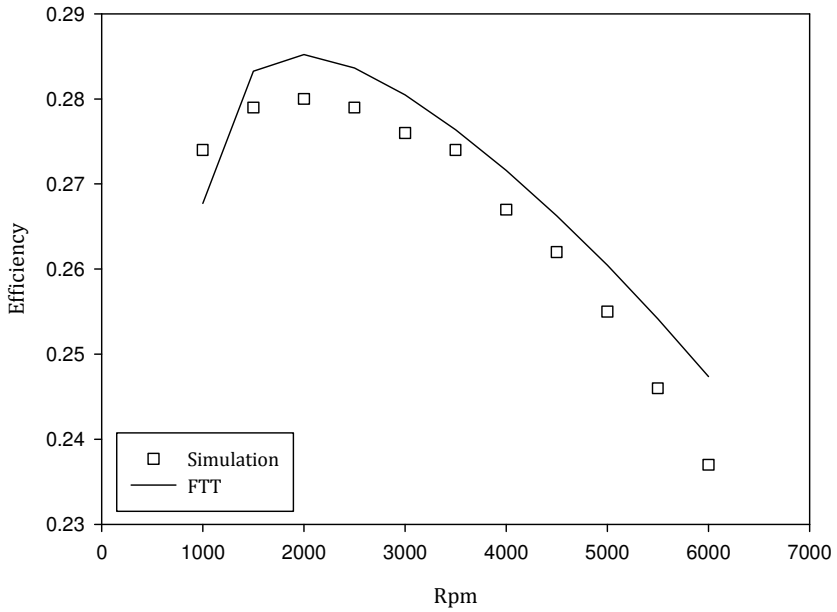

Figure 4.14 Engine brake efficiency against rpm

4.6.7 Cycle Temperatures

Central to the calculation of the exhaust gas temperature in the FTT model is the calculation of the cycle temperatures within the engine. Remembering that the FTT model utilises the air standard cycle as a reference point, cycle temperatures for the FTT model are easily delineated numerically in the appropriate sequence: 1–2–3–4–5. This can be seen in Figure 4.5. Temperatures within the actual engine—in this case the engine simulation—are less easily pinpointed. The actual engine utilises a continuous crank motion which necessarily eliminates clearly defined start and end points for the cycle processes. This in turn is evident from Figure 4.6. It is therefore more meaningful to analyse the cycle temperatures over the whole cycle. This is shown in Figure 4.15. The plot shows the spatially averaged, in-cylinder gas temperature as a function of the crank angle.

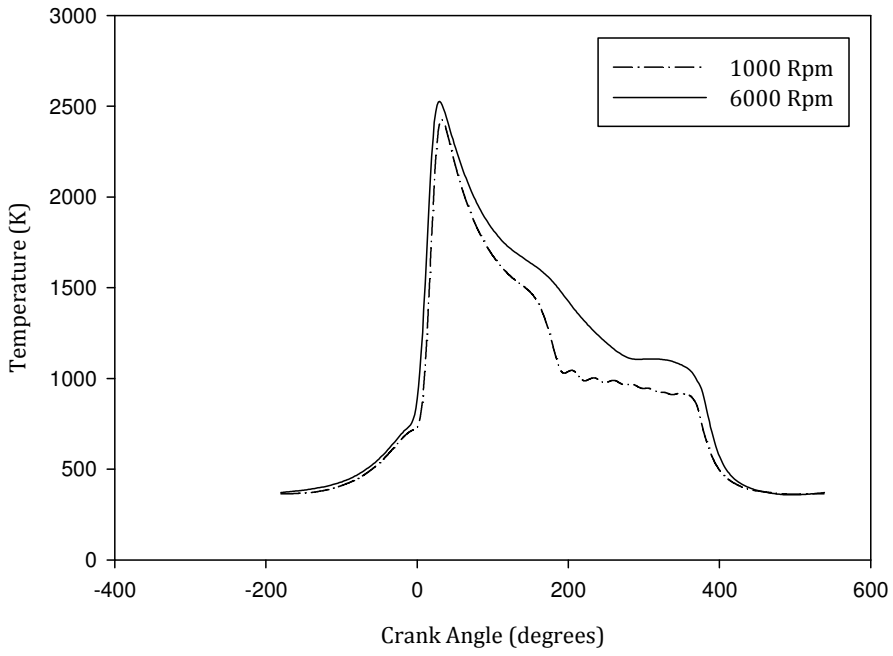

Figure 4.15 Engine simulation—cycle temperature against crank angle

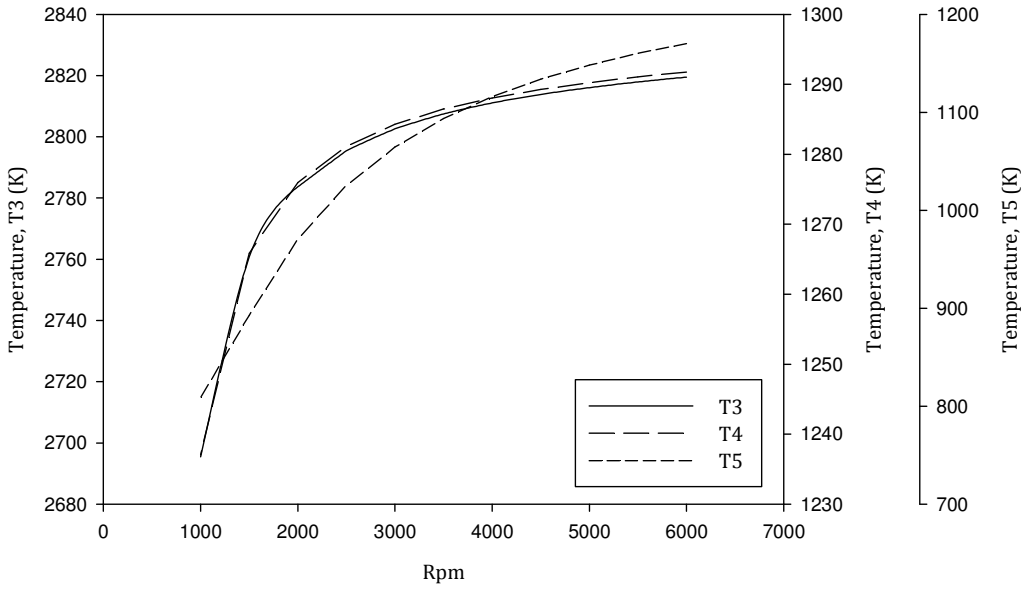

Figure 4.16 FTT model cycle temperatures against rpm

The cycle can be divided approximately into individual strokes of 180° each over the full 540°, or two crank revolutions, of the complete cycle. Therefore, as per Figure 4.15, compression begins at −180°, expansion at 0°, exhaust at 180° and induction at 360°. With this in mind, approximate locations for the cycle temperatures can be specified in accordance with the crank coordinates specified above, i.e. the cycle starting temperature, T_1 can be taken as that at crank angle −180°, the beginning of compression; T_2 as that at 0°; T_3 can be read from the plot as the peak in-cylinder temperature, evident at approximately 30° crank angle; T_4 can be taken as the temperature immediately prior to blowdown, approximately visible in Figure 4.15 at 180° crank angle; and T_5, the in-cylinder temperature after blowdown has occurred, can be read from the plot at approximately 190°.

4.6.7.1 Cycle Temperatures Variation across Operating Speed Range

Figure 4.16 is useful in that it can allow insight into the temperature variation at each approximate cycle point over the full operating frequency range. For instance, the maximum cycle temperature T_3 can be seen to vary by approximately 100 K over the full speed range. This supports the results of the FTT model, presented in Figure 4.16. This plot shows the calculated cycle temperatures for the engine against the operating speed in rpm. From this plot it can be seen that the maximum cycle temperature varies by approximately 120 K.

The variation in T_4 and T_5 can be estimated from Figure 4.15 in similar fashion. It can be seen that the variation in T_4 is approximately 300 K across the range, while for T_5 the variation is approximately 430 K. Comparing this with the FTT calculation it can be seen that the theoretical variation of T_4 is approximately 60 K while that for T_5 is approximately 370 K. In the case of T_4 the disparity between the simulation and theoretical values is considerable, however for T_5 the difference is not quite as pronounced, although still notable. This variance is tolerable however, as the overall magnitudes of the temperatures remain within acceptable percentage difference values over the full operating speed range.

4.6.7.2 Cycle Temperature Magnitudes across Operating Speed Range

There is slight disparity in the magnitudes of T_3; the maximum temperature recorded during the simulation was 2417 K at 1000 rpm, whilst for the FTT model the temperature at this point was 2695 K.

Similarly, the magnitudes for T_4 and T_5 differ between the models. For T_4 the simulation recorded a value of approximately 1170 K at 1000 rpm, whilst the

FTT model calculated a value of 1237 K at this speed. T_5 was recorded as 1040 K approximately during the simulation, whilst the FTT model calculated a value of 808 K.

These variations in the temperature magnitudes remain tolerable however, as they still display acceptable percentage difference for the model to be deemed satisfactory. Also, as noted previously, the simulated and theoretical exhaust gas temperatures remain close, such that overall the FTT model can be considered a reasonable representation of the actual cycle performance.

4.6.8 Power vs. Efficiency

It is common for heat engine performance to be expressed on a plot of brake power against brake efficiency. This is done so as to compare maximum power and maximum efficiency operating points. The resulting plot is typically a loop shape with clear maxima at locations on each of the axes.

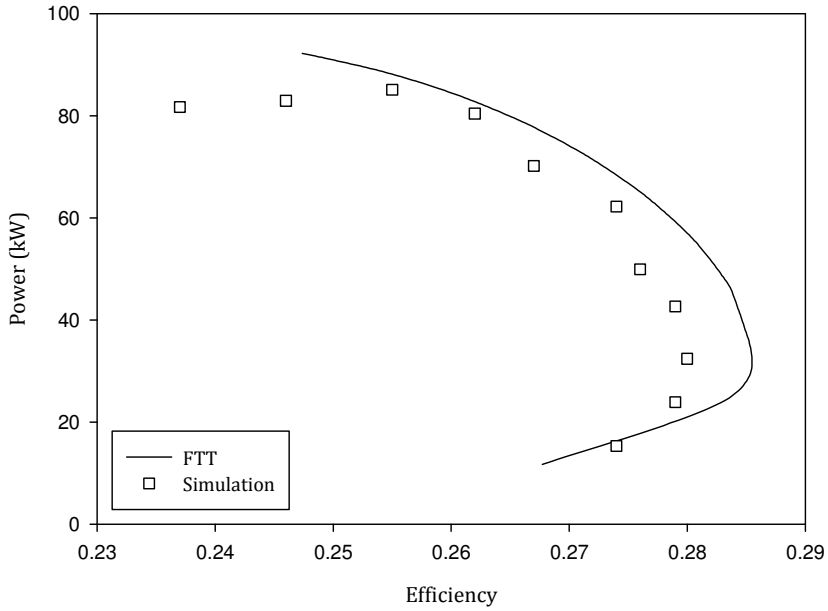

Figure 4.17 Brake power against brake efficiency

Figure 4.17 shows plots of the Ricardo Wave simulation data and the FTT model data on the P–η plane. It is evident that the FTT model offers a good approximation of the engine performance, as the relevant magnitudes are similar and the loop-shape graphs are similar in trend.

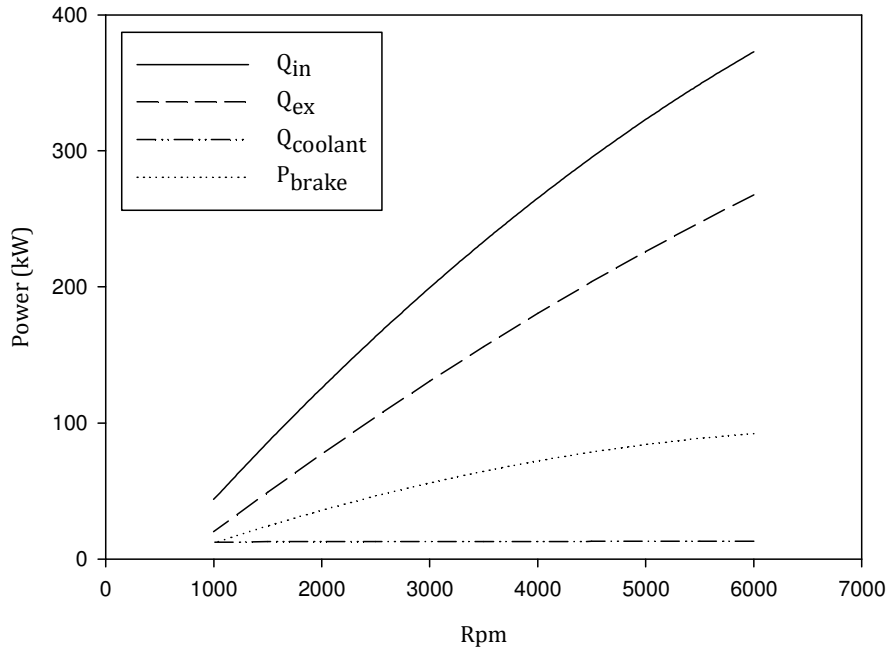

Figure 4.18 Energy balance—magnitudes

4.6.9 Overall Energy Balance

Figure 4.18 and Figure 4.19 show plots of the overall energy balance of the engine. Figure 4.18 shows a plot of the different energy sinks accounted for in the FTT model. Figure 4.19 shows the relative proportions of the energy transfer to each sink as a function of engine operating speed.

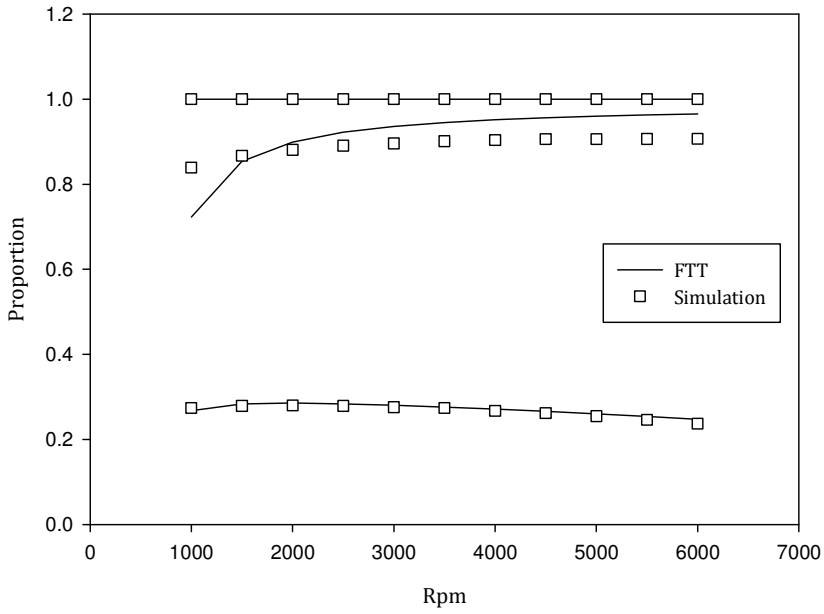

Figure 4.19 Energy balance—proportions

It can be seen from Figure 4.18 that the FTT model offers a reasonable approximation of the overall energy balance of the engine over the full operating range of engine speeds. The calculated brake power is a good match for the recorded simulation data, whilst the proportions attributed to the exhaust and coolant reservoirs offer slightly less accuracy. These are considered to be allowable however as the range of percentage difference for each is quite satisfactory. This data is presented in Figure 4.20, where it can be seen that only at very low rpm does the percentage difference vary significantly from a 10% difference value, and at higher rpm the difference value for all plots clusters around 5%, indicating that the two models are comparable.

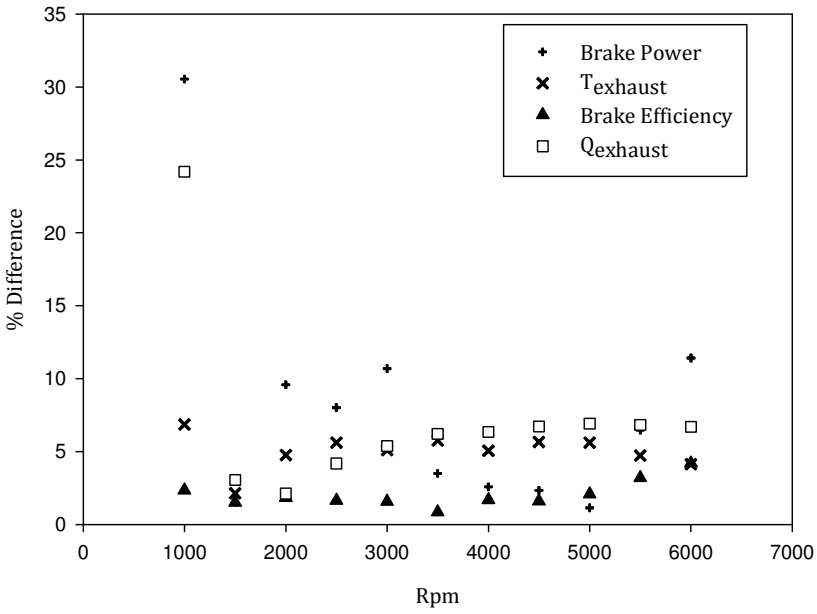

Figure 4.20 Percentage differences between FTT model and recorded simulation data

4.7 Conclusions

Extensive verification of the FTT model of the Otto cycle engine presented in Chapter 3 has been completed and is presented in the current chapter. A commercial virtual engine simulation software, Ricardo Wave, was used to model and simulate a 4-cylinder, 4-stroke naturally aspirated gasoline fired SI engine. The same engine was then modelled in the FTT environment using the model derived in the current work. Results of the FTT simulation were then compared against those recorded from the Ricardo Wave software. This permitted an analysis of the capabilities of the FTT model as a means of predicting the performance of the Otto cycle.

The FTT model compared favourably with the Ricardo Wave simulation for the given engine. Extensive results have been presented, demonstrating how the brake power, brake efficiency, exhaust heat content, exhaust gas temperature,

cycle temperatures, working mass and specific work of the engine can be calculated in the FTT model within acceptable percentage difference limits.

5 DEVELOPMENT OF A FINITE TIME THERMODYNAMICS MODEL OF A STIRLING CYCLE ENGINE

5.1 Introduction

The Stirling cycle engine is gaining significant interest in recent times as a potential alternative prime mover technology for both fossil and renewable energy systems. Numerous applications have been investigated in recent years, including micro-CHP, solar thermal generation and automotive hybrid applications.

Thermodynamic modelling of the Stirling cycle is well established; however, accurate simulation of the practical cycle has traditionally proven difficult. This is generally understood to be due largely to the inclusion of a regenerator in the cycle and the consequent complex flow and heat transfer regime. Accommodation of the regenerator performance within a reasonably simple analytical regime has proven difficult; however, significant progress has been made in recent years. In this chapter, an FTT model of the Stirling is derived which offers good predictive modelling capability with relatively little complexity in the analysis.

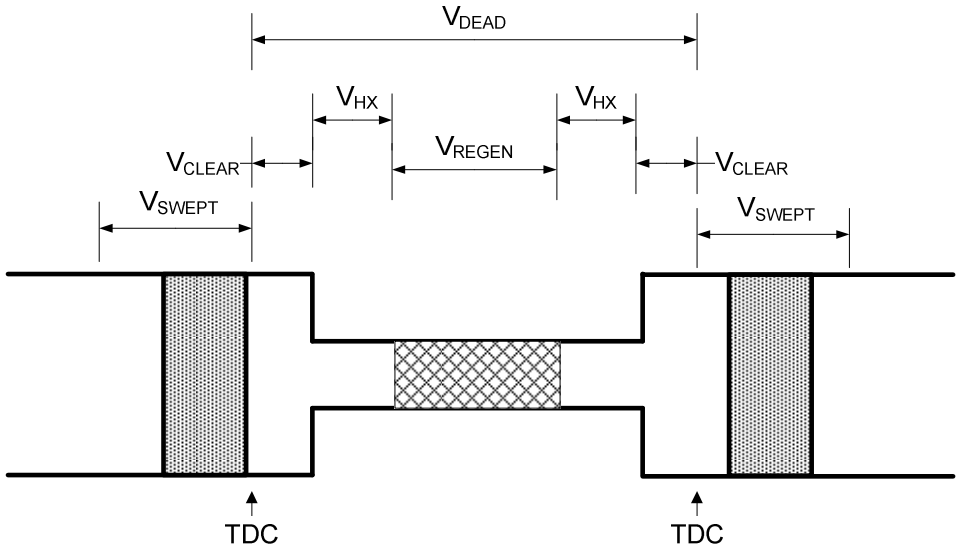

Figure 5.1 Stirling cycle engine 5-space configuration

In this model of the Stirling cycle engine, we use the method presented by Angulo-Brown et al [117, 118, 142] for the Otto cycle engine, in which it was proposed to use a generalised friction loss term to represent mechanical friction and thermal losses within the engine. The technique has been used numerous times for modelling cycles such as the Otto and Diesel cycles [88, 119, 122, 123, 124]. Here we apply the principle to the Stirling engine.

The process adopted involves generating a reversible model of the cycle, then correcting it using the friction power loss term derived from the above. An irreversibility parameter, I_R, is then introduced to account for irreversibility in the gas processes. The method is similar in principle to the decoupled methods used in previous works [98, 62], whereby a representation of the ideal cycle is corrected through loss terms identified through analysis of the specific engine components. The method proposed here differs in its level of complexity; friction power loss irreversibilities are approximated but the specific loss mechanisms are not identified. The intention is to provide a simple model of the

endoreversible Stirling cycle engine with reasonable quantitative and qualitative agreement with real engine performance.

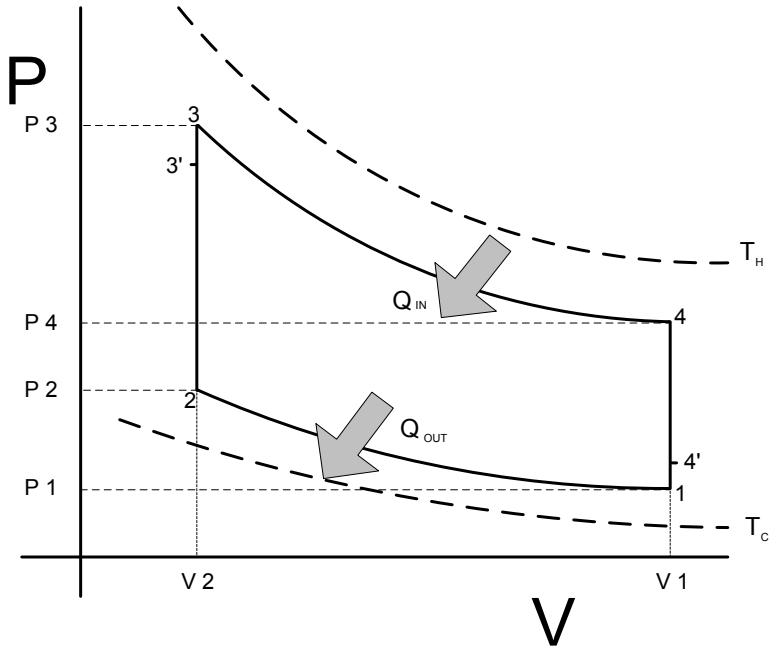

(a)

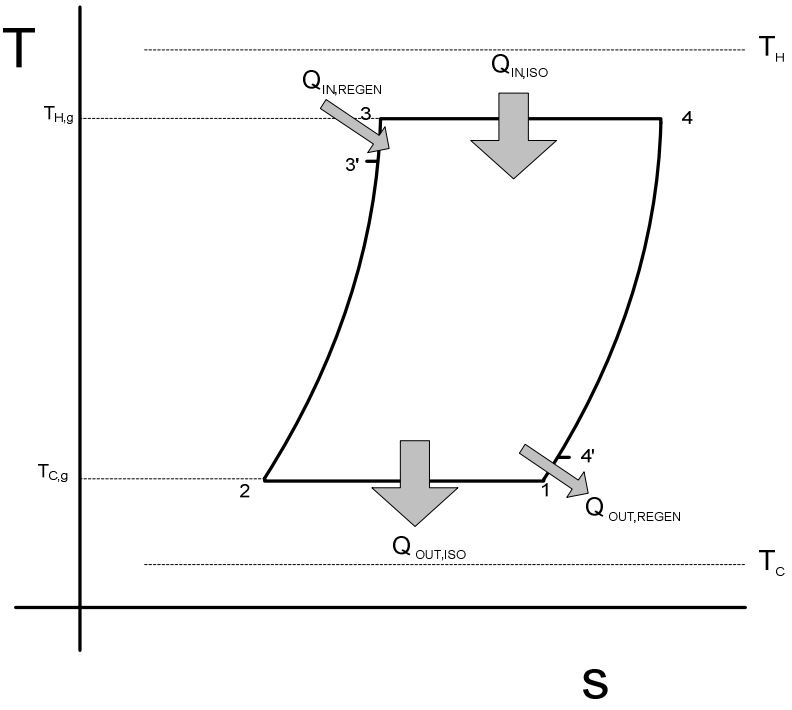

(b)

Figure 5.2 The Stirling cycle (a) p–V diagram (b) T–S diagram

5.2 Detail of the Model

The irreversible power output of the Stirling cycle engine will be shown in this chapter to be expressible in the form:

$$P_{\text{irrev}} = P_{\text{I}} - P_{\mu} - P_{\text{p}} - \dot{Q}_{\text{cond}} - \dot{Q}_{\text{ex}} \tag{5-1}$$

where P_{I} is the power output of the cycle with consideration of irreversibility within the gas processes, P_{μ} is a friction power loss that describes the loss due to generalised mechanical friction within the cycle, and P_{p} is the power loss due to pumping of the working fluid through the heat exchangers. This loss is considered here and not in the Otto cycle model as the nature of the Stirling engine geometry with its tubular heat exchangers and regenerator mesh mean that it becomes more pronounced for this engine. $\dot{Q}_{\text{cond}}$ is a heat loss term used to describe the heat loss due to conduction through the engine body from the heated side to the cooled side, and $\dot{Q}_{\text{ex}}$ is the heat loss directly from the engine exhaust.

As per prior similar analyses, the friction loss term can be expressed in generalised forms as:

$$P_{\text{f}} = \mu \bar{v}^2 \tag{5-2}$$

In this analysis we include a generalised pumping loss term to account for the losses in the heat exchangers particular to the Stirling engine. This is computed as:

$$P_{\text{p}} = \alpha_{\text{p}} \bar{v}^3 \tag{5-3}$$

where α_{p} is the pumping loss coefficient. Note that the pumping loss is proportional to the cube of the gas velocity whereas the friction term is

proportional to the square of the velocity. The development of analytical relationships to describe the constants μ and α_p is detailed in this chapter.

5.2.1 The Ideal Stirling Cycle with Imperfect Heat Exchangers

The work output of the Stirling cycle is:

$$W_{\text{rev}} = Q_{\text{in}} - Q_{\text{out}} \tag{5-4}$$

For the ideal air standard cycle, this becomes:

$$W_{\text{rev}} = mR_g \ln(R_v)(T_{\text{H}} - T_{\text{C}}) \tag{5-5}$$

where T_{H} and T_{C} are the temperatures of the thermal source and sink respectively (K), R_v is the compression ratio of the cycle, $V_{\max}/V_{\min}$, R is the specific gas constant (J/kgK) of the working fluid and m is the mass of gas in the cycle (kg). It should be noted that r_v is computed from the total cycle volume variation and therefore includes the dead space within the engine. The heat input to the cycle in Joules, Q_{in}, is comprised of the heat addition required due to imperfect regeneration, process 3'–3 in Figure 5.2, and that due to isothermal heat exchange, process 3–4 in Figure 5.2:

$$Q_{\text{in}} = Q_{3'3} + Q_{34} \tag{5-6}$$

$$Q_{\text{in}} = mc_v(1 - \varepsilon_R)(T_{\text{H}} - T_{\text{C}}) + \varepsilon_H mR_g T_{\text{H}} \ln(R_v) \tag{5-7}$$

where c_v is the specific heat capacity at constant volume of the gas (J/kgK), ε_R is the regenerator effectiveness and ε_H is the effectiveness of the hot side heat exchanger. In this analysis, it is assumed that the heat exchanger effectiveness values effectively refer explicitly to thermal resistance losses across the heat exchanger walls. The working spaces therefore remain isothermal, as presented in Figure 5.2. This is a common assumption of FTT, the net effect being an assumption of endo-reversibility within the cycle, all irreversibilities being confined to the system boundary.

Similarly the heat rejection from the cycle can be specified as the heat rejection required due to imperfect regeneration, process 4'–1 in Figure 5.2, and that which occurs at isothermal conditions, process 1–2 in Figure 5.2:

$$Q_{\text{out}} = Q_{4'1} + Q_{12} \tag{5-8}$$

$$Q_{\text{out}} = mc_v(1 - \varepsilon_{\text{R}})(T_{\text{H}} - T_{\text{C}}) + \varepsilon_{\text{C}} mR_g T_{\text{C}} \ln(R_v) \tag{5-9}$$

where ε_{C} is the effectiveness of the cold side heat exchanger. For each heat exchanger it is assumed that the maximum heat transfer that could occur corresponds to the process involved in the ideal cycle, i.e. constant volume heat transfer during the regeneration processes and isothermal heat transfer during the expansion and contraction processes. The actual heat transfer is therefore calculated from the relationship $\dot{q} = \varepsilon \dot{q}_{\text{max}}$. The work output of the engine with account of heat exchanger performance can therefore be given from (5-4):

$$W_{\text{rev}} = \varepsilon_{\text{H}} mR_g T_{\text{H}} \ln(R_v) - \varepsilon_{\text{C}} mR_g T_{\text{C}} \ln(R_v) \tag{5-10}$$

$$W_{\text{rev}} = mR_g \ln(R_v)(\varepsilon_{\text{H}} T_{\text{H}} - \varepsilon_{\text{C}} T_{\text{C}}) \tag{5-11}$$

This is the work output of the ideal cycle with imperfect heat exchange. It implies irreversibility generation associated with the heat exchanger performance, but does not make any account for other irreversibility mechanisms within the engine such as friction losses or gas throttling losses.

However, a key departure of the ideal cycle over the practical cycle is the exclusion of kinematically varying working volumes within the thermodynamic circuit. The ideal air-standard cycle such as that represented in Figure 5.2 assumes discontinuous piston motion within the circuit. This has the effect of enlarging the enclosed area of the *p*–*V* diagram and thereby increasing the cycle work performed by the cycle. The inclusion of kinematic crank mechanisms has

the effect of rounding off the extremities of the graph, resulting in a *p*–*V* diagram which is closer in appearance to that presented in Figure 5.3.

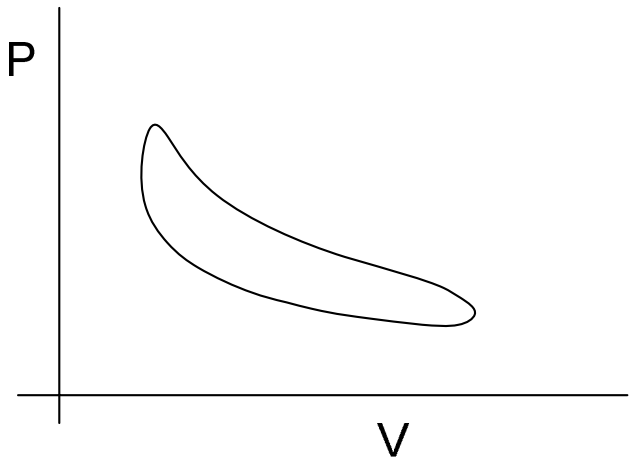

Figure 5.3 The practical Stirling cycle

It is therefore necessary to accommodate the cyclic volume variations in the analysis in order to fully account for the work lost due to the use of continuous piston motion. Traditionally, this has been done using the Schmidt Stirling cycle analysis. This method is summarised in the following section.

5.2.2 Schmidt Cycle Model

The Schmidt model is a mathematical treatment of the Stirling cycle. It was the first mathematically rigorous attempt to describe the cycle and remains to this day the foundation of Stirling cycle analysis [58, 91]. The model makes a number of simplifying assumptions about the cycle, and consequently is not a realistic description of the practical cycle experienced in actual engines. The assumptions made to facilitate analysis are:

1) Heat transfer in the heat exchangers and working spaces is isothermal

2) Instantaneous pressure is homogenous throughout the complete working circuit

3) The mass of working fluid is constant, i.e. there are no leaks from the gas circuit

4) The working gas is assumed to behave as a perfect gas

5) The speed of the machine is constant and cyclic steady state has been achieved

6) The potential and kinetic energies of the gas are assumed negligible

The above assumptions are highly idealised and lead to extremely optimistic predictions of work output and efficiency for the engine. For example, the assumption of isothermal heat transfer leads to the prediction of a thermal efficiency equal to the Carnot efficiency for the given source and sink temperatures. Also, the assumption of instantaneously homogenous pressure within the circuit neglects the losses due to fluid friction within the heat exchangers and the working spaces. The work output of the engine is therefore significantly higher than that which is practically achievable. Previous studies have indicated the Schmidt model and its variants to over-predict the work output and efficiency by a factor of approximately 2, sometimes higher [58, 57, 98]. The major contribution of the Schmidt model and its variants is the inclusion of kinematically varying working space volumes within the analysis, as well as the specific inclusion of dead volume, crank angle and phase angle within the analysis, something which is only implicit in the air-standard cycle analysis. This has the notable effect of providing pressure–volume indicator diagrams similar to those that would be expected of real engines. Therefore, the work output of the Schmidt model is lower than that of the equivalent air-

standard cycle by an amount equivalent to the difference in enclosed area of the respective p–V diagrams.

A number of variants on the Schmidt analysis exist in the literature. For the current study, the variant proposed by Walker [58] is utilised. This particular version is viewed as suitable in that it presents the analysis in terms of four dimensionless parameters pertaining to the engine geometry. These ratios are:

i) The temperature ratio, $\Gamma = \frac{T_{\mathrm{C}}}{T_{\mathrm{H}}}$

ii) The swept volume ratio, $\kappa = \frac{V_{\mathrm{C}}}{V_{\mathrm{E}}}$

iii) The dead volume ratio, $\chi = \frac{V_{\mathrm{D}}}{V_{\mathrm{E}}}$

iv) The phase angle,α; the angle by which volume variations in the expansion space lead those in the compression space.

where T_{H} and T_{C} are the source and sink temperatures, $V_{\mathrm{C}}$and $V_{\mathrm{E}}$are the swept volumes of the compression and expansion space respectively and $V_{\mathrm{D}}$is the total dead volume in the system. A summary of the equations used by Walker in the Schmidt-type analysis is presented below.

5.2.3 Summary of Schmidt-type Analysis Equations

Instantaneous volume of expansion space:

$$V_{\mathrm{e}} = \frac{1}{2} V_E \left(1 + \cos\left(\phi\right)\right) \tag{5-12}$$

where ϕ is the crank angle. Instantaneous volume of compression space:

$$V_{\mathrm{c}} = \frac{1}{2} \kappa V_{\mathrm{E}} \left(1 + \cos\left(\phi - \alpha\right)\right) \tag{5-13}$$

Instantaneous volume of total working space:

$$V_{t,\mathrm{instant}} = V_{\mathrm{e}} + V_{\mathrm{c}} + V_{\mathrm{dead}} \tag{5-14}$$

Instantaneous cycle pressure:

$$p = \frac{p_{\max}(1-\delta)}{[1+\delta\cos(\phi-\theta)]} \tag{5-15}$$

where

$$\delta = \frac{(\Gamma^2 + 2\Gamma\kappa\cos(\alpha) + \kappa^2)^{0.5}}{(\Gamma + \kappa + 2\Sigma)} \tag{5-16}$$

$$\tan(\theta) = \frac{\kappa\sin(\alpha)}{\left(\Gamma + \kappa\cos(\alpha)\right)} \tag{5-17}$$

$$\Sigma = \frac{2X\Gamma}{(\tau+1)} \tag{5-18}$$

Pressure ratio:

$$\frac{p_{\max}}{p_{\min}} = \frac{(1+\delta)}{(1-\delta)} \tag{5-19}$$

Mean cycle pressure:

$$p_{\text{mean}} = p_{\max}\left[\frac{(1-\delta)}{(1+\delta)}\right]^{0.5} \tag{5-20}$$

Net cycle work:

$$W_{\text{Schmidt}} = \frac{(p_{\max}V_T)\pi(1-\Gamma)}{(\kappa+1)}\left[\frac{(1-\delta)}{(1+\delta)}\right]^{0.5}\left[\frac{\delta\sin(\theta)}{[1+(1-\delta^2)^{0.5}]}\right] \tag{5-21}$$

where

$$V_{\text{T}} = V_{\text{E}} + V_{\text{C}} = (1+\kappa)V_{\text{E}} \tag{5-22}$$

Thermal efficiency:

$$\eta = \frac{T_{\text{H}} - T_{\text{c}}}{T_{\text{H}}} = (1-\Gamma) \tag{5-23}$$

The above equations allow the calculation of the ideal cycle work for the Stirling cycle with consideration of the sinusoidal volume variations within the working spaces. All other assumptions are identical to those made in the air standard cycle analysis, such that the difference between the two effectively amounts to

the work lost due to the use of the continuous crank motion. For the FTT analysis, it is therefore possible to specify a loss ratio, N_{L} to account for the mechanical losses and to align the ideal air standard expression for cycle work with that of the Schmidt type analysis. This ratio is specified as:

$$N_{\mathrm{L}} = \frac{W_{\mathrm{Schmidt}}}{W_{\mathrm{rev}}} \tag{5-24}$$

As will be shown in the next chapter, a typical value for N_{L} is approximately 0.3. This indicates that there are significant losses associated with the use of the sinusoidal volume variations over the discontinuous motion inherent in the air-standard cycle. The work output of the cycle with consideration of the heat exchanger performances can therefore be expressed in terms of the loss ratio:

$$W_{\mathrm{rev,L}} = N_{\mathrm{L}} m R_g \ln(R_v)(\varepsilon_{\mathrm{H}} T_{\mathrm{H}} - \varepsilon_{\mathrm{c}} T_{\mathrm{c}}) \tag{5-25}$$

5.2.4 Internal Irreversibility—the Irreversibility Ratio

A common method used in the field of FTT to account for irreversibilities within the cycle is to include an irreversibility parameter, I_{R} [84], where $I_{\mathrm{R}} > 1$. This irreversibility parameter is derived from the Clausius inequality, which can be expressed as:

$$I_{\mathrm{R}} \frac{|Q_{\mathrm{in}}|}{T_{\mathrm{H}}} - \frac{|Q_{\mathrm{out}}|}{T_{\mathrm{c}}} = 0 \tag{5-26}$$

In this case, the work output of the cycle can be given as [122]:

$$W_{\mathrm{I}} = |Q_{\mathrm{in}}| - I_{\mathrm{R}} |Q_{\mathrm{out}}| \tag{5-27}$$

Considering the ideal Stirling cycle, Equation (5-25) becomes:

$$W_{\mathrm{I}} = N_{\mathrm{L}} m R_g \ln(R_v)(T_{\mathrm{H}} - I_{\mathrm{R}} T_{\mathrm{c}}) \tag{5-28}$$

It is seen that for the limiting case of $I_{\mathrm{R}} = 1$, the work output equals the ideal cycle work. To get some further insight into the irreversibility generation, Equation (5-26) can be rearranged to give:

$$I_{\mathrm{R}} = \frac{|Q_{\mathrm{out}}|T_{\mathrm{H}}}{|Q_{\mathrm{in}}|T_{\mathrm{c}}} = \frac{s_2 - s_1}{s_4 - s_3} \tag{5-29}$$

Considering the Stirling cycle with imperfect regeneration as shown in Figure 5.2 (a), there are two mechanisms by which heat is transferred to and from the surroundings; isothermal heat transfer in the heat exchangers, as per the ideal air-standard cycle; and isochoric heat transfer, required to compensate for the imperfect regeneration process. The entropy generation in the heat addition and heat rejection processes can be considered separately. Considering the entropy transfer into the system:

$$s_{\mathrm{in}} = \frac{|Q_{\mathrm{isothermal}}|}{T_{\mathrm{H}}} + \int \frac{|Q_{\mathrm{isochoric}}|}{T} \tag{5-30}$$

Which becomes:

$$s_{\mathrm{in}} = \frac{N_L \varepsilon_H m R_g T_H \ln(R_{\mathrm{v}})}{T_{\mathrm{H}}} + N_{\mathrm{L}} m c_v \int_{3'}^{3} \frac{dT}{T} \tag{5-31}$$

Completing the integration, Equation (5-31) becomes:

$$s_{\mathrm{in}} = N_{\mathrm{L}} \varepsilon_{\mathrm{H}} m R_g \ln(R_v) + N_{\mathrm{L}} m c_v \ln\left(\frac{T_3}{T_{3'}}\right) \tag{5-32}$$

Similarly, the entropy leaving the system can be summarised as:

$$s_{\mathrm{out}} = N_{\mathrm{L}} \varepsilon_{\mathrm{c}} m R_g \ln(R_v) + N_{\mathrm{L}} m c_v \ln\left(\frac{T_{4'}}{T_1}\right) \tag{5-33}$$

The entropy generation ratio, I_{R} can therefore be expressed as:

$$I_{\mathrm{R}} = \frac{s_{out}}{s_{in}} = \frac{\left[\varepsilon_{\mathrm{c}} R_g \ln(R_v) + c_v \ln\left(\frac{T_{4'}}{T_1}\right)\right]}{\left[\varepsilon_{\mathrm{H}} R_g \ln(R_v) + c_v \ln\left(\frac{T_3}{T_{3'}}\right)\right]} \tag{5-34}$$

Equation (5-34) allows an expression for the I_{R} term with respect to the physical parameters of the system. The temperatures after regeneration, $T_{3'}$ and $T_{4'}$ can be calculated with knowledge of the effectiveness of the regenerator through the equation:

$$Q_{\text{regen,comp}} = mc_v(1 - \varepsilon_{\text{R}})(T_3 - T_2) = mc_v(T_3 - T_{3,}) \tag{5-35}$$

where $\text{Q}_{\text{regen,comp}}$ denotes the heat that must be transferred to the system to compensate for the regenerator heat losses. Equation (5-35) can be rearranged to give:

$$T_{3,} = \varepsilon_{\text{R}}(T_3 - T_2) + T_2 \tag{5-36}$$

Similarly, the temperature after regeneration when the gas moves from the heated space to the cooled space can be expressed as:

$$T_{4,} = T_1 - \varepsilon_{\text{R}}(T_3 - T_1) \tag{5-37}$$

Remembering that $T_{\text{H}} = T_3 = T_4$ and $T_{\text{c}} = T_1 = T_2$. It is seen from Equation (5-34) that the irreversibility generated within the cycle is a function of the specific heat capacity at constant volume, c_v, the source and sink temperatures, the specific gas constant, R_g, the volume compression ratio, r_v and the effectiveness of each of the heat exchangers; ε_{H}, ε_{R} and ε_{c}. This has implications for the specification of:

1) The working fluid (c_v, R_g)
2) The operating regime ($T_{\text{H}}, T_{\text{c}}$) and
3) The engine geometry ($R_v, \varepsilon_{\text{R}}, \varepsilon_{\text{H}}, \varepsilon_{\text{c}}$).

The FTT method involves the imposition of a time constraint on the process. In this instance, we introduce the thermodynamic cycle period,τ as a constraint, derived from the imposed engine operating frequency, f (Hz):

$$\tau = \frac{1}{f} \tag{5-38}$$

Consequently the ideal cycle power, with accommodation for cycle irreversibilities, P_{I} , is:

$$P_{\text{I}} = \frac{W_{\text{I}}}{\tau} = \frac{N_L m R_g}{\tau} \ln(\text{R}_v)(T_{\text{H}} - I_{\text{R}} T_{\text{C}}) \tag{5-39}$$

Inclusion of the cycle irreversibilities in this manner is a common practice in the finite time method. Examples include work by Ozkaynak et al [146, 147], Curto-Risso et al [122]. However, whilst being a simple and effective means of apportioning magnitude to the losses inherent in the cycle, it is limited in its facility to investigate actual loss mechanisms. In the following sections, a global friction loss term is derived similar to that proposed by Angulo-Brown et al for the Otto cycle and a pumping power loss term is introduced to account for the flow losses inherent in the heat exchangers.

5.2.5 Heat Exchanger Performance

5.2.5.1 Regenerator Effectiveness

The performance of the regenerative heat exchanger can be modelled to gain some insight into its dependence on gas speed. The regenerator can be modelled as a counter flow heat exchanger [101, 148, 149]. In this case, the effectiveness is usually determined using the expression:

$$\varepsilon = \frac{\mathrm{NTU}}{2 + \mathrm{NTU}} \tag{5-40}$$

The number of transfer units (NTU) is computed as:

$$\mathrm{NTU} = \frac{h_{\mathrm{R}} A_{\mathrm{w}}}{\dot{m} c_p} \tag{5-41}$$

where h_{R} is the convective heat transfer coefficient. The wetted area of the regenerator mesh, A_{w}, can be calculated from:

$$A_{\mathrm{w}} = \left(\frac{1}{4}\right)\left(\frac{\pi^2 D_{\mathrm{R}}^2 L_{\mathrm{R}}}{b + d}\right) \tag{5-42}$$

where $D_R$is the regenerator diameter, $L_R$is the regenerator length, b is the mesh wire gap distance and d is the mesh wire diameter. Figure 5.4 shows a simplified representation of a wire mesh screen with these parameters shown.

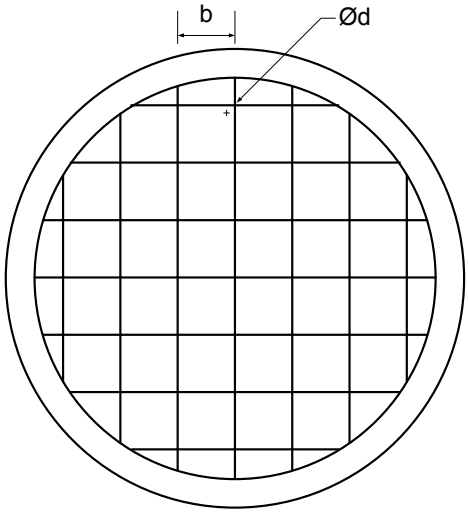

Figure 5.4 Regenerator mesh screen showing mesh wire diameter and wire gap

The regenerator is a gas-to-solid heat exchanger; therefore the overall heat transfer coefficient, U_{R}, becomes simply the convective coefficient for the gas flowing over the wire mesh. The convective heat transfer coefficient h_{R} is computed from [105]:

$$h_{\mathrm{R}} = \frac{0.395\left(\frac{4p_m}{R_g T_L}\right) v_g^{0.424} c_p \upsilon}{(1+\tau)\left(1 - \frac{\pi}{4\left(\left(\frac{b}{d}\right)+1\right)}\right) D_{\mathrm{R}}^{0.576} \mathrm{Pr}^{\frac{2}{3}}} \tag{5-43}$$

where $v_g$is the gas velocity in the regenerator, υ is the kinematic viscosity and Pr is the Prandtl number of the working gas. The mass flow of gas through the regenerator $\dot{m}$ is computed using the assumption that only a mass equivalent to that contained in the working spaces at any given instant is transported through the regenerator. Assuming again that the pressure throughout the circuit is instantaneously homogenous, the ratio of working mass to total cycle mass is given by the mass ratio:

$$N_m = \frac{\left(\frac{V_\mathrm{e}}{T_\mathrm{H}} + \frac{V_\mathrm{c}}{T_\mathrm{c}}\right)}{\left(\frac{V_e}{T_\mathrm{H}} + \frac{V_\mathrm{h}}{T_\mathrm{H}} + \frac{2V_\mathrm{R}}{(T_\mathrm{H} + T_\mathrm{c})} + \frac{V_k}{T_\mathrm{c}} + \frac{V_\mathrm{c}}{T_\mathrm{c}}\right)} \tag{5-44}$$

where V_k and V_h are the volumes of the cooler and heater respectively. Assuming that the total mass of gas in the cycle passes through the regenerator twice every revolution, the mass flowrate is therefore:

$$\dot{m} = 2N_m mf \tag{5-45}$$

These relationships offer a piston-speed dependant method for calculating the approximate regenerator effectiveness.

5.2.5.2 Hot Side Heat Exchanger Effectiveness

For the source side heat exchanger, we will assume a cross flow, compact heat exchanger configuration with both gases unmixed.

The effectiveness-NTU relationship for this scenario is:

$$\varepsilon = 2\left\{1 + C_\mathrm{r} + (1 + C_\mathrm{r}^2)^{0.5}\left[\frac{1 + \exp(-\mathrm{NTU}(1 + C_\mathrm{r}^2)^{0.5})}{1 - \exp(-\mathrm{NTU}(1 + C_\mathrm{r}^2)^{0.5})}\right]^{-1}\right\} \tag{5-46}$$

where

$$NTU = \frac{U_\mathrm{H} A}{C_\mathrm{min}} \tag{5-47}$$

$$C_\mathrm{r} = \frac{C_\mathrm{min}}{C_\mathrm{max}} \tag{5-48}$$

And the heat capacity rate $C = \dot{m}c_p$. The overall heat transfer coefficient, U, is defined for an unfinned cylindrical heat exchanger as [149]:

$$U = \frac{1}{R_\mathrm{total} A} = \frac{1}{\left[\left(\frac{1}{h_1 \pi d_\mathrm{o} L_\mathrm{H}}\right) + \left(\frac{\ln\left(\frac{d_\mathrm{o}}{d_\mathrm{i}}\right)}{2\pi k L_\mathrm{H}}\right) + \left(\frac{1}{h_2 \pi d_\mathrm{i} L_\mathrm{H}}\right)\right]} \tag{5-49}$$

h_1 and h_2 are the convective heat transfer coefficients for the exhaust gas and working gas sides respectively, L_H is the heat transfer length of the heat exchanger, k is the conduction coefficient for the heat exchanger wall and d_i and $d_o$are the inner and outer diameters of the heat exchanger tubes respectively. The convective heat transfer coefficient on the hot exhaust gas side, h_1, can be computed by modelling the system as a compact heat exchanger. The methodology for analysis of such heat exchangers is well represented in the literature.

The case of unfinned heat exchange surface area will be considered first. The convective coefficient can be defined as [149]:

$$h_1 = \frac{j_{\mathrm{H}} G c_p}{\mathrm{Pr}^{\frac{2}{3}}} \tag{5-50}$$

where j_{H} is the Colburn j factor for the heater tubes, G is the mass velocity (kg/sm^2) and Pr is the Prandtl number. To calculate the convective coefficient on the source side, the mass velocity must be calculated first:

$$G = \frac{\dot{m}}{\sigma A_{\mathrm{fr}}} \tag{5-51}$$

where σ is the ratio of the minimum free-flow area of the finned passages and A_{fr} is the frontal area of the heat exchanger tubes. These quantities are particular to the given heat exchanger geometry.

In order to ascertain the j_{H} factor, it is necessary to compute the Reynolds number for the flow regime involved. For the combustion gas side of the heat exchanger the Reynolds number can be given as:

$$\mathrm{Re} = \frac{G D_{\mathrm{h}}}{\mu} \tag{5-52}$$

With the Reynolds number calculated it is therefore possible to determine j_H from the heat exchanger correlations provided in the literature [149]. The convective coefficient for the combustion gas side can then be calculated using Equation (5-50).

The conduction resistance term in Equation (5-49) can be calculated by modelling the exchanger tubes as cylindrical tubes in crossflow conditions. The radial conduction resistance is therefore:

$$R_{\mathrm{t,cond}} = \frac{\ln\left(\frac{d_o}{d_i}\right)}{2\pi k L_{\mathrm{H}}} \tag{5-53}$$

where L_{H} is the heat transfer length of the exchanger, ie the effective length available for heat transfer interaction.

In order to compute the heat transfer coefficient for the working fluid side of the heat exchanger, h_2, it is necessary to account for the atypical flow regime involved: that of periodically reversing flow. Kanzaka and Iwabuchi [150] performed a study of heat transfer in the heat exchangers in the Stirling engine in which a specific relationship for the Reynolds number is computed for the special case of periodically reversing flow that is found particularly in the Stirling engine:

$$\overline{\mathrm{Re}} = \left|\frac{\overline{dg}}{d\theta}\right| \left(\frac{6\bar{P}V_C}{\bar{p}R_g T_1} N\right)\left(\frac{4}{\pi\mu d_i}\right) \tag{5-54}$$

where $\left|\frac{\overline{\mathrm{d}g}}{\mathrm{d}\theta}\right|$ is the mean mass flow of the working fluid within the heat exchanger. The Nusselt number for the condition of periodically reversing flow is presented by Kanzaka and Iwabuchi as:

$$\mathrm{Nu} = 0.021\overline{\mathrm{Re}}^{0.8}\mathrm{Pr}^{0.4}\left(\frac{T_{\mathrm{w}}}{T_{\mathrm{b}}}\right)^{-0.5}(C') \tag{5-55}$$

where the correction term, C′ is given as:

$$C' = 0.923 + 0.75\left(\frac{T_{\mathrm{w}}}{1000}\right) \tag{5-56}$$

It is then a reasonably simple step to calculate h_2:

$$h_2 = \frac{k_f \mathrm{Nu}}{L_{\mathrm{H}}} \tag{5-57}$$

where k_f is the conduction coefficient of the working gas. This gives a speed dependant term for the convective coefficient on the working fluid side of the heat exchanger. The wall temperature on the interior of the heat exchanger, T_{w}, can be approximated using a simple conduction analysis when the convective coefficient of the hot combustion gas, the heat exchanger material and geometry are specified. The same relationships can be used to compute the convective coefficient in the cooling side heat exchanger, with accommodation made for the temperatures and the mass flow-rates of the fluids interacting.

5.2.6 Static Thermal Losses

5.2.6.1 Static Conduction Losses

Another important thermal loss in the Stirling engine system is the static thermal conduction loss. This loss arises due to the thermal gradient across the engine from the source to sink [98]. It is an important thermal loss to account for as it remains approximately constant for a given source and sink temperature regime, such that for different engine speeds and mean operating pressures it contributes a varying proportion of the total losses. The thermal conduction loss is dependant on the physical construction of the given engine, and therefore must be measured experimentally to be accurately accounted for.

It is most easily represented as a proportion of the total heat admitted to the cycle:

$$\dot{Q}_{\text{cond}} = N_{\text{cond}}(\dot{Q}_{\text{in}}) \tag{5-58}$$

where N_{cond} is the experimentally measured ratio of the conduction losses to the total heat input to the cycle.

5.2.6.2 Exhaust Stack Losses

Another major loss from the engine is the loss from the exhaust system. These losses are usually termed 'stack losses' and represent a significant proportion of the total loss from the engine. Due the complex nature of the fluid interaction in the heat exchangers of the Stirling engine, these losses are difficult to quantify analytically without recourse to complex fluid flow simulation, however an estimation of the losses is possible. To accommodate the losses in the current simulation, it was noted from the experimental energy balance data that the exhaust losses maintain an approximately constant proportion of the engine heat addition over the different mean cycle pressure regimes. It was decided for the validation simulation to account for the exhaust losses using the product:

$$\dot{Q}_{\text{exhaust}} = N_{\text{ex}}\dot{Q}_{\text{in}} \tag{5-59}$$

where $N_{\text{ex}} \cong 0.3$. This offered a simple but effective means for accounting for the exhaust stack losses of the engine. The physical reality of the N_{ex} term can be discussed with reference to the heat exchanger effectiveness as follows.

A methodology for calculation of the heat exchanger effectiveness is detailed in the previous section. The heat exchanger effectiveness is defined as ratio of actual heat transfer to the maximum possible heat transfer:

$$\varepsilon = \frac{\dot{Q}_{\text{actual}}}{\dot{Q}_{\text{max}}} \tag{5-60}$$

where the maximum heat transfer is defined in terms of the fluid entrance temperatures:

$$\dot{Q}_{\text{max}} = \dot{C}_{\text{min}}\left(T_{\text{h,i}} - T_{\text{c,i}}\right) \tag{5-61}$$

For the heater of the Stirling cycle engine, $T_{\text{h,i}}$ is the temperature of the combustion gas and $T_{\text{c,i}}$ is the temperature of the gas immediately after the regenerator and before entrance to the heater tubes, calculated previously as $T_{3'}$. This maximum heat transfer can be represented as a proportion of the total heat available in the combustion gas stream:

$$R_Q = \frac{\dot{Q}_{\text{max}}}{\dot{Q}_{\text{in,eng}}} \tag{5-62}$$

The engine uses a preheater system which recovers heat from the exhaust to preheat combustion air entering the combustion chamber. Therefore, the heat actually entering the engine via the hot side heat exchanger is less than the total heat released during combustion. This heat input to the engine is represented by $\dot{Q}_{\text{in,eng}}$ in Equation (5-62). The heat loss from the exhaust (after the preheater) to atmosphere can therefore be described as the difference between the heat input to the system via the combustion gases and the actual heat transfer into the engine:

$$\dot{Q}_{\text{exhaust}} = \dot{Q}_{\text{in,eng}} - \varepsilon\dot{Q}_{\text{max}} \tag{5-63}$$

This in turn becomes:

$$\dot{Q}_{\text{exhaust}} = \left(1 - \varepsilon R_Q\right)\dot{Q}_{\text{in,eng}} \tag{5-64}$$

As can be seen, while the heat exchanger effectiveness, $\boldsymbol{\varepsilon}$ will be available from previous calculations, computation of the $\boldsymbol{\dot{Q}}_{\text{in,eng}}$ term and by extension the $\boldsymbol{R_Q}$

term is problematic. This is because the calculation of the $\dot{Q}_{\text{in,eng}}$ term relies on knowledge of the temperature of the exhaust gas immediately before entering the preheater. However, for the current study a value for this temperature was not available, meaning that in order to complete the computation an estimate would be necessary. Because this is essentially equivalent to estimating the N_{ex} term from the experimental heat balance data, it was decided to simply use the N_{ex} estimate to quantify the exhaust heat losses.

Note that the exhaust stack loss is treated as a loss from the sink of the thermodynamic cycle, whereas in actuality it would be more appropriate to specify it as a bypass loss, as it effectively does not interact with the hot side heat exchanger but rather is despatched directly to the exhaust flue. It was considered in the current simulation to include it as a cycle loss for the sake of congruence with thermodynamic pedagogy.

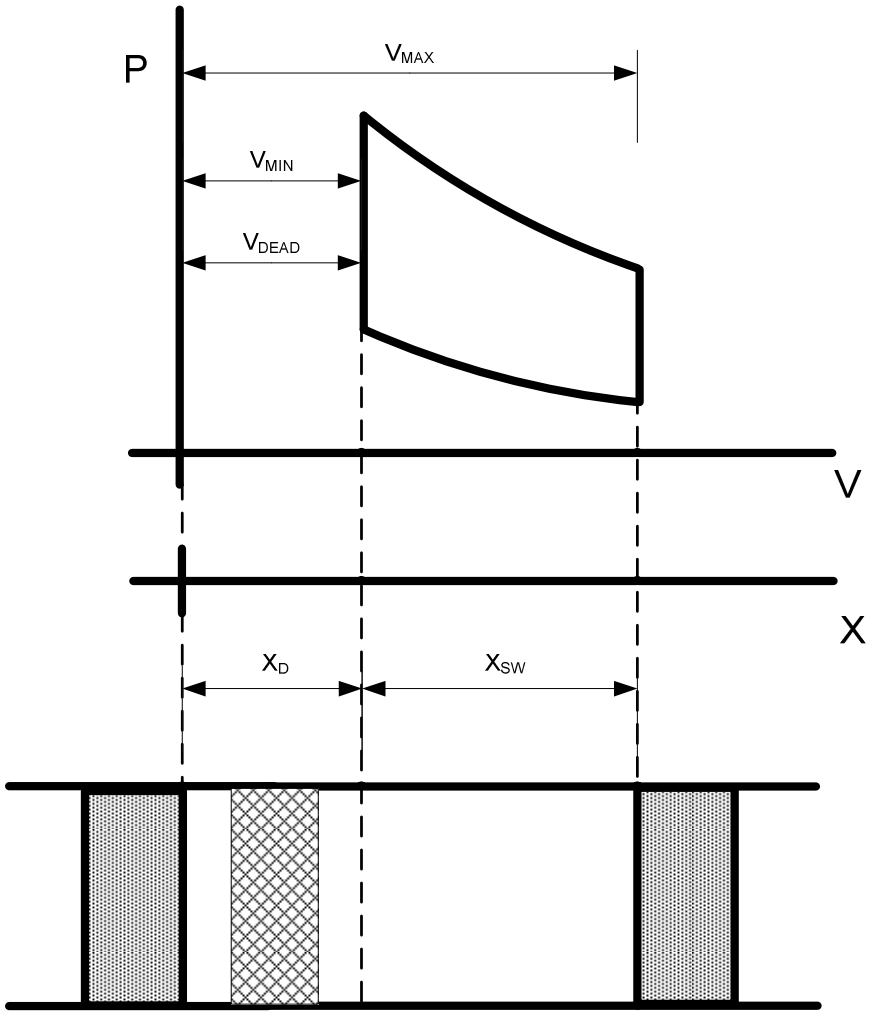

(a)

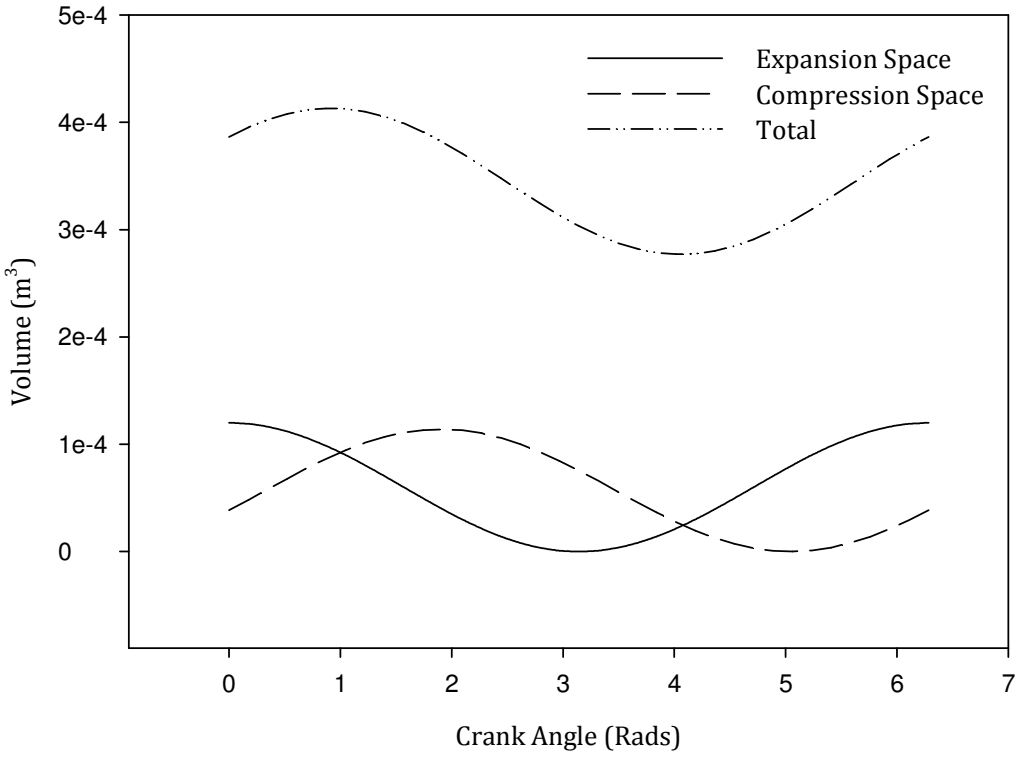

(b)

Figure 5.5 Working volumes of the Stirling cycle

(a) pV–pX diagram of the pseudo single cylinder Stirling cycle (b) example of the volume variations in the rhombic drive mechanism, including total volume variation

5.2.7 Global Friction Losses

We will consider a dissipation term to approximate the global friction losses within the cycle due to mechanical and thermal losses. This method was developed by Mozurkewich and Berry [144] for an Otto engine and used to good effect by several others subsequently [117, 118, 122]. The friction power loss is calculated as:

$$P_{\mu} = \mu_s \bar{v}_p{}^2 \tag{5-65}$$

where μ_s is a coefficient of friction which takes into account the global losses for the Stirling engine and $\bar{v}$ is the mean piston velocity (m/s). The procedure to evaluate μ for an Otto cycle engine is detailed by Mozurkewich and Berry. A modified version of this procedure is offered here to accommodate some of the particular characteristics of the Stirling engine. The aim is to present a generalised methodology for analysis of the Stirling cycle.

5.2.7.1 Calculation of Friction Coefficient

μ_s is related to the frictional work loss, W_f, through the expression:

$$\mu_s = \frac{2\tau W_f}{\pi^2 {x_s}^2} \tag{5-66}$$

where x_s is the stroke of the piston under consideration. The procedure to derive Equation (5-66) is the same as that detailed by Mozurkewich and Berry [144] for the Otto cycle (cf. Equation (3-16), Chapter 3), with the exception that the Stirling cycle is a two stroke cycle and so this must be accommodated accordingly as a reduced cycle period. Mozurkewich and Berry indicate that in the case of four stroke, single piston cycles such as the Otto cycle, W_f can be considered equal to $0.15(W_{rev})$. Detailed data concerning the losses inherent in the Stirling cycle engine are less easily retrieved. Martini [98] provides some of the most comprehensive performance figures concerning real Stirling engines. Data for the General Motors GPU-3 engine demonstrate mechanical losses varying between 24% and 57% of the measured indicated power in the engine, depending on several variables such as working fluid, mean pressure and cycle frequency. Similar figures are suggested for the General Motors 4L23 engine. Makhkamov and Ingham [151], who consider mechanical losses in an experimental solar thermal Stirling engine further corroborate this. As these

can essentially be considered high-performance engines that were subject to considerable development, we can reasonably take these figures as representative of state of the art. The actual indicated power is usually significantly below the ideal indicated power calculated from the classical thermodynamics treatment of the cycle. The cycle efficiency is consequently significantly degraded from the Carnot value inherent in the ideal analysis. Walker suggests a factor of 0.5 as a reasonable estimate of the difference between the two [58, 57]. This is corroborated by Urieli and Berchowitz [91] through comparison of experimental data for the Ford-Philips 4-215 engine and the GM GPU-3 with an ideal isothermal analysis. If we proceed on this assumption, and assume also a mean value for the mechanical losses of 30%, then we can say that the friction power losses for the Stirling for the FTT analysis are approximately 15% of the ideal cycle work, or $W_{\mathrm{f}} = 0.15(W_{\mathrm{rev}})$. This information therefore permits the calculation of μ_{s} for the Stirling cycle engine as per Equation (5-66).

In conjunction with μ, it is required to calculate mean piston velocity for the Stirling cycle. Mean piston velocity, $\bar{v}_{\mathrm{p}}$ is related to the cycle frequency through:

$$\bar{v}_p = 2x_{\mathrm{s}}f \tag{5-67}$$

Both μ_s an $\bar{v}$ are dependent on the stroke, x_{s}. In the Stirling engine, cycle volume changes are achieved through the complimentary movement of two working pistons, as in the α-type engine, or a piston and displacer, as in the β- and γ-type engines. In the case of the β- and γ-type engines, the stroke of the cycle can be defined simply as the stroke of the power piston, as the displacer space operates as a constant volume. In the case of the two-piston α-type engines, the relative displacements of the two working volumes at any given

time make the definition of a stroke more difficult from a kinematic point of view than for a single piston cycle such as the Otto or Diesel cycles. Pressure is generally assumed instantaneously uniform across the working chambers, however, so that we can assume, in a twin piston engine at least, that friction effects are divided equally between the two working pistons. This allows us to simplify analysis; it is proposed here to develop an effective stroke, $x_{\mathrm{S,eff}}$ and subsequent compression ratio, R_v, by considering the total cycle volume variations as being realised by one operating piston-cylinder configuration and by considering the dead volume within the cycle as being analogous to a clearance volume in this hypothetical single cylinder configuration. This is shown in Figure 5.2 (a), which offers a *pV–pX* diagram for an ideal Stirling cycle and Figure 5.2 (b), which shows the realisation of the total volume in the Rhombic drive mechanism. The dead volumes in the heat exchangers and cylinders can be gathered into one effective volume and arranged to allow calculation of an effective clearance distance:

$$x_{\mathrm{D}} = \frac{4V_{\mathrm{D}}}{\pi d^2} \tag{5-68}$$

where d is the cylinder bore. The cycle has a compression ratio, R_v that can thus be expressed as:

$$R_v = \frac{x_{\mathrm{S,eff}} + x_{\mathrm{D}}}{x_{\mathrm{D}}} \tag{5-69}$$

It is straightforward to express the effective stroke, $x_{\mathrm{S,eff}}$ as:

$$\mathrm{x_{S,eff}} = \mathrm{x_D}(R_v - 1) \tag{5-70}$$

where $x_D$is the clearance depth in the cylinder. This effective stroke is then used to compute μ_s and $\bar{v}$ as previously described.

5.2.7.2 Pumping Losses

In addition to the global friction losses, the use of heat exchangers in the Stirling cycle engine results in pumping losses arising from the pressure losses inherent in fluid flow in the heat exchanger tubes and the regenerator matrix. Flow acceleration losses are also pertinent to the regenerator matrix. Martini [98] provides simplified relationships to quantify the pressure drops in each of the heat exchangers.

Considering the regenerator, pressure losses associated with flow through the mesh screens can be divided into flow acceleration losses and core friction losses. Furthermore, the flow acceleration losses will be different at different points in the cycle depending on whether the gas is flowing to or from the heated space. It is therefore necessary to consider the losses as divided between two processes; a) flow of the gas from hot space to cold space and b) flow from cold space to hot space. Assuming gas flow in the engine approximates that which occurs in the ideal cycle, it is possible to assume that each process occurs once during the complete cycle, so that the cumulative effects over the full cycle are the algebraic sum of the losses on each pass.

a) Flow from hot to cold side:

$$\Delta p_{\mathrm{H-C}} = \frac{G_R^2}{2}\left[\frac{1}{\rho_{\mathrm{H}}}(1+\sigma^2)(\psi-1) + \frac{C_{f,\mathrm{R}} L_{\mathrm{R}}}{R_H \rho_{\mathrm{R}}}\right] \tag{5-71}$$

b) Flow from cold to hot side:

$$\Delta p_{C-H} = \frac{G_R^2}{2}\left[\frac{1}{\rho_C}(1+\sigma^2)\left(\frac{1}{\psi}-1\right) + \frac{C_{f,R} L_{\mathrm{R}}}{R_{\mathrm{H}} \rho_{\mathrm{R}}}\right] \tag{5-72}$$

where $\sigma = \frac{A_{ff,R}}{A_{fr,R}}$, $\psi = \frac{\rho_H}{\rho_C}$. and R_H is the hydraulic radius of the regenerator matrix and is a function of the mesh porosity, ϕ, and the heat transfer area per unit volume of the exchanger:

$$R_H = \frac{\phi}{A_{vol}} \tag{5-73}$$

The total pressure loss for flow through the regenerator can therefore be summarised as:

$$\Delta p_{regen} = \Delta p_{H-c} + \Delta p_{c-H} \tag{5-74}$$

$$\Delta p_{regen} = \frac{G_R^2}{2}(1+\sigma^2)\left[\frac{1}{\rho_H}(\psi - 1) + \frac{1}{\rho_c}\left(\frac{1}{\psi} - 1\right)\right] + \left[\frac{C_{f,R} G_R^2 L_R}{R_H \rho_R}\right] \tag{5-75}$$

The pressure losses in the heater and cooler can similarly be computed:

$$\Delta p_{heater} = \left(\frac{2C_{f,H} {G_H}^2 L_H}{d_{i,H}\rho_H}\right) \tag{5-76}$$

$$\Delta p_{cooler} = \left(\frac{2C_{f,c} {G_c}^2 L_c}{d_{i,c}\rho_c}\right) \tag{5-77}$$

where in each case C_f is the friction factor, which is a function of the Reynolds number, L is the heat exchanger length, d_i is the internal diameter of the heat exchanger tube in question and ρ is the gas density in the given space. Correlations for C_f for the stacked screens usually used in Stirling engines are provided by Martini. The Reynolds number for flow through the regenerator matrix can be computed as:

$$Re_R = \frac{4R_H G_R}{\mu} \tag{5-78}$$

The Reynolds correlation for the heater and cooler is given by Equation (5-54). G is the mass velocity and is calculated in a manner similar to Equation (5-51). When considering the pressure drop in the regenerator, G becomes:

$$G_{\mathrm{R}} = \frac{\dot{m}_{\mathrm{R}}}{A_{\mathrm{ff,R}}} \tag{5-79}$$

The pumping power loss associated with these pressure drops are computed with knowledge of the volumetric flowrate of the fluid in each space:

$$P_{\mathrm{p}} = \Delta p Q \tag{5-80}$$

By considering the volume flow rate $Q = Av$ and by substituting $\dot{m}_{\mathrm{R}} = \rho_{\mathrm{R}} A_{\mathrm{R}} v_{\mathrm{R}}$ the power dissipated in the regenerator heat exchanger can be demonstrated to be proportional to the cube of the fluid velocity. For the flow acceleration losses:

$$P_{\mathrm{p,flow\,acc}} = \left[(1+\sigma^2)\left[\frac{1}{\rho_{\mathrm{H}}}(\psi - 1) + \frac{1}{\rho_{\mathrm{c}}}\left(\frac{1}{\psi} - 1\right)\right]\left(\frac{\rho_{\mathrm{H}}^3}{\rho_{\mathrm{R}}}\right)\left(\frac{A_p^3}{A_{\mathrm{ff,R}}^2}\right)\right] v_p^3 \tag{5-81}$$

and for the core friction pumping losses:

$$P_{p,\mathrm{core}} = \left[\frac{\rho_R C_{\mathrm{f,R}} L_{\mathrm{R}} A_{\mathrm{ff,R}}}{R_{\mathrm{H}}}\right] v_p^3 \tag{5-82}$$

Such that the pumping losses in the regenerator can be expressed as:

$$P_{\mathrm{p,regen}} = \left[(1+\sigma^2)\left[\frac{1}{\rho_{\mathrm{H}}}(\psi - 1) + \frac{1}{\rho_{\mathrm{c}}}\left(\frac{1}{\psi} - 1\right)\right]\left(\frac{\rho_{\mathrm{H}}^3}{\rho_{\mathrm{R}}}\right)\left(\frac{A_p^3}{A_{\mathrm{ff,R}}^2}\right) + \frac{\rho_{\mathrm{R}} C_{\mathrm{f,R}} L_{\mathrm{R}} A_{\mathrm{ff,R}}}{R_{\mathrm{H}}}\right] v_p^3 \tag{5-83}$$

where the substitution:

$$v_{\mathrm{R}} = \frac{\rho_{\mathrm{H}} A_{\mathrm{p}}}{\rho_{\mathrm{R}} A_{\mathrm{R}}} \bar{v}_p \tag{5-84}$$

is made to express the flow in the regenerator in terms of the mean piston speed. Flow through the regenerator is understood to be through the free flow area of the mesh and not the full tube area, as might be used for standard tube flow conditions. The free-flow area of the regenerator mesh can be computed with knowledge of the frontal area of the mesh, when the porosity of the mesh is known:

$$A_{\mathrm{fr,R}} = A_{\mathrm{R}}(1-\phi) \tag{5-85}$$

A_{R} is the cross sectional area of the regenerator. Consequently:

$$A_{\mathrm{ff,R}} = A_{\mathrm{R}} - A_{\mathrm{fr,R}} \tag{5-86}$$

Similarly for the hot side heat exchanger, the pumping power losses are:

$$P_{\mathrm{p,heater}} = 2C_{\mathrm{f,H}}L_{\mathrm{H}}\rho_{\mathrm{H}}\pi d_{i,\mathrm{H}}{v_{\mathrm{H}}}^3 \tag{5-87}$$

and for the cooler:

$$P_{\mathrm{p,cooler}} = 2C_{\mathrm{f,c}}L_{\mathrm{c}}\rho_{\mathrm{c}}\pi d_{i,\mathrm{c}}{v_{\mathrm{c}}}^3 \tag{5-88}$$

Considering the power losses as a grouped fluid power loss term:

$$P_{\mathrm{pump}} = P_{\mathrm{p,regen}} + P_{\mathrm{p,heater}} + P_{\mathrm{p,cooler}} \tag{5-89}$$

it is possible to express the velocities in each of the heat exchanger spaces in terms of the piston velocity, $\bar{v}_{\mathrm{p}}$ by arranging the mass continuity equations in each space to give:

$$v_{\mathrm{H}} = \frac{A_p}{A_{\mathrm{H}}}\bar{v}_p \tag{5-90}$$

$$v_{\mathrm{c}} = \frac{\rho_{\mathrm{R}}A_p}{\rho_{\mathrm{c}}A_{\mathrm{c}}}\bar{v}_p \tag{5-91}$$

so that the total pumping power term can be summarised as:

$$\begin{aligned} P_{\mathrm{pump}} = \Bigg\{\Bigg[(1+\sigma^2)\left[\frac{1}{\rho_{\mathrm{H}}}(\psi-1)+\frac{1}{\rho_{\mathrm{c}}}\left(\frac{1}{\psi}-1\right)\right]\left(\frac{\rho_{\mathrm{H}}^3}{\rho_{\mathrm{R}}}\right)\left(\frac{A_p^3}{A_{\mathrm{ff,R}}^2}\right) \\ + \frac{\rho_R C_{\mathrm{f,R}} L_R A_{ff,R}}{R_H}\Bigg] + 2C_{\mathrm{f,H}}L_{\mathrm{H}}\rho_{\mathrm{H}}\pi d_{i,\mathrm{H}}\left(\frac{A_p}{A_{\mathrm{H}}}\right) \\ + 2C_{\mathrm{f,C}}L_{\mathrm{c}}\rho_{\mathrm{R}}\pi d_{i,\mathrm{c}}\left(\frac{A_p}{A_{\mathrm{c}}}\right)\Bigg\}\bar{v}_p^3 \end{aligned} \tag{5-92}$$

5.2.8 Irreversible Cycle Power Output

The power output of the engine can be expressed as the irreversible power less the dissipated frictional power and the pumping power losses:

$$P_{\mathrm{irrev}} = P_{\mathrm{I}} - P_{\mu} - P_{\mathrm{pump}} - \dot{Q}_{\mathrm{cond}} - \dot{Q}_{\mathrm{e}} \tag{5-93}$$

5.2.9 Irreversible Cycle Efficiency

The efficiency is therefore calculated as:

$$\eta_{\text{Total}} = \frac{P_{\text{irrev}}}{\dot{Q}_{\text{in}}} \tag{5-94}$$

where $\dot{Q}_{\text{in}} = Q_{\text{in}}/\tau$. These equations provide the parabolic curves for power and efficiency against compression ratio, as well as the loop shape power against efficiency graph common to all practical heat engines.

5.3 Conclusions

An FTT model of the Stirling cycle has been developed and presented in this chapter. The model incorporates elements common to the FTT method used for other heat engine cycles but not previously used for the Stirling cycle engine. In particular, a method for calculating global friction losses within the engine is described. Similarly, a new method for including pumping power losses in the engine heat exchangers is described. A numerical study is provided in the next chapter.

6 VALIDATION OF THE STIRLING CYCLE FINITE TIME THERMODYNAMICS MODEL

6.1 Introduction

In this chapter the FTT model of the Stirling cycle engine developed in Chapter 5 is validated using engine specifications and experimental test data available in the literature. The effectiveness of the FTT modelling method for prediction of basic performance parameters such as brake power and brake efficiency is assessed. Engine simulation is performed using the model, and the results compared to experimental data presented in the literature.

6.2 Methodology

The methodology adopted for the validation of the FTT Stirling cycle model comprises use of the specific engine geometric specifications in the model, simulation of the engine operation using these specifications and subsequent comparison of performance results with published experimental results for the same engine. The model is validated using specifications for the General Motors GPU-3 Stirling engine operating with helium as the working gas over a range of operating speeds, Figure 6.1. As with the validation procedure for the Otto cycle model presented previously, a number of criteria for comparison of the FTT model with the experimental results are desirable; however, due to the limited quantity of data available concerning experimental performance of the engine, available criteria for comparison were more limited than for the Otto cycle model. The primary data available were the brake power and brake-efficiency of the engine over the given operational speed range; therefore, comparison of

the FTT model with the experimental data focused on these as the basis for the validation.

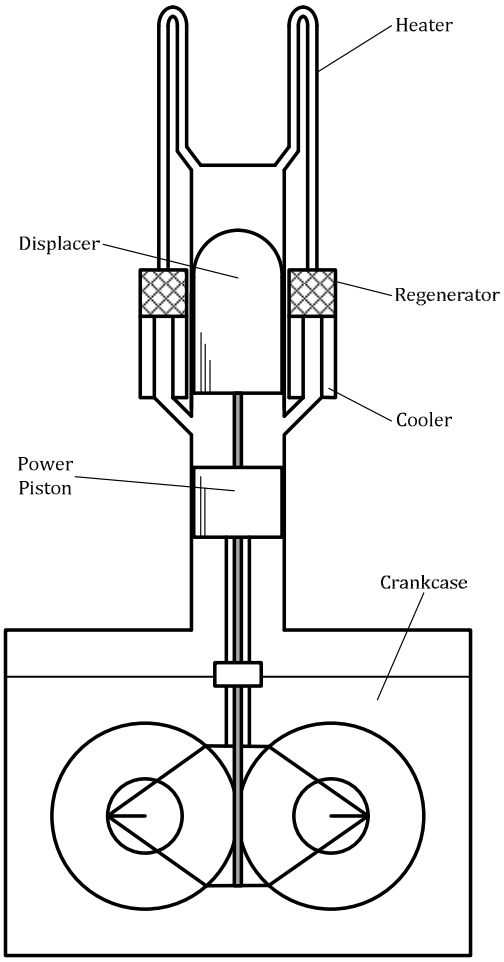

Figure 6.1 GPU-3 Stirling engine configuration

Central to the analysis was the modelling of the heat exchangers. The Stirling cycle engine has three main heat exchangers, connected in series, which enable realisation of the thermodynamic cycle. The FTT model utilises heat exchanger effectiveness as a specified parameter for each of the exchangers. For the validation procedure, it was necessary to model the heat exchangers to gain insight into the variation of the effectiveness over the full operating speed range of the engine. The analytical expressions for this are detailed in Chapter 5.

These expressions are utilised here with the geometric, thermodynamic and heat balance data available from the literature.

6.3 The General Motors GPU-3 Stirling Engine Specifications

The geometric specifications for the GPU-3 engine are presented in Table 6.1. Table 6.2 presents detailed specification of the dead volumes within the engine. The data is reproduced from the extensive reports compiled by Martini [98] and Thieme [152]. These data represent the most detailed description of a functioning experimental Stirling engine available in the literature and consequently have been used numerous times for analysis and validation of various thermodynamic models [91, 148, 153].

6.4 Modelling of the GPU-3

6.4.1 Working Gas Properties

The properties of all fluids utilised in the simulation are detailed in Table 6.3. The working fluid is helium; water is used as coolant on the cold side of the engine, and the combustion gases are modelled as heated-air at the specified temperature. The source and sink are approximated as isothermal, as are the hot and cold spaces of the gas. Gas properties for the heater were approximated at a temperature of 600 K, corresponding to an approximated mean temperature between the source temperature and the ambient temperature. On the cooler side, gas properties were approximated at a temperature of 290 K, which represents a rounding up of the cold gas temperature. This was done to enable expedient reference to tabulated data.

6.5 Polynomial Expressions for Imposed Parameters

As for the Otto cycle engine, the FTT model for the Stirling engine is simplified by the inclusion of fitted polynomial curves for specified parameters to the model. In this case, the cycle heat addition is specified from a fitted polynomial curve. This procedure offers the advantage of allowing interpolative simulation of the model outside the specified values. Extrapolative simulation is also possible, although as will be seen in a later section, caution is advised as the model is sensitive to variation in the fitting of the polynomial. The engine is simulated in four loading regimes corresponding to different mean cycle pressure values. The values for mean cycle pressure used were 2.76 MPa, 4.14 MPa, 5.52 MPa and 6.9 MPa. The fitted polynomials for the experimentally measured heat addition for each case are detailed in the following section.

6.5.1 Heat Input—Fitted Polynomial Curves for Experimental Data

Figure 6.2 shows the experimentally measured heat input to the GPU-3 engine for all cases of mean cycle pressure. The fitted polynomial curves for each set of experimental data are shown also.

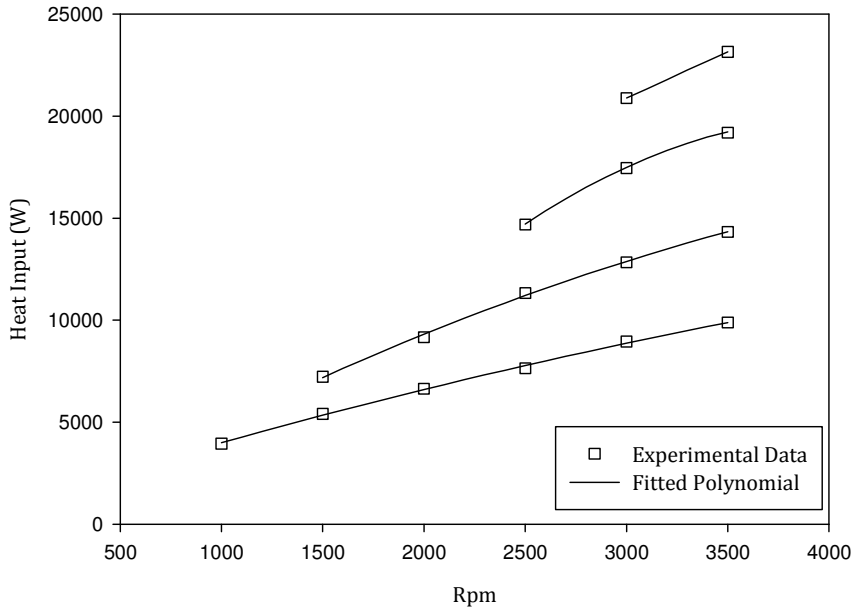

Figure 6.2 Experimentally measured heat addition to GPU-3 Stirling engine with fitted polynomials for various mean cycle pressure values

The polynomial expression for the 2.76 MPa case is:

$$\dot{Q}_{in@2.76MPa} = [-0.0006f^2 + 0.1864f + 1.051] \times 10^3 \quad (6\text{-}1)$$

The polynomial is a function of the cycle frequency, f, in units of Hz. Similarly, the polynomial expressions for each of the remaining regimes are:

$$\dot{Q}_{in@4.14MPa} = [-0.0016f^2 + 0.3478f + 0.5069] \times 10^3 \quad (6\text{-}2)$$

$$\dot{Q}_{in@5.52MPa} = [-0.0074f^2 + 1.011f + 14.56] \times 10^3 \quad (6\text{-}3)$$

$$\dot{Q}_{in@6.9MPa} = [0.2724f^2 + 7.26] \times 10^3 \quad (6\text{-}4)$$

Table 6.1 GM GPU-3 engine dimensions

[98]

Specifications	**Value**
Heater	
Mean tube length (cm)	24.53
Heat transfer length (cm)	15.54
Cylinder tube (cm)	11.64
Regenerator tube (cm)	12.89
Tube inside diameter (cm)	0.302
Tube outside diameter (cm)	0.483
No. tubes per cylinder	40
No. tubes per regenerator	5
Cooler	
Tube length (cm)	4.61
Heat transfer length (cm)	3.55
Tube inside diameter (cm)	0.108
Tube outside diameter (cm)	0.159
No. tubes per cylinder	312
No. tubes per regenerator	39
Regenerators	
Length (inside) (cm)	2.26
Diameter (inside) (cm)	2.26
No. per cylinder	8
Material	Stainless steel wire cloth
No. wires, per cm	79 x 79
Wire diameter (cm)	0.004
No. layers	308
Filler factor, (%)	30.3

Angle of rotation between adjacent screens (deg)	5
Mesh porosity	0.8
Cold End Connecting Ducts	
Length (cm)	1.59
Duct inside diameter (cm)	0.597
No. ducts per cylinder	8
Cooler end cap (cm^3)	0.279
Drive	
Connecting rod length (cm)	4.6
Crank radius (cm)	1.38
Eccentricity (cm)	2.08
Miscellaneous	
Cylinder bore at liner (cm)	6.99
Cylinder bore above liner (cm)	7.01
Displacer rod diameter (cm)	0.952
Piston rod diameter (cm)	2.22
Displacer diameter (cm)	6.96
Displacer wall thickness (cm)	0.159
Displacer stroke (cm)	3.12
Expansion space clearance (cm)	0.163
Compression space clearance (cm)	0.03
Buffer space maximum volume (cm^3)	521
Total working space minimum volume (cm^3)	233.5

Table 6.2 GM GPU-3 engine dead volumes

[98]

Specifications—Engine Dead Volume	**Value (cm^3)**
Heater	
Insulated portion of heater tubes next to expansion space	9.68
Heated portion of heater tubes	47.46
Insulated portion of heater tubes next to regenerator	13.29
Additional volume in four heater tubes used for instrumentation	2.74
Volume in header	7.67
Total	**80.8**
Cooler	
Volume in cooler tubes	13.13
Regenerators	
Entrance volume into regenerator	7.36
Volume within matrix and retaining disks	53.4
Volume between regenerators and coolers	2.59
Volume in snap ring grooves at end of coolers	2.18
Total	**65.5**
Expansion Space Clearance Volume	
Displacer clearance (around displacer)	3.34
Clearance volume above displacer	7.41
Volume from end of heater tubes into cylinder	1.74
Total	**12.5**
Compression Space Clearance Volume	
Exit volume from cooler	3.92

Volume in cooler end caps	2.77
Volume in cold end connecting ducts	3.56
Power piston clearance (around power piston)	7.29
Clearance volume between displacer and power piston	1.14
Volume at connections to cooler end caps	2.33
Volume in piston "notches"	0.06
Volume around rod in bottom of displacer	0.11
Total	**21.18**
Total dead volume	193.15
Minimum live volume	39.18
Calculated minimum total working space volume	**232.3**
Measured value of minimum total working space volume (by volume displacement)	233.5
Change in working space volume due to minor engine modification	2.5
Total	**236.0**

Table 6.3 Working fluid properties GM GPU-3

Specifications	**Value**
Gas	
Working Gas	Helium
System Temperatures	
Source temperature (K)	1100
Hot side gas temperature (K)	922
Sink temperature (K)	286
Cold side gas temperature (K)	286

Ambient temperature (K)	293
Properties—Helium	
Specific heat capacity, constant volume C_v (J/kgK)	3120
Specific heat capacity, constant pressure c_p (J/kgK)	5197
Specific gas constant, R (J/kgK)	2077
Kinematic viscosity, ν (@600K) (m^2/s)	394×10^{-6}
Prandtl number, Pr_{helium}	0.676
Conductivity, k (@600K) (W/mK)	252×10^{-3}
Conductivity, k (@290K) (W/mK)	149×10^{-3}
Dynamic viscosity, μ (@600K) (Ns/m^2)	320×10^{-7}
Dynamic viscosity, μ (@290K) (Ns/m^2)	195×10^{-7}
Properties—Air	
Specific heat capacity, constant pressure c_p (J/kgK)	1120
Prandtl Number, Pr_{air} (1100K)	0.72
Properties – Water	
Specific heat capacity, (J/kgK)	4198
Prandtl number, Pr_{water} (286K)	8.8

6.5.2 Combustion Mass Flowrate

In order to compute the effectiveness of the hot side heat exchanger, knowledge of the mass flowrate of combustion gases is required. Only a limited quantity of data was available in the literature; therefore it was necessary to develop a reasonable approximation to proceed. This was done by rearranging the first law heat equation to specify the mass flowrate as the subject. Assuming the combustion gas flow to be an open, steady flow system with negligible kinetic and potential energy changes and also assuming that the gas is cooled completely to ambient temperature, the expression becomes:

$$\dot{m}_{\text{comb}} = \frac{\dot{Q}_{\text{in}}}{\left[c_{p,\text{air}}(T_{\text{source}} - T_{\text{amb}})\right]} \tag{6-5}$$

where $\dot{Q}_{\text{in}}$ is the heat addition to the cycle, $c_{p,\text{air}}$ is the specific heat capacity at constant pressure of the hot combustion gases, approximated as air at the combustion temperature. T_{source} and T_{amb} are the combustion and ambient temperatures respectively. Figure 6.3 shows the computed mass flowrate for each of the mean pressure regimes specified. For this case, the heat input polynomials used were those presented previously, whilst the specific heat capacity and system temperatures are as specified in Table 6.3.

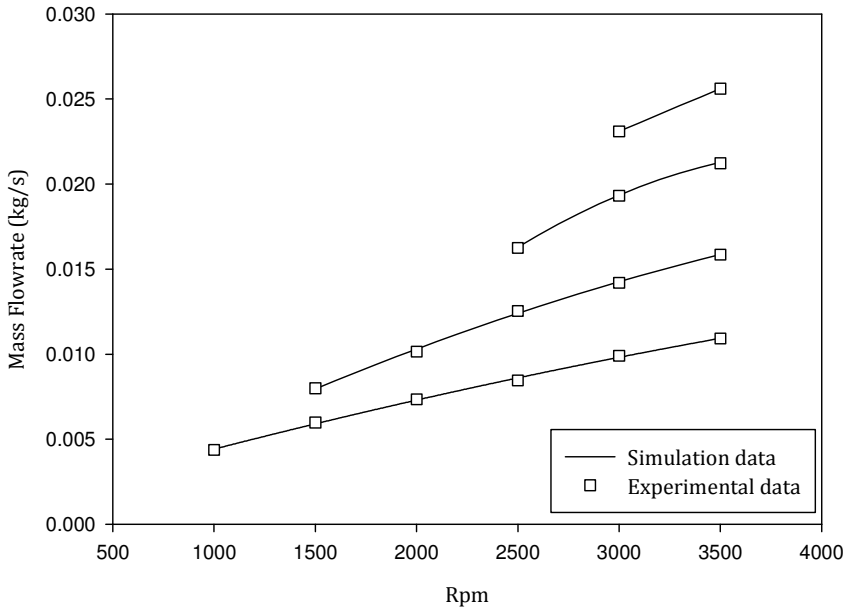

Figure 6.3 Calculated combustion mass flowrate using fitted polynomial expressions for the heat input

6.6 Schmidt Analysis

6.6.1 Specification of Dimensionless Parameters

Consideration of the engine specifications and dead volumes presented in Table 6.1 and Table 6.2, along with the analytical expressions for the kinematic motion of the working pistons given in the preceding chapter, permit calculation of the swept volume ratio and the dead volume ratio for use in the Schmidt analysis. The temperature ratio can be calculated from the source and sink temperatures given in Table 6.3 and the phase angle is provided in the literature [91]. These data are summarised in Table 6.4. The output parameter of concern with the Schmidt style model is the cyclic work performance of the engine. This is computed as per the analytical expression, Equation (5-21), given in Chapter 5.

This work expression gives the work output of the ideal cycle for the given engine geometry with consideration of the lost work inherent in the use of the continuous piston motion. The ratio of this work output to the ideal air standard cycle work output gives the loss ratio, N_L. These parameters are given in Table 6.4 also.

6.7 Calculation of Heat Exchanger Parameters

6.7.1 Hot Side Heat Exchanger

In order to offer an approximate characterisation of the hot side heat exchanger performance, it is necessary to make several simplifying assumptions concerning the behaviour of the gases interacting across the exchanger. These assumptions can be summarised as follows:

1) The heat exchanger geometry is simplified to that presented in Figure 6.4. The heat exchanger is assumed to be a gas-to-gas un-finned circular tube bank compact heat exchanger.

2) Heat transfer from the combustion gases to the tube exterior walls is one dimensional and occurs normal to the transfer surface.

3) The frontal area of the individual heater tubes, A_{fr}, is calculated as the product of the outside diameter of the tubes, $d_{t,h}$, and the heat transfer length of the tube, $L_{t,h}$, as seen in Figure 6.4 (c).

4) The free flow area of the combustion gas through the tube bank is calculated as the difference between the total frontal area of all tubes and the surface area of a hypothetical cylinder of radius R_{HEX} which represents a plane passing through the central axis of the tube-passes, as shown in

Figure 6.4 (a). The free flow area, A_{ff}, around individual tubes is simply the total area divided by the number of tubes. It is assumed to be divided equally around the tube as shown in Figure 6.4 (c).

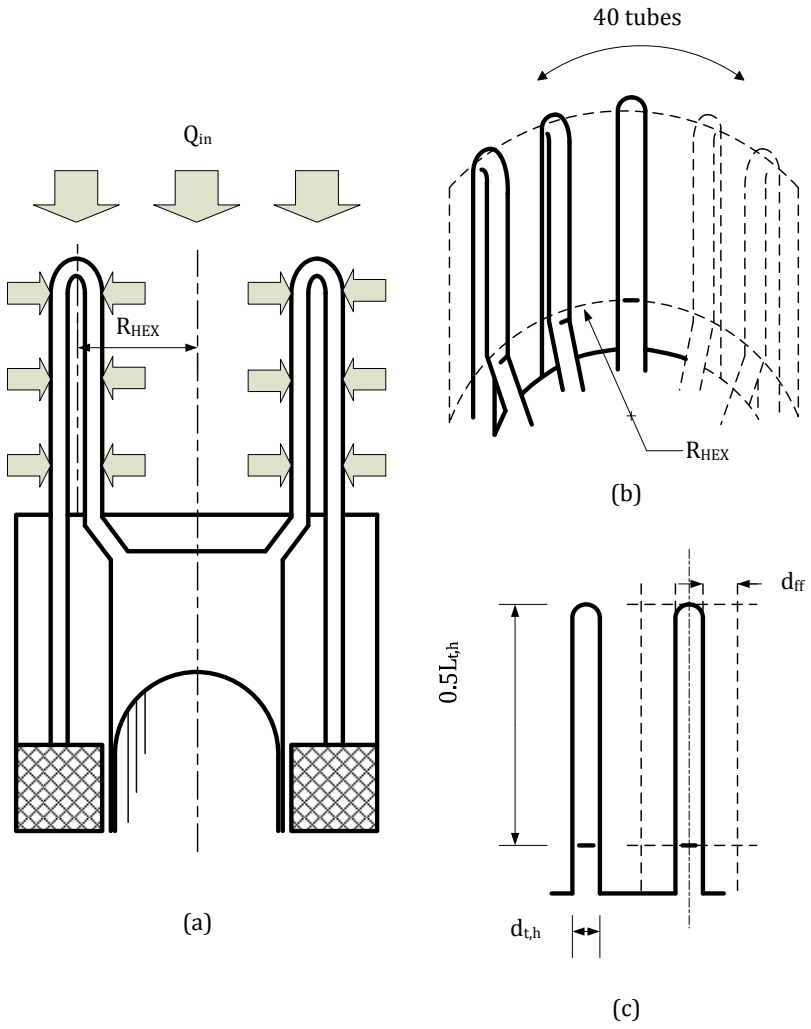

Figure 6.4 Hot side heat exchanger arrangement

(a) assumption of heat transfer normal to transfer surface (b) frontal area plane

(c) dimensions for calculation of frontal area and free-flow area

Table 6.4 Results of Schmidt analysis, GPU-3, 2.76 MPa

Dimensionless Parameter	**Value**
Dead volume ratio, χ	1.93
Swept volume ratio, κ	0.95

Temperature ratio, τ		0.3102		
Phase angle, α		1.9		
Mean cycle pressure (MPa)	2.76	4.14	5.52	6.9
Cycle work, W_{Schmidt} (J)	107	160	213	267
N_{L}	0.3021	0.3021	0.3021	0.3021

For the GPU-3 engine, R_{HEX} is not explicitly available and must be estimated by scaling from the schematics provided in the published data. When this was done the value determined for R_{HEX} was 0.07 m. A_{ff} was then computed to be 0.0191m^2 for the given assumptions.

The Colburn j_{H} value is dependent on the Reynolds number and is computed from analytical expressions available in the literature [153]:

$$\text{Re} \leq 3000 \qquad j_{\text{H}} = \exp(0.337 - 0.812\log(\text{Re})) \tag{6-6}$$

$$3000 \leq \text{Re} \leq 4000 \qquad j_{\text{H}} = 0.0021 \tag{6-7}$$

$$4000 \leq \text{Re} \leq 7000 \qquad j_{\text{H}} = \exp(13.31 + 0.861\log(\text{Re})) \tag{6-8}$$

$$7000 \leq \text{Re} \leq 10000 \qquad j_{\text{H}} = 0.0034 \tag{6-9}$$

$$10000 \leq \text{Re} \qquad j_{\text{H}} = \exp(-3.575 - 0.229\log(\text{Re})) \tag{6-10}$$

These assumptions are then employed in the analytical expressions given in Chapter 5 to determine the hot side heat exchanger effectiveness and NTU.

6.7.2 Cold Side Heat Exchanger

Similar to the hot side heat exchanger, several simplifying assumptions are made for the characterisation of the cold side heat exchanger. These can be summarised as follows.

1) The heat exchanger geometry is simplified to that presented in Figure 6.5.

2) The cooler is a gas-to-liquid un-finned circular tube bank compact heat exchanger with all heat exchange assumed to be one dimensional and occurring normal to the heat transfer area.

3) The frontal area of the individual heater tubes, A_{fr} is calculated as the product of the outside diameter of the tubes, $d_{t,c}$ and the heat transfer length of the tube, $L_{t,c}$ as seen in Figure 6.5 (c)

4) The free flow area of the combustion gas through the tube bank is calculated as the difference between the total frontal area of all tubes and the surface area of a hypothetical cylinder of diameter d_{regen}, which represents a plane passing through the central axis of the tubes, similar in principle to the method employed for the heater tubes. The free flow area, A_{ff} around individual tubes is simply the total divided by the number of tubes at the circumference of the tube bank. Complex flow through the tube bank is not accounted for.

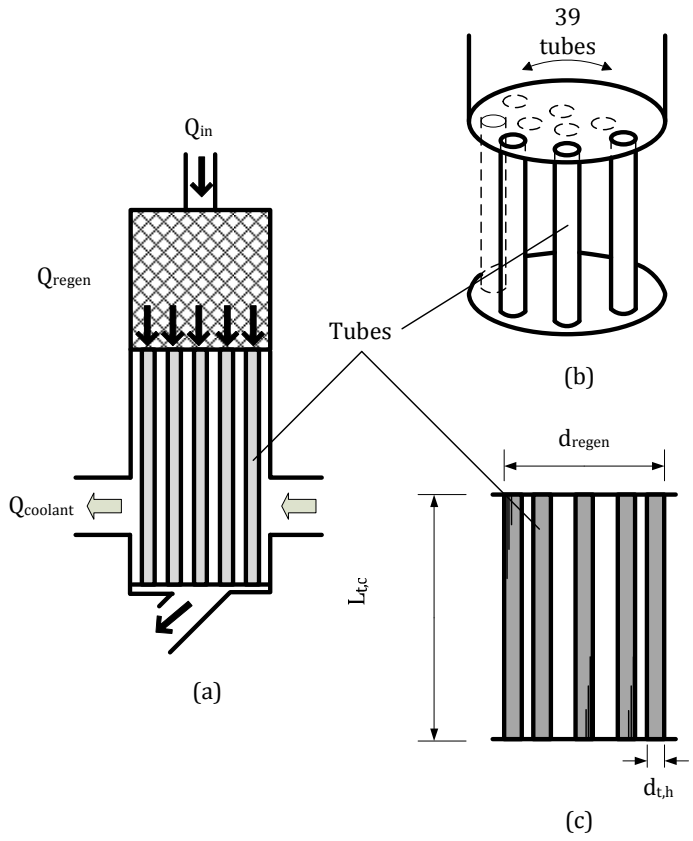

Figure 6.5 Cold side heat exchanger arrangement

(a) Regenerator and Cooler layout (b) gas tube bank (c) dimensions for calculation of frontal area and free-flow area

Calculation of the Colburn j_H value for the compact heat exchanger is done in the same manner as for the heater tube bank. The heat exchanger NTU and effectiveness can then be calculated using the analytical expressions presented in Chapter 5.

6.8 Dynamic Losses - Global Friction Losses

6.8.1 Calculation of Friction Coefficient at Different Mean Pressure Values

The general method for calculation of the friction coefficient is detailed in the preceding chapter. Consultation of the experimental data however

demonstrates that the proportion of the heat added to the cycle that is ultimately lost to mechanical friction in the system is not constant for different operating loads. A decline in the proportion is noted for increasing mean cycle pressure. As indicated in the previous chapter, this mechanical friction loss proportion is calculated using an expression of the form:

$$W_{\mathrm{f}} = N_{\mathrm{ml}} W_{\mathrm{REV}} \tag{6-11}$$

where N_{ml} is an empirical coefficient relating to the mechanical losses, and $0 < N_{\mathrm{ml}} < 1$. For the simulation using the FTT model it was therefore necessary to specify values of N_{ml} for each of the mean cycle pressure regimes under investigation. These values were obtained from the experimental data presented by Thieme [152, 154], Thieme and Tew [155] and Martini [98]. Energy balance tests on the engine completed by Thieme [152] indicate that the mechanical losses in the system decrease as a proportion of the heat input with increasing mean cycle pressure. Therefore, if it is assumed that the reversible thermodynamic cycle work of the engine increases linearly with the heat addition to the cycle, it can be said that N_{ml} decreases with increasing mean cycle pressure. The values of N_{ml} used in the present simulation are given in Table 6.5. Due to a lack of comprehensive data in the literature, it was necessary to approximate the values for cases of mean cycle pressure 4.14 MPa and 5.52 MPa. This was done using a trial and error process of values between those given for the 2.76 MPa and 6.9 MPa cases to approximate the known Brake Power curve for the engine. The values for the friction loss coefficient computed as a result of this analysis for the GPU-3 engine are presented in Table 6.5 also.

6.8.2 Calculation of Pumping Loss Coefficient at Different Mean Pressure Values

The fluid pumping loss coefficient, α_p is calculated for the GPU-3 engine as per the analytical expression derived in the previous chapter. The values for this coefficient for each mean cycle pressure regime are presented in Table 5-5. The values of α_p are given as exponential functions of the engine rotational speed due to the presence of the frictional loss coefficients used for the heat exchanger tubes. These coefficients are functions of the Reynolds number of the working gas in each heat exchanger and therefore must be accommodated across the operational speed range. The expressions are taken from fitted curves applied to the model data.

Table 6.5 Static and dynamic loss terms used in simulation

Mean cycle pressure (MPa)	2.76	4.14	5.52	6.9
Parameter				
Friction loss coefficient, N_{ml}	0.15	0.1	0.075	0.05
Conduction Loss, Q_{cond} (W)	500	500	500	500

6.9 Static Losses—Conduction and Exhaust Stack Loss

6.9.1 Conduction Losses

Conduction losses through the engine are considered a static loss on the system. Thieme [152] indicates that for a given source temperature the conduction losses remain approximately constant through the engine for different loads and operating frequencies. The magnitude of this loss could therefore be

approximated for the GPU-3 engine under the given operating source and sink temperatures from energy balance data provided from experimental data.

The estimated conduction loss values for the given temperature regime taken from the experimental data are given in Table 6.5. As with the mechanical friction loss terms there was some variation of the term required over the various mean cycle pressures. In particular it can be seen that the conduction losses are slightly higher at lower cycle pressure values. As with the mechanical loss coefficient, the intermediate values for the cases of 4.14 MPa and 5.52 MPa mean cycle pressures were estimated due to absence of experimental data.

6.9.2 Exhaust Stack Losses

As detailed in the previous chapter, quantification of the exhaust stack loss term is reliant on the experimental data available in the literature. For the current simulations therefore, the exhaust losses are quantified as:

$$\dot{Q}_{\text{exhaust}} = N_{ex}\dot{Q}_{\text{in}} \tag{6-12}$$

where$N_{ex} \cong 0.3$.

6.10 Results of Simulation and Comparison with Experimental Data—Helium Working Gas

This section presents the main body of results gained from the FTT simulation and compares them with the body of experimental data available from the literature. The section is divided into subsections pertaining approximately to the simulation of the heat exchanger components and then to the overall performance of the engine. Heat exchanger performance is analysed through the computation of the effectiveness over the range of operating frequencies for each of the three heat exchangers used in the system. Of interest when

computing the heat exchanger effectiveness are the Reynolds numbers for the gas in each of the heat exchangers and the subsequent calculation of the convective heat transfer coefficients for the fluids interacting across each exchanger. Results for the calculation of these parameters using the analytical expressions presented in the previous chapter are analysed in this section also. The analysis of the heat exchangers extends to the computation of the irreversibility parameter, I_R. Results for the computation of this parameter are provided also.

Overall engine performance is analysed using the brake power output and the brake thermal efficiency. These are compared against the known experimental values. Percentage difference values are given for the brake power and brake thermal efficiency values to indicate the fidelity of the FTT model to the actual engine performance.

6.10.1 Heat Exchanger Reynolds Numbers

Computation of the Reynolds numbers for the fluids in heat exchangers is necessary for the computation of the convective heat transfer coefficients, the subsequent calculation of the overall heat transfer coefficients (U-values) and ultimately the computation of the heat exchanger effectiveness. The results for the computation of the Reynolds numbers for the combustion gas and the oscillating flow in the hot side heat exchanger are presented in Figure 6.6 and Figure 6.7 respectively. The Reynolds number for flow in the regenerator is plotted in Figure 6.8, whilst the Reynolds number for the oscillating flow of the working gas in the cold side heat exchanger is plotted in Figure 6.9. The Reynolds number of the coolant is not plotted as, due to the constant mass flowrate of the cooling water, the Reynolds number holds a constant value of

Re = 95. The exponential rise of the Reynolds number in the oscillating flow regimes is notable in the figures.

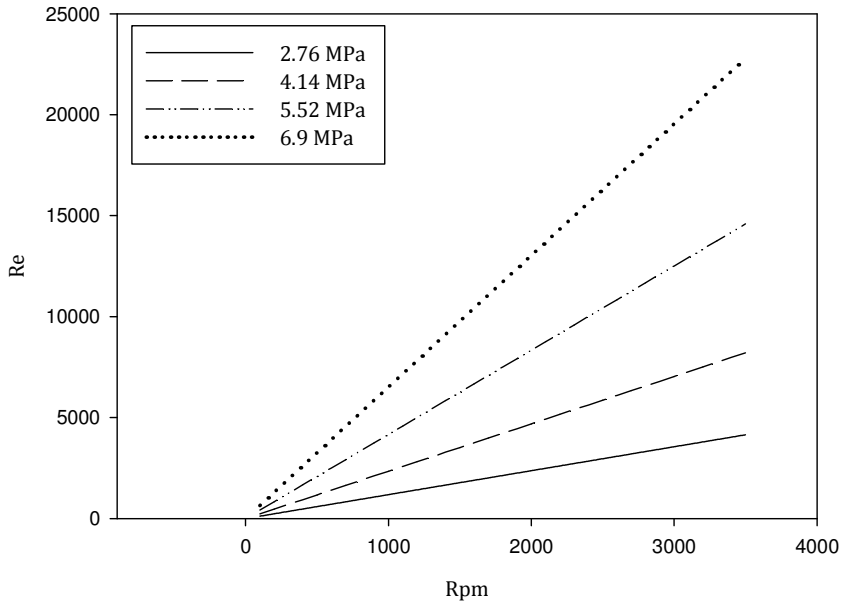

Figure 6.6 Reynolds number for oscillating flow in circular tubes , hot side heat exchanger

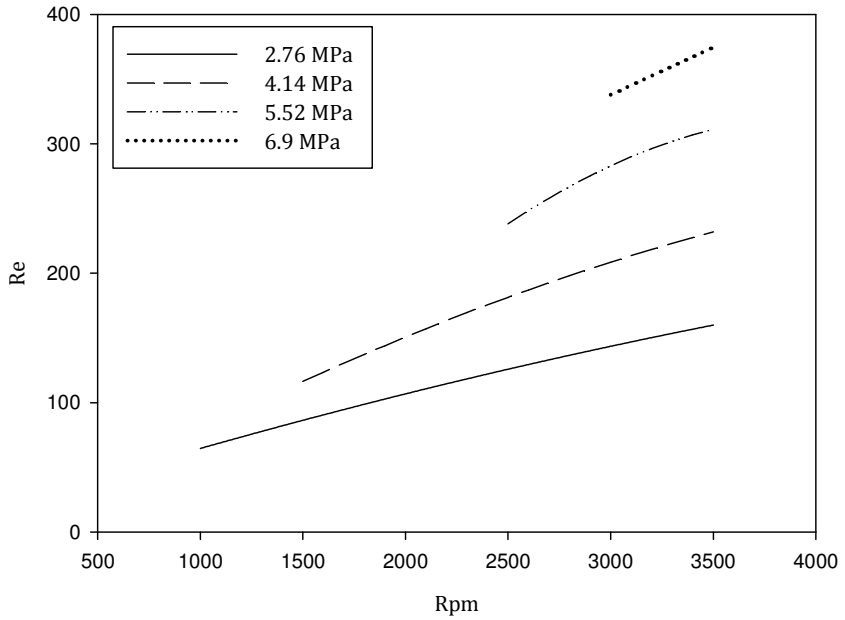

Figure 6.7 Reynolds number for combustion gas flow over tube bank, hot side heat exchanger

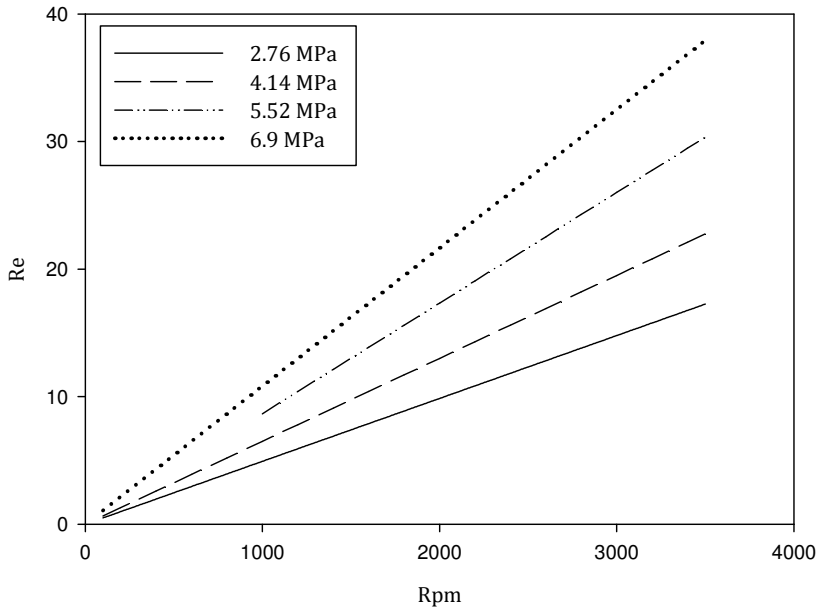

Figure 6.8 Reynolds number for gas flow through regenerator

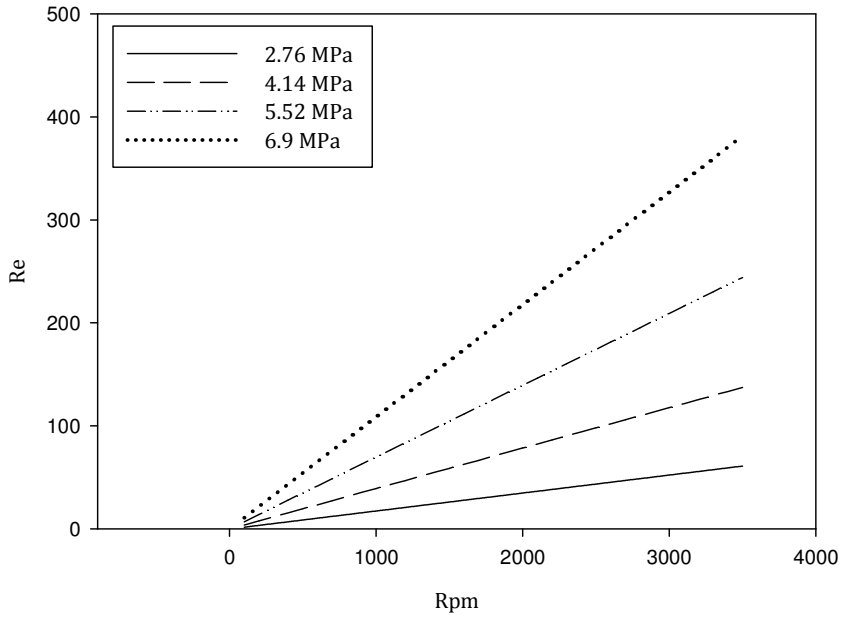

Figure 6.9 Reynolds number for oscillating flow in circular tubes, cold side heat exchanger

6.10.2 Convective Heat Transfer Coefficients

Calculation of the convective heat transfer coefficients for each of the heat exchangers and for both the internal and external transfer fluids was necessary

for the analysis of the heat exchangers. Knowledge of the h values permits computation of the U-values for each exchanger and consequently the exchanger NTU value. The analytical relationships involved are detailed in the previous chapter. The simulation results are present here.

6.10.2.1 Hot Side

Figure 6.10 and Figure 6.11 show the working gas convective heat transfer coefficient and the combustion gas heat transfer coefficient respectively.

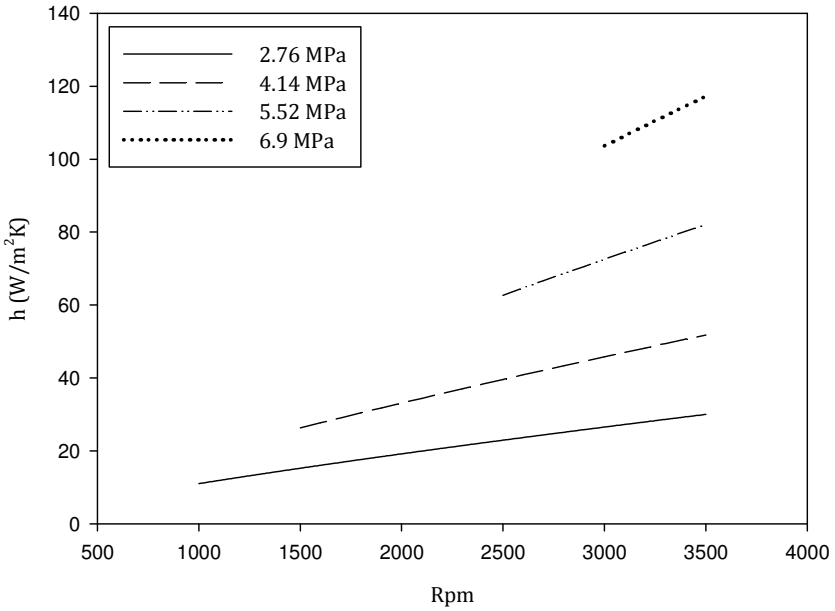

Figure 6.10 Hot side working gas heat transfer coefficient

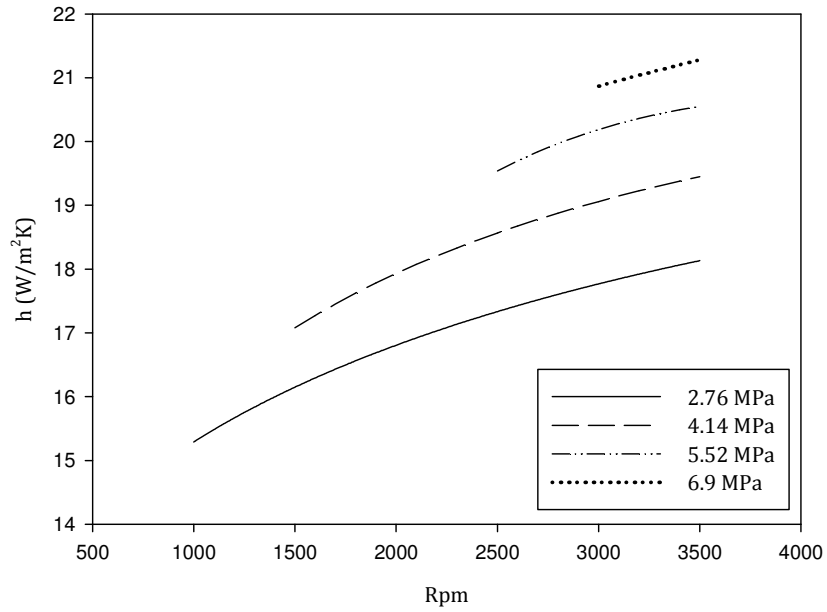

Figure 6.11 Hot side combustion gas heat transfer coefficient

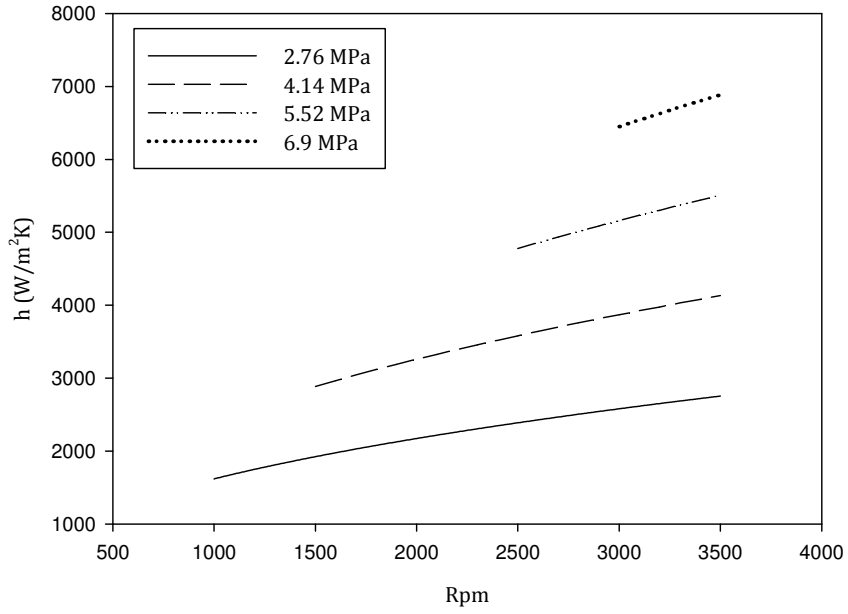

Figure 6.12 Regenerator convective heat transfer coefficient

6.10.2.2 Regenerator

Figure 6.12 shows the variation of the regenerator convective heat transfer coefficient over the full operating frequency range for each of the mean cycle pressures under investigation.

6.10.2.3 Cold Side

Figure 6.13 and Figure 6.14 show the variation of the convective heat transfer coefficient for the cooler working gas and the coolant respectively.

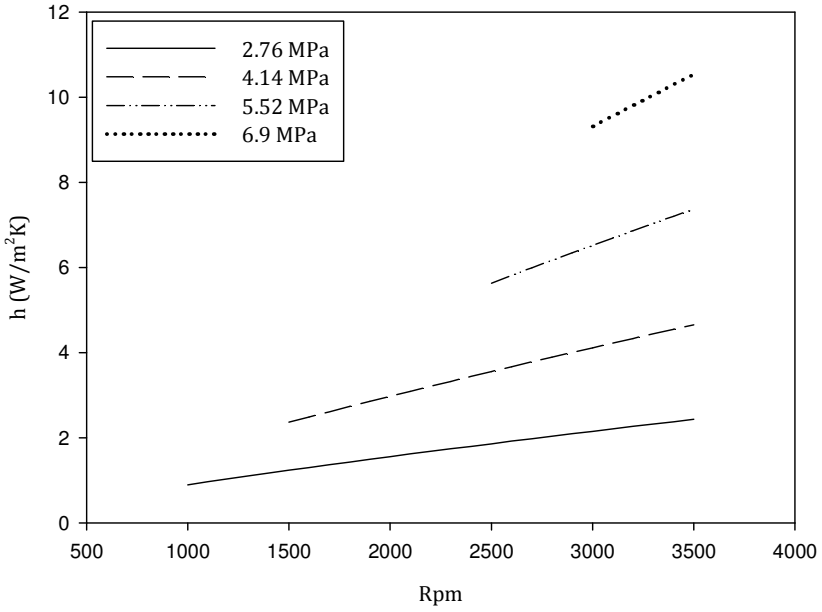

Figure 6.13 Cold side working gas convective heat transfer coefficient

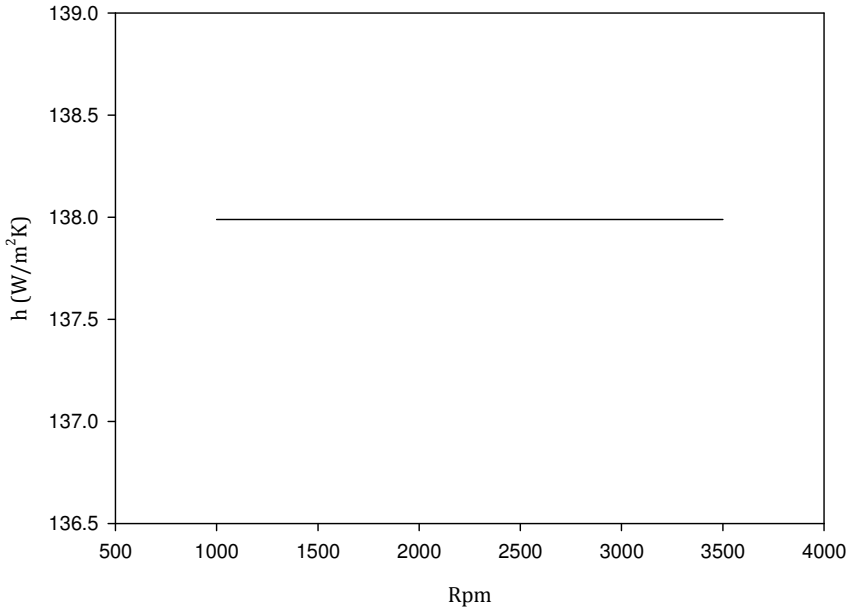

Figure 6.14 Cold side coolant convective heat transfer coefficient

6.10.3 Heat Exchanger Effectiveness

Figure 6.15 shows the results for the simulation of the hot side heat exchanger effectiveness for the GPU-3 engine under investigation. The overall trend visible from the plots for the different operating conditions suggests that increasing mean cycle pressure and operating frequency have a detrimental effect on heat exchanger effectiveness. However a maximum is visible for the case of 2.76 MPa mean cycle pressure. This maximum suggests that heat exchanger effectiveness is optimised for operation at approximately 1300 rpm for these constraints. It was not possible to further investigate this for the other operating regimes due to a lack of experimental data. It is notable though from the plot presented that heat exchanger effectiveness remains relatively high for the operating frequency range given, with many of the values above 90% effectiveness.

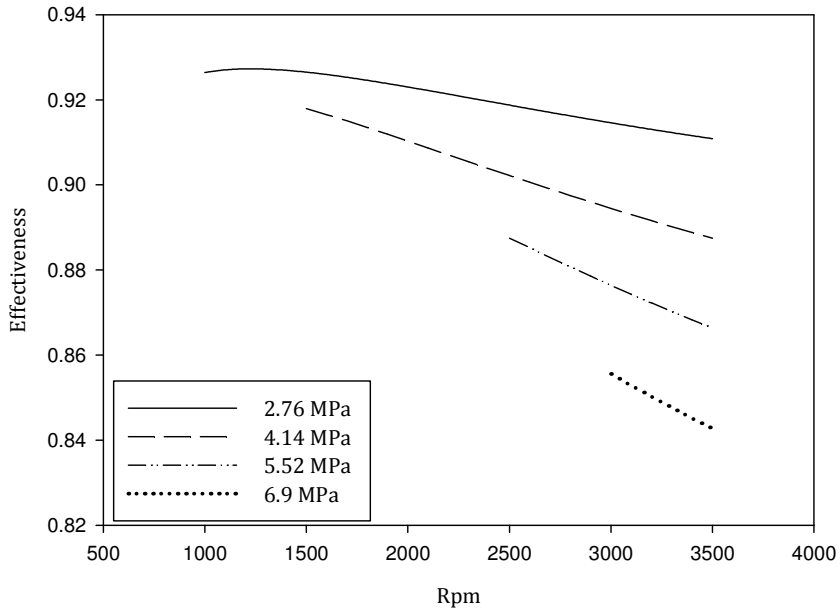

Figure 6.15 Hot side heat exchanger effectiveness against engine rpm

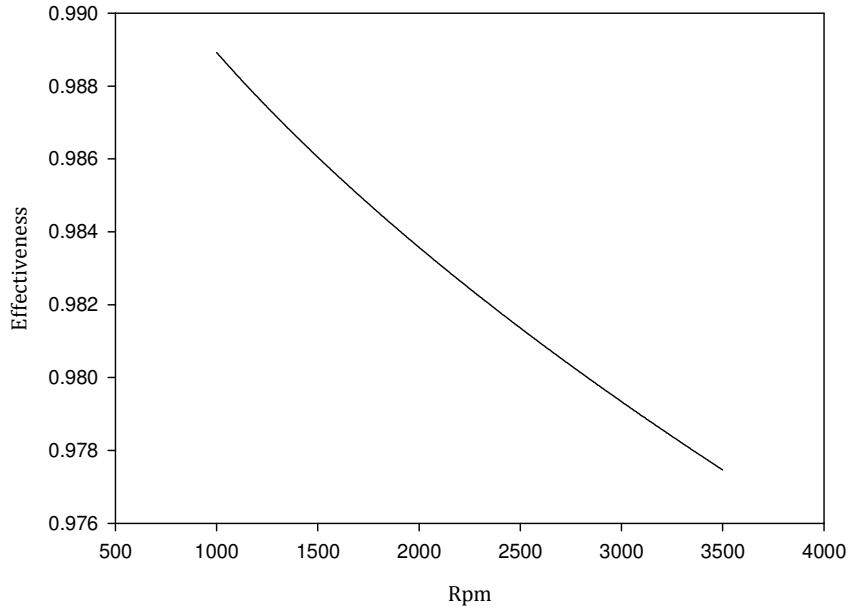

Figure 6.16 Regenerator effectiveness against engine rpm

Figure 6.16 presents data for the effectiveness calculation for the regenerative heat exchanger. The effectiveness of the regenerator is notable for being almost identical at all operating mean cycle pressures. This appears to be due to the ratio (h/ṁ) used in the calculation of the NTU being approximately equal at each load regime. As with the hot side heat exchanger, the trend over the operating frequency range is towards a reduction in effectiveness, however the magnitude remains high, above 97% in all cases.

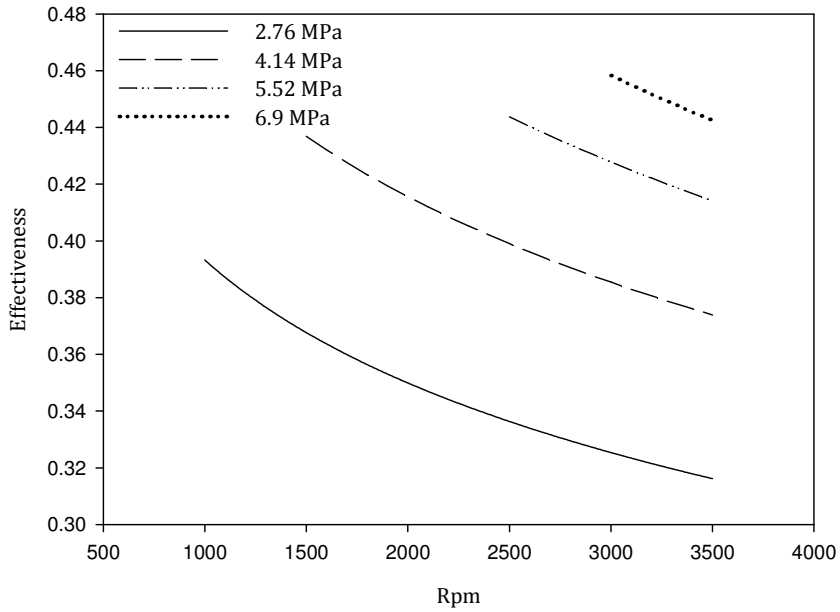

Figure 6.17 Cold side heat exchanger effectiveness

Figure 6.17 shows the effectiveness value for the cooler side heat exchanger. The trend visible on the graph indicates that increasing mean cycle pressure corresponds to an increase in heat exchanger effectiveness, whilst increasing cycle frequency corresponds to a decline in effectiveness.

6.10.4 Irreversibility Parameter, I_R

The cycle irreversibility parameter is computed according to the analytical method presented previously. Figure 6.18 shows plots of the values of I_R for each of the mean cycle pressure regimes under investigation and for the full operating speed range. It is evident from the data that the ratio increases with engine operating speed and with mean cycle pressure. This implies that changes in these conditions involve increases in the entropy generation within the working gas circuit due to processes such as throttling, free expansion, friction etc. The magnitude of the ratio is in line with that expected for other heat engines.

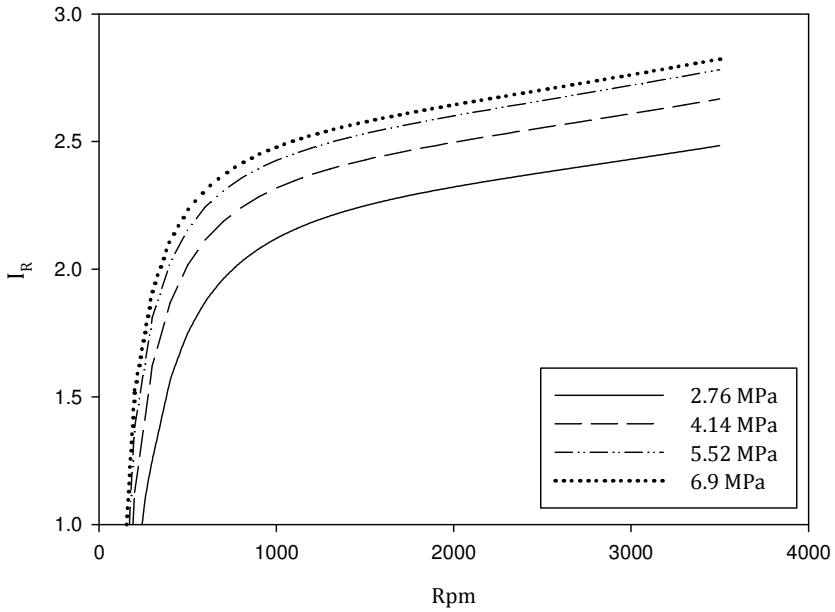

Figure 6.18 Variation of irreversibility parameter I_R with engine operating speed

6.10.5 Brake Power Output

The brake power output of the engine is important for appraisal of the model as it is among the only experimental performance data known for the engine. In conjunction with the brake thermal efficiency and the heat requirement, the brake power output computed from the FTT model is compared against the experimental data to gauge the fidelity of the FTT model. Figure 6.19 depicts the results of the simulation model plotted against the experimental data for the GPU-3 engine.

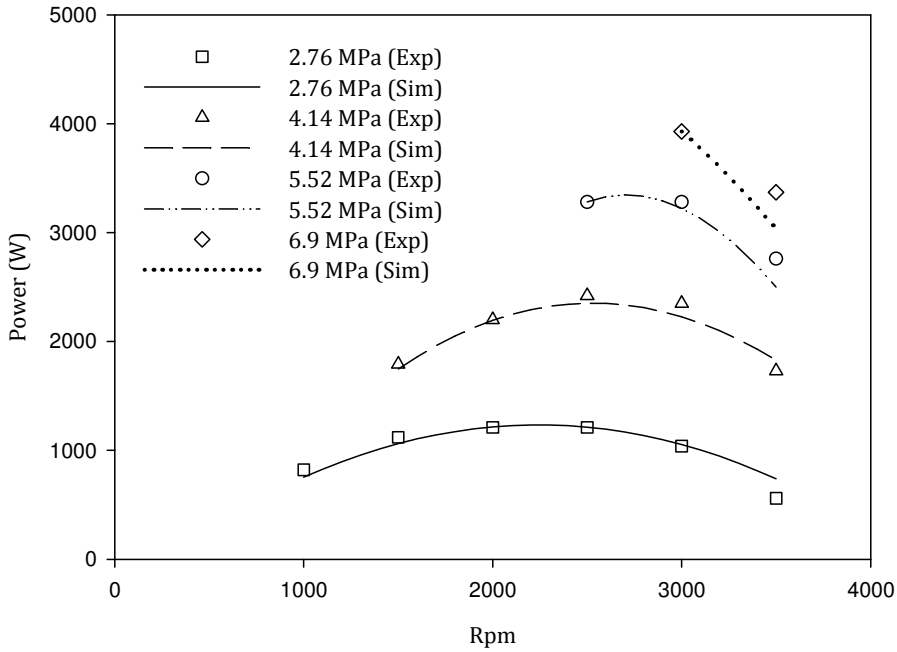

Figure 6.19. Brake power output, experimental and simulation data

6.10.6 Brake Thermal Efficiency

As with the brake power output, the brake thermal efficiency of the GPU-3 engine is used as a criterion for comparison of the capability of the FTT simulation model against real performance data. The results are presented in Figure 6.20.

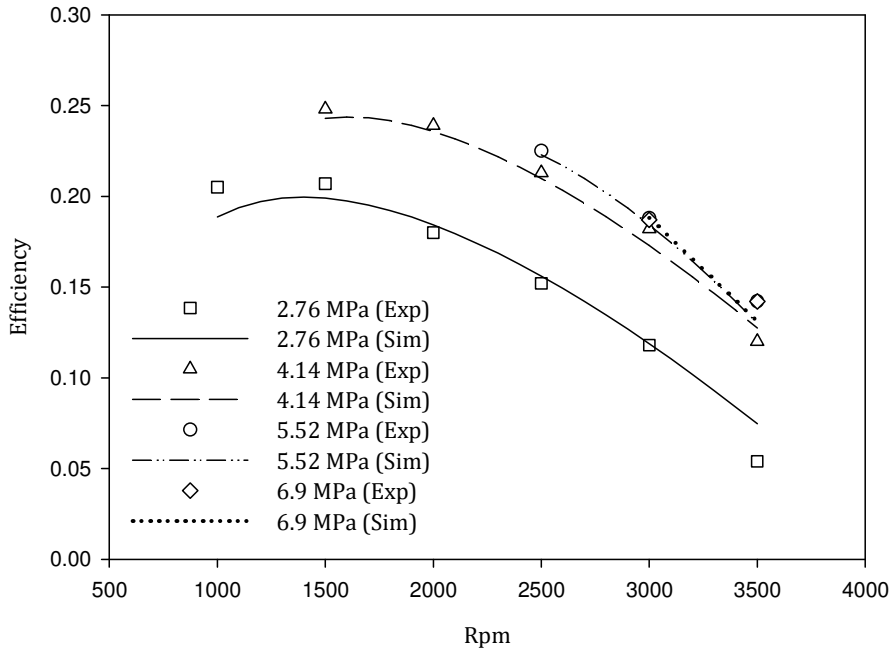

Figure 6.20 Brake thermal efficiency, experimental and simulation data

6.10.7 Power vs. Efficiency

Heat engine performance is routinely displayed by means of a plot of brake power against brake thermal efficiency. The advantage of such a plot is the ability to identify the proximity of the power and efficiency maxima to each other; all heat engines display a loop shaped *P*–η diagram similar to those shown in Figure 6.21 and Figure 6.22. These plots show the results of the FTT simulation plotted against the experimental data on the *P*–η plane. It can be seen that the simulation data displays the loop shape expected of a heat engine and that it corresponds well to the plot of the experimental data presented also.

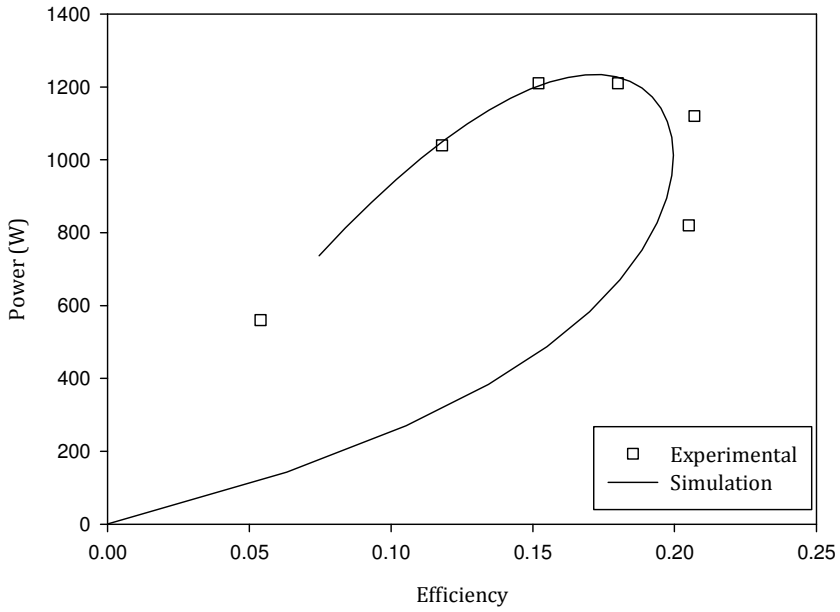

Figure 6.21. Brake power against brake efficiency, 2.76 MPa

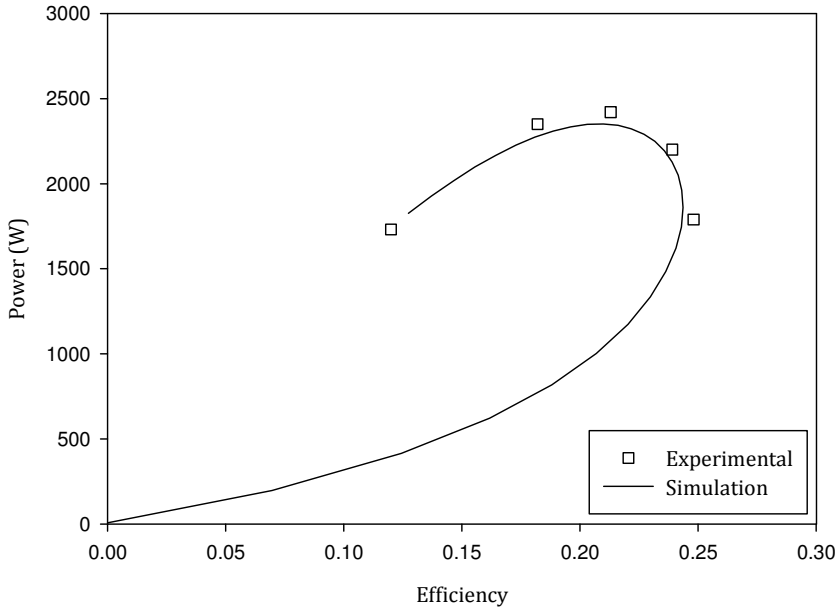

Figure 6.22 Brake power against brake efficiency, 4.14 MPa

6.11 Error Analysis

Figure 6.23and Figure 6.24 show the results of error analyses for the brake power and brake thermal efficiency analyses respectively. It can be readily appreciated from these plots that the model demonstrates good agreement with

the experimental data, with difference values within 10% in the majority of instances in each case.

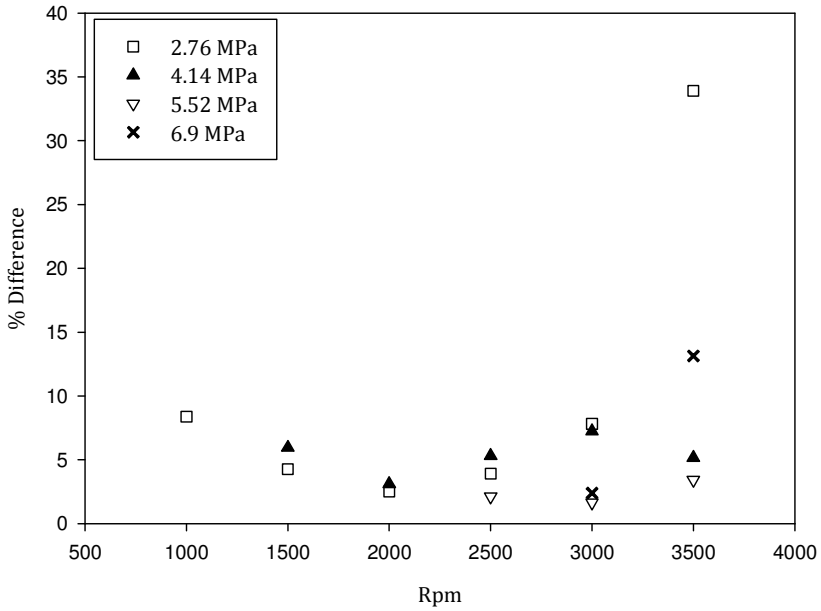

Figure 6.23 Brake power percentage difference against engine rpm

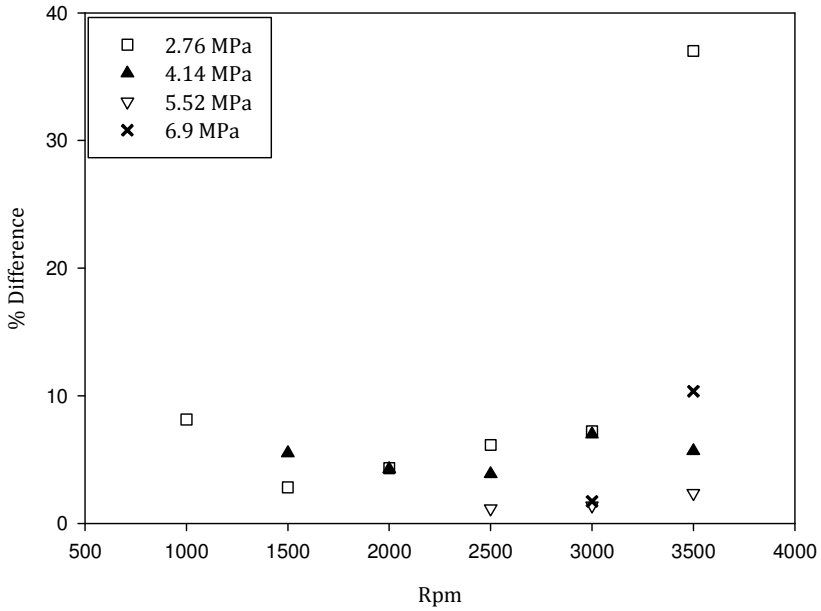

Figure 6.24 Brake thermal efficiency percentage difference against engine rpm

6.12 Heat Input—Sensitivity to Polynomial Order

Due to a lack of complete experimental data for all mean cycle pressure regimes, cycle heat requirement was not known for all operating frequencies at all loads.

Therefore, as detailed previously, fitted polynomials were used for the data that was available, allowing interpolation of data between the experimental data points.

Using the fitted polynomials it was also possible to extrapolate data in an attempt to assess performance of the engine outside of the experimentally measured data points. However, this extrapolation proved problematic as it was highly sensitive to the polynomial order. In this section, the effect of variation of polynomial order on the outputs of the model is briefly assessed. Linear and second order polynomial relationships for the heat input are assessed and their effect on the power output and brake thermal efficiency are investigated.

6.12.1 Specification of Fitted Polynomials for Heat Input

The fitted second order polynomials for the heat input to the engine are presented in Section 6.5. These expressions are summarised along with their 'coefficient of determination' values in Table 6.6.

Table 6.6 Polynomial and linear curve fits for heat input experimental data

P_{mean}	*Polynomial*	R^2
2.76MPa	$[-0.0006f^2 + 0.1864f + 1.051] \times 10^3$	0.9986
4.14 MPa	$[-0.0016f^2 + 0.3478f + 0.5069] \times 10^3$	0.9988
5.52 MPa	$[-0.0074f^2 + 1.011f + 14.56] \times 10^3$	1
6.9 MPa	$[0.2724f + 7.26] \times 10^3$	1

P_{mean}	Linear	R^2
2.76MPa	$[0.1415f + 1.7722] \times 10^3$	0.996
4.14 MPa	$[0.2141f + 2.056] \times 10^3$	0.9934
5.52 MPa	$[0.2694f + 3.636] \times 10^3$	0.9828
6.9 MPa	$[0.2724f + 7.26] \times 10^3$	1

The limited data set made it possible to fit linear expressions to the data without a considerable decrease in the accuracy of the fit. These linear expressions are also presented with their coefficients of determination in Table 6.6. It can be seen that although the polynomials offer better fits for the experimental data, the linear expressions also offer good agreement, well within acceptable limits.

Figure 6.25 shows plots of the brake power output of the engine extrapolated over the full operating speed range for the case of the polynomial heat addition expressions. It is evident from the plot that for the cases of increased mean cycle pressure the brake power output at low rpm is significantly below what would be expected; contrary to what would be expected for actual engines it can be seen from the data plots that the engine power output at high mean cycle pressure and low rpm is actually lower than that for a lower mean cycle pressure at the same rpm. This can be offset partially by the use of a linear heat input; this can be seen from Figure 6.26. This condition satisfies the expected result of higher power output at higher mean cycle pressure and low rpm. It is notable though that when the linear expression is used, it results in the power output at lower rpm being somewhat high.

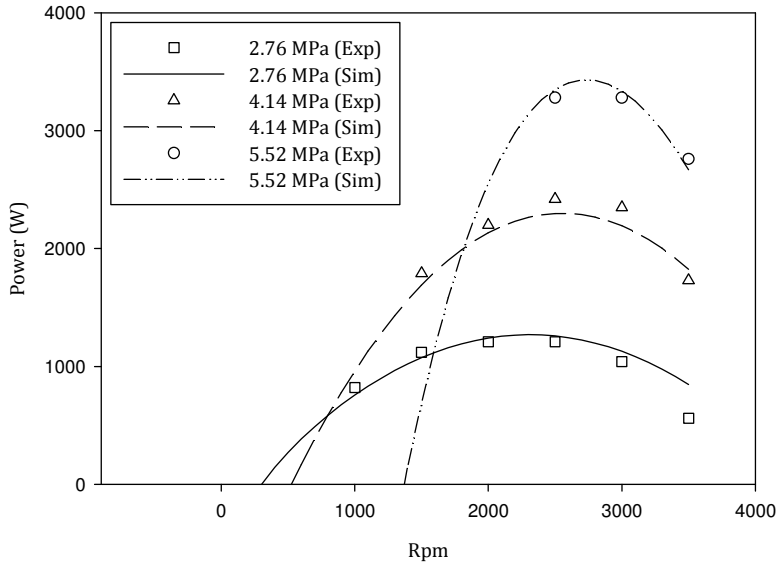

Figure 6.25 Brake power against rpm, polynomial heat input

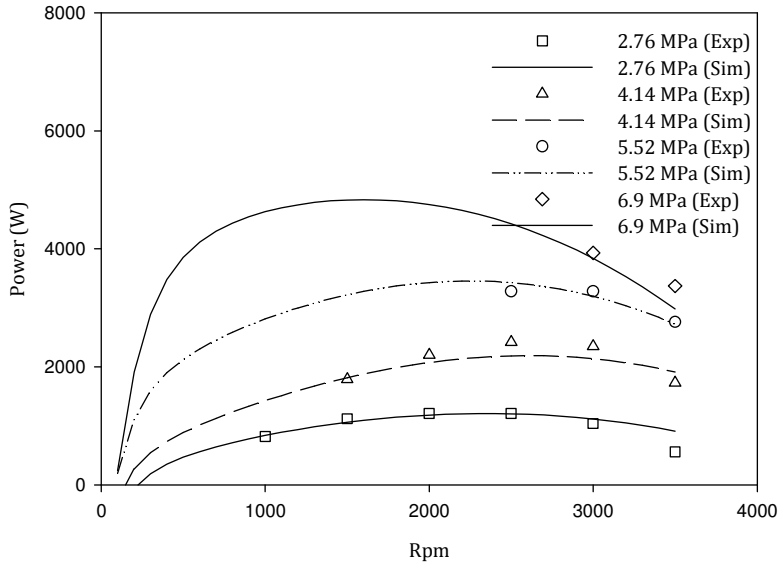

Figure 6.26 Brake power against rpm, linear heat input

Figure 6.25 and Figure 6.26 allow a comparison of the brake power output of the engine for each mean cycle pressure value for the cases of linear and polynomial heat inputs. It is clear from these plots that with increasing mean

cycle pressure, the disparity between the power outputs for the linear and polynomial cases becomes significantly more pronounced.

Although this is by no means a conclusive analysis due to the lack of experimental data, it is possible to suggest that the heat input for the actual engine would be a polynomial of order somewhere between the linear and second order case. However, it is not possible to investigate this more fully in the present work.

6.12.2 Extrapolation of Heat Input using Scaled Polynomials

A further possibility for extrapolating heat input data for the higher mean cycle pressure load regimes is to scale the polynomial from a regime with a more complete data set. This essentially assumes that the heat demand for the engine scales linearly with the mean cycle pressure. There is some justification of this in the literature, as increasing mean cycle pressure is an accepted method of scaling the power output of the engine, therefore it can reasonably be assumed that the heat requirement scales in a similar manner.

Figure 6.27 shows the polynomial heat input expressions scaled from the 2.76 MPa regime plotted against the experimental heat input data. It can be seen that this offers a reasonable approximation to the experimental data. Figure 6.28 gives a plot of the brake power output of the engine under these new polynomial heat input expressions. Again, it can be seen that this model offers a reasonable fit to the experimental data, although the error is considerably higher than with the explicitly fitted polynomials. Figure 6.29 gives a similar plot for the brake efficiency of the engine. Figure 6.30 to Figure 6.32 give plots

of the percentage differences for the heat input, the brake power and the brake efficiency plots discussed above.

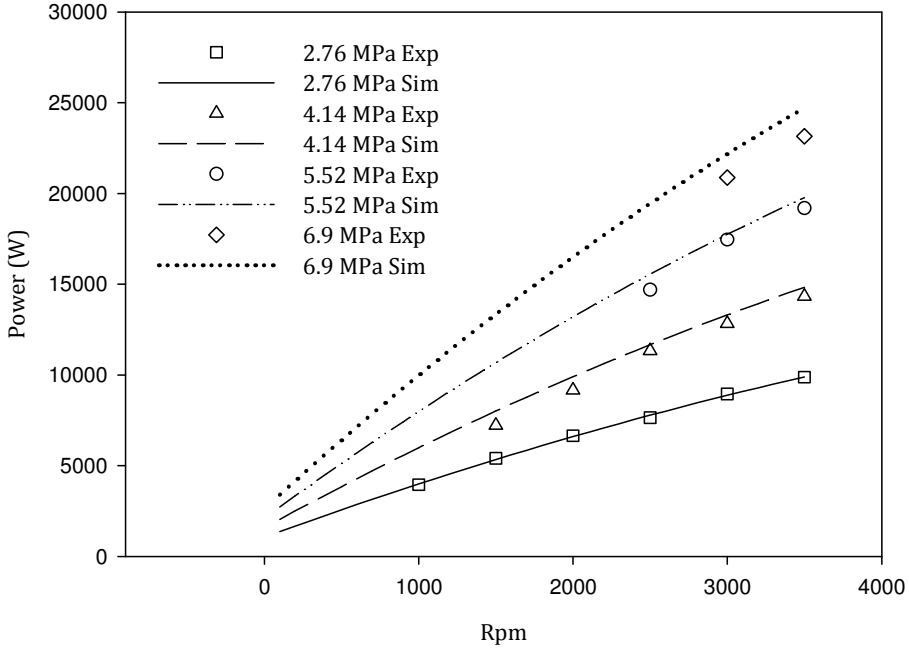

Figure 6.27 Scaled polynomial expressions for heat input to GPU-3 Stirling engine

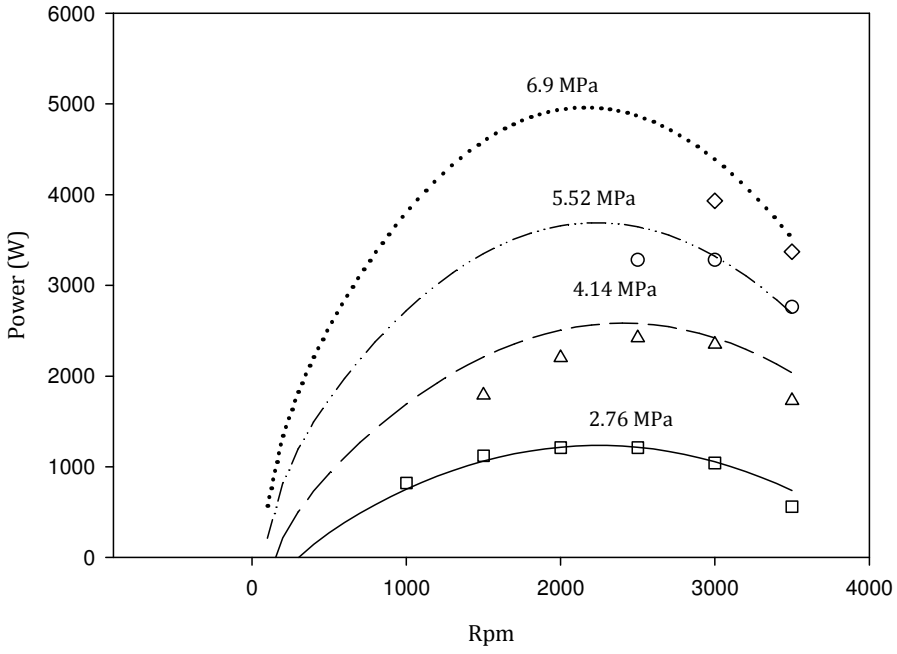

Figure 6.28 Brake power output for case of scaled polynomial heat input expressions

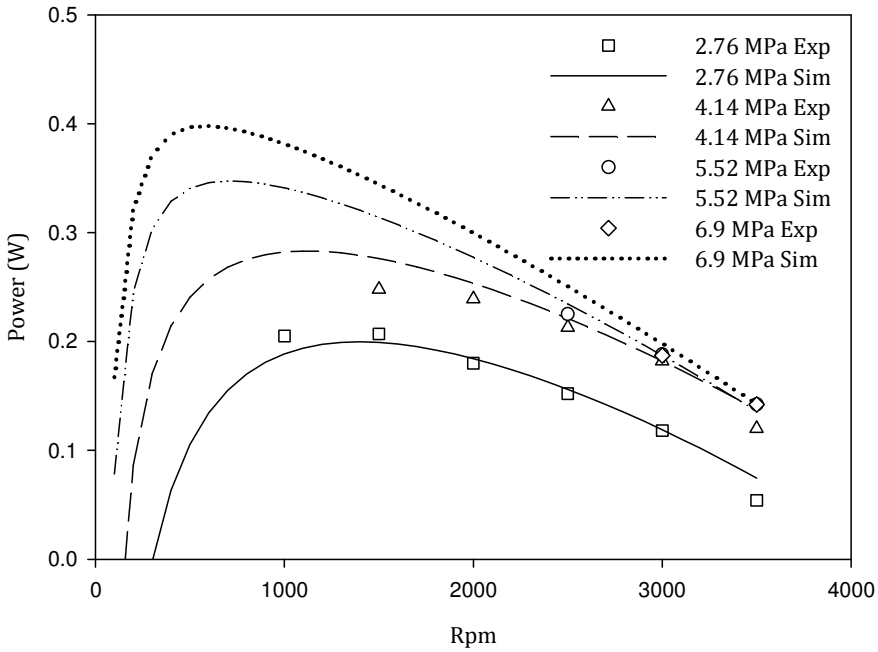

Figure 6.29 Brake thermal efficiency for case of scaled polynomial heat input expressions

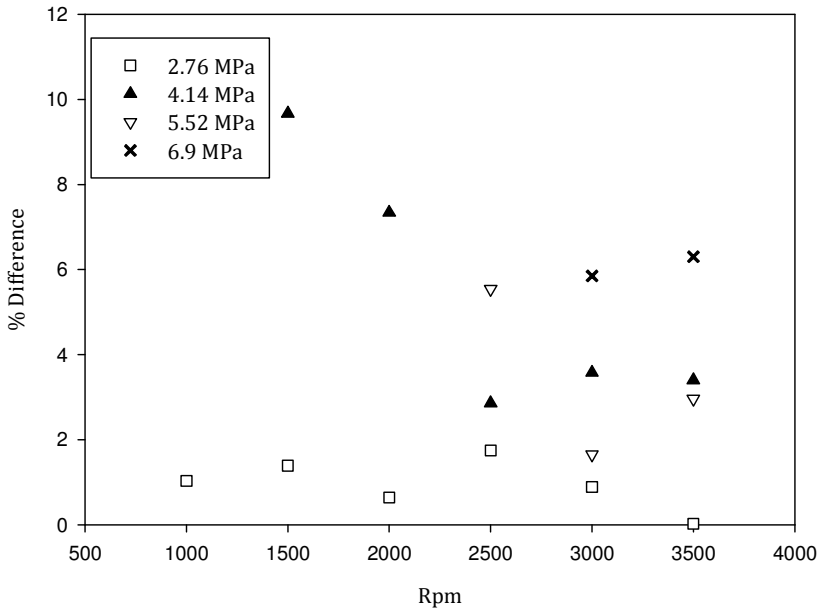

Figure 6.30 Percentage difference, scaled polynomial heat input expressions

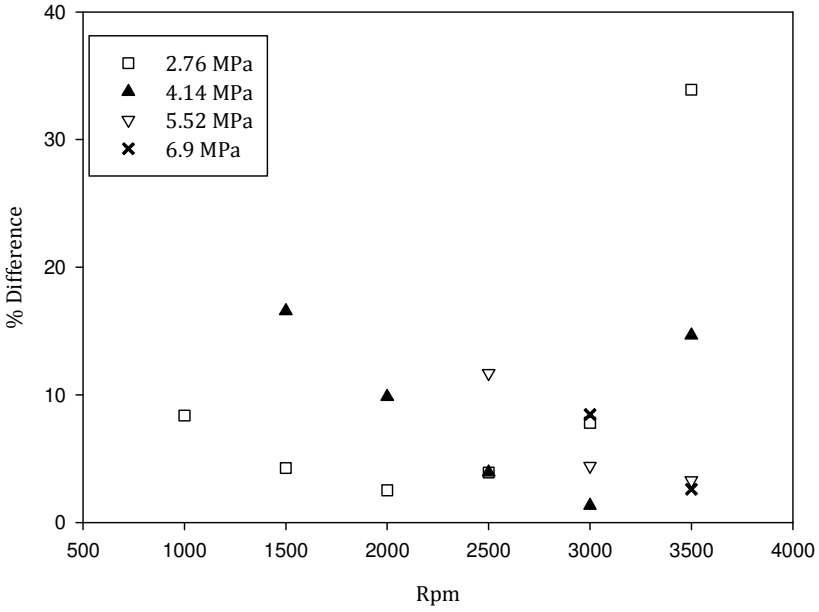

Figure 6.31 Percentage difference, brake power output

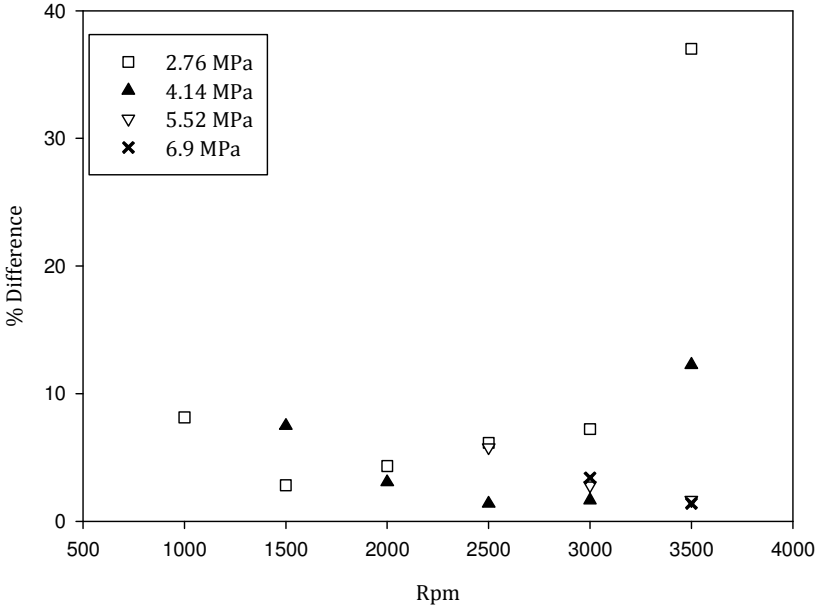

Figure 6.32 Percentage difference, brake thermal efficiency

6.13 Results of Simulation and Comparison with Experimental Data—Hydrogen Working Gas

In addition to the validation conducted for the helium charged GPU-3 Stirling engine it was possible to perform a brief validation using the case of hydrogen as working gas in the engine. Although the data available was more limited for the performance of the hydrogen charged engine, it was possible to perform a brief analysis to add to the overall validation of the FTT model. The results of this are presented in Figure 6.33 to Figure 6.35.

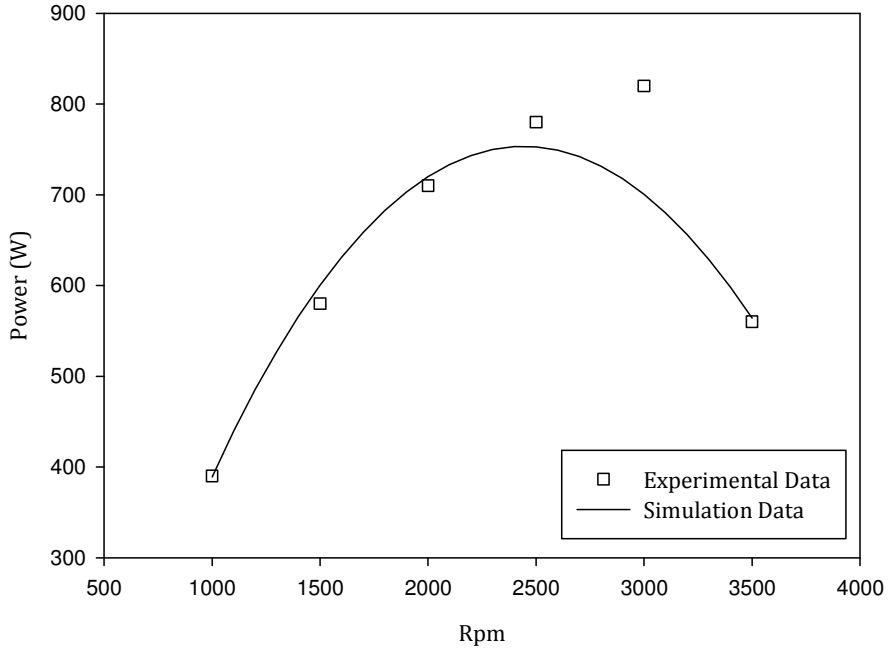

Figure 6.33 Brake power output for hydrogen charged GPU-3 Stirling engine, 1.38 MPa mean cycle pressure

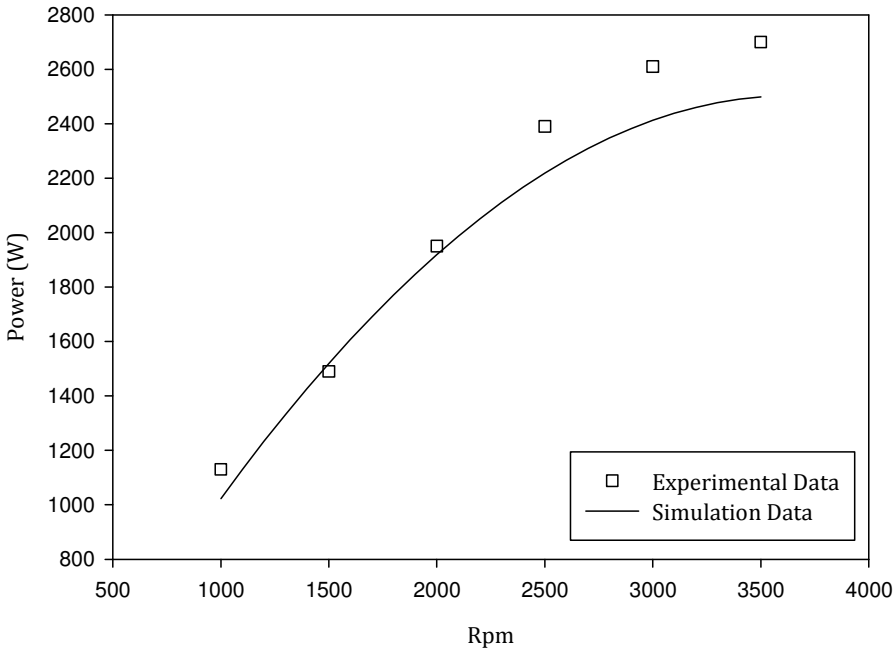

Figure 6.34 Brake power output for hydrogen charged GPU-3 Stirling engine, 2.76 MPa mean cycle pressure

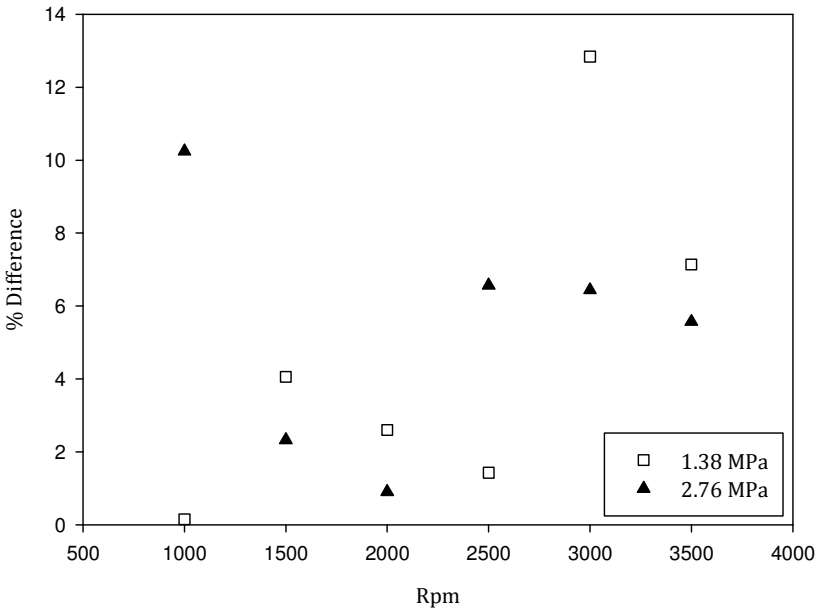

Figure 6.35 Percentage differences for experimental and simulation data, hydrogen charged GPU-3 Stirling engine

6.14 Conclusions

The FTT model for the Stirling cycle engine presented in Chapter 5 has been validated against experimental data available in the literature for the General Motors GPU-3 Stirling engine. The GPU-3 is capable of operation with either helium of hydrogen as working fluid and under a variety of mean cycle pressure regimes. Test data for operation with helium working fluid was utilised as a basis for validation of the FTT model.

The FTT model was found to offer good agreement with the experimental data, with percentage difference values for both brake power and brake thermal efficiency being within 10% for a large part of the operational test points.

The sensitivity of the model to the form of polynomial curve utilised for the heat input is addressed. Due to the lack of experimental data available, there exists the possibility that the fitted polynomial curves for the limited data do not adequately represent the actual data trend. It was therefore necessary to accommodate this possibility. This was done by investigating the modelled scenarios for two sets of imposed heat addition polynomials; firstly for the second order polynomial curve fitted to the experimental data and secondly for a linear expression fitted to the data. The linear expression offers a slightly less accurate fit to the data, however the coefficient of determination remains high, indicating a good fit.

7 ANALYSIS OF THE COMBINED CYCLE

7.1 Introduction

This chapter presents the analysis of the combination of the Otto and Stirling thermodynamic cycles, using the FTT models presented in the preceding chapters. The Otto cycle acts as the topping cycle in the arrangement, with the Stirling cycle recovering heat from the exhaust stream with the primary goal of generating additional mechanical power.

The FTT models allow analysis of the two cycles in more detail than the ideal air standard cycles, as they permit inclusion of generalised speed-dependent friction loss terms, pumping loss terms and thermal losses. The FTT Otto model has been specifically developed from others available in the literature to include exhaust thermal power losses and to calculate the enthalpy-averaged temperature of the flow at the exhaust port. The FTT Stirling model is a new addition to the literature and draws upon the FTT modelling conventions used in the analysis of other engines such as the Otto and Diesel cycle engines. The Otto and Stirling FTT models are easily combined analytically through the Otto cycle exhaust stream, permitting analysis of the combined cycle and its optimisation. The analytical expressions linking the two models are developed in this chapter, and the results of the simulated combined cycle are assessed.

7.2 Methodology

The validation processes detailed in the preceding chapters looked at individual engines of each of the thermodynamic cycles under investigation in isolation of each other. In order to analyse the combined cycle, it would be possible to

simply use both engines as they were studied in the validation simulations and couple them together. This would represent a sub-optimal combined configuration; however, it would still be possible to gauge the performance gains possible through the combination. It was desirable though to attempt to optimise the configuration, to assess the maximum power and efficiency gains possible.

With this in mind, the Otto cycle engine was scaled down to 25% size to a one cylinder version of that analysed previously. This was done as an *ad hoc* optimisation—it was known that the engines could be scaled to better complement each other by inspection of the energy balances, and the multi-cylinder Otto engine was much easier to scale down than was the single cylinder Stirling engine to scale up, due to the sophisticated heat exchangers used in the design. The combined cycle was then analysed in terms of use as a stationary power generator. With this in mind, two operating scenarios were investigated:

1. the two engines operating at the same rotational speed, i.e. a "synchronised operating frequency" operation and;
2. the two engines operating at different speeds i.e. an "asynchronous operating frequency" operation. It is assumed in both scenarios that both engines have achieved steady state operation.

The parameter of most interest for modelling of the combined cycle is the Otto cycle exhaust temperature. This is computed using the analytical method specified in Chapter 3. The enthalpy-averaged temperature of the gas in the exhaust port is calculated. By assuming this temperature to be maintained for a short, but unspecified, distance along the exhaust line, it is possible to use this as the entry temperature of the heating fluid for the Stirling cycle source heat

exchanger. It is seen that the exhaust gas temperature from the Otto cycle engine is very close to the combustion gas temperature for the Stirling cycle engine in its normal operation mode. Therefore, the reduction in performance below rated conditions is minor.

7.3 Analysis of Stirling Cycle Temperatures

The central point of coupling between the two thermodynamic cycles is the Otto cycle exhaust stream. This acts as the thermal source for the Stirling cycle. It is therefore necessary to develop analytical relationships for the Stirling cycle thermal source and sink temperatures in terms of the Otto exhaust stream gas properties.

7.3.1 Stirling Hot Side Working Gas Temperature

It is possible for the heat admitted to the Stirling cycle through the hot side heat exchanger to be expressed as:

$$\dot{Q}_{i,\text{Stirling}} = \varepsilon_{\text{H}} \dot{Q}_{\text{max}} \tag{7-1}$$

where $\dot{Q}_{\text{max}}$ is the maximum possible heat consumption of the Stirling cycle engine taken from the heat release in the combustion chamber. As detailed in Chapter 5, it is assumed in Equation (7-1) that the maximum possible heat transfer to the Stirling engine would equate to a proportion of the total sensible thermal content of the combustion gas flow, $\dot{Q}_{\text{in}}$. As was also seen in Chapter 5, the maximum heat transfer to the cycle can be related to the heat released during combustion through the ratio R_Q. Therefore, the maximum heat transfer possible across the heat exchanger can be represented by the term $R_Q \dot{Q}_{\text{in}}$. This actual heat transfer through the heat exchanger wall can be expressed in terms

of the free-stream temperatures of the interacting gases, the overall heat transfer coefficient and the heat transfer area by Equation (7-2) [149]:

$$\dot{Q}_{i,\text{Stirling}} = U_{\text{H}} A_{\text{H}} \left(T_{\infty,1} - T_{\infty,2} \right) \tag{7-2}$$

where $T_{\infty,1}$ and $T_{\infty,2}$ are the free stream temperatures of the two gases, U is the overall heat transfer coefficient and A the heat transfer area. In this case, the free-stream temperatures correspond to the temperature of the exhaust gas of the Otto engine and the gas temperature in the Stirling engine heat exchanger. For the current study, it is desired to compute the internal gas temperature of the Stirling engine heat exchanger when the maximum heat input and the combustion gas temperature are known. Equation (7-2) can thus be rearranged to give:

$$T_{\infty,2} = T_{\infty,1} - \frac{\varepsilon_H R_Q \dot{Q}_{\text{in}}}{U_{\text{H}} A_{\text{H}}} \tag{7-3}$$

It is evident from the above equation that in order to compute the gas temperature in the Stirling heat exchanger, it is necessary to know the overall heat transfer coefficient, the heat exchange area and the heat exchanger effectiveness. It will be shown in the following section that these three factors are related and can be determined for a given heat exchanger.

7.3.1.1 Computation of the $\frac{\varepsilon R_Q}{UA}$ term

The effectiveness of a given heat exchanger is related to the overall heat transfer coefficient and the heat transfer area through the NTU value. The NTU can be calculated as:

$$\text{NTU} = \frac{UA}{\dot{C}_{\text{min}}} \tag{7-4}$$

Incropera and Dewitt [149] indicate that it is suitable to approximate U as constant for a given heat exchanger for different operating regimes of fluid flows, pressures and temperatures. Considering also that the heat exchanger area will not change, the UA product will not change for the heat exchanger under investigation. It is also possible to suggest that for all reasonable cases of deployment of the heat exchanger, the $\dot{C}_{\min}$ term will fluctuate only mildly so that it is possible to suggest that the NTU will not vary considerably for these values. Calculation of the heat exchanger effectiveness when the NTU is known is dependent on specific correlations for differing exchanger types. Examples of such ε– NTU correlations are given in [149] and [156] also. It is possible to generalise, however, and say that small fluctuations in NTU will give rise only to small fluctuations in ε, and by extension R_Q. Therefore, allowing the conclusion that, for a given heat exchanger, the term $\frac{\varepsilon R_Q}{UA}$ will remain approximately constant for all operating scenarios. With regard to the computation of the gas temperature in the heat exchanger as in Equation (7-3), it is possible therefore to conclude that for a heat exchanger of known performance, it is sufficient to know the sensible thermal content of the source, the value of the $\frac{\varepsilon R_Q}{UA}$ term and the free stream temperature of the combustion exhaust gases in order to compute the internal temperature of the gas in the heat exchanger.

7.3.2 Stirling Cold Side Working Gas Temperature

The heat rejected from the cold side to the water cooling circuit is:

$$\dot{Q}_{\text{coolant}} = \varepsilon_{\text{c}} \dot{Q}_{o,\text{Stirling}} \tag{7-5}$$

In this instance, the maximum possible heat transfer is understood to be that which is rejected from the gas cycle, $\dot{Q}_{\mathrm{o,Stirling}}$, and therefore that which is recovered by the coolant is restricted by the heat exchanger effectiveness:

$$\dot{Q}_{o,\mathrm{Stirling}} = \frac{\dot{Q}_{\mathrm{coolant}}}{\varepsilon_{\mathrm{c}}} \tag{7-6}$$

where $\dot{Q}_{\mathrm{coolant}}$ is the heat actually recovered in the engine coolant circuit. The heat that the cycle is rejecting, $\dot{Q}_{\mathrm{o,Stirling}}$, is necessarily greater than that actually recovered as a consequence of the imperfect heat exchange in the exchanger. It is possible then to express the free stream temperature of the working gas in the cooling heat exchanger in terms of the temperature of the cooling fluid, the recovered heat in the coolant, the heat exchanger effectiveness and the heat exchanger $U_{\mathrm{c}}A_{\mathrm{c}}$ term:

$$T_{\infty,3} = T_{\infty,4} + \frac{\dot{Q}_{\mathrm{coolant}}}{\varepsilon_c U_{\mathrm{c}} A_{\mathrm{c}}} \tag{7-7}$$

7.3.3 Summary of Analytical Expressions for Stirling Gas Temperatures

The gas temperatures in the Stirling engine can therefore be summarised in terms of the experimentally recordable values of T_{ex}, T_{coolant}, $\dot{Q}_{\mathrm{in}}$ and $\dot{Q}_{\mathrm{coolant}}$, and the heat exchanger geometric parameters ε, U and A :

$$T_{\mathrm{H,g}} = T_{\mathrm{ex}} - \frac{\varepsilon_{\mathrm{H}} R_Q \dot{Q}_{\mathrm{in}}}{U_{\mathrm{H}} A_{\mathrm{H}}} \tag{7-8}$$

$$T_{\mathrm{c,g}} = T_{\mathrm{coolant}} + \frac{\dot{Q}_{\mathrm{coolant}}}{\varepsilon_{\mathrm{c}} U_{\mathrm{c}} A_{\mathrm{c}}} \tag{7-9}$$

It is important to note that the term $\dot{Q}_{\mathrm{in}}$ denotes the heat consumption of the Stirling engine, i.e. the heat released in the combustion chamber. In the combined cycle system set-up, this heat requirement is drawn from the Otto engine exhaust, which acts as a thermal reservoir for the Stirling cycle. The

limit for the reservoir occurs when the heat demand of the Stirling reaches the limit of the that available from the exhaust stream.

7.3.4 Calculated Operating Temperatures

The maximum and minimum temperatures of the gas in the thermodynamic cycle were computed using Equations (7-8(7-3) and (7-9) given in the previous section. These are compared against the rated cycle temperatures computed for the GPU-3 engine in Table 7.1. The combustion temperature for the rated operating test data is computed using the first law heat equation. This is possible as the heat supplied to the cycle, the fuel mass flow rate, the air mass flow rate and the ambient temperature are known from the experimental data given in [98].

Table 7.1 Comparison of Stirling cycle gas temperatures

	T_{source} (K)	$T_{\text{H,g}}$ (K)
Rated	1167	922
Combined cycle	1059	814

7.4 The Combined Cycle—Simulation Results

The combined cycle was simulated using the FTT models connected using the temperature expressions presented in the preceding section. A series of scenarios have been analysed in order to assess the optimal combination of the two cycles. These scenarios can be divided into first law and second law analyses. In the first law analysis, the optimisation of the combined cycle engine is addressed with reference to the operating frequencies of the engines. The

heat balance of the plant is also investigated and compared to that of the Otto engine operating alone. This is of interest when considering the plant for deployment as a cogeneration unit. In the second law analysis, the combined cycle optimisation is addressed with reference to the second law efficiency of the combined cycle, minimisation of the irreversibility parameter, I_R, and analysis of the exergy destruction associated with the degradation of the waste heat from *high grade* in the exhaust flow to *low grade* in the jacket-water circuit. This is particularly pertinent to the deployment of the engine as a cogeneration system.

7.4.1 First Law Analysis of the Combined Cycle System

7.4.1.1 Optimal Operating Frequency—Synchronous Operation

The power output of any engine is directly proportional to the operating frequency of the cycle. However, the presence of speed-dependant gas flow effects and friction effects acts to limit the power output at higher rpm, thereby suggesting an optimum speed for maximum power output. The same is true for the maximum efficiency of the engine.

The two engines analysed in the present work have separate operational characteristics and therefore have individual maximum power points in terms of their individual operating speeds. Similar optima would have existed for their brake thermal efficiencies. This suggested the possibility that there existed maximum power and efficiency points for the combined cycle system.

In a situation where the Otto cycle engine is assumed to have a constant operating frequency, it would be possible to maximise the power output from a bottoming Stirling cycle by running it at a different speed to the Otto cycle, in

accordance with its optimum power output point. Alternatively, it would be possible to increase the specific work output of the Stirling engine by increasing the mean cycle pressure and subsequently running it at the same speed as the Otto engine. This might have the advantage of simplifying the transmission system required for coupling the two engines.

The standard operational mode for stationary power generators is to operate at a fixed speed, with engine loading being ultimately controlled by variation of the fuel availability through a throttle or fuel governor system. It may therefore be considered that the primary goal of any optimisation procedure for the combined cycle is to maximise the power output of the component engines at a single common speed. The most common operational speed for such industrial engines in the European market is 1500 rpm. Therefore, the first scenario analysed is the operation of both constituent engines at 1500 rpm. This would also likely be the simplest embodiment with regard to the mechanical transmission system.

Figure 7.1 shows the heat consumption profiles for the GPU-3 Stirling engine operating at different mean cycle pressures and across its full operating speed range. The curves utilised are the scaled polynomials developed in the preceding chapters. Shown intersecting these curves is the sensible thermal power content of the Otto cycle engine exhaust stream when operating at 1500 rpm. The drop line indicates the Stirling engine heat requirement for each of the operating regimes at 1500 rpm. This demonstrates that, in all but the 6.9 MPa mean-cycle-pressure case, the Otto exhaust would represent at good thermal source for this Stirling engine. For the 6.9 MPa case, the heat requirement from the source is too great to be accommodated from this source.

This implies that a slightly lower mean cycle pressure would satisfy the constraint at this operating speed. Alternatively, the engine could be loaded at a lower speed to accommodate the heat availability in the Otto exhaust. This scenario will be investigated more fully in the next section.

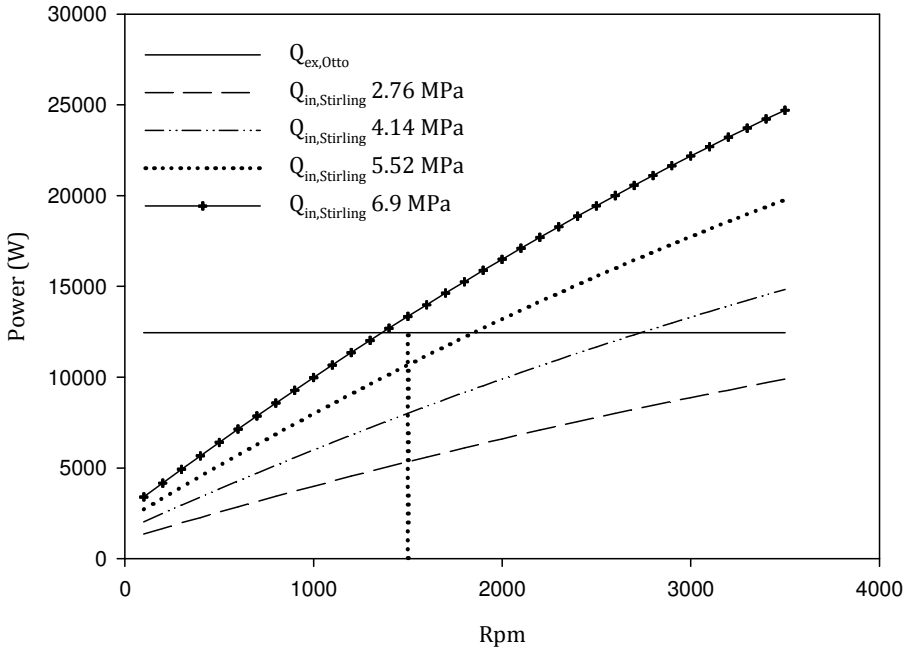

Figure 7.1 Synchronous loading of the GPU-3 engine operating on Otto exhaust thermal reservoir, heat consumption curves

Figure 7.2 shows the plots for the brake power corresponding to these heat input curves. It can be seen that at each mean cycle pressure regime the engine is operating below its maximum power output. This is also the case for the Stirling engine brake thermal efficiency, which is shown in Figure 7.3. The brake power output and brake thermal efficiencies for the Otto engine, the Stirling engine and the combined cycle engine are presented in Table 7.2 Combined cycle performance, synchronous operation. The performance gains are presented also as percentages for both the power and efficiency. It can be

seen that for the engines under consideration, considerable performance gains are possible. The maximum gain is seen for the case of GPU-3 at 5.52 MPa mean cycle pressure. In this case a power output of 9.04kW is possible, corresponding to a gain of 48.9% over the Otto cycle alone. The efficiency gain is approximately 13.9% absolute, corresponding to a relative gain of 49.1% over the Otto cycle alone.

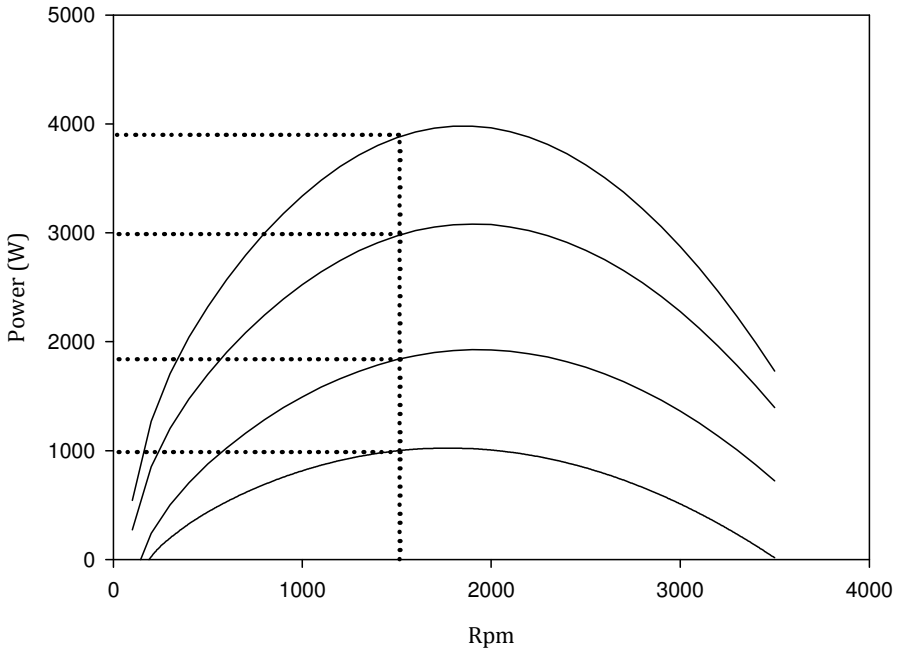

Figure 7.2 Synchronous loading of the GPU-3 Stirling engine operating on Otto exhaust thermal reservoir, brake power curves

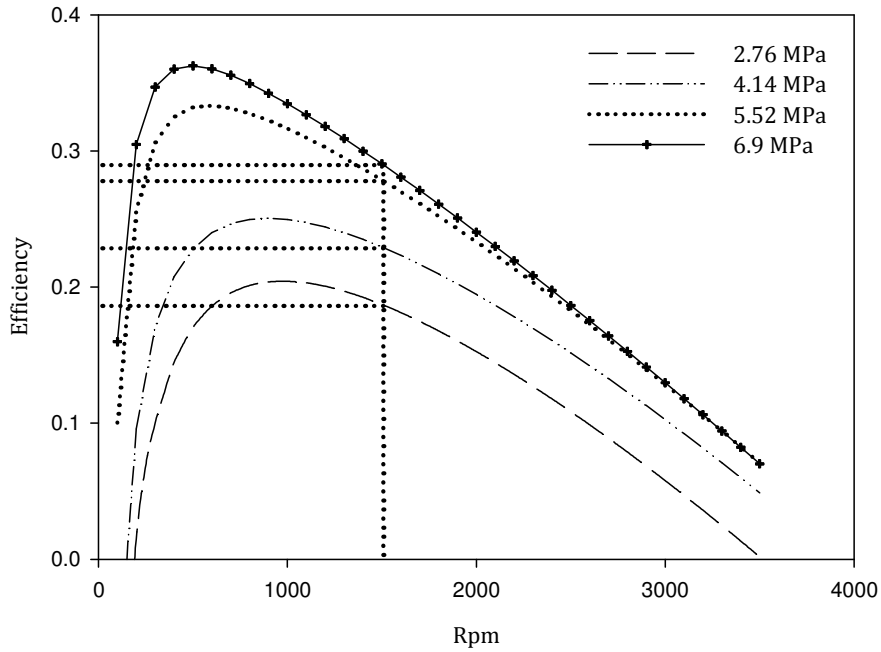

Figure 7.3 Synchronous loading of the GPU-3 Stirling engine operating on Otto exhaust thermal reservoir, brake thermal efficiency curves

Table 7.2 Combined cycle performance, synchronous operation

Otto Cycle Performance		**Value**		
P_{fuel} (@1500 rpm)(kW)		21.43		
P_{brake}(@1500 rpm)(kW)		6.07		
η_{brake} (@1500 rpm)(%)		28.3		
Mean Cycle Pressure (MPa)	2.76	4.14	5.52	6.9
Stirling Cycle Performance				
P_{brake} (@1500 rpm) (kW)	0.99	1.82	2.97	N/A*
η_{brake} (@P_{max}) (%)	18.6	22.9	27.6	N/A*
Combined Cycle Performance				
P_{brake} (kW)	7.06	7.89	9.04	N/A*
$\eta_{CC,brake}$ (%)	32.9	36.8	42.2	N/A*

Performance Gain				
P_{brake} (@1500 rpm) (%)	16.3	29.9	48.9	N/A*
η_{brake} (%) (absolute)	4.6	8.5	13.9	N/A*
η_{brake} (%) (relative)	16.25	30	49.1	N/A*

*heat consumption exceeds availability from Otto exhaust

7.4.1.2 Optimal Operating Frequency—Asynchronous Operation

Although the scenario that might most reasonably be expected would be for the two engines in the hybrid arrangement to operate at identical rotational speeds, an alternative scenario is suggested whereby the two engines operate at asynchronous rotational speeds. This situation could feasibly serve to maximise the total plant efficiency by allowing the bottoming cycle engine to be loaded at its optimum speed. This concept is investigated in this section.

Figure 7.4 shows the heat demand curves for the GPU-3 engine under the same mean cycle pressure conditions as before. The rotational speeds at which each curve intersects the enthalpy availability from the Otto exhaust are shown. It can be seen that for the case of 2.76 MPa mean cycle pressure, the heat demand curve does not intersect the heat supply from the Otto exhaust. This indicates that the engine may require higher operating speed or else is simply undersized under these conditions. The latter would seem to be the case, as the brake power output at this speed is near zero, as can be seen from Figure 7.5.

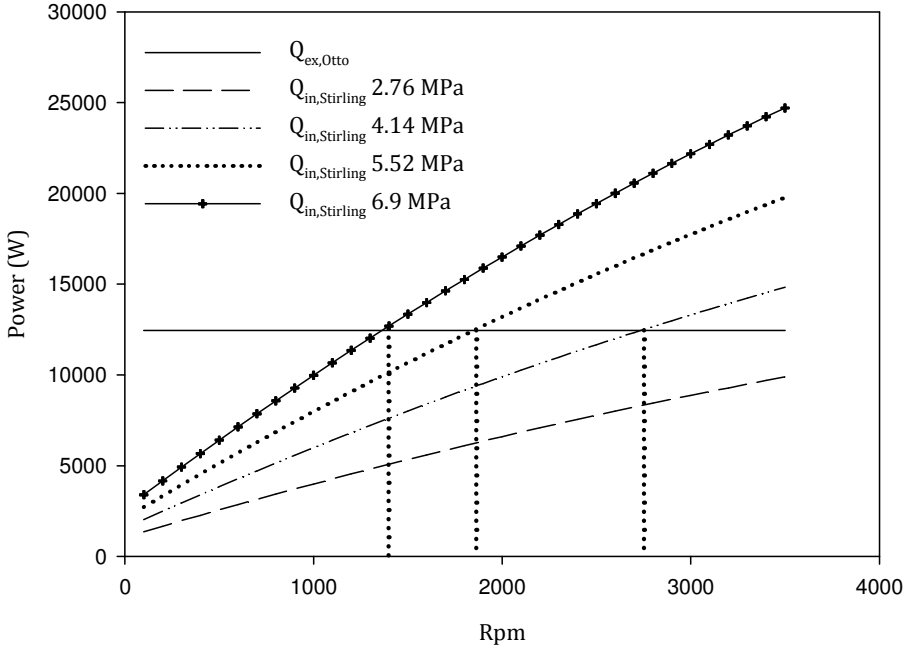

Figure 7.4 Otto cycle exhaust enthalpy availability plotted with GPU-3 Stirling cycle engine heat consumption curves, asynchronous operation

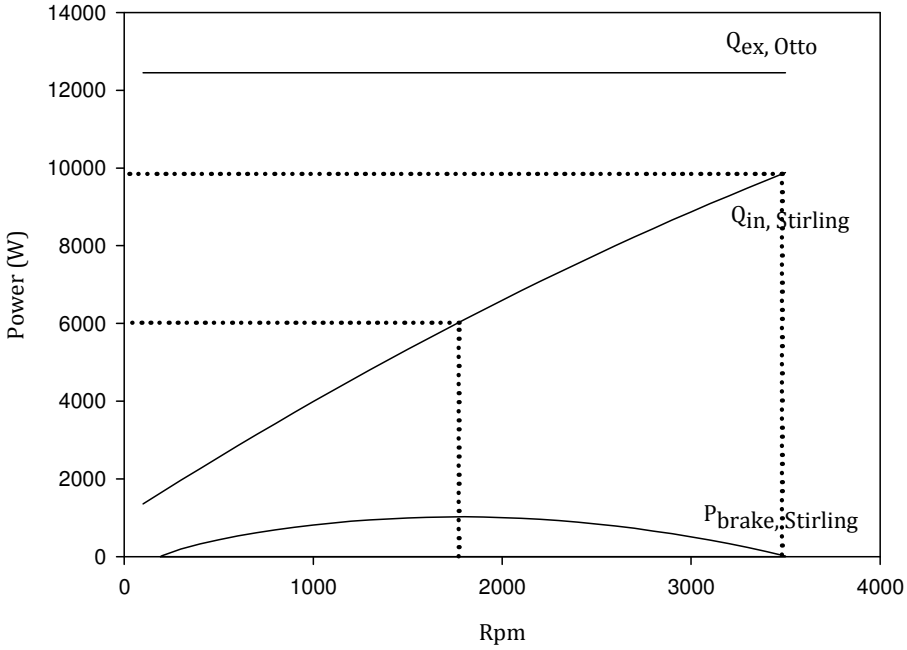

Figure 7.5 Asynchronous loading of the GPU-3 engine operating on Otto exhaust thermal reservoir, 2.76 MPa mean cycle pressure

Figure 7.6 shows the case of the GPU-3 Stirling engine with a mean cycle pressure 4.14 MPa. In this case, the brake power output at the point of intersection of the heat supply and demand curves corresponds to a brake power output below the maximum power output of the engine, which occurs at a lower rpm. The option therefore exists to load the engine at a lower speed, where it would be more efficient and would produce a higher brake power output. The additional unused enthalpy left in the exhaust stream would be dispersed to atmosphere. Similarly to the previous case, this suggests that the engine is underpowered at this mean cycle pressure. The most desirable case is where the maximum power output occurs at the point at which the heat demand matches the supply from the Otto cycle exhaust. This is more closely approximated at the higher mean cycle pressure of 5.52 MPa, as can be seen in Figure 7.7. In this case, the maximum brake power output occurs at a point close to that at which the required heat input matches the heat available from the exhaust.

Figure 7.8 shows the plot for the case of the GPU-3 engine with a mean cycle pressure of 6.9 MPa. In this instance, the power output where the heat supply matches the heat demand occurs at a point below the speed for maximum power, as opposed to above it, as in the previous cases. This negates the possibility of running the engine at a higher rpm to achieve maximum power. Also, it is notable that the power point that is achievable occurs at a rotational speed below the 1500 rpm of the Otto cycle engine. This may have advantages from the perspective of engine wear and component fatigue, both of which become issues with increased operating frequencies.

As before, the brake power output and brake thermal efficiencies for the Otto engine, the Stirling engine and the combined cycle engine are collated and are presented in Table 7.3 for the asynchronous rotational speed scenario under investigation in the present section. The performance gains are presented also as percentages for both the power and efficiency.

The efficiency gains represented in this analysis are the first law efficiency gains. Second law performance can be investigated too for the given combined cycle system, both through the inclusion of the I_R term, as a means of accounting for the irreversibility generated within the cycle, and through investigation of the second law efficiency, η_{II}. Second law performance is analysed in the following section.

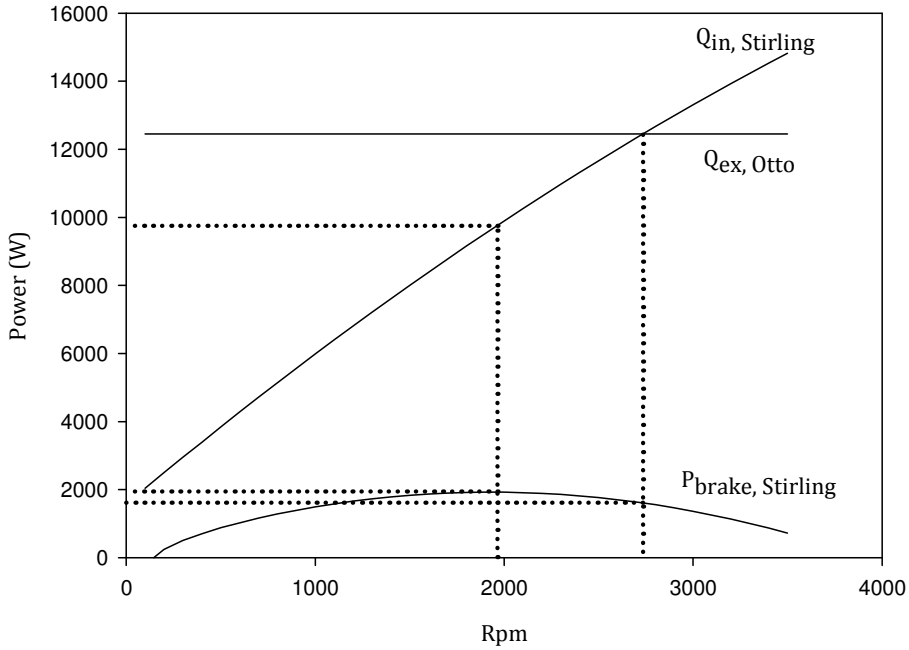

Figure 7.6 Asynchronous loading of the GPU-3 engine operating on Otto exhaust thermal reservoir, 4.14 MPa mean cycle pressure

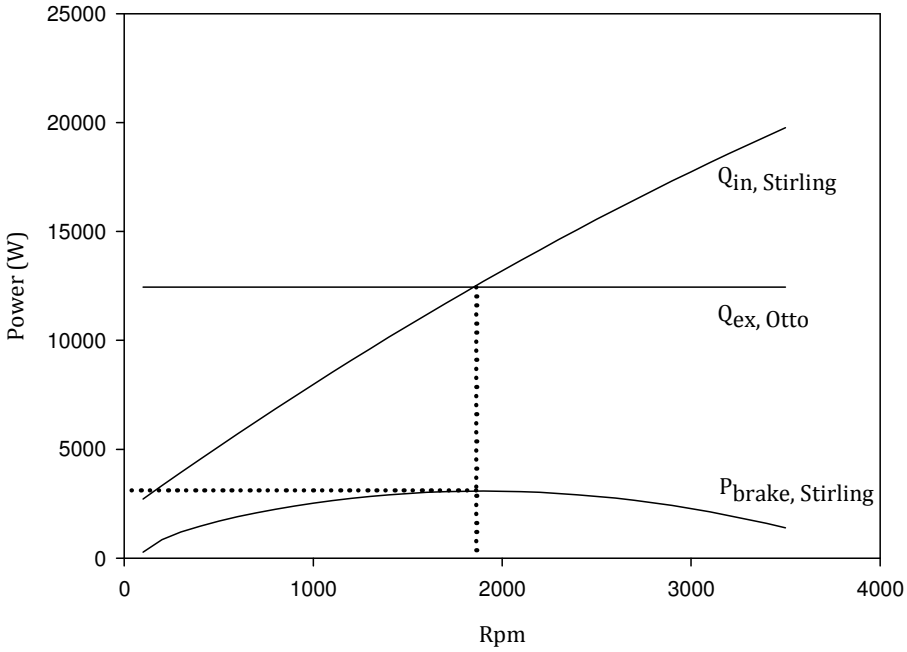

Figure 7.7 Asynchronous loading of the GPU-3 engine operating on Otto exhaust thermal reservoir, 5.52 MPa mean cycle pressure

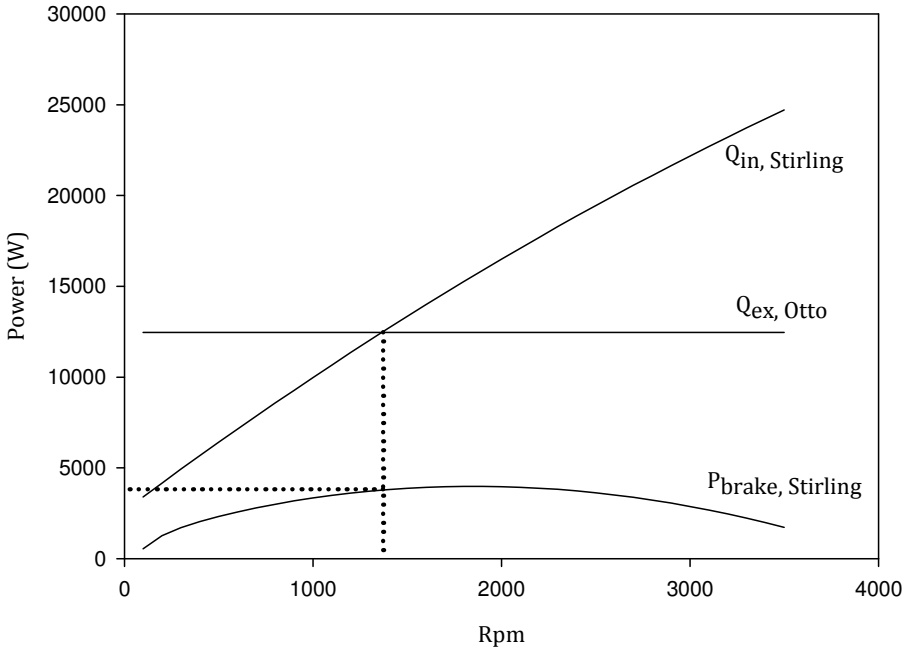

Figure 7.8 Asynchronous loading of the GPU-3 engine operating on Otto exhaust thermal reservoir, 6.9 MPa mean cycle pressure

Table 7.3 Combined cycle performance, asynchronous operation

Otto Cycle Performance				
P_{fuel} (@1500Rpm)(kW)		21.43		
P_{brake} (@1500Rpm)(kW)		6.07		
η_{brake} (@1500 Rpm)(%)		28.3		
Mean Cycle Pressure (MPa)	2.76	4.14	5.52	6.9
Stirling Cycle Performance				
P_{brake} (max) (kW)	1.04	1.92	3.08	3.78
η_{brake} @ P_{max} (%)	16.7	20.0	24.3	25.7
Combined Cycle Performance				
P_{brake} (kW)	7.11	7.99	9.15	9.85
$\eta_{CC,brake}$ (%)	33.2	37.3	42.7	46.0
Speed @ P_{max} (rpm)	1770	1924	1860	1380
Performance Gain				
P_{brake} (max) (%)	17.1	31.6	50.7	65.6
η_{brake} (%) (absolute)	4.9	9.0	14.4	18.6
η_{brake} (%) (relative)	17.31	31.8	50.9	65.7

7.4.2 Second law Analysis of the Combined Cycle System

7.4.2.1 Second law Efficiency of the Combined Cycle

The second law efficiency of a power plant is defined as the ratio of the actual irreversible plant efficiency to the efficiency of the same plant operating reversibly. It is used to investigate the performance of the plant in terms of its

maximum possible performance and inherently characterises the entropy generation and related exergy destruction within the cycle. It therefore serves as a useful design-aid when considering performance improvements for power plant. It can be simply expressed as:

$$\eta_{\mathrm{II}} = \frac{\eta_{\mathrm{irrev}}}{\eta_{\mathrm{rev}}} \tag{7-10}$$

In the case of the combined cycle under investigation, it is necessary to derive an expression for the reversible power output of the power plant. By considering the ideal air standard cycles, the reversible power output of the combined cycle system can be expressed as:

$$P_{\mathrm{CC,rev}} = P_{\mathrm{Otto}} + P_{\mathrm{Stirling}} \tag{7-11}$$

which becomes:

$$P_{\mathrm{CC,rev}} = \dot{C}_{\mathrm{O}}[(T_3 - T_4) + (T_1 - T_2)] + m_{\mathrm{St}} f \mathrm{R}_{\mathrm{St}} \ln(R_v)\left(T_{\mathrm{H,g}} - T_{\mathrm{c,g}}\right) \tag{7-12}$$

where $\dot{C}_{\mathrm{O}}$ is the heat capacity rate of the Otto cycle, m_{St} is the mass of working gas in the Stirling cycle and f is the cycle frequency of the Stirling cycle. The efficiency of the combined cycle is given as:

$$\eta_{\mathrm{CC,rev}} = \frac{P_{\mathrm{CC,rev}}}{\dot{Q}_{\mathrm{in,rev}}} \tag{7-13}$$

where the heat admitted to the combined cycle, $\dot{Q}_{\mathrm{in,rev}}$, is that which is supplied to the Otto cycle:

$$\dot{Q}_{\mathrm{in,rev}} = \dot{C}_{\mathrm{O}}(T_3 - T_2) \tag{7-14}$$

$\dot{C}_{\mathrm{O}}$ is the heat capacity rate of the mass flow through the Otto cycle. For the combined cycle the maximum efficiency that would be obtainable by the plant would correspond to the reversible efficiency. The second law efficiency for the plant would therefore be the ratio of the actual combined plant efficiency to this reversible efficiency:

$$\eta_{\mathrm{II,CC}} = \frac{\eta_{\mathrm{CC,brake}}}{\eta_{\mathrm{CC,rev}}} \tag{7-15}$$

The previous analyses of the cycle focused on optimisation of the combination in terms of the rotational speed of the engines. It is also possible to investigate the evolution of $\eta_{II,CC}$ with the operating speed of the plant. This can be seen in Figure 7.9, which presents plots of the second law efficiency of the plant against the operating rotational speed and at each of the different mean cycle pressure values already investigated for the Stirling cycle engine.

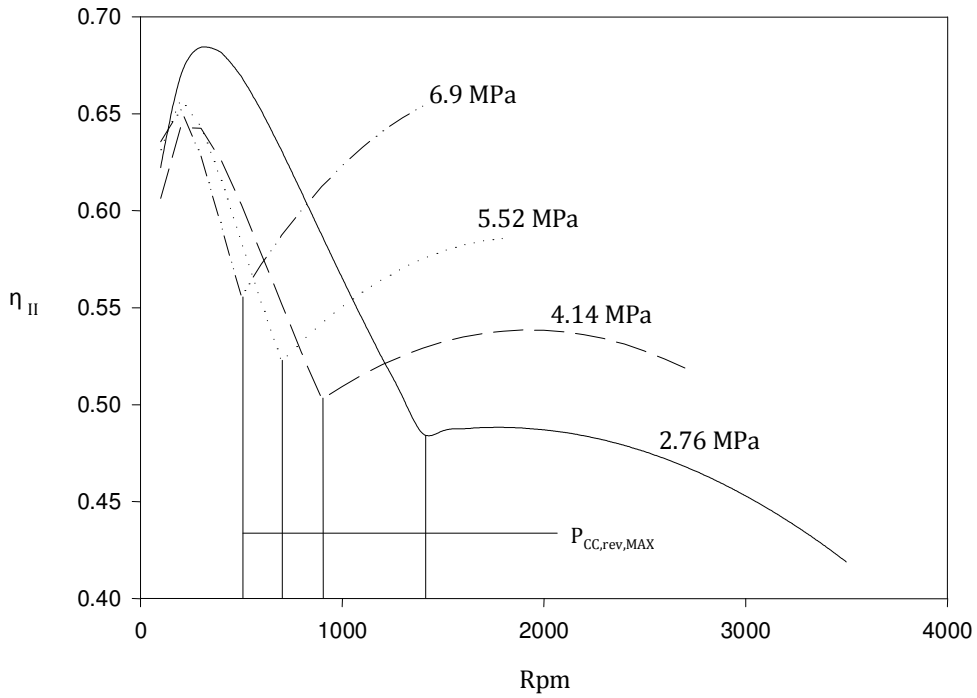

Figure 7.9 Second law efficiency of the combined cycle plant against Stirling engine rotational speed

It can be seen from Figure 7.9 that two local maxima exist for the second law efficiency of the plant, corresponding to part load operation and maximum power operation of the plant. The part load scenario describes the case of the heat addition to the reversible Stirling cycle being less than that available from the reversible Otto cycle. The maximum power scenario involves the case of the

heat addition to the reversible Stirling cycle being equal to that available from the Otto cycle exhaust. This scenario therefore represents the maximum reversible power possible from the combined cycle, for each mean-cycle-pressure value of the Stirling engine.

It can also be seen from Figure 7.9 that for each mean-cycle-pressure regime, the second law efficiency curve terminates at the point of maximum power output from the practical combined cycle engine. As is seen in previous examples, this is the point at which the actual irreversible engine heat requirement exceeds the heat available from the Otto cycle exhaust. For the 5.52 MPa and 6.9 MPa mean cycle pressure cases it can be seen that the second law efficiency curves terminate before a clear optimum point is reached. However, in the case of the 4.14 MPa and 2.76 MPa regimes, clear optima are visible.

The part load and maximum power regimes can be understood with reference to Figure 7.10, which illustrates the point of intersection of the heat requirement for the reversible Stirling cycle engine and the heat rejection from the reversible Otto cycle engine. Also, Figure 7.11 shows plots of the first law efficiencies of the reversible and irreversible versions of the combined cycle system. This plot is used to demonstrate the origin of the two maxima present in each of the second law curves. This can be inferred, as the second law efficiency is the ratio of the irreversible efficiency to the reversible efficiency, as mentioned previously.

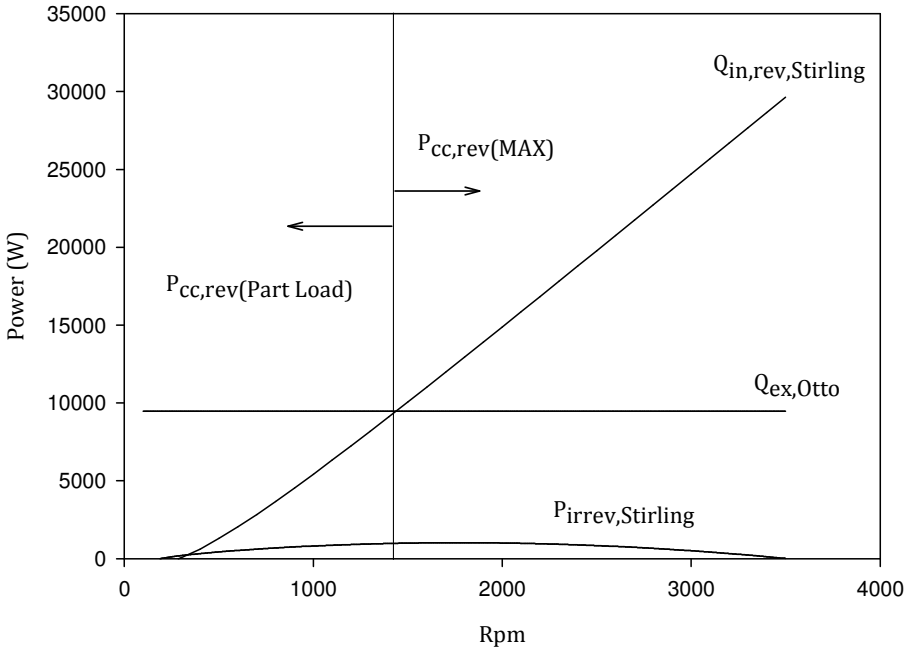

Figure 7.10 Part load and maximum power operation zones for reversible combined cycle system, 2.76 MPa mean cycle pressure

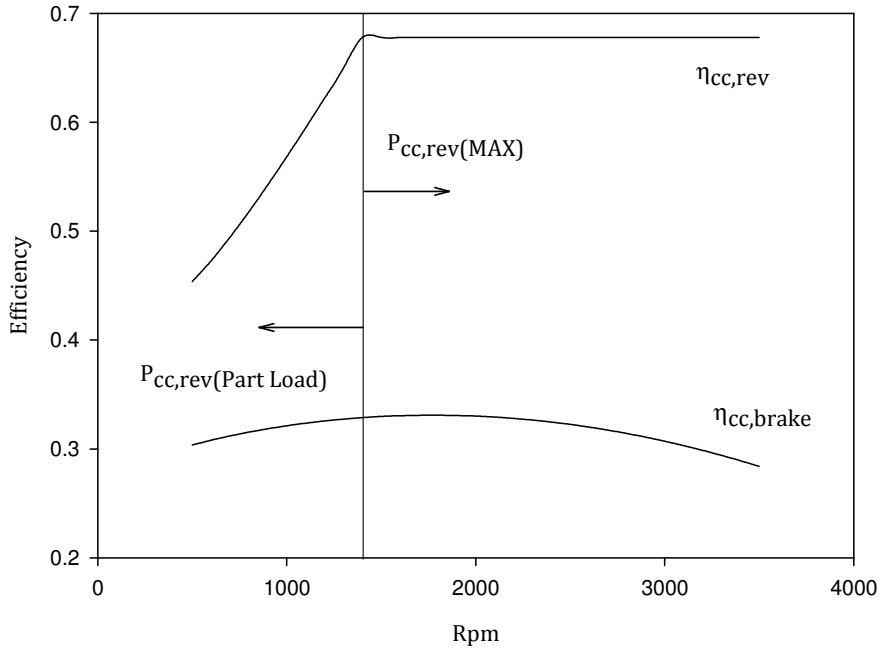

Figure 7.11 First law efficiencies of reversible and irreversible combined cycle, 2.76 MPa mean cycle pressure

It is possible to conclude from Figure 7.9 that under maximum power conditions, second law efficiency is positively affected by an increase in mean cycle pressure. Maximum second law efficiency occurs for the case of 6.9 MPa mean cycle pressure. However, under part-load conditions, the opposite is the case, with peak second law efficiency occurring for the case of 2.76 MPa mean cycle pressure. It may be inferred, however, that the local maxima for the part-load cases occur at impractically low speeds for the engine in question and so are not particularly relevant to the analysis. For the maximum-power cases, by definition, the maximum second law efficiencies occur at the point of maximum total power output from the combined cycle system.

7.4.2.2 Optimal Irreversibility Parameters

It is possible to use the FTT models for the Otto and Stirling cycles developed previously to further investigate the operating regimes that offer the minimum entropy generation within the gas circuits. This is done by analysing the irreversibility parameter, I_R, for each cycle. As this is the ratio of the entropy exiting the system to that entering, it effectively represents the entropy generation within the cycle—see Chapter 5, Equation (5-29). It should be noted that investigation of I_R is not equivalent to investigation of η_{II}. The I_R term accounts for irreversibilities within the gas processes only, whereas the η_{II} term accounts also for mechanical friction and pumping losses due to its inclusion of the total brake power of the cycles.

Figure 7.12 shows the variation of the parameter I_R over the full range of operation for the one-cylinder gasoline-fired Otto cycle engine analysed previously.

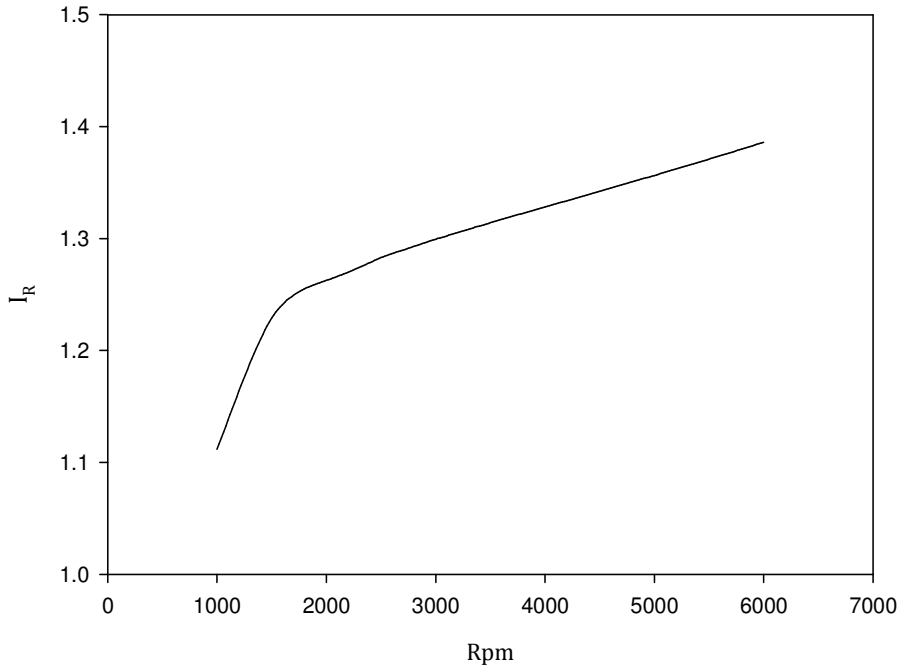

Figure 7.12 Irreversibility parameter, I_R, for the 1-cylinder naturally aspirated gasoline-fired Otto cycle engine investigated in Chapter 4

A similar plot is given in Figure 7.13 for the Stirling cycle engine analysed previously, the GPU-3. On this plot can be seen the variation of I_R over the full operating speed range for this engine, for the four mean-cycle-pressure regimes under investigation. As with the Otto cycle engine, it can be seen from the plot that the I_R value does not show an explicit minimum value at any point, but rather displays a monotonic increase for all mean-cycle-pressure regimes over the given speed range. In this case it can therefore be suggested that in order to minimise the irreversibility generation within the gas circuit of the engine it is simply necessary to load the engine at as low an operating frequency as possible and to reduce the mean cycle pressure. This is contrary to the maximum power conditions of the engine, which indicate that increasing the mean cycle pressure has the effect of increasing the attainable power output of the cycle.

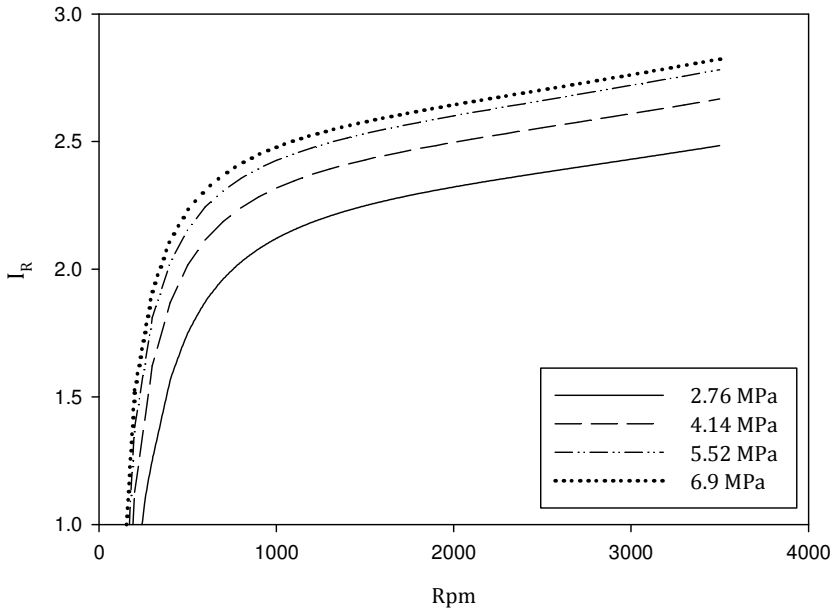

Figure 7.13 Irreversibility parameter, I_R, for the GPU-3 Stirling engine investigated in Chapter 6

7.5 Applications of the Combined Cycle—Distributed Generation and Combined Heat and Power

The combined cycle system that has been developed in the present work is envisaged as being suitable for application in the *DG* market. This would include application both for *mono*-generation—the generation of electrical power only—and for *poly*-generation, which involves the recovery of waste heat in addition to the electrical output. This heat may be used as space or process heating (CHP), or the plant may provide both heating and cooling (tri-generation).

The advantages of the combined cycle system are immediately obvious in the case of simple electrical generation, as the increase in primary energy efficiency would translate directly into fuel-cost savings to the operator. The revenue gains, however, need to be balanced against the increased plant size and

complexity. A full economic analysis of the system is detailed in the following chapter, in which case the cost-benefit analysis with regard to the additional plant complexity is assessed.

In the case of cogeneration, the economic value of the heat recovered from the plant must be included in the economic analysis of the engine deployment. The high-grade heat available from the exhaust stream of a combustion engine is typically desirable as a thermal source for raising steam or for heating water in situations with a suitable heat demand. In the case of the combined cycle, a proportion of this high grade heat would be effectively diverted to mechanical work via the bottoming cycle engine. However, although the work output has a higher economic value than the high-grade heat output, the increased low-grade heat present in the cooling water circuit would have to be accommodated.

7.5.1 Heat Balance of the Combined Cycle Plant for Cogeneration

Figure 7.14 shows the heat balance for the various permutations of the combined cycle plant under the synchronous operating regime detailed previously. The heat balance of the Otto cycle engine is presented at the extreme left. The other plots represent the combined cycle with the Stirling cycle operating at different mean cycle pressures. It can be seen that with increasing power output from the Stirling cycle, brought about by increased mean cycle pressure, the proportion of the heat admitted to the cycle that is diverted to each energy sink changes considerably. In particular, the proportion diverted to the low-grade jacket cooling water circuit increased significantly compared to the single cycle case. It should be noted again that the 6.9 MPa case cannot be included in the synchronous regime analysis due to a heat demand in excess of that available from the Otto cycle exhaust stream. It can

however, be used as an indicative value. As before, the actual limiting mean cycle pressure would lie somewhere between this and the 5.52 MPa value and could be determined through interpolation.

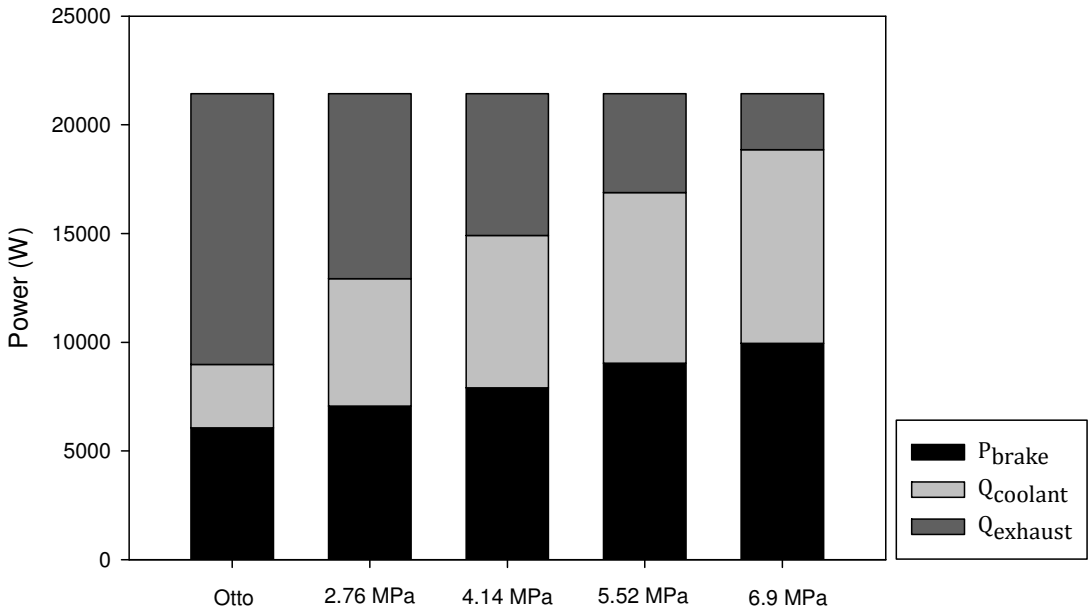

Figure 7.14 Energy balance of the combined cycle plant for cogeneration—synchronous frequency operation

Figure 7.15 shows the same series of data for the case of asynchronous loading of the combined engines. Similar trends in the proportions of the energy sinks are visible although, as before, it is noted that the brake thermal efficiency in this case is higher than that attainable for the synchronous operation regime. It is also noted that the exhaust energy proportion for the 5.52 MPa and 6.9 MPa cases is approximately the same. The increase in brake thermal efficiency at the higher mean cycle pressure appears to come at the expense of the jacket water cooling sink.

The economic significance of the change in the energy balance of the plant from the perspective of a cogeneration plant will be dealt with in detail in the following chapter.

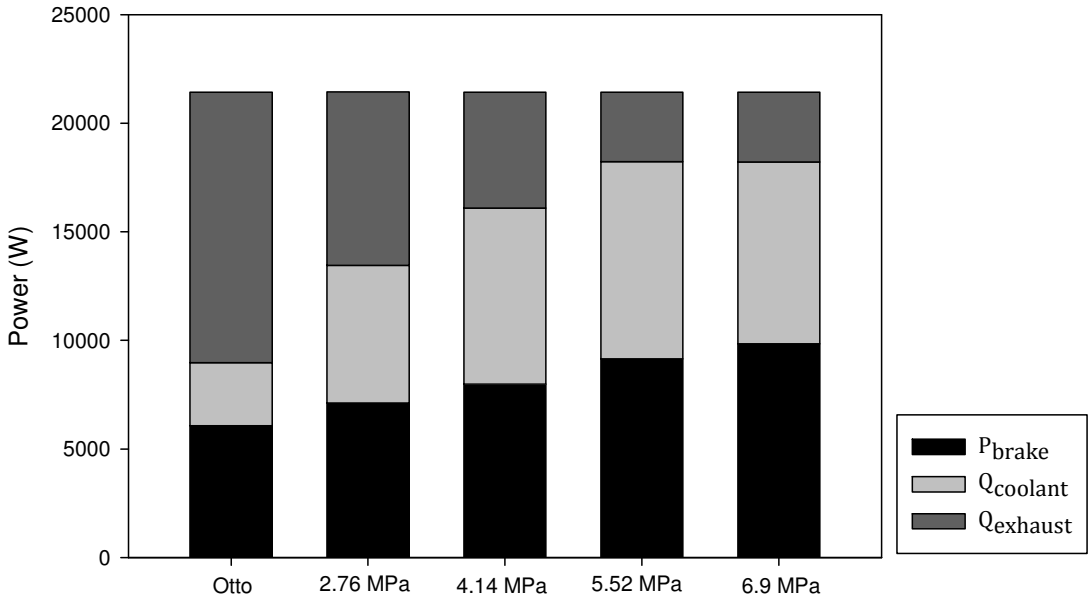

Figure 7.15 Energy balance of combined cycle plant for cogeneration—asynchronous frequency operation

7.5.2 Variation of the Heat Balance of the Combined Cycle Plant

It is of interest at this point to discuss the implications of variation of the Otto cycle energy balance and its effect on the combined cycle operation. Any bottoming cycle is necessarily dependant on both the quantity and quality of the energy available in the exhaust stream of the topping engine, in this case the Otto cycle engine. Steps to improve the efficiency of such Otto engines such as those mentioned in Chapter 2 generally have the effect of reducing both the quantity of energy expelled in the exhaust stroke but also the temperature at which it is expelled. It can therefore be implied that such improvements in the Otto cycle technology will negatively affect the potential output of the Stirling

bottoming cycle. This is a critical concern for the economic deployment of the combined cycle, however it should be noted that even the most advanced Otto-type engines have sufficiently high exhaust temperatures to permit some level of bottoming cycle operation. Similarly, the nature of the Otto cycle energy sinks and their behaviour at different loads is introduced in Chapter 2. The energy balance of the Otto engine is affected under different loading regimes, with the tendency to be towards reduced exhaust energy proportion at part-loads. Such a reduction in the exhaust energy proportion will necessarily have a detrimental effect on the performance of the bottoming cycle. A complete study of part load performance is not completed here, as the design point of industrial prime-movers is generally full load operation. This regime is therefore prioritised in the present work.

7.5.3 Exergy Analysis of the Combined Cycle Energy Sinks

To more fully investigate the thermodynamic implications of using the combined cycle system in a cogeneration scenario, it was necessary to appraise the quality of heat sinks and to compare the combined cycle system to the single cycle Otto engine. This was deemed necessary as the quality of the thermal sinks are of importance in such scenarios; for example, any degradation in the high grade heat present in the exhaust stream may negatively impact the ability of the plant to raise high pressure steam for industrial use. This is an issue very much concerning the economics of plant deployment, and while an estimation of the exergy losses in the combined cycle system will not be fully representative of the utility of the plant from a heat recovery viewpoint, it is still of interest due to the high value of the mechanical work output, which ultimately would be

converted to electrical power. The exergy balance was therefore completed as a complementary study to the second law analysis. It involved performing an exergy analysis on each of the energy sinks and the subsequent comparison of the total exergy balance with that of the Otto cycle operating in a single cycle system.

7.5.3.1 Calculation of Exergy for Finite Capacity Reservoirs

The exergy content of the thermal sinks associated with the combined cycle is assessed by assuming the sinks to be finite-capacity thermal reservoirs. This assumption means that the temperature of each sink changes with the transit of heat across the boundary. The Carnot efficiency for reservoirs of finite thermal capacity is [157]:

$$\eta_{C,fr} = 1 + \left(\frac{(1-\eta_C)}{\eta_C}\right)\ln(1-\eta_C) \tag{7-16}$$

where

$$\eta_C = 1 - \left(\frac{T_c}{T_H}\right) \tag{7-17}$$

This modified version of the Carnot cycle efficiency is therefore used to calculate the exergy value of the reservoirs using the relationship:

$$B = \eta_{C,fr} Q \tag{7-18}$$

where Q is the heat transfer of the reservoir expressed in watts and B is the associated exergy transfer of the reservoir, expressed in watts.

7.5.3.2 Exergy Analysis—Synchronous and Asynchronous Operation

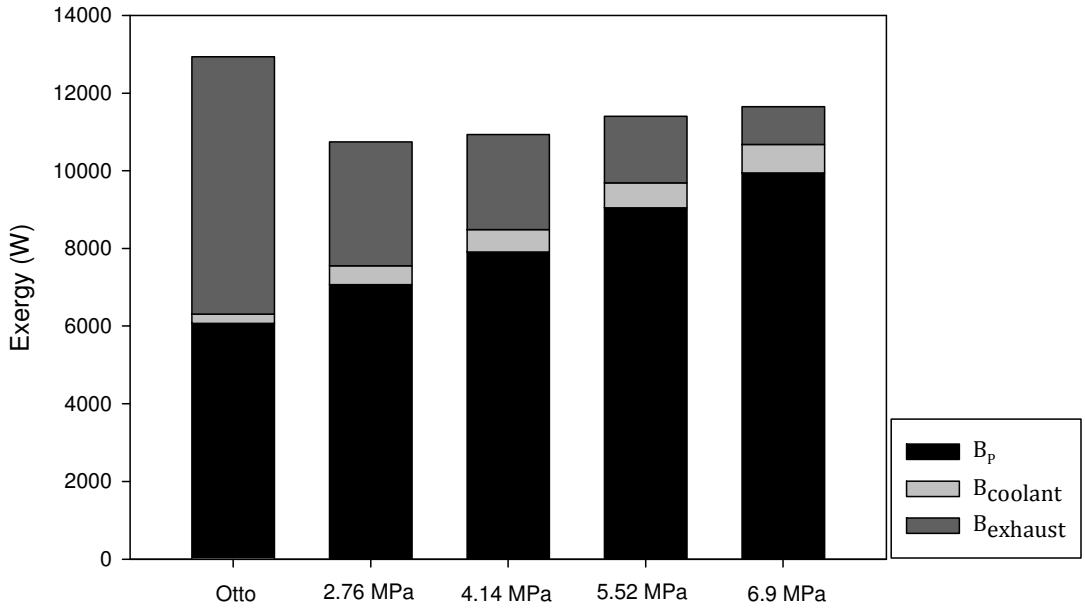

Figure 7.16 Exergy balance of combined cycle plant for cogeneration—synchronous frequency operation

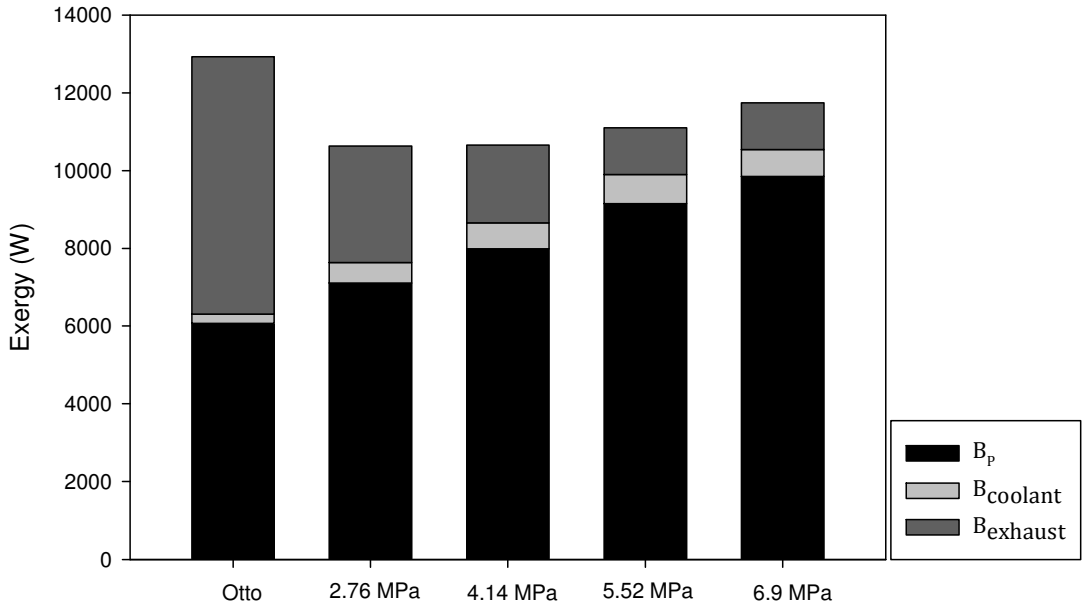

Figure 7.17 Exergy balance of combined cycle plant for cogeneration—asynchronous frequency operation

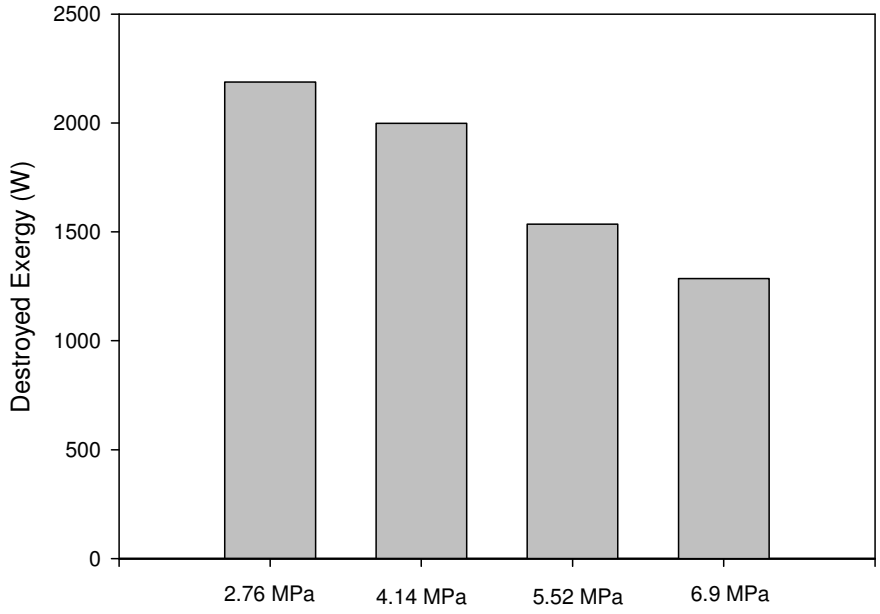

Figure 7.18 Destroyed exergy of combined cycle plant—synchronous frequency operation

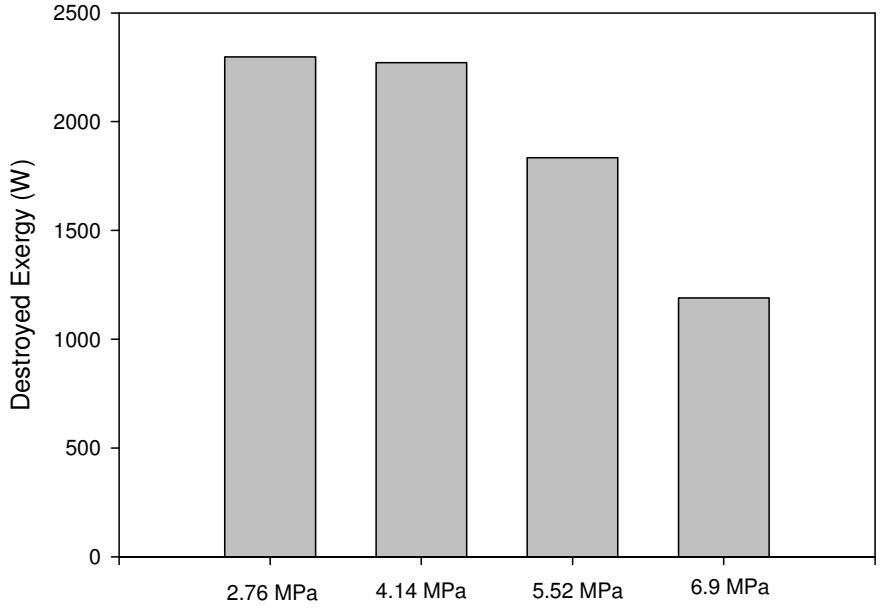

Figure 7.19 Destroyed exergy of combined cycle plant—asynchronous frequency operation

Figure 7.16 shows a plot of the exergy balance of the combined cycle plant for the different configurations under investigation and in the synchronous operation scenario. Figure 7.17 shows a similar plot for the case of asynchronous operation.

Figure 7.18 and Figure 7.19 show the actual quantities of exergy destroyed for the synchronous and asynchronous cases of the combined plant, over and above that destroyed in the Otto cycle engine acting in a single cycle mode. A bottoming cycle does not reduce the endogenous exergy destruction of a single cycle plant. In the case of this particular combined cycle plant the benefit is that the exergy of the exhaust gas stream of the Otto cycle engine is converted to three exergetic outputs mechanical work (brake power), heat transfer to the cooling jacket water and the exergy of exhaust from the bottoming Stirling cycle.

For many practical applications the reduced grade of the exhaust heat from the combined cycle plant would not be a serious disadvantage. The published experimental data indicates an approximate average exhaust gas temperature from the Stirling exhaust of 717 K. This is of the similar magnitude to the temperature of the direct exhaust of some commercially available cogeneration engines and indicates that there remains the possibility for some recovery of heat from the combined cycle exhaust, with the proportion being reduced compared to a single cycle plant.

7.6 Conclusions

Simulation results for the combined Otto/Stirling thermodynamic cycle are presented. Both first law and second law analyses are conducted to investigate

the thermodynamic benefits of using the combined cycle rather than the single cycle.

The use of the combined cycle is analysed for both a mono-generation scenario and a cogeneration scenario. In the case of mono-generation, only an increase in mechanical power is of particular interest, as this would be converted directly to electrical energy. The higher brake thermal efficiency made possible by the combined cycle would therefore offer direct economic benefits through fuel cost savings to the operator.

For the case of cogeneration, the magnitude and quality of the heat sinks must be accounted for in the analysis. While the increased electrical output is of primary importance for the cogeneration scenario, the grade of the thermal sinks is important also, as it will affect the possibility for economic heat recovery and utilisation from the plant.

First law analysis indicates that significant increase in brake thermal efficiency and brake power output is feasible with the combined cycle. It is also seen that the waste heat production of the plant becomes concentrated in the low grade coolant water circuit for the combined cycle system. Two optimisation scenarios are studied: synchronous operation whereby the two engines are loaded at the same rotational speed, and asynchronous operation, whereby the Stirling cycle engine is loaded at a different speed. This is done to enable the Stirling cycle engine to be run as close to the maximum power point as possible and therefore to maximise total plant efficiency.

Second law analysis indicates optimal regimes for the maximum second law efficiency and for the minimisation of the irreversibility parameter, I_R. The

exergy destruction of the bottoming cycle is greater for the lower mean cycle pressure variants of the Stirling engine.

8 ECONOMIC ANALYSIS OF THE COMBINED CYCLE SYSTEM

8.1 Introduction

This chapter presents an economic analysis of the combined cycle system when deployed as a prime mover for both mono-generation and cogeneration scenarios. As the technical merit of any technology is largely secondary to its market attractiveness, the argument for or against the use of the combined cycle system necessarily must include an appraisal of the economic return on investment over and above that of the current market standard.

There are a host of methods available to perform economic analysis of power generation systems. Central among these are the *Simple Payback Period* (SPP), the *Net Present Value* (NPV) and the *Internal Rate of Return* (IRR) methods. The SPP is conceptually the simplest of these, being the ratio of the capital cost of the project to the periodical net revenue of the investment, typically measured as annual revenue. The SPP therefore describes the length of time required for the investment revenue to completely offset the initial investment cost. It therefore acts as a measure of project risk; however it does not offer any insight into the long term profitability of the project. This can be more clearly assessed using the NPV. The NPV quantifies the total net revenue over the life of the project and discounts it to its *Present Value* (PV). The difference, therefore, between the capital cost and the Present Value of the net revenue indicates whether the project will add value to the company. A positive NPV indicates a worthwhile investment and competing investment opportunities with individual positive

NPVs may be compared, based on the relative magnitudes of these NPVs, to decide upon the most attractive investment.

8.2 Methodology

Both the single cycle Otto engine and the combined cycle system were appraised using standard economic appraisal techniques. These were the SPP, the NPV and the IRR. The engine plant investigated was that detailed in the preceding chapter. A comparison was also made between the Otto engine used previously and another Otto engine with higher efficiency. This was done to investigate the economic benefit of increasing the Otto cycle plant efficiency in a single cycle plant.

The system was analysed in each of four scenarios: as a cogeneration system acting under synchronous and asynchronous engine loading and as a mono-generation system for AD gas, again under synchronous and asynchronous operation.

The NPV of the system was analysed on a per-kW basis in order to generalise the analysis. Both the electrical power output and the fuel power input were used as reference points for this in order to assess the long term investment viability of the plant. Economic analysis of power plant is typically done with reference to the electrical power output. However, with NPV analysis this method does not necessarily account for the sensitivity of the model to the plant efficiency. This can be accommodated by performing the NPV analysis with respect to the fuel power input. Therefore, rather than computing the savings or revenue per kW of electrical power generated, the savings or revenue per kW of fuel power consumed is calculated. The intention is to provide a metric for

assessing plant profitability as a function of the quantity of fuel consumed by the plant. This is of particular relevance in situations involving the use of the plant for recovery and conversion of a fuel from a finite reservoir such as an AD gas source or a landfill gas source. In such cases, the requirement for maximum efficiency is evident, as efficiency gains translate directly into revenue gains for the operator. In this regard, the NPV of the plant investment per kW of fuel consumed would be the most important, as it accounts directly for the benefits of using higher-efficiency plant.

8.3 Economic Model

The economic model used accounted for the SPP, the NPV and the IRR for the combined cycle system.

8.3.1 Primary Energy Savings

The *Primary Energy Saving* (PES) associated with a cogeneration plant is the cost difference between the cost to purchase the *equivalent power cost*, EC, from the local utility providers the *running cost* (RC) of the plant, including fuel and maintenance costs:

$$\mathrm{PES_{chp}} = \mathrm{EC_{chp}} - \mathrm{RC_{chp}} \tag{8-1}$$

In the simplest scenario, the running costs can be summarised as the fuel cost plus the maintenance cost of the unit plus any fixed overhead costs associated with connection to the utility grids:

$$\mathrm{RC_{chp}} = (P_\mathrm{F} C_\mathrm{F} N_\mathrm{H}) + C_\mathrm{m} + C_\mathrm{E,fixed} + C_\mathrm{G,fixed} \tag{8-2}$$

where P_F is the fuel power content, C_F is the unit cost of the fuel, N_H is the number of operating hours, C_m is the unit cost for maintenance of the plant, $C_\mathrm{E,fixed}$ is the cost associated with maintaining electrical grid connection and

$C_{\mathrm{G,fixed}}$ is the unit cost associated with maintaining grid connection to the fuel gas grid. Similarly, the cost to purchase the equivalent power from the utility suppliers can be given as:

$$\mathrm{EC}_{\mathrm{chp}} = (P_{\mathrm{m}}\eta_{\mathrm{alt}}N_{\mathrm{H}}C_{\mathrm{E}}) + N_{\mathrm{HUF}}\left(\left(\frac{\dot{Q}}{\eta_{\mathrm{B}}}\right)N_{\mathrm{H}}C_{\mathrm{G}}\right) \tag{8-3}$$

where P_{m} is the mechanical power output of the plant, η_{alt} is the efficiency of the alternator, C_{E} is the electrical unit tariff, N_{HUF} is the Heat Usage Factor, $\dot{Q}$ is the thermal power output of the plant, $\eta_{\mathrm{B}}$is the efficiency of the equivalent sized boiler and C_{G} is the unit tariff for the boiler fuel gas. The Heat Usage Factor, $N_{\mathrm{HUF}} \leq 1$. The Heat Usage Factor is used to accommodate situations in which not all of the available heat is utilised. This is a common feature of such systems and arises from the unpredictability of space heating requirements on a given site over such a protracted timespan.

These expressions account only for simple electrical and gas fuel tariffs by assuming only one tariff in each case. In practical cases, the model would be expanded to include various different tariffs as dictated by the local utility suppliers. It is common to have tariffs which use a *time of day* structure, whereby peak demand hours are charged a higher tariff than off-peak hours. The core structure of the economic model remains the same though, such that the simplified form is appropriate for the current analysis.

When considering novel gas recovery systems such as power generation from landfill or AD gas, there is no unit cost associated with the actual gas fuel itself. Running costs are therefore generally limited to the maintenance costs and the overheads for connection to the grid. The plant output, typically confined to the

electrical output, is sold directly to the utility. It is therefore more appropriate to discuss the plant economy in terms of the annual revenue from selling power directly to the grid rather than the savings made over purchasing of the equivalent power from the grid. The net annual revenue is the difference between the gross revenue and the annual running costs for the plant:

$$\mathrm{AR_{NG}} = \mathrm{AR_{NG,gross}} - \mathrm{RC_{NG}} \tag{8-4}$$

where $\mathrm{AR_{NG,gross}}$ is the gross annual revenue associated with the novel gas applications and $\mathrm{RC_{NG}}$ is the running cost of the plant associated with novel gas applications. Most jurisdictions offer a special rate to power producers generating from renewable energy sources such as these special gas applications. This tariff can be given as C_{R} and included in the analysis of the plant gross annual revenue:

$$\mathrm{AR_{gross}} = P_{\mathrm{m}}\eta_{\mathrm{alt}}N_{\mathrm{H}}C_{\mathrm{R}} \tag{8-5}$$

The annual running costs for the unit are the maintenance costs and the fixed overheads associated with maintaining grid connection:

$$\mathrm{RC_{NG}} = C_{\mathrm{m,NG}} + C_{\mathrm{E,fixed,NG}} \tag{8-6}$$

where $\mathrm{C_{m,NG}}$ is the cost associated with the maintenance of the novel gas fired unit and $C_{\mathrm{E,fixed,NG}}$ is the fixed overhead cost associated with connection to the electrical utility grid.

8.3.2 Capital Cost

The capital cost of the plant is central to the economic analysis. To generalise analysis it is typical to specify the capital cost of the plant on a per kW basis, typically taking the electrical power output as the reference point. For the case of the single cycle plant this is straightforward, as generalised specific cost values for such engines are readily available in the literature. When calculating

the specific capital cost of the combined cycle plant, however, it is necessary to incorporate the specific costs of two different engine technologies. The resulting cost must therefore account for the relative proportions of the final delivered-power taken from each engine. The specific costs used in the present analysis are presented in Table 8.1. X^1_{Otto} refers to the specific cost of the original Otto cycle engine used in analysis to this point, and X^2_{Otto} refers to the high-efficiency Otto cycle engine analysed for comparative purposes. Note that the increase in specific capital cost for the latter is a somewhat arbitrary assumption, made to reflect the increased plant complexity inherently required for achieving the improvement in performance.

Table 8.1 Specific capital cost for each of the prime movers under investigation [158, 159]

$X^1_{\text{Otto,E}}$ (€/kW$_e$)	1000
$X^1_{Otto,F}$ (€/kW$_f$)	283
$X^2_{\text{Otto,E}}$ (€/kW$_e$)	1100
$X^2_{\text{Otto,F}}$ (€/kW$_f$)	495
X_{Stirling} (€/kW$_e$)	2000

The specific capital cost for the combined cycle plant can therefore be calculated from the expression:

$$X_{\text{CC}} = X_{\text{Otto}}\eta_{\text{alt}}\left(\frac{P_{\text{m}}}{P_{\text{CC}}}\right) + X_{\text{Stirling}}\eta_{\text{alt}}\left(\frac{P_{\text{Stirling}}}{P_{\text{CC}}}\right) \tag{8-7}$$

where P_{CC} is the total power output of the combined cycle and $P_{Stirling}$ is the power output of the Stirling cycle engine.

8.3.3 Simple Payback Period

The SPP for an investment is the ratio of the initial capital investment to the net annual revenue from the investment. It indicates the time, in years, required for the revenue to pay back the investment cost. It is a simple analysis tool and therefore has limitations, however it finds widespread use as a "back of the envelope" indicator for the risk associated with an investment. For the case of a cogeneration plant, the SPP is the ratio of the capital cost to the PES:

$$\mathrm{SPP}_{\mathrm{chp}} = \frac{X_{\mathrm{capital,chp}}}{\mathrm{PES}} \tag{8-8}$$

where $X_{\mathrm{capital,chp}}$ is the capital cost associated with the given CHP unit. For the case of a novel gas-recovery power generation plant, the SPP is the ratio of the capital cost to the net annual revenue:

$$\mathrm{SPP}_{\mathrm{NG}} = \frac{X_{\mathrm{capital,NG}}}{\mathrm{AR}_{\mathrm{net}}} \tag{8-9}$$

where $X_{\mathrm{capital,NG}}$ is the capital cost associated with the plant when used for novel gas applications.

8.3.4 Net Present Value

The NPV is calculated as the difference between the capital cost of the plant and the sum of all discounted net annual revenue payments for the lifetime of the plant. For the case of the cogeneration unit, the NPV of the investment is:

$$\mathrm{NPV}_{\mathrm{chp}} = \sum_{t=1}^{n} \left(\frac{PES_{\mathrm{chp}}}{(1+i)^t} \right) - X_{\mathrm{capital}} \tag{8-10}$$

where n is the lifetime of the plant under investigation, usually measured in years and i is the discount rate. Similarly, the NPV for the novel gas application can be expressed as:

$$\mathrm{NPV_{chp}} = \sum_{t=1}^{n} \left(\frac{AR_{NG}}{(1+i)^t} \right) - X_{\mathrm{capital}} \tag{8-11}$$

In order to generalise the results, the NPV can be expressed on a per-kW basis, as described previously. To do this, the capital costs and the annual revenues must be expressed as a fraction of either the electrical power output of the plant or the fuel power input. Depending on which analysis is being done, X_{capital} will be defined by Equation (8-7) in terms of either $X_{\mathrm{Otto,E}}$ or $X_{\mathrm{Otto,F}}$.

8.3.5 Internal Rate of Return

The IRR of an investment is defined as that interest rate value at which the NPV of all cash flows into and out from the investment equal zero [160]. It is an indicative tool used to appraise the return on an investment. A higher IRR typically indicates a more desirable investment and, provided all other factors are maintained the same, the project with the higher IRR will typically be favoured.

The method has limitations, however, and a higher IRR is not always representative of a better investment. Where two available investment opportunities have different initial capital investment requirements, one investment project may have a lower projected IRR than the other, but a higher NPV. As the NPV dictates the ultimate profitability of the project, the project with the higher NPV would be preferable. This is evident in the following analysis results where it can be seen that, while the IRR of the different project

variants declines, the NPV increases with the increasing capital cost of the projects.

Table 8.2 Techno-economic model parameters

C_E (€/kWh)	0.1527
C_G (€/kWh)	0.03641
C_R(€/kWh)	0.11
$C_{M,Otto}$(€/kW/annum)	50
$C_{M,Stirling}$(€/kW/annum)	50
N_H	5420
N_{HUF}	0.8
η_B	0.9
Plant lifetime, n (years)	10
Discount rate, i (%)	8

8.4 Results and Discussion

The parameters used in the techno-economic analysis are presented in Table 8.2. The results of the economic analyses of the combined cycle system are presented in Table 8.3 to Table 8.6. In each case, the capital cost, as computed using Equation (8-7), the annual net cashflow and the SPP are calculated. Presented also are the NPV and IRR values computed with respect to the annual cashflow per kW of electrical power and per kW of fuel power converted.

Table 8.3 presents the results of the analysis as performed for the case of the combined cycle system being used in a cogeneration scenario with the engines operating in synchronous mode. As can be seen, the annual cashflow is positive

and increasing for the increasing power output of the combined cycle system. However, the capital cost is seen also to increase, such that the SPP for the plant is noted to increase from a minimum of 2.35 years for the single cycle Otto engine to 2.76 years for the combined cycle with the 5.52 MPa mean cycle pressure GPU-3 Stirling engine. Note that the capital cost of the combined cycle plant is shown to increase with the increasing mean cycle pressure of the Stirling engine, even though the same engine geometry is used in each case. This is an approximation, which is made in order to account for the increasing plant complexity that would be seen due to the requirement for larger electrical conversion hardware and for possible increases in the reserve gas storage system.

Table 8.3 Economic analysis, single and combined cycle system for CHP applications, synchronous operation

	Otto	**Combined cycle (at mean cycle pressure)**			
		2.76 MPa	4.14 MPa	5.52 MPa	6.9 MPa
Capital cost (€/kW_e)	1000	1140	1231	1326	N/A
(annual net incoming cashflow) : (Primary Energy Savings) (€/kW_e)	425	438	457	477	N/A
SPP (Years)	2.35	2.6	2.69	2.76	N/A
NPVe (€/kW_e)	2537	2500	2567	2638	N/A
IRR_e	0.41	0.37	0.35	0.34	N/A
NPVf (€/kW_{fuel})	619	741	851	1002	N/A

IRR_f	0.366	0.37	0.35	0.34	N/A

Although an increase in the SPP is noted for the combined cycle over the single cycle, it is also notable that the NPV_e for the combined cycle increases steadily for the increasing mean cycle pressure of the Stirling engine. It surpasses that of the single cycle Otto engine at 4.14 MPa mean cycle pressure, indicating a more attractive investment. The NPV_f also increases in similar fashion although in this case it surpasses that of the single cycle plant immediately, indicating that the investment-attractiveness scales with the total plant efficiency. In each case, however, the IRR is seen to decrease from that for the single cycle, although it remains high in all instances.

Similar trends are visible in Table 8.4, which presents the analysis for the case of asynchronous operation of the combined cycle plant. For this case the 6.9 MPa mean cycle pressure Stirling engine is included for reasons described in the previous chapter.

Table 8.4 Economic analysis, single and combined cycle system for CHP application, asynchronous operation

	Otto	$CC_{2.76MPa}$	$CC_{4.14MPa}$	$CC_{5.52MPa}$	$CC_{6.9MPa}$
Capital cost (€/kW_e)	1000	1140	1240	1337	1384
(annual net incoming cashflow): (Primary Energy Savings) (€/kW_e)	425	438	459	479	488
SPP (Years)	2.35	2.6	2.7	2.79	2.83
NPV_e (€/kW_e)	2573	2500	2574	2644	2678

IRR_e	0.41	0.37	0.35	0.34	0.33
NPV_f (€/kW_{fuel})	619	741	864	1016	1108
IRR_f	0.366	0.37	0.35	0.34	0.33

Table 8.5 and Table 8.6 present the results of the analysis for the mono-generation scenario, such as would be used for AD gas operation. In this case, a renewable energy tariff is assumed to be paid for the power exported to the grid. This is quantified based on the Renewable Energy Feed-In Tariff (REFIT) offered in the Republic of Ireland [161]. Table 8.5 shows the results of the analysis for the case of synchronous operation. Similar trends are present as for the cogeneration system; however, the NPV magnitudes are larger. Notable is the fact that the NPV_e value indicates that the combined cycle system is most profitable when the low-power Stirling engine is included in the combined system. This seems counter intuitive, even when the increased maintenance costs for higher power output are considered. The NPV_f values corroborate this, as it can be seen that the magnitudes of these increase with increasing mean cycle pressure of the Stirling engine. This can be understood as meaning that the NPV per kW of fuel-power consumed increases with increasing power output of the Stirling engine, indicating greater profitability with a higher-efficiency engine system.

Table 8.5 Economic analysis, single and combined cycle system for AD gas application, synchronous operation

	Otto	$CC_{2.76MPa}$	$CC_{4.14MPa}$	$CC_{5.52MPa}$	$CC_{6.9MPa}$
Capital cost (€/kW_e)	1000	1140	1231	1329	N/A

	Otto	$CC_{2.76MPa}$	$CC_{4.14MPa}$	$CC_{5.52MPa}$	$CC_{6.9MPa}$
(annual net incoming cashflow): (Primary Energy Savings) (€/kW_e)	546	582	579	576	N/A
SPP (Years)	1.83	1.95	2.12	2.31	N/A
NPV_e (€/kW_e)	3543	3704	3587	3459	N/A
IRR_e	0.54	0.50	0.46	0.42	N/A
NPV_f (€/kW_{fuel})	875	1098	1189	1313	N/A
IRR_f	0.48	0.50	0.46	0.42	N/A

Table 8.6 shows the results of the analysis for the system under asynchronous operation. Again, similar trends are seen as per the synchronous operation scenario with the inclusion of the 6.9 MPa mean cycle pressure Stirling engine.

Table 8.6 Economic analysis, single and combined cycle system for AD gas application, asynchronous operation

	Otto	$CC_{2.76MPa}$	$CC_{4.14MPa}$	$CC_{5.52MPa}$	$CC_{6.9MPa}$
Capital cost (€/kW_e)	1000	1146	1240	1337	1384
(annual net incoming cashflow): (Primary Energy Savings) (€/kW_e)	546	582	579	575	574
SPP (years)	1.83	1.97	2.14	2.32	2.41
NPV_e (€/kW_e)	3543	3696	3574	3448	3386
IRR_e	0.54	0.5	0.46	0.42	0.4

NPV_f (€/kW_{fuel})	875	1104	1200	1325	1401
IRR_f	0.48	0.5	0.46	0.42	0.4

Table 8.7 shows the results of a comparison of the given Otto-cycle engine with a more efficient engine of the same type. The engine specification used in this case was sourced from a manufacturer's data sheet [162] and represents what might be considered the current market leader in terms of plant efficiency. This comparison was performed to gain insight into the possible profitability gain that may arise from using a higher-specification topping engine. It can be seen that while the high-efficiency Otto-cycle engine represents a marked improvement in NPV_f in both cases, the combined cycle plant is at least as profitable in the case of cogeneration, and more profitable in the case of the AD gas-fuelled operation. It is not particularly appropriate to compare the high-efficiency Otto-cycle engine with the combined cycle plant in this way though, as this engine could still act as a topping engine in its own right; however, it is interesting to compare the combined cycle plant to the best-in-class of the Otto-cycle engine in a single cycle arrangement [162].

Table 8.7 Comparative economic analysis of Otto cycle generator for CHP and AD operation

	CHP		**AD**	
	Otto[1]	Otto[2]	Otto[1]	Otto[2]
Capital cost (€/kW_e)	1000	1100	1000	1100
Annual net incoming cashflow:				
Primary Energy Savings (€/kW_e)	425	478	546	546

SPP (years)	2.35	2.29	1.83	2.01
NPV_e (€/kW_e)	2573	2878	3543	3443
IRR_e	0.41	0.42	0.54	0.49
NPV_f (€/kW_{fuel})	619	1112	875	1272
IRR_f	0.366	0.374	0.48	0.42

8.5 Conclusions

A series of economic analyses are performed to assess the suitability of the combined cycle system for use in both a mono-generation and a cogeneration situation. The mono-generation situation of interest was that of a novel gas-fuelled operation such as landfill gas site or an AD gas site. Cogeneration was assumed to be natural-gas-fired, with limited heat recovery accounted-for through the use of the Heat Usage Factor, N_{HUF}.

The economic analyses indicate that for both the mono-generation and cogeneration situations the Otto / Stirling combined cycle represents an economically attractive option for a system prime mover. When evaluated on the net revenue per kW fuel requirement of the engine, the combined cycle system is significantly more profitable over the expected lifetime of the plant than the Otto engine acting alone as a single cycle prime mover. The economic analysis indicated that the expected increase in plant capital cost required for the inclusion of the Stirling cycle engine offsets the increased annual revenue such that the SPP is caused to increase slightly over that of the single cycle plant. However, the NPV is seen to increase with the addition of the second cycle, indicating a more profitable arrangement over the full lifetime of the plant.

The Otto cycle used in the analysis is compared against a high-efficiency engine operating on the same cycle. It is seen from this analysis that while considerable improvement in profitability is seen with the improvement in the efficiency, even after accounting for an increase in specific capital cost, the combined cycle system is still potentially a more profitable arrangement.

9 CONCLUSIONS

9.1 Summary of Aims and Objectives

The overarching aim of this research work, stated in Chapter 1, was to investigate the Otto / Stirling combined cycle as a prime mover for use in the DG industry. Assessment of the techno-economic performance of the proposed combined cycle plant through thermodynamic simulation and established economic appraisal techniques was to be performed. From this then the final aim was to draw conclusions regarding the suitability of the plant for use as both a mono-generation and a poly-generation prime mover.

Within these aims, the central objectives of the work were

- Conduct a literature survey to establish the current market and technology status in the DG industry.

- Generate a thermodynamic simulation model for the Otto cycle engine capable of accounting for the energy balance of the three main energy sinks

- Verification of the Otto cycle thermodynamic simulation model against a commercially available virtual engine simulation software package.

- Generate a thermodynamic simulation model for the Stirling cycle engine capable of accounting for the energy balance of the three main energy sinks

- Validation of this thermodynamic model against technical specifications and experimental data available in the literature.

- Simulation of the combined cycle system and a full techno-economic appraisal of the potential of the system to perform as a prime mover for the DG scenarios mentioned previously.

- Draw conclusions as to the viability of the proposed combined cycle plant as a prime mover for stationary power generation. Provide discussion on these results and detail proposed future work on the concept.

9.2 Summary of Major Conclusions and Contributions

The success of the project can therefore be gauged against the objectives mentioned above and the degree to which they were achieved. The major conclusions and contributions of the research work are:

- The study presents a detailed analysis of the Otto and Stirling combined cycle as a prime mover for DG applications. This work represents the first comprehensive study of the novel combined cycle system involving the Otto and Stirling thermodynamic cycles available in the literature

- The extension of an existing FTT model for the Otto cycle engine to include exhaust sensible enthalpy and temperature was completed

- A verification of the extended FTT Otto cycle model against a commercial simulation package was performed. The model demonstrated good agreement with the commercial simulation model.

- A new FTT model for the Stirling cycle engine incorporating heat transfer and friction irreversibilities has been developed. This model represents a new addition to the literature both for Stirling cycle analysis and for FTT.

- Validation of the FTT model of the Stirling cycle engine against experimental data for the General Motors GPU-3 Stirling engine was completed. The validation procedure showed the model to offer good agreement to known performance data.

- Economic appraisal of the novel combined cycle was performed in order to offer a preliminary assessment of market attractiveness of the technology. It was seen that the novel combined cycle represents a technically viable and an economically attractive potential technology, with power gains of up to approximately 67% and efficiency gains of up to approximately 19% possible over the single cycle plant. Analysis was completed for both Natural Gas fired cogeneration and AD gas fired mono-generation. In both cases it was seen that whilst the SPP of the plant was somewhat increased, the NPV of the plant revenue over its lifetime was enhanced in comparison to the single cycle system. This leads to the conclusion that the novel combined cycle system represents an economically viable prime mover system.

It is therefore possible to state that the project was successful as it achieved the objectives laid out at the beginning.

9.3 Future Work

Possibilities for further work on the combined cycle concept at hand are numerous. From an academic viewpoint, there remain a large number of possibilities for building upon the work presented here for the FTT models of each cycle. In particular it would be interesting to model other Stirling cycle

engines using the FTT method developed here. This would permit further validation of the model. It would also allow the formation of a database of the empirical factors employed, allowing the compilation of operational bounds on the engine. This may prove useful as a modelling and design aid to engineers interested in the Stirling cycle engine.

From a commercial viewpoint, the major possibility for future work would be the development of the combined cycle system to a prototype stage and ultimately towards full commercial deployment. This would foreseeably require focus on a number of key areas. Firstly, the most suitable Stirling engine configuration should be selected with consideration of the overall plant layout and size, the predicted performance output and the ease of maintenance. Secondly, it would be necessary to optimise the heat exchangers for the novel heat reservoirs involved – the Otto cycle exhaust stream and the water cooling circuit. In addition to the thermodynamic design, it would be necessary to identify a suitable transmission system by which to integrate the work outputs of the two engines involved. The options would likely involve using either an electrical or mechanical coupling to combine the shaft outputs. This would be a particularly important aspect, because although different clutch mechanisms exist for combined cycle power plant, these usually do not have plant footprint as a strict constraint and so size and layout is secondary to optimal performance. In the combined cycle system under analysis, plant footprint is a prime consideration and therefore optimal configuration of the transmission mechanism is important meaning that the dual optimisation of size and performance must be considered.

REFERENCES

1. IPCC, 2007: *Climate Change 2007: Synthesis Report. Contribution of Working Groups I, II and III to the Fourth Assessment Report of the Intergovernmental Panel on Climate Change* [Core Writing Team, Pachauri, R.K and Reisinger, A. (eds.)]. IPCC, Geneva, Switzerland, 104 pp. Available from: http://www.ipcc.ch/publications_and_data/publications_ipcc_fourth_assessment_report_synthesis_report.htm.
2. Giannantoni, C. and M. Zoli, *The Derivative 'Drift' in Complex Systems Dynamics The Case of Climate Change and Global Warming*, in *22nd International Conference on Efficiency, Cost, Optimization, Simulation and Environmental Impact of Energy Systems*. 2009: Foz do Iguacu, Brazil. pp. 1031–1040.
3. International Energy Agency. *World Energy Outlook 2008*. 2008.
4. Aleklett, K., et al, *The Peak of the Oil Age—Analyzing the World Oil Production Reference Scenario in World Energy Outlook 2008*. Energy Policy. **38**(3): pp. 1398–1414.
5. Almeida, P.D. and P.D. Silva, *The peak of oil production—Timings and market recognition*. Energy Policy, 2009. **37**: pp.1267–1276.
6. Verbruggen, A. and M. Al Marchohi, *Views on peak oil and its relation to climate change policy*. Energy Policy. 2010. **38**(10): pp. 5572–5581.
7. Friedrichs, J., *Global energy crunch: How different parts of the world would react to a peak oil scenario*. Energy Policy, 2010. **38**: pp. 4562–4569.
8. Zevenhoven, R. and A. Beyene, *Global Warming: A Result of Greenhouse Gas Emissions of of Heat-Up of the Surroundings by Power Plants?* , in *22nd*

International Conference on Efficiency, Cost, Optimization, Simulation and Environmental Impact of Energy Systems. 2009: Foz do Iguacu, Brazil. pp. 987–994.

9. Toth, F.L. and H.-H. Rogner, *Oil and nuclear power: Past, present, and future*. Energy Economics, 2006. **28**(1): pp. 1–25.
10. Boykoff, M.T. and J.M. Boykoff, *Climate change and journalistic norms: A case-study of US mass-media coverage*. Geoforum, 2007. **38**(6): pp. 1190–1204.
11. Antilla, L., *Climate of scepticism: US newspaper coverage of the science of climate change*. Global Environmental Change Part A, 2005. **15**(4): pp. 338–352.
12. Doulton, H. and K. Brown, *Ten years to prevent catastrophe?: Discourses of climate change and international development in the UK press*. Global Environmental Change, 2009. **19**(2): pp. 191–202.
13. Sampei, Y. and M. Aoyagi-Usui, *Mass-media coverage, its influence on public awareness of climate-change issues, and implications for Japan's national campaign to reduce greenhouse gas emissions*. Global Environmental Change, 2009. **19**(2): pp. 203–212.
14. Winstanley, D., *In support of skepticism*. Environmental Science & Policy, 2000. **3**(1): pp. 19–20.
15. Engineers Ireland, *Engineers Ireland - Code of Ethics*, 2010.
16. *American Society of Mechanical Engineers - Code of Ethics*. 2010, ASME.
17. IEEE, IEEE Code of Ethics. 2010. Available from: http://www.ieee.org/membership_services/membership/ethics_code.html

18. Cengel, Y.A. and M.A. Boles, *Thermodynamics An Engineering Approach*. Fourth ed. 2002: McGraw Hill.

19. Mayhew, Y. and G. Rogers, *Engineering Thermodynamics*. Fourth ed. 1992, Essex: Longman Scientific & Technical.

20. Petrescu, S., Petre, C., Costea, M., Malancioiu, O.,Boriaru, N.,Dobrovicescu, A., Feidt, M., Harman, C., *A Methodology of Computation, Design and Optimization of Solar Stirling Power Plant using Hydrogen/Oxygen Fuel Cells*. Energy, 2010. **35**(2): pp. 729–739.

21. Kongtragool, B. and S. Wongwises, *A review of solar-powered Stirling engines and low temperature differential Stirling engines.* Renewable and Sustainable Energy Reviews, 2003. **7**(2): pp. 131–154.

22. Tlili, I., Y. Timoumi, and S.B. Nasrallah, *Analysis and design consideration of mean temperature differential Stirling engine for solar application.* Renewable Energy, 2008. **33**(8): pp. 1911–1921.

23. Brandhorst Jr, H. W. and P. A. Chapman Jr, *New 5 kW free-piston Stirling space convertor developments.* Acta Astronautica, 2008. **63**(1-4): pp. 342–347.

24. Onovwiona, H. I. and V. I. Ugursal, *Residential cogeneration systems: review of the current technology.* Renewable and Sustainable Energy Reviews, 2006. **10**(5): pp. 389–431.

25. De Paepe, M., P. D'Herdt, and D. Mertens, *Micro-CHP systems for residential applications.* Energy Conversion and Management, 2006. **47**(18-19): pp. 3435–3446.

26. Stone, R., *Introduction to Internal Combustion Engines*. 1999: Macmillan Press Ltd

27. Van Basshuysen, R. and F. Schafer, *Internal Combustion Engine Handbook*. 2004: SAE International

28. Heywood, J.B., *Internal Combustion Engine Fundamentals*. 1988: McGraw Hill Book Company

29. Smil, V., *The two prime movers of globalization: history and impact of diesel engines and gas turbines.* Journal of Global History, 2007(2): pp. 373–394.

30. Badami M, C.A., Campanile P, and Anzioso F, *Performance of an Innovative 120kWe Natural Gas Cogeneration System*. Energy, 2007.**32**: pp. 823–833.

31. Deutz Power Systems, *Technical Circular 0199 - 99 - 3017 en 2nd Exchange*. 2004.

32. Roubaud, A. and D. Favrat, *Improving performances of a lean burn cogeneration biogas engine equipped with combustion prechambers*. Fuel, 2005. **84**: pp. 2001–2007.

33. Cho, H.M. and B.-Q. He, *Spark ignition Natural Gas engines--A review.* Energy Conversion and Management, 2007. **48**(2): pp. 608–618.

34. Schneider, E.W. and D.H. Blossfeld, *Radiotracer Method For Measuring Real Time Piston Ring and Cylinder Bore Wear in Spark Ignition Engines*. Nuclear Instruments and Methods in Physics Research, 2003. **505**: pp. 559–563.

35. Taylor, Alex M.K.P., *Science review of internal combustion engines.* Energy Policy, 2008. **36**: pp. 4657–4667.

36. Pariotis, E.G., et al, *Comparing the results obtained from a CFD and a Quasidimensional model used to investigate the effect of various piston bowl geometries of a HSDI Diesel engine under motoring conditions*, in *Proceedings of the 21st International Conference on Efficiency, Cost,*

Optimization, Simulation and Environmental Impact of Energy Systems. 2008: Cracow-Gliwice, Poland.

37. Rakopoulos, C.D. and C.N. Michos, *Biogas Composition Effects on the Combustion Characteristics of a SI Engine using a Quasi-dimensional, Turbulent Combustion Model*, in *Proceedings of the 21st International Conference on Efficiency, Cost, Optimization, Simulation and Environmental Impact of Energy Systems*. 2008: Cracow-Gliwice, Poland.
38. Reynolds, C.C.O.B. and R.L. Evans, *Improving emissions and performance characteristics of lean burn Natural Gas engines through partial stratification.* International Journal of Engine Research, 2004: **5**(1): pp. 105–114.
39. Hannah, J. and M. Hillier, *Applied Mechanics*. 1995. Longman Scientific & Technical.
40. Silva, F.S., *Fatigue on Engine Pistons - A Compendium of Case Studies*. Engineering Failure Analysis 2006. **13**: pp. 480–492.
41. Kajiwara, H., Fujioka, Y, Susuki, T. and Negishi, H, *An Analytical Approach for Prediction of Piston Temperature Distribution in Diesel Engines*. JSAE Review 2002. **23**: pp. 429 –434.
42. Al-Sarkhi, A., J.O. Jaber, and S.D. Probert, *Efficiency of a Miller Engine*. Applied Energy 2006. **83**(4): pp. 343–351.
43. Zhao, Y. and J. Chen, *Performance analysis of an irreversible Miller heat engine and its optimum criteria*. Applied Thermal Engineering. 2006 (doi: 1 0.10 16/j.applthermaleng.2006.12.002).

44. Wu, C., P.V. Puzinauskas, and J.S. Tsai, *Performance analysis and optimisation of a supercharged Miller cycle Otto engine*. Applied Thermal Engineering, 2003. **23**: pp. 511–521.

45. Wang, Y., et al, *Application of the Miller cycle to reduce NOx emissions from petrol engines.* Applied Energy, 2008. **85**(6): pp. 463–474.

46. Wang, Y., et al, *An analytic study of applying miller cycle to reduce NOx emission from petrol engine*. Applied Thermal Engineering 2007, 27(11-12) p 1779-1789.

47. Mikalsen, R., Y.D. Wang, and A.P. Roskilly, *A comparison of Miller and Otto cycle Natural Gas engines for small scale CHP applications.* Applied Energy, 2009. **86**(6): pp. 922–927.

48. Wang, Y., et al *Experimental investigation of applying Miller cycle to reduce NOx emission from diesel engine*. in Proceedings of IMechE Part A, J. Power and Energy. 2005.

49. Kesgin, D., *Effect of Turbocharging System on the Performance of a Natural Gas Engine*. Energy Conversion and Management, 2005. **46**: pp. 11–32 .

50. Galindo, J., et al, *Impact of two-stage turbocharging architectures on pumping losses of automotive engines based on an analytical model.* Energy Conversion and Management. 1010.**51**(10): pp. 1958–1969.

51. Nakonieczny, K., *Entropy generation in a diesel engine turbocharging system.* Energy, 2002. **27**(11): pp. 1027–1056.

52. Katrasnik, T., V. Medica, and F. Trenc, *Analysis of the dynamic response improvement of a turbocharged diesel engine driven alternating current generating set*. Energy Conversion and Management, 2005. **46**: pp. 2838–2855.

53. West, M., *Electromagnetic, Continuously Variable Transmission Power Split Turbo Compound And Engine And Vehicle Comprising Such A Turbo Coompound*, W.P. Office, Editor. 2010.

54. Berger, J., M. Kley, and S. Bartosch, *Turbocharger turbo compound system*, W.P. Office, Editor. 2009.

55. Vuk, C.T., *Turbo Compounding - A Technology Who's Time Has Come*, in *11th Diesel Engine Emissions Reduction Conference*. 2005: Chicago. illinois.

56. Finkelstein, T. and A.J. Organ, *Air Engines*. 2001. Professional Engineering Publishing Ltd.

57. Walker, G., Fauvel, O. R., Reader, G., Bingham, E. R. , *The Stirling Alternative.* 1994. Gordon and Breach Science Publishers.

58. Walker, Graham, *Stirling Engines*. 1980, Oxford: Clarendon Press.

59. Organ, A.J., *The Air Engine — Stirling cycle power for a sustainable future*. 2007, Cambridge: Woodhead Publishing Limited.

60. Thombare, D.G. and S.K. Verma, *Technological Development in the Stirling Cycle Engines*. Renewable and Sustainable Energy Reviews, 2008.12(1), pp. 1–36.

61. Fang, H.W., et al *A novel Stirling engine with am elliptic drive*. in *Energy Conversion Engineering Conference, 1996. IECEC 96. Proceedings of the 31st Intersociety*. 1996.

62. Hargreaves, C.M., *The Philips Stirling Engine*. 1991, Amsterdam: Elsevier Science Publishers B.V.

63. Stine, W.B. and R.B. Diver, *A Compendium of Solar Dish/Stirling Technology*. 1994, Sandia Laboratories.

64. Stirling Engine Systems, Inc. (SES), *Stirling Energy Systems Announces $100 Million Investment by NTR PLC*. 2008, http://www.stirlingenergy.com/pdf/2008-04-17.pdf [accessed 2 Oct. 2010).

65. Timmerman, Luke, *Infinia Raises $11.5M To Make New Solar-Power Generators, Entices Paul Allen Again*. 2 May, 2010. http://www.xconomy.com/seattle/2010/02/05/infinia-raises-11-5m-to-make-new-solar-power-generators-entices-paul-allen-again/ [accessed 2 Oct. 2010] on Xconomy web site (http://www.xconomy.com).

66. *Stirling Solar Dish System*. 2007 [cited; Available from: http://www.energylan.sandia.gov/photo/photos/9999/999961U3.jpg

67. Hammond, G. P., Stapleton, A. J., *Exergy analysis of the United Kingdom energy system*. Discussion. Proceedings of the Institution of Mechanical Engineers, Part A: Journal of Power and Energy, 2001:(**215**) (A2), pp. 141–162.

68. Fleten, S.E., K.M.Maribu, and I. Wangensteen, *Optimal Investment Strategies in Decentralized Renewable Power Generation Under Uncertainty*. Energy, 2007. **32**: pp. 803–815.

69. Fraser, P., *Distributed Generation in Liberalised Electricity Markets*. OECD/lEA. 2002.

70. Themelis, N. J. and P. A. Ulloa, *Methane Generation in Landfills*. Renewable Energy 2007. **32**: pp. 1243–1257

71. Western Development Commission, *Meeting Ireland's Electricity Needs post-2020 - Submission to the Joint Oireachtas Committee on Climate Change and Energy Security* 2009.

72. Byrne O Cleirigh, *Combined Heat and Power (CHP) Potential in Ireland*. 2009, Report prepared for Sustainable Energy Ireland.

73. *Directive 2004/8/EC of the European Parliament and of the Council of 11 February 2004, on the promotion of cogeneration based on a useful heat demand in the internal energy market, amending Directive 92/42/EEC*. 2004.

74. Oh, S.-D., H.-S. Oh, and H.-Y. Kwak, *Economic Evaluation for Adoption of Cogeneration System*. Applied Energy, 2007. **84**: pp. 266 –278

75. *Delivering a Sustainable Energy Future for Ireland - The Energy Policy Framework 2007 - 2020*. 2007, The Government of Ireland - Department of Communications, Marine and Natural Resources.

76. DIT Energy Bureau. 2008. Available from: http://bms.dit.ie/.

77. Panno, D., A. Messineo, and A. Dispenza, *Cogeneration Plant in a Pasta Factory: Energy Saving and Environmental Benefit*. Energy, 2007. **32**: pp. 746–754.

78. Energy and Environmental Analysis , Inc. *CHP in the Hotel and Casino Market Sectors*. 2005. Available from: http://www.epa.gov/chp/documents/hotel_casino_analysis.pdf.

79. Madrano, M., et al., *Integration of Distributed Generation systems into generic types of commercial buildings in California*. Energy and Buildings, 2008. **40**: pp. 537–548.

80. Denton, J.C., *Thermal cycles in classical thermodynamics and nonequilibrium thermodynamics in contrast with Finite Time Thermodynamics*. Energy Conversion and Management, 2002. **43**(13): pp. 1583–1617.

81. Sekulic, D.P., *A fallacious argument in the Finite Time Thermodynamics concept of endoreversibility.* Journal of Applied Physics, 1998. **83**(9): pp. 4561–4565.

82. Lavenda, B.H., *The thermodynamics of endoreversible engines.* American Journal of Physics, 2007. **75**(2): pp. 169–175.

83. Novikov, I.I., *The efficiency of atomic power stations (a review)*. Journal of Nuclear Energy, 1958. **7**(1-2): pp. 125–128.

84. Feidt, M., *Optimal Thermodynamics —New Upperbounds*. Entropy, 2009. **11**: pp. 529-547.

85. Curzon, F.L. and B. Ahlborn, *Efficiency of a Carnot engine at maximum power output*. American Journal of Physics, 1975. **43**(1): pp. 22–24.

86. Bejan, A., Entropy generation minimization: The new thermodynamics of finite-size devices and finite-time processes. Journal of Applied Physics, 1996. **79**(3): pp. 1191–1218.

87. Chen, L., C. Wu, and F. Sun, Finite Time Thermodynamic Optimization or Entropy Generation Minimization of Energy Systems. Journal of Non-Equilibrium Thermodynamics, 1999. **24**: pp. 327–359.

88. Qin, Xiaoyong, et al, *The universal power and efficiency characteristics for irreversible reciprocating heat engine cycles.* European Journal of Physics, 2003. **24**: pp. 359–366.

89. Lingen, C. Junlin Zheng, Fengrui Sun and Chih Wu, *Optimum distribution of heat exchanger inventory for power density optimization of an endoreversible closed Brayton cycle.* Journal of Physics D: Applied Physics, 2001. **34**(3): p. 422.

90. Kongtragool, B. and S. Wongwises, Investigation on power output of the gamma-configuration low temperature differential Stirling engines. Renewable Energy, 2005. **30**(3): pp. 465–476.

91. Urieli, Israel and David M. Berchowitz, *Stirling Cycle Engine Analysis*. 1984, Bristol: Hilger.

92. Organ, Allan J., *Thermodynamics and Gas Dynamics of the Stirling Cycle Machine*. 1992: Cambridge University Press.

93. Reader, G.T. and C. Hooper, *Stirling Engines*. 1983, London: E. & F.N. Spon.

94. Carlson, H., M.B. Commisso, and B. Lorentzen. *Maximum Obtainable Efficiency For Engines And Refrigerators Based On The Stirling Cycle*. in *Energy Conversion Engineering Conference, 1990. IECEC-90. Proceedings of the 25th Intersociety*. 1990.

95. Finkelstein, T., *A new isothermal theory for Stirling machine analysis and a volume optimization using the concept of 'ancillary' and 'tidal' domains.* Proceedings of the Institution of Mechanical Engineers, Part C: Journal of Mechanical Engineering Science, 1998. **212**(3): pp. 225–236.

96. Kongtragool, B. and S. Wongwises, *Thermodynamic analysis of a Stirling engine including dead volumes of hot space, cold space and regenerator.* Renewable Energy, 2006. **31**(3): pp. 345–359.

97. Dyson, R.W., S.D. Wilson, and R.C. Tew, *Review of Computational Stirling Analysis Methods*. 2004, NASA.

98. Martini, William R., *Stirling Engine Design Manual*. 2nd Edition. 1983: DOE/NASA.

99. Senft, J.R., *Optimum Stirling engine geometry.* International Journal of Energy Research, 2002. **26**(12): pp. 1087–1101.

100. Organ, Allan J., *The Regenerator and the Stirling Engine*. 1997: London Mechanical Engineering Publications.

101. Feidt, M., Lesaos, K., Costea, M., Petrescu, S. , *Optimal allocation of HEX inventory associated with fixed power output or fixed heat transfer rate input.* International Journal of Applied Thermodynamics, 2002. **5**(1): pp. 25–36.

102. Feidt, M., Costea, M., Petrescu, S., *Heat Transfer Conductance or Area Minimization in a Stirling Cycle Engine*, in *ECOS 2000*. 2000: Universiteit Twente, Nederlands.

103. Kuosa, M., J. Kaikko, and L. Koskelainen, *The impact of heat exchanger fouling on the optimum operation and maintenance of the Stirling engine.* Applied Thermal Engineering, 2007. **27**(10): p. 1671-1676.

104. Domingo, N., *Comparative Analysis of a Stirling Heat Pump with Second and Third Order Computer Models*. 1985, Oak Ridge National Laboratory.

105. Petrescu, S., Costea, M., Harman, C., Florea, T., *Application of the Direct Method to irreversible Stirling cycles with finite speed.* International Journal of Energy Research, 2002. **26**(7): pp. 589–609.

106. Petrescu, S. and C. Harman, *The Connection Between the First Law and Second Law of Thermodynamics for Processes with Finite Speed—A Direct Method for Approaching and Optimization of Irreversible Processes* Journal of the Heat Transfer Society of Japan, 1994. **33**(128): p. 60.

107. Petrescu, S., Stanescu, G., Constantinescu, R., Dobrovicescu, A., *The First Law of Thermodynamics for Closed Systems, Considering the Irreversibilities Generated by the Friction Piston-Cylinder, the Throttling of the Working*

Medium and the Finite Speed of the Mechanical Interaction, in ECOS'92. 1992, ASME: Zaragoza, Spain.

108. Erbay, L. Berrin and Yavuz Hasbi, *Optimization of the irreversible Stirling heat engine.* International Journal of Energy Research, 1999. **23**(10): pp. 863–873.
109. Erbay, L. Berrin and Hasbi Yavuz, *Analysis of the Stirling heat engine at maximum power conditions.* Energy, 1997. **22**(7): pp. 645–650.
110. Feidt, M., Costea, M., Popescu, G., *Optimal Design of a Stirling Engine using a Generalized Heat Transfer Law Model*, in ROMA '95 CIRCUS Centro Internazionale di Ricerca e Calcolo Universitario Scientifico 1995: Rome, Italy.
111. Senft, James R., *Theoretical Limits on the Performance of Stirling Engines.* International Journal of Energy Research, 1998. **22**: pp. 991–1000.
112. Tlili, I., Y. Timoumi, and S.B. Nasrallah, *Thermodynamic analysis of the Stirling heat engine with regenerative losses and internal irreversibilities.* International Journal of Engine Research, 2008. **9**(1): pp. 45–56.
113. Descieux, D. and M. Feidt, *One Zone Thermodynamic Model Simulation of an Ignition Compression Engine.* Applied Thermal Engineering, 2007. **27**: pp. 1457–1466.
114. Sakhrieh, A., et al, *Computational thermodynamic analysis of compression ignition engine.* International Communications in Heat and Mass Transfer. 2010.**37**(3): pp. 299–303.
115. RICARDO. *Ricardo Wave - Available Technical Papers*. 2010, http://www.ricardo.com/en-gb/Software/Products/WAVE/Available-papers/ [accessed 24th August 2010].

116. Gamma Technologies. *GT Suite Publications*. 2010. http://www.gtisoft.com/publications/pub_%20GT_SUITE_Publications.php [accessed 24th August 2010]

117. Angulo-Brown, F., J. Fernandez-Betanzos, and C. Diaz-Pico, *Compression ratio of an optimized air standard Otto-cycle model*. European Journal of Physics, 1994. **15**: pp. 38–42.

118. Angulo-Brown, F. and et al, *A non-endoreversible Otto cycle model: improving power output and efficiency*. Journal of Physics D: Applied Physics, 1996. **29**(1): p. 80.

119. Hernandez, A.C., Medina, A., Roco, J.M.M., Valesco, S., *On an irreversible air standard Otto-cycle model*. European Journal of Physics, 1995. **16**(2): pp. 73–75.

120. Ge, Y., et al, *Thermodynamic simulation of performance of an Otto cycle with heat transfer and variable specific heats of working fluid*. International Journal of Thermal Sciences, 2005. **44**(5): pp. 506–511.

121. Chen, J., Y. Zhao, and J. He, *Optimization criteria for the important parameters of an irreversible Otto heat-engine*. Applied Energy, 2006. **83**(3): pp. 228–238.

122. Curto-Risso, P.L., A. Medina, and A.C. Hernandez, *Theoretical and simulated models for an irreversible Otto cycle*. Journal of Applied Physics, 2008, **104**(9): 094911(11pp.).

123. Curto-Risso, P.L., A. Medina, and A.C. Hernandez, *Optimizing the operation of a spark ignition engine: Simulation and theoretical tools.* Journal of Applied Physics, 2009. **105**.

124. Curto-Risso, P.L., A. Medina, and A.C. Hernandez, *Thermodynamic Optimization of a Spark Ignition Engine*, in 22nd International Conference on Efficiency, Cost, Optimization, Simulation and Environmental Impact of Energy Systems. 2009: Foz do Iguacu, Brazil. pp. 1979–1988.

125. Engelbert, C., et al, *Introducing the 1S.W501G Single-Shaft Combined-Cycle Reference Power Plant*, in *ASME Power 2004*. 2004, ASME: Baltimore, Maryland.

126. Franco, A. and C. Casarosa, *On some perspectives for increasing the efficiency of combined cycle power plants.* Applied Thermal Engineering, 2002. **22**(13): pp. 1501–1518.

127. Clawson, L.G., *High Efficiency Otto Cycle Engine with Power Generating Expander*, U.S.P. Office, No. US7062915. 2006: United States.

128. Badami, M., et al, *Design and performance evaluation of an innovative small scale combined cycle cogeneration system.* Energy, 2008. **33**(8): pp. 1264–1276.

129. Hiroshi Yaguchi and Daisaku Sawada, *Exhaust Heat Recovery Apparatus*, United States Patent Office, No. PCT/JP04/13952, 2003, Toyota Jidosha Kabushiki Kaisha: United States.

130. Mori, M., *Power Device Equipped with Combustion Engine and Stirling Engine*, European Patent Office, No. EP1624177A1. 2004, Honda Motor Co. Ltd.

131. Sawada, D.Y., Hiroshi; Mitani, Shinichi, *Exhaust Heat Recovery Apparatus*, World Intellectual Property Organisation, No. PCT/IB2007/000481. 2007, Toyota Jidosha Kabushiki Kaisha.

132. Johansson, L., *Exhaust Gas Alternator System*, U.S.P. Office, No. 09/881,112, 2003, STM Power Inc.: United States of America.
133. Lopes, J.A.P., et al, *Integrating Distributed Generation into electric power systems: A review of drivers, challenges and opportunities.* Electric Power Systems Research, 2007. **77**(9): pp. 1189–1203.
134. Chicco, G. and P. Mancarella, *Distributed multi-generation: A comprehensive view.* Renewable and Sustainable Energy Reviews, 2009. **13**(3): pp. 535–551.
135. Pepermans, G., et al, *Distributed Generation: definition, benefits and issues.* Energy Policy, 2005. **33**(6): pp. 787–798.
136. Bayod-Rújula, A.A., *Future development of the electricity systems with Distributed Generation.* Energy, 2009. **34**(3): pp. 377–383.
137. Gambarotta, A. and I. Vaja, *Internal Combustion Engines bottoming with Organic Rankine Cycles—A thermodynamic analysis*, in *21st International Conference on Efficiency, Cost, Optimization, Simulation and Environmental Impact of Energy Systems*. 2008, AGH University of Science & Technology, The Silesian University of Technology: Cracow-Gliwice, Poland:pp 715 - 723
138. Endo, T., Kawajiri, S., Kojima, Y., Takahashi, K., Baba, T., Ibaraki, S., Takahashi, T., Shinohara, M., *Study on Maximizing Exergy in Automotive Engines*, in *2007 SAE World Congress*. 2007, SAE International: Detroit, Michigan.
139. Chammas, R.E. and D. Clodic, *Combined Cycle for Hybrid Vehicles*, in *2005 SAE World Congress*. 2005, SAE International: Detroit, Michigan:Paper No. 2005-01-1171

140. Yaguchi, H., Sawada,D. , *Exhaust Heat Recovery Apparatus*, United States Patent Office, PCT/JP04/13952, 2003, Toyota Jidosha Kabushiki Kaisha: United States.

141. Curto-Risso, P.L., A. Medina, and A.C. Hernandez, *Optimizing the operation of a spark ignition engine: Simulation and theoretical tools.* Journal of Applied Physics, 2009. **105**(9): 094904(10pp.).

142. Angulo-Brown, F., T.D. Navarrete-Gonzalez, and J.A. Rocha-Martinez, *An Irreversible Otto Cycle Model Including Chemical Reactions,* in *Recent Advances in Finite Time Thermodynamics*, C. Wu, L. Chen, and J. Chen, Editors. 1999, Nova Science Publishers Inc.

143. Abu-Nada, E., et al, *Thermodynamic modeling of spark-ignition engine: Effect of temperature dependent specific heats*. International Communications in Heat and Mass Transfer, 2006. **33**(10): pp. 1264–1272.

144. Mozurkewich, Michael and R. Stephen Berry, *Optimal paths for thermodynamic systems: The ideal Otto cycle*. Journal of Applied Physics, 1982. **53**(1): pp. 34–42.

145. Stas, M.J., *Effect of Exhaust Blowdown Period on Pumping Losses in a Turbocharged Direct Injection Diesel Engine*, in SAE International Congress and Exposition. 1999, SAE: Detroit, Michigan.

146. Ozkaynak, S., *The theoretical efficiency limits for a combined cycle under the condition of maximum power output.* Journal of Physics D: Applied Physics, 1995. **28**(10): p. 2024.

147. Ozkaynak, S. and et al, *Finite-time thermodynamic analysis of a radiative heat engine with internal irreversibility.* Journal of Physics D: Applied Physics, 1994. **27**(6): p. 1139.

148. Timoumi, Youssef, Iskander Tlili, and Sassi Ben Nasrallah, *Design and performance optimization of GPU-3 Stirling engines.* Energy, 2008. **33**(7): pp. 1100–1114.

149. Incropera, Frank P. and David P. DeWitt, *Fundamentals of Heat and Mass Transfer*. Fifth ed. 2002: John Wiley & Sons.

150. Kanzaka, Mitsuo and Makio Iwabuchi, *Study on Heat Transfer of Heat Exchangers in the Stirling Engine : Heat Transfer in a Heated Tube under the Periodically Reversing Flow Condition.* JSME international journal. Ser. 2, Fluids engineering, heat transfer, power, combustion, thermophysical properties, 1992. **35**(4): pp. 641–646.

151. Makhkamov, Kh. Kh. and D.B. Ingham, *Analysis of the Working Process and Mechanical Losses in a Stirling Engine for a Solar Power Unit.* Journal of Solar Energy Engineering, 1999. **121**: pp. 121–127.

152. Thieme, L.G., *Low Power Baseline Test for the GPU - 3 Stirling Engine.* 1979. NASA Lewis Research Center.

153. Formosa, F. and G. Despesse, *Analytical model for Stirling cycle machine design*. Energy Conversion and Management, 2010. 51(10): pp.1855-1863

154. Thieme, L.G., *High-Power Baseline and Motoring Test Results for the GPU-3 Stirling Engine*. 1981. NASA Lewis Research Center.

155. Thieme, L.G. and R.C. Tew Jr, *Baseline Performance of the GPU-3 Stirling Engine*, in Highway Vehicle Systems Contractors Coordination Meeting sponsored by the U.S. Department of Energy. 1978. NASA Lewis Research Centre: Dearborn, Michigan.

156. Kays, W.M. and A.L. London, *Compact Heat Exchangers*. 2nd ed. 1964: McGraw Hill.

157. Ondrechen, M.J. et al, *Maximum work from a finite reservoir by sequential Carnot cycles*. American Journal of Physics, 1980. **49**(7): pp. 681–685.

158. Electric Power Research Institute, *Stirling Engine Assessment*. 2002, Palo Alto, California.

159. Giaccone, L. and A. Canova, *Economical comparison of CHP systems for industrial user with large steam demand.* Applied Energy, 2009. **86**(6): pp. 904–914.

160. Newnan, D.G., J.P. Lavelle, and T.G. Eschenbach, *Essentials of Engineering Economic Analysis*. 2002, New York: Oxford University Press.

161. Department of Communications, Energy and Natural Resources, Sustainable and Renewable Energy Division, *Electricity from Renewables inc REFIT and AER*. 2010, Ireland, web page [accessed 21 August 2010], http://www.dcenr.gov.ie/Energy/Sustainable+and+Renewable+Energy+Division/Electricity+from+Renewables+inc+REFIT+and+AER.htm.

162. MWM, *MWM TCG 2020 Gas Engine Specification* 2010, Germany, data sheet [accessed 20 August 2010], http://www.mwm.net/modules/wfdownloads/singlefile.php?cid=20&lid

APPENDIX A

A.1 FTT Otto Cycle Model Validation

```
%% Ricardo 4 cylinder NA SI gasoline engine model
%This model presents a validation of the Otto cycle thermodynamic
model as %presented in Chapter 3. It is validated against a sample
engine from the Ricardo WAVE simulation file

%% Step 1: Define Engine Cylinder Geometry

%Number of Cylinders
Ncyl = 4;

%Bore (m)
B=0.085;

%Stroke (m)
S = 0.088;

%Piston Face Area (m^2)
Ap = (pi()*B^2)./4;

%Crank radius (m)- this is half the stroke
a = S/2;

%Crank Radius to Con Rod length ratio,f
f = 0.29;

%Con Rod Length (m)
L=a/f;

%Compression Ratio
Rv = 9;

%Total Displaced Volume (m^3)
Vtot = 0.002;

%Volume per cylinder (m^3)
Vcyl = Vtot/Ncyl;

% Starting temperature for the cycle (K)
T1 = 383;

% Specify gamma, the specific heat ratio (taken from simulation)
gamma = 1.3;

%% Step 2: Specify Engine Operating Frequency

% Engine operating speed (Rpm)
N = 1000:500:6000;

% Engine Rotational Frequency (Hz)
freq = N./60;
```

```
% Thermodynamic Frequency (Hz) - The thermodynamic cycle takes two
full revolutions to complete
freq1 = freq./2;

% Thermodynamic Cycle period (s)
t = 1./freq1;

% Mechanical Cycle period (s)
t1 = 1./freq;

% Time on power stroke, t34
t34 = 0.25.*t;

% Angular velocity (rads/sec)
AngVel = 2*pi().*freq;

%% Step 3: Calculate the Clearance Volume
% We need to know the clearance volume. We can calculate this as the
% difference between the total volume and the swept volume

% Clearance Volume, calculated by using the compression ratio and
the dispaced volume of the cylinder
Vclear = Vcyl/Rv;

%% Step 4: Calculate the Average Piston Position, x34
% First, calculate the clearance depth, x0
x0 = (4*Vclear)./(pi()*B^2);

x34 = S./2+x0;

%% Step 5: Specify the Crank Angle

% Specify the crank angle as a vector (rads)

phi = 0:0.04:2*pi();

%% Step 6: Calculate the Instantaneous Volume as a function of Crank
Angle

Vinst = Vclear+((Rv-1)*Vclear./2)*((1./f)+1-cos(phi)-
(sqrt((1./f.^2)-sin(phi).^2)));

%% Step 7: BEGIN CALCULATION OF ENGINE WORK

% We will now begin calculating the engine work
% We need to specify the heat added to the cycle (W). The heat added
to the entire 4 cylinder engine is:

Q = (((-4E-6).*(N.^2))+(0.0938.*N)-45.978).*1000./Ncyl;

% To determine the heat addition per cylinder per thermodynamic
cycle (J/cycle)
q = (Q./(freq1));

% We need to specify the mass of gas within the cycle. This is
available from the engine specifications. First, we are given the
mass flowrate through one cylinder (kg/s)
Mf = (((-6E-10).*N.^2)+((1E-5).*N)-0.0065);
```

```
% However, as only two of the working cylinders are working at any
one time, (assuming that at any one time one cylinder is inhaling,
one exhausting, one compressing and one powering)
Mflow = 2.*Mf;

% the mass per cylinder per cycle is therefore (kg/cycle)
M = (Mflow./(freq1));

% Temperature T2, the temperature after compression
T2 = T1.*Rv.^(gamma-1);

%% Step 8: Calculation of required Temperatures and Specific Heat
Capacity Terms

% We require values for the specific heat capacities at constant
pressure and constant volumes for a variety of temperatures (the
cycle temperatures) We then compute averages for these later.  In
order to calculate the specific heats, we use the Abu-Nada
polynomial expression as advocated by Ge et al

Cp1      =      (((2.506E-11)*T1.^2)+((1.454E-7).*T1.^1.5)-((4.246E-
7).*T1)+((3.162E-5).*T1^0.5)+(1.3303)-((1.512E4).*T1.^-
1.5)+((3.063E5).*T1^-2)-((2.212E7).*T1^-3))*10^3;
Cp2      =      (((2.506E-11).*T2.^2)+((1.454E-7).*T2.^1.5)-((4.246E-
7).*T2)+((3.162E-5).*T2.^0.5)+(1.3303)-((1.512E4).*T2.^-
1.5)+((3.063E5).*T2^-2)-((2.212E7).*T2.^-3))*10^3;

% Gas Constant (J/kgK)
R = 287;

% Cv, the specific heat at constant pressure (J/kgK)
Cv1 = Cp1-R;
Cv2 = Cp2-R;

%Also, let Cv3 = Cv2. We must do this as we used Cv2 to calculate
T3, therefore there is no point in evaluating at T3, it will just
give Cv2 anyway

Cv3 = Cv2;

% and

Cp3 = Cv3+R;

% Temperature T3, the temperature after combustion (K)
T3 = (q./(M.*Cv2))+T2;

% We must include the cylinder wall temperature, Tw. This is taken
from the Ricardo WAVE simulation(K)
Tw = 480;

% T4 is the temperature after the adiabatic expansion stroke. It is
the temperature at which heat transfer begins from the cylinder (K)
T4    =    ((T3.*t./8).*((B+(Vclear./Ap).*(1+Rv)).*(1+Rv.^(1-gamma)-
2.*(Tw./T3))))./((B./2+x34).*t34))+2.*Tw-T3;

% The temperature ratio
tau = T1./T3;
```

```
% The Specific Heat Capacities at T4 (J/kgK)
Cp4 = (((2.506E-11).*T4.^2)+((1.454E-7).*T4.^1.5)-((4.246E-
7).*T4)+((3.162E-5).*T4.^0.5)+(1.3303)-((1.512E4).*T4.^-
1.5)+((3.063E5).*T4.^-2)-((2.212E7).*T4.^-3))*10^3;

Cv4 = Cp4-R;

% calculate the temperature averaged gamma values required
gamma12 = (Cp1+Cp2)./(Cv1+Cv2);
gamma34 = (Cp3+Cp4)./(Cv3+Cv4);

%calculate the average specific heat at constant volume for process
41. We %also require the same value for process 23, however as
already mentioned these are taken as equal, so we use Cv2 as the
average value

Cv41 = 0.5.*(Cv4+Cv1);

%% Step 9: Calculate the Work Loss due to Heat Transfer

% Coefficient of convective heat transfer (Averaged over the full
expansion stroke)
h = 1000;

% Phenomenological constant
epsilon = 0.1;

WQ =
((pi.*epsilon.*h.*B.*t.*T3)/16)*(B+(Vclear./Ap).*(1+Rv)).*(1+(Rv.^(1
-gamma34))-(2.*(Tw./T3)));

%% Step 10: Calculate the heat loss to the cylinder walls

QL = WQ./epsilon;

%% Step 11: Calculate the Friction Loss Work
%In this section we calculate the lost work due to friction
according to the relationship offered by Curto Risso et al This
method is favourable in that it allows calculation with respect to
cylinder geometry

%The reversible work is

Wrev = M.*(((Cv2.*(T3-T2)))-(Cv41.*(T4-T1)));

%% Step 11-1: Calculate the friction coefficient

%the power lost to friction is specified as 15% of the reversible
work (Mozurkewich & Berry 1981)

Wf = 0.15.*Wrev;

% to calculate the alpha friction coefficient

alpha = (2.*t1.*Wf)./(7*(pi^2).*(S.^2));

% to calculate the friction coefficient, mu

mu = 7.*alpha;
```

```
%% Step 11-2: Calculate the Irreversible Power for a set Rv range

%we need to calculate the averaged piston velocity (m/s)

ve = 2.* S .* freq;

% The friction power losses are therefore (W)

Pf = mu.*(ve.^2);


%% Step 12: Calculate the Irreversible Work

% Specify the Experimental Power polynomial - this is the curve
fitted to the experimental data from Ricardo Wave
Pexp = (((-2E-6).*N.^2)+(0.0301.*N)-16.368).*1000./Ncyl;

% Calculate the Irreversibility Factor, IR
IR   =   (-1./(Cv41.*(T4-T1))).*((t./M).*(Pexp+(WQ./t)+Pf)-(Cv2.*(T3-
T2)));

% we are now in a position to calculate the irreversible work, WI
(J)
WI = M.*(((Cv2.*(T3-T2)))-(IR.*Cv41.*(T4-T1)));

%% Step 13: Calculate the Final Irreversible Power

Ptotal = (WI.*freq1)-(WQ.*freq1)-(Pf);

Ptotal_1 = Ptotal.*Ncyl;

Qin = Q.*Ncyl;

%% Step 14: Calculate the Final Brake Thermal Efficiency

eff = Ptotal./Q;

%% Step 15: Calculate the Heat Loss through the Exhaust

% the exhaust heat can be approximated as the balance of heat left
in the cylinder after the brake power and thermal loss to the
cylinder walls have been accounted for

Qex = Q-Ptotal-(QL.*freq1);

% The results of this caluclation offer good agreement with the
engine ratings given in the literature

%% Step 16: Calculate the FTT Cycle Work at each speed

Wmodel=Ptotal./freq1;

%% Step 17: Calculate the Actual Cycle Work at each speed

Wact = Pexp./freq1;

%% Step 18: Calculate the Exhaust Temperature
```

```
% We use the method described in Chapter 3 to calculate the exhaust
temperature.    We estimate the mass flow during blowdown by
calculating the mass flowrate through the exhaust valves and
multiplying this by the estimated time that blowdown occurs for.  We
assume a four valve pent roof configuration

% number of exhaust valves
nv = 2;

% stagnation pressure - taken as the pressure in the cylinder at
exhaust valve opening (Pa)

p0 = (M.*R.*T4)./Vcyl;

% stagnation temperature - taken as the temperature in the cylinder
at exhaust valve opening (K)

T0 = T4;

% Valve diameter (Heywood p222) (m)
Dv = 0.3.*B;

% We assume the best possible performance of the valve(see figure 6-
18 pp 229 Heywood (1988))
Lv = 0.1.*Dv;

% Orifice Area (Heywood (1988) pp 226) (m^2)
Ac = pi.*Dv.*Lv;

% Dicharge coefficient
CD = 0.6;

% Choked mass flow during blowdown (kg/s)
Mflow_bd =
((nv.*CD.*Ac.*p0)./sqrt(R.*T0)).*(gamma34.^0.5).*(2./(gamma34+1)).^(
(gamma34+1)./(2.*(gamma34-1)));

% Estimate blowdown time - in the absence of specific information
regarding the valve timing of this engine we use approximations.
Stas (1999) and Heywood (1988) indicate that blowdown typically
takes between 40deg and 60deg CA. If we assume a median of 50deg CA,
then we see that this represents 50/720 = 7% of total cycle
duration.  This enables us to calculate a blowdown duration (s)

t_bd= 0.03.*t;

% we are now positioned to calculate the quantity of mass evacuated
from each cylinder during the blowdown as (kg)

Mbd=Mflow_bd.*t_bd;

% and the mass remaining in the cylinder is (kg)

Mrem = M-(Mbd);

%The proportion of mass left to total mass that was in it is

Rm = Mrem./M;
```

```
Rm_bd=Mbd./M;

Qbd = (Rm_bd.*Qex)./(freq1);

% This proportion applies to the heat remaining in the cycle also

Qrem = (Rm.*Qex)./(freq1);

% Exhaust final temperature per cycle per cylinder (K)
CvE = 900;

T5 = T4-((Qbd)./(M.*Cp4));

%% Step 19: Enthalpy Averaged Temperature

% Due to the highly irregular mass flow, we see that two thirds of
the mass leaves the cylinder during the blowdown process.  We assume
that this gas is at the temperature T4 of blowdown. The remaining
third we take as being at the lower temperature T5.  Heywood (p234)
indicates that to accomodate the mass flux, an enthalpy averaged
temperature is more indicative of the exhaust temperature

% constant pressure specific heat of exhaust gas at temperature T5
(J/kgK)
Cp5      =      (((2.506E-11).*T5.^2)+((1.454E-7).*T5.^1.5)-((4.246E-
7).*T5)+((3.162E-5).*T5.^0.5)+(1.3303)-((1.512E4).*T5.^-
1.5)+((3.063E5).*T5.^-2)-((2.212E7).*T5.^-3)).*10^3;

Cp45 = 0.5.*(Cp4+Cp5);

Cp51 = 0.5.*(Cp5+Cp1);

% Enthalpy of blowdown gas (J)

Hbd = Mbd.*Cp45.*T4;

% Enthalpy of remaining gas in cylinder (J)

Hrem = Mrem.*Cp51.*T5;

% Total enthalpy of exhaust gas (J)

Hex = Hbd+Hrem;

%  To calculate the average temperature, we require an averaged
specific heat value (J/kgK)

Cp_avg = 0.5.*(Cp45+Cp51);

% The average temperature of this enthalpy is therefore (K)

Tex_avg=Hex./(M.*Cp51);
```

APPENDIX B

B.1 FTT Stirling Cycle Model Validation

```
%This model details a Finite Time Thermodynamic model of the
Stirling
%cycle. The model begins with the ideal cycle and corrects for
%irreversibility associated with the heat exchangers.Heat exchanger
effectiveness
%terms are included in the model.  This ideal model is then
corrected through the use of a global friction loss
%parameter, as first suggested by Mozurkewich & Berry and later
deployed to
%significant effect by Angulo-Brown et al

%% Step 1: Specify the engine parameters

% we will specify the temperatures, pressure and volume of the
% thermodynamic cycle, as well as the gas constant R

% Engine Rpm (for calculation of friction coefficient)
N = 2500;

% Engine Rpm range (for calculation of Power and Efficiency)
N1 = 100:100:3500;

%% Step 1-1: Calculate engine cycle frequencies (relevent to
analysis across speed
%% range)

f1 = N1./60;

t1 = 1./f1;

tp1=t1/2;

% Heat Input (from performance data)
Qin1 = (1000.*(((-0.0016).*f1.^2)+(0.3478.*f1)-0.5069));
%Qin1 = (1000.*((0.2141.*f1)+2.056));
%Qin1 = (4.14./2.76).*1000.*((-0.0006.*(f1.^2))+(0.1864.*f1)+1.051);

% Mean Pressure (Pa)
P = 4.14E6;

% Compression ratio
Rv = 1.39;

% Cylinder bore (m)
d = 0.07;

%Regenerator diameter (diameter of 1 tube)
Dr = 0.0226;

%length of regenerator
Lr = 0.0226;
```

```
% mesh wire diameter
d_wire=0.00004;

%Diameter of piston
Dp=0.0699;

% Annular Gap
xg = 0.00163;

%Length of Displacer Piston
Lp = 0.04359;

% Expansion Space Inner Diameter
DCE=0.0696;

% Number of Heater Tubes
Nh=40;

% Number of Cooler Tubes
Nc=312;

% Source Temperature (K)
Tsource = 1170;

% Sink Temperature (K)
Tsink = 286;

% Hot Side Gas Temperature (K)
T3=922;

% Cold Side Gas Temperature (K)
T1 = 286;

%Ambient Temperature (20 deg C)(K)
Tamb= 293;

% Exhaust Temperature after preheater (K)
Texh = 523;

%Average Temperature of thermodynamic source and sink (K)
Tavg = (T3+T1)./2;

% Volume of Expansion Space
Vex = 0.00012;

% Volume of Compression Space
Vcomp = 0.000114;

%Average Volume of cycle. This is computed from the cyclic volume
variation
%equations. For the GPU-3 engine, a rhombic drive is used, and the
mean
%total cycle volume is,(m3)
Vavg = 0.000369;

% Specify the system dead volume. This is available from engine
specs (m3)
Vdead = 0.000232;
```

```
% Volume in Hot Side HEX
Vh = 8.08E-5;

% Volume in Cold Side HEX
Vk = 1.313E-5;

% Volume in Regenerator
Vr = 6.55E-5;

% Gas constant, Helium (J/kgK)
R = 2077;

% Specify the Specific Heat at Constant Volume for the working fluid
% (Helium)(J/kgK)
Cv = 3120;

%Viscosity of gas (m2/s) (Helium)
visc = 396E-6;

%dynamic viscosity of Helium @750K approx
mu_helium = 364E-7;

%dynamic viscosity of Helium @300K approx
mu_helium_C = 195E-7;

%Conductivity of working Gas (Helium @ 600K)
kf = 252E-3;

%Conductivity of working Gas (Helium @ 300K)
kf_w = 149E-3;

% Prandtl Number (Helium)
Pr = 0.676;

% Specific heat at constant pressure, air (922K) (J/kgK)
Cp_air = 1120;

% Specific heat at constant pressure, air (500K) (J/kgK)
Cp_air1 = 1030;

% Specify internal and external diameters of the heater tubes
di=0.00302; %Inner diameter
do=0.00483; %Outer diameter

% Specify internal and external diameters of the cooler tubes
di_w=0.00108; %Inner diameter
do_w=0.00159; %Outer diameter

%conduction coefficient, stainless steel
kwC = 15;

% Length of cooler tubes
LH_w = 0.0355;

%conduction coefficient, stainless steel
kwH = 22.8;
LH = 0.154;
```

```
% Dynamic viscosity of Cooling water
mu2 = 1422E-6;

%Prandtl number, air at 900K
Pr_w=10.26;

%Specific Heat Capacity of Cooling Water
Cp_w=4198;

% Regenerator porosity
Por = 0.8;

%% Step 2: Schmidt - Style Isothermal model of Stirling

% this model is used to provide an estimate of Stirling engine work
output
% when losses due to continuous piston movement are accounted for.
The
% model retains the dead volume, temperatures and isothermal
assumptions of
% the ideal case, and so it is a reasonable comparison against the
ideal
% cycle to ascertain the work losses associated with the piston
motion.

%SPECIFY DIMENSIONLESS PARAMETERS

% Crank Angle (rads)
phi = 0:2*pi();

% Temperature Ratio
TR = T1./T3;

% Dead Volume Ratio
CHI = Vdead./Vex;

% Swept volume Ratio
KAPPA = Vcomp./Vex;

% Phase Angle;
ALPHA = 1.9;

% Expansion space volume variations
Ve_inst = 0.5.*Vex.*(1+cos(phi));

% Compression space volume variations
Vc_inst = 0.5.*KAPPA.*Vex.*(1+cos(phi-ALPHA));

% Instantaneous volume of total working space
Vtot_inst = Ve_inst+Vc_inst+Vdead;

% Calculate Substitution terms
SIGMA = 2.*CHI.*TR./(TR+1);

THETA = atan(KAPPA.*sin(ALPHA)./(TR+KAPPA.*cos(ALPHA)));

DEL =
(((TR.^2)+2.*TR.*KAPPA.*cos(ALPHA)+KAPPA.^2).^0.5)./(TR+KAPPA+2.*SIG
MA);
```

```
% Calculate the Max Pressure
Pmax = P./(((1-DEL)./(1+DEL)).^0.5);

Pmin = Pmax./((1+DEL)./(1-DEL));

% Calculate the Instantaneous Pressure in the cycle

p_inst = Pmax.*(1-DEL)./(1+DEL.*cos(phi-THETA));

% Calculate the cycle work output
VT = Vex+Vcomp;

W = (Pmax.*VT).*pi().*((1-TR)./(KAPPA+1)).*(((1-
DEL)./(1+DEL)).^0.5).*(DEL.*sin(THETA))./(1+(1-DEL.^2).^0.5);

%% Step 3: Calculate the Cycle Mass

% we calculate the mass of gas in the engine using the ideal gas law
and
% the averaged properties

M = (P*Vavg)./(R*Tavg);

%% Step 4: Determine the ratio of Schmidt cycle work to ideal cycle
work

Nw = W./(M.*R.*log(Rv).*(T3-T1));

% This ratio gives an insight into the work losses inherent in the
use of
% continuous piston motion. The only difference between the two is
the
% accomodation of the volume variations. We can therefore use this
ratio to
% correct the ideal cycle in the FTT method to account for work
losses
% through continuous piston motion

%% Step 5: Calculate the Mass flowrate of the combustion gases

% Combustion gas mass flowrate at each operating point

Mcomb=Qin1./(Cp_air.*(Tsource-Tamb));

%% Step 6: Calculate the Heat that goes to the cycle and the heat
lost to Exhaust

Qex = 0.3.*Qin1;

%% Step 7: Specify the Conduction Losses within the engine

% This is calculated from the experimental data given by Thieme

Qcond = 500; %(W)

%% Step 8: Calculate the engine frequency and the thermodynamic
cycle period, t
```

```
%% (relevant to calculation of mu term)

f = N./60;

t = 1/f;

%% Step 9: Calculate the effective Stroke

% Effective Clearance Displacement
xD = (4*Vdead)./(pi*(d^2));

% Effective Stroke
Se = xD.*(Rv-1);

%% Step 10: Now Calculate the effective Piston Velocity

ve1 = 2.*Se.*f1;

%% Step 11: Calculate the Regenerator Effectiveness - GPU-3 Engine

% we model the regenerator as a balanced counter flow heat exchanger
(Feidt
% 2002). We use the model for heat transfer coefficienct as
described by
% Petrescu et al (2002). This requires specification of certain
parameters
% to assist calculation. Details of the GPU-3 engine regenerator are
given
% by Martini. There are 8 regenerators in the engine

b=1.5*d_wire;

% WETTED AREA OF REGENERATOR (TOTAL)
Aw = 8*(1/4)*((pi^2)*(Dr^2)*Lr)/(b+d_wire);

% Calculate the gas velocity in the regenerator - we assume
incompressible
% flow in the regenerator, therefore we use the continuity equation
to
% calculate the velocity in the regenerator

%Cross sectional area of regenerator
Ar = 8*(pi*Dr^2)/4;

%Cross sectional area of piston
Ap = (pi*Dp^2)/4;

%Velocity of gas in cylinder - assumed equal to piston velocity
Vc = ve1;

% Therefore the velocity of gas in the regenerator
vr=(Ap*Vc)/Ar;

% We calculate the temperature ratio, tau.
tau = T3/T1;

% Specific Heat Capacity at constant pressure, Helium
Cp = Cv+R;
```

```
% CALCULATE CONVECTIVE COEFFICIENT

h = (0.395*((4*P)/(R*T1))*(vr.^0.424)*Cp*(visc.^0.576))/((1+tau)*(1-
(pi/(4*((b/d_wire)+1))))*(Dr^0.576)*(Pr^(2/3)));

% CALCULATE THE MASS FLOW THROUGH THE REGENERATOR
% To estimate the mass flow rate through the regenerator, we assume
that only a mass equivalent to that contained in the
% working volumes at any instant is transported through the
regenerator ie only a "live mass" is accounted for, the "dead mass"
% contained in the dead volumes is not accounted for. To estimate
the instantaneous mass
% in each working space, we determine the ratio of instaneous
working space
% volume to the total dead space volume in the system

Nm_1=((Ve_inst./T3)+(Vc_inst./T1))./((Vh./T3)+(Vr./((T3+T1)./2))+(Vk
./T1)+(Ve_inst./T3)+(Vc_inst./T1));

% this gives a range of values over the full cycle. The mean value
is taken
% to give an approximation of the ratio over one full cycle.

Nm = mean(Nm_1);

% It is assumed that over

Mr = Nm.*2.*Nw.*M.*f1;

% CALCULATE THE NTU OF THE REGENERATOR

NTU = (h*Aw)./(Cp*Mr);

%% Step 12: Regenerator Effectiveness

eR = NTU./(2+NTU);

%% Step 13: CALCULATE THE HOT SIDE HEX EFFECTIVENESS

%% Step 13-1: First calculate the convective coefficient on the
combustion gas side

% Free Flow Area (calculated for GPU-3 3/5/2010)
Aff = 0.01912;

%Hydraulic Diameter of Hot Side HEX flow passages
Dh = 0.0115;

% Dynamic viscosity of Combustion Gases
mu1 = 411.3E-7;

% First Calculate the Mass Velocity
G=(Mcomb)./Aff;

% Reynolds number of gas flow
Re=G.*Dh./mu1;

%Colburn jH value (Formosa 2010)
jH = exp(0.337-0.812.*log(Re));
```

```
%Prandtl number, air at 900K
Pr_air=0.72;

% Convective Coefficient
h1=(jH.*G.*(Cp_air))./(Pr_air.^(2/3));

%% Step 13-2: Second calculate the thermal resistance in the wall of
the HEX tubes

% Calculate the Thermal resistance associated with radial conduction
% through the HEX tube walls
Rt=(log((do./2)./(di./2)))./(2.*pi.*kwH.*LH);

%% Step 13-3: Calculate the convective coefficient of the Stirling
Working gas side

% Calculate the Reynolds number of the working fluid flow in the HEX
% (Kanzaka (1992))

p_dash = (1./40).*(P.*Vex)./((Nm.*M).*R.*T3);

Re_St =
(1./40).*(1./(2.*pi().*f1)).*(Mr).*((6.*P.*Vex.*N1)./(p_dash.*R.*T3)
).*(4./(pi.* mu_helium.*di));

%estimate the interior wall temperature and the bulk fluid
temperature for
%the working fluid

Tw = T3;
Tb = 600;

%Calculate substitution term
C=0.923+0.75.*(Tw./1000);

% Calculate the Nusselt Number
Nu = 0.021.*(Re_St.^0.8).*(Pr.^0.4).*((Tw./Tb).^(-0.5)).*C;

% Calculate the convective heat transfer coefficient
h2 = (kf.*Nu)./LH;

%% Step 13-4: Calculate U, the overall heat transfer coefficient of
the HEX on the
%% combustion gas side

%Thermal resistance values

R1 = 1./(h1.*pi.*do.*LH);

R2 = Rt;

R3 = 1./(h2.*pi.*di.*LH);

% Calculate the heat transfer area on the working gas side

AH = pi.*di.*LH;
```

```
Uh = 1./(AH.*(R1+R2+R3));

% Specify the Cmin term. In this case it is the combustion side gas
Ch

Cmin = (1./Nh).*Mcomb.*Cp_air;

Cmax = (1./Nh).*Mr.*Cp;

Cr = (Cmin./Cmax);

% The NTU then becomes(for total 40 tubes)
NTUh = Nh.*(Uh.*AH)./(Cmin);

% The Effectiveness becomes (Crossflow exchanger, Cmin mixed, Cmax
unmixed)
eH=1-exp((-Cr.^-1).*(1-exp(-Cr.*NTUh)));

%% Step 14: CALCULATE THE COLD SIDE HEX EFFECTIVENESS

%% Step 14-1: First calculate the convective coefficient on the
water coolant side

% Free Flow Area (Calculated as per assumptions, Chapter 5)
Aff_w = 0.008272;

%Hydraulic Diameter (Calculated as per assumptions, Chapter 5)
Dh_w = 0.00859;

%Average Mass flowrate of cooling water
Mw=0.13;

% First Calculate the Mass Velocity
G_w=(Mw)./Aff_w;

% Reynolds number of gas flow
Re_w=G_w.*Dh_w./mu2;

%jH value (Formosa 2010)
jH_w= exp(-3.575-0.229.*log(Re_w));

% Convective Coefficient
h1_C=(jH_w.*G_w.*(Cp_w))./(Pr_w.^(2/3));

%% Step 14-2: Second calculate the thermal resistance in the wall of
the HEX tubes

% Cooler side thermal conductivity resistance
Rt_w=(log((do_w./2)./(di_w./2)))./(2.*pi.*kwC.*LH_w);

%% Step 14-3: Calculate the convective coefficient of the Stirling
Working gas side

p_dash_C = (P.*Vcomp)./((Nm.*M).*R.*T1);

Re_St_C =
(1./(Nc)).*(1./(2.*pi().*f1)).*(Mr).*((6.*P.*Vcomp.*N1)./(p_dash_C.*
R.*T1)).*(4./(pi.* mu_helium_C.*di_w));
```

```
% estimate the interior wall temperature and the bulk fluid
temperature for
% the working fluid

Tw_C = T1;

% Estimate the fluid temperature
Tb_C = 320;

% Calculate the Nusselt Number

%Substitution term
C_w=0.923+0.75.*(Tw_C./1000);

Nu_C = 0.021.*(Re_St_C.^0.8).*(Pr.^0.4).*((Tw_C./Tb_C).^(-
0.5)).*C_w;

%Convective Coefficient
h2_C = (kf_w.*Nu_C)./LH_w;

%% Step 14-4: Calculate U, the overall heat transfer coefficient of
the HEX on the
%% coolant side

% Thermal resistance values

R1_w = 1./(h1_C.*pi.*do_w.*LH_w);

R2_w = Rt_w;

R3_w = 1./(h2_C.*pi.*di_w.*LH_w);

% Calculate the heat transfer area on the working gas side

AH_C = pi.*di_w.*LH_w;

Uc = 1./(AH_C.*(R1_w+R2_w+R3_w));

% Specify the Cmin term. In this case it is the combustion side gas
C

Cmin_C = (1./Nc).*Mr.*Cp;

Cmax_C = (1./Nc).*Mw.*Cp_w;

Cr_C = (Cmin_C./Cmax_C);

% The NTU then becomes

NTUc = Nc*(Uc.*AH_C)./Cmin_C;

% The Effectiveness becomes (Cmin mixed, Cmax unmixed)
eC=1-exp((-Cr_C.^-1).*(1-exp(-Cr_C.*NTUc)));

%% Step 15: Calculate the ideal (reversible) cycle Work

Wrev = (eH.*Qin1.*t1)-(Nw.*eC.*M.*R.*T1.*log(Rv));
```

```
%% Step 16: Calculate the ideal (reversible) cycle Power at the
given frequency

Prev = Wrev./t1;

%% Step 17: Calculate the Friction Work

% In this section, we calculate the lost friction work.  We use the
method
% laid out in Chapter 4. This method introduces the concept of the
effective stroke and the effective
% piston velocity.
% To quantify the global friction type losses, we assume that losses
are
% comprised of 1) Pumping losses and 2) Mechanical friction losses.

%Calculate friction Work, Wf as a function of the reversible work,
Wrev

Wf = 0.1*Wrev;

%% Step 18: Calculate the Friction Power

% we use the same procedure as that used by Angulo Brown et al for
the Otto
% engine, P = mu*(ve)^2

%% Step 19: Calculate the friction coefficient, mu

mu = (2.*t*Wf)./((pi^2).*(Se^2));

%% Step 20: Finally calculate the friction power

Pf = mu.*(ve1.^2);

%% Step 21: Calculation of Pumping Power Losses

% First it is necessary to specify the Cf terms for each of the
operating
% spaces. This requires knowledge of the Reynolds Number in each
section.
% Referring to Martini (1983), the Cf values are calculated from:

CfH = exp(-1.34-0.2.*log(Re_St));

CfC = exp(-1.34-0.2.*log(Re_St_C));

% To calculate the Cf in the Regenerator, it is necessary to
calculate the
% Reynolds number of the fluid flow. This is related to the mesh
properties
% through the Hydraulic Radius of the mesh

% Heat transfer area per unit volume of the regenerator
Avol = Aw./(Ar.*Lr);

% Hydraulic Radius
R_H = Por./Avol;
```

```
% Frontal area of regenerator mesh
Afr_R = Ar.*(1-Por);

% Freeflow area of regenerator mesh
Aff_R = Ar - Afr_R;

% Mass Velocity of flow through regenerator
G_R = Mr./(Aff_R);

% Reynolds Number
Re_R = (4.*R_H.*G_R)./mu_helium;

% Therefore the Cf value for the regenerator is
CfR = exp(0.015-0.125.*log(Re_R));

% Calculate the density of the gas in each space
rho_H = P./(R.*T3);
rho_R = P./(R.*Tavg);
rho_C = P./(R.*T1);

% Frontal Area of heater tubes
Ah = Nh.*pi().*(di.^2);

% Frontal Area of cooler tubes
Ac = Nc.*pi().*(di_w.^2);

% Pumping Power Loss
sigma2 = Aff_R./Afr_R;
psi = rho_H./rho_C;

Pp = (8.*((1+sigma2.^2).*((1./rho_H).*(psi-1)+(1./rho_C).*((1./psi)-
1)).*((rho_H.^3)./rho_R).*((Ap.^3)./(Aff_R.^2))+((rho_R.*CfR.*Lr.*Af
f_R)./R_H))+Nh.*((1./2).*CfH.*LH.*rho_H.*pi().*di.*(Ap./(Ah./Nh)))+1
.*Nc.*((1./2).*CfC.*LH_w.*rho_R.*pi().*di_w.*(Ap./(Ac./Nc)))).*ve1.^
3;

alpha_S = (8.*((1+sigma2.^2).*((1./rho_H).*(psi-
1)+(1./rho_C).*((1./psi)-
1)).*((rho_H.^3)./rho_R).*((Ap.^3)./(Aff_R.^2))+((rho_R.*CfR.*Lr.*Af
f_R)./R_H))+Nh.*((1./2).*CfH.*LH.*rho_H.*pi().*di.*(Ap./(Ah./Nh)))+1
.*Nc.*((1./2).*CfC.*LH_w.*rho_R.*pi().*di_w.*(Ap./(Ac./Nc))));

%% Step 22: Fitted Polynomial for Experimental Power Output

Pexp = (-2E-7).*(N1.^3)+(0.0011).*(N1.^2)-0.9329.*N1+1462.3;

%% Step 23: Calculate the Engine Irreversibility Parameter

% Calculate the regenerator exit temperatures
Tx2 = eR.*(T3-T1)+T1;

Tx4 = T3 - eR.*(T3-T1);

IR = (T3./T1)-(t1./(M.*R.*T1.*log(Rv))).*(Pexp+Pf+Pp+Qcond+Qex);

%% Step 24: Calculate the irreversible cycle work for the series of
%% Operating Speeds - IR varies with eR
```

```
Wrev1 = (eH.*Qin1.*t1)-IR.*(Nw.*eC.*M.*R.*T1.*log(Rv));

%% Step 25: Calculate the ideal (reversible) cycle Power at the
given frequency

Prev1 = Wrev1./t1;

%% Step 26: Calculate the Irreversible Power

Pirrev = (Prev1  - Pf - Pp-Qcond -Qex);

%% Step 27: Calculate the Cycle Efficiency
eff=Pirrev./Qin1;
```

APPENDIX C

C.1 Combined Cycle Model

```
%% THIS MODEL IS THE COMBINED CYCLE MODEL FOR THE FINAL ANALYSIS.
IT USES THE RICARDO WAVE 4-CYLINDER N/A ENGINE MODEL AND COMBINES IT
WITH THE STIRLING CYCLE FTT MODEL DEVELOPED PREVIOUSLY

%% Ricardo 4 cylinder NA SI gasoline engine model
%This model presents an Otto cycle thermodynamic model as
%published in the ASME Energy Sustainability 2010 conference.  The
model
%presents the 4 cylinder engine model used for the FTT model
validation

%% Step 1: Define Engine Cylinder Geometry


%Number of Cylinders
Ncyl = 1;

%Bore (m)
B=0.085;

%Stroke (m)
S = 0.088;

%Piston Face Area
Ap = (pi()*B^2)./4;

%Crank radius (m)- this is half the stroke
a = S/2;

%Crank Radius to Con Rod length ratio,f
f = 0.29;

%Con Rod Length
L=a/f;

%Compression Ratio
Rv = 9;

%Total Displaced Volume (m3)
Vtot = 0.0005;%0.0263;

%Volume per cylinder (m3)
Vcyl = Vtot/Ncyl;

%% Step 2: Specify Engine Operating Frequency

% ASSUME THE ENGINE OPERATING SPEED TO BE 1500 RPM

% Engine operating speed (Rpm)
N = 1500;

% Engine Rotational Frequency (Hz)
```

```
freq = N./60;

% Thermodynamic Frequency (Hz) - The thermodynamic cycle takes two
full
% revolutions to complete
freq1 = freq./2;

% Thermodynamic Cycle period (s)
t = 1./freq1;

% Mechanical Cycle period (s)
t1 = 1./freq;

% Time on power stroke, t34
t34 = 0.25.*t;

% Angular velocity (rads/sec)
AngVel = 2*pi().*freq;

%% Step 3: Calculate the Clearance Volume
% We need to know the clearance volume. We can calculate this as the
% difference between the total volume and the swept volume

%Clearance Volume, calculated by using the compression ratio and the
%dispaced volume of the cylinder
Vclear = Vcyl/Rv;

%% Step 4: Calculate the Average Piston Position, x34
% First, calculate the clearance depth, x0
x0 = (4*Vclear)./(pi()*B^2);

x34 = S./2+x0;

%% Step 5: Specify the Crank Angle

% Specify the crank angle as a vector, in radians

phi = 0:0.04:2*pi();

%% Step 6: Calculate the Instantaneous Volume as a function of Crank
Angle

Vinst = Vclear+((Rv-1)*Vclear./2)*((1./f)+1-cos(phi)-
(sqrt((1./f.^2)-sin(phi).^2)));

%% Step 7: BEGIN CALCULATION OF ENGINE WORK

% We will now begin calculating the engine work
% We need to specify the heat added to the cycle (W). The heat added
per cylinder to the
% 4 cylinder engine is:
Q = (((-4E-6).*(N.^2))+(0.0938.*N)-45.978).*1000./4;
%Q = (((-4E-9).*N.^3)+((3E-5).*N.^2)-
(0.0231.*N)+52.792).*1000./Ncyl;

% To determine the heat addition per cylinder per thermodynamic
cycle (J/cycle)
q = (Q./(freq1));
```

```
% We need to specify the mass of gas within the cycle. This is
available
% from the engine sepcifications. First, we are given the mass
flowrate
% through one cylinder (kg/s)
%Mf = (((-3E-10).*N.^2)+((7E-6).*N)-0.0032);
%Mf = ((-2E-13).*N.^3)+((2E-9).*N.^2)-((3E-7).*N)+0.0029;
Mf = 2.*(((-6E-10).*N.^2)+((1E-5).*N)-0.0065);

% However, as only two of the working cylinders are working at any
one
% time, (assuming that at any one time one cylinder is inhaling, one
% exhausting, one compressing and one powering)

Mflow = 1.*Mf;

% the mass per cylinder per cycle is therefore (kg/cycle)
M = (Mflow./(freq1));

% First input the starting temperature for the cycle (K)
T1 = 383;

% Now we must specify gamma, the specific heat ratio (taken from
% simulation)
gamma = 1.3;

% Temperature T2, the temperature after compression
T2 = T1.*Rv.^(gamma-1);

%% Step 8-1: Calculation of required Temperatures and Specific Heat
Capacity Terms

% We require values for the specific heat capacities at constant
pressure
% and constant volumes for a variety of temperatures (the cycle
% temperatures) We then compute averages for these later.  In order
to
% calculate the specific heats, we use the Abu-Nada polynomial
expression
% as advocated by Ge et al

Cp1 = (((2.506E-11)*T1.^2)+((1.454E-7).*T1.^1.5)-((4.246E-
7).*T1)+((3.162E-5).*T1^0.5)+(1.3303)-((1.512E4).*T1.^-
1.5)+((3.063E5).*T1^-2)-((2.212E7).*T1^-3))*10^3;
Cp2 = (((2.506E-11).*T2.^2)+((1.454E-7).*T2.^1.5)-((4.246E-
7).*T2)+((3.162E-5).*T2.^0.5)+(1.3303)-((1.512E4).*T2.^-
1.5)+((3.063E5).*T2^-2)-((2.212E7).*T2.^-3))*10^3;

% Gas Constant (J/kgK)
R = 287;

% Cv, the specific heat at constant pressure

Cv1 = Cp1-R;
Cv2 = Cp2-R;

%Also, let Cv3 = Cv2. We must do this as we used Cv2 to calculate
T3,
%therefore there is no point in evaluating at T3, it will just give
Cv2
```

```
%anyway

Cv3 = Cv2;

% and

Cp3 = Cv3+R;

% Temperature T3, the temperature after combustion. We assume the
specific
% heat Cv2 value, although it should really be at T3 - obviously
this is
% not possible as we are using it to estimate T3.
T3 = (q./(M.*Cv2))+T2;

% We must include the cylinder wall temperature, Tw. This is
difficult to approxmiate, but can be taken from the Ricardo WAVE
simulation. (K)
Tw = 480;

% T4 is the temperature after the adiabatic expansion stroke. It is
the
% temperature at which heat transfer begins from the cylinder
T4 = ((T3.*t./8).*((B+(Vclear./Ap).*(1+Rv)).*(1+Rv.^(1-gamma)-
2.*(Tw./T3))./((B./2+x34).*t34))+2.*Tw-T3;

% The temperature ratio
tau = T1./T3;

% The Specific Heat Capacities at T4
Cp4 = (((2.506E-11).*T4.^2)+((1.454E-7).*T4.^1.5)-((4.246E-
7).*T4)+((3.162E-5).*T4.^0.5)+(1.3303)-((1.512E4).*T4.^-
1.5)+((3.063E5).*T4.^-2)-((2.212E7).*T4.^-3))*10^3;

Cv4 = Cp4-R;

% calculate the temperature averaged gamma values required
gamma12 = (Cp1+Cp2)./(Cv1+Cv2);
gamma34 = (Cp3+Cp4)./(Cv3+Cv4);

%calculate the average specific heat at constant volume for process
41. We
%also require the same value for process 23, however as already
mentioned
%these are taken as equal, so we use Cv2 as the average value

Cv41 = 0.5.*(Cv4+Cv1);

%% Step 9: Calculate the Work Loss due to Heat Transfer

% Coefficient of convective heat transfer (Averaged over the full
expansion
% stroke)
h = 330;

epsilon = 0.1;
```

```
WQ =
((pi.*epsilon.*h.*B.*t.*T3)/16)*(B+(Vclear./Ap).*(1+Rv)).*(1+(Rv.^(1
-gamma34))-(2.*(Tw./T3)));

%% Step 9-1: Calculate the heat loss to the cylinder walls

QL = WQ./epsilon;

%% Step 10: Calculate the Fricition Loss Work
%In this section we calculate the lost work due to friction
according to
%the relationship offered by Curto Risso et al This method is
favourable
%in that it allows calculation with respect to cylinder geometry

%The Reversible work is

Wrev = M.*(((Cv2.*(T3-T2)))-(Cv41.*(T4-T1)));

%% Step 10-1: Calculate the friction coefficient

%the power lost to friction is specified as 15% of the reversible
work
%(Mozurkewich & Berry 1981)

Wf = 0.15.*Wrev;

% to calculate the alpha friction coefficient

alpha = (2.*t1.*Wf)./(7*(pi^2).*(S.^2));

% to calculate the friction coefficient, mu

mu = 7.*alpha;

%% Step 10-2: Calculate the Irreversible Power for a set Rv range

%we need to calculate the averaged piston velocity

ve = 2.* S .* freq;

% The friction power losses are therefore

Pf = mu.*(ve.^2);


%% Step 11: Calculate the Irreversible Work

% Specify the Experimental Power polynomial - this is the curve
fitted to
% the experimental data from Ricardo Wave
Pexp = (((-2E-6).*N.^2)+(0.0301.*N)-16.368).*1000./4;

IR = (-1./(Cv41.*(T4-T1))).*((t./M).*(Pexp+(WQ./t)+Pf)-(Cv2.*(T3-
T2)));

% we are now in a position to calculate the irreversible work, WI
```

```
WI = M.*(((Cv2.*(T3-T2)))-(IR.*Cv41.*(T4-T1)));


%% Calculate the Final Irreversible Power

Potto = (WI.*freq1)-(WQ.*freq1)-(Pf);

Potto_1 = Potto.*Ncyl;

Qin = Q.*Ncyl;

%% Calculate the Final Efficiency

eff = Potto./Q;

% This method demonstrates good approximation of the real operation
of the
% TCG 2016 V12 engine
% Actual Power: 600kW
% Theoretical Power: 599.7kW
% Actual Efficiency (electrical): 0.408
% Theoretical Efficiency (mechanical): 0.4218

%% Calculate the Heat Loss through the Exhaust

% the exhaust heat can be approximated as the balance of heat left
in the
% cylinder after the brake power and thermal loss to the cylinder
walls
% have been accounted for (W)

Qex = Q-Potto-(QL.*freq1);

Qex_1 = Qex.*Ncyl;

% The results of this caluclation offer good agreement with the
engine
% ratings given in the literature

%% Calculate the FTT Cycle Work at each speed

Wmodel=Potto./freq1;

%% Calculate the Actual Cycle Work at each speed

Wact = Pexp./freq1;

%% Calculate the Exhaust Temperature

% We use the method described in the paper to calculate the exhaust
% temperature.  We estimate the mass flow during blowdown by
calculating
% the mass flowrate through the exhaust valves and multiplying this
by the
% estimated time that blowdown occurs for.  We assume a four valve
pent
% roof configuration

% number of  exhaust valves
```

```
nv = 2;

% stagnation pressure - taken as the pressure in the cylinder at
exhaust
% valve opening

p0 = (M.*R.*T4)./Vcyl;

% stagnation temperature - taken as the temperature in the cylinder
at
% exhaust valve opening

T0 = T4;

% Orifice Area - we use the valve curtain area from Heywood (1988)
pp 226
% Ac = pi*Dv*Lv

% Valve diameter - Heywood p222
Dv = 0.3.*B;

% We assume the best possible performance of the valve - see figure
6-18 p
% 229 Heywood (1988)
Lv = 0.1.*Dv;

% Orifice Area
Ac = pi.*Dv.*Lv;

% Dicharge coefficient

CD = 0.6;

% Choked mass flow during blowdown

Mflow_bd =
((nv.*CD.*Ac.*p0)./sqrt(R.*T0)).*(gamma34.^0.5).*(2./(gamma34+1)).^(
(gamma34+1)./(2.*(gamma34-1)));

% Estimate blowdown time - in the absence of specific information
regarding
% the valve timing of this engine we use approximations.  Stas
(1999) and
% Heywood (1988) indicate that blowdown typically takes between
40deg and
% 60deg CA. If we assume a median of 50deg CA, then we see that this
% represents 50/720 = 7% of total cycle duration.  This enables us
to
% calculate a blowdown duration

t_bd= 0.03.*t;

% we are now positioned to calculate the quantity of mass evacuated
from each cylinder during
% the blowdown as

Mbd=Mflow_bd.*t_bd;

% and the mass remaining in the cylinder is
```

```
Mrem = M-(Mbd);

%The proportion of mass left to total mass that was in it is

Rm = Mrem./M;

Rm_bd=Mbd./M;

Qbd = (Rm_bd.*Qex)./(freq1);

% This proportion applies to the heat remaining in the cycle also

Qrem = (Rm.*Qex)./(freq1);

% Exhaust final temperature per cycle per cylinder
CvE = 900;
%T5 = T4+((Qrem)./(Mrem.*Cv4));

T5 = T4-((Qbd)./(M.*Cp4));

%% Enthalpy Averaged Temperature

% due to the highly irregular mass flow, we see that two thirds of
the mass
% leaves the cylinder during the blowdown process.  We assume that
this gas
% is at the temperature T4 of blowdown. The remaining third we take
as
% being at the lower temperature T5.  Heywood (p234) indicates that
to
% accomodate the mass flux, an enthalpy averaged temperature is more
% indicative of the exhaust temperature

% constant pressure specific heat of exhaust gas at temperature T5

Cp5 = (((2.506E-11).*T5.^2)+((1.454E-7).*T5.^1.5)-((4.246E-
7).*T5)+((3.162E-5).*T5.^0.5)+(1.3303)-((1.512E4).*T5.^-
1.5)+((3.063E5).*T5.^-2)-((2.212E7).*T5.^-3)).*10^3;

Cp45 = 0.5.*(Cp4+Cp5);

Cp51 = 0.5.*(Cp5+Cp1);

% Enthalpy of blowdown gas

Hbd = Mbd.*Cp45.*T4;

% Enthalpy of remaining gas in cylinder

Hrem = Mrem.*Cp51.*T5;

% Total enthalpy of exhaust gas

Hex = Hbd+Hrem;

% To calculate the average temperature, we require an averaged
specific
```

```
% heat value

Cp_avg = 0.5.*(Cp45+Cp51);

% The average temperature of this enthalpy is therefore

Tex_avg=Hex./(M.*Cp51);

%Tex_avg1=Hex./(0.0011.*Cp5);


%% STIRLING ENGINE MODEL - BELOW IS THE FTT STIRLING MODEL ALTERED
TO
%% INCLUDE THE OTTO CYCLE EXHAUST AS THE THERMAL SOURCE

%% Specify the engine parameters

% we will specify the temperatures, pressure and volume of the
% thermodynamic cycle, as well as the gas constant R

% Engine Rpm (for calculation of friction coefficient)
Ns = 2500;

% Engine Rpm range (for calculation of Power and Efficiency)
N1 = 100:100:3500;

%% Calculate engine cycle frequencies (relevent to analysis across
speed
%% range)

f1 = N1./60;

t1_S = 1./f1;

tp1=t1_S/2;

% Mean Pressure (Pa)
P = 2.76E6;

% Compression ratio
Rv_S = 1.39;

% Cylinder bore (m)
d = 0.07;

%Regenerator diameter (diameter of 1 tube)
Dr = 0.0226;

%length of regenerator
Lr = 0.0226;

% mesh wire diameter
d_wire=0.00004;

%Diameter of piston
Dp=0.0699;

% Annular Gap
```

```
xg = 0.00163;

%Length of Displacer Piston
Lp = 0.04359;

% Expansion Space Inner Diameter
DCE=0.0696;

% Number of Heater Tubes
Nh=40;

% Number of Cooler Tubes
Nc=312;

% Exhaust Temperature after preheater (K)
Texh = 523;

%Ambient Temperature (20 deg C)(K)
Tamb= 293;

% Volume of Expansion Space
Vex = 0.00012;

% Volume of Compression Space
Vcomp = 0.000114;

%Average Volume of cycle. This is computed from the cyclic volume
variation
%equations. For the GPU-3 engine, a rhombic drive is used, and the
mean
%total cycle volume is,(m3)
Vavg = 0.000369;

% Specify the system dead volume. This is available from engine
specs (m3)
Vdead = 0.000232;

% Volume in Hot Side HEX
Vh = 8.08E-5;

% Volume in Cold Side HEX
Vk = 1.313E-5;

% Volume in Regenerator
Vr = 6.55E-5;

% Gas constant, Helium (J/kgK)
R_S = 2077;

% Specify the Specific Heat at Constant Volume for the working fluid
% (Helium)(J/kgK)
Cv = 3120;

%Viscosity of gas (m2/s) (Helium)
visc = 396E-6;

% Prandtl Number (Helium)
Pr = 0.676;
```

```
% Specific heat at constant pressure, air (922K) (J/kgK)
Cp_air = 1120;

% Specific heat at constant pressure, air (500K) (J/kgK)
Cp_air1 = 1030;

% Specify internal and external diameters of the heater tubes
di=0.00302; % as per engine Specifications
do=0.00483; % as per engine Specifications

% Specify internal and external diameters of the cooler tubes
di_w=0.00108;
do_w=0.00159;

%conduction coefficient, stainless steel, heater
kwC = 15;

%conduction coefficient, stainless steel, cooler
kwH = 22.8;

% Length of heater tubes
LH = 0.154;

% Length of cooler tubes
LH_w = 0.0355;

% Dynamic viscosity of Combustion Gases
mu1 = 411.3E-7;

% Dynamic viscosity of Cooling water
mu2 = 1422E-6;

%dynamic viscosity of Helium @750K approx
mu_helium = 364E-7;

%dynamic viscosity of Helium @300K approx
mu_helium_C = 195E-7;

%Prandtl number, air at 900K
Pr_air=0.72;

%Prandtl number, water
Pr_w=8.8;

%Specific Heat Capacity of Cooling Water
Cp_w=4198;

% Porosity
Por = 0.8;

%% Specify the temperatures for the GPU-3 under tested conditions

% Heat Input (from performance data)
Qin_S_exp = (2.76./2.76).*1000.*((-
0.0006.*(f1.^2))+(0.1864.*f1)+1.051);

% Heat Rejection (from experimental data)
Qcoolant_S_exp = (2.76./6.9).*(0.0006.*N1.^2)+(1.7591.*N1)+493.77;
```

```
% Source Temperature (K)
Tsource=1167;

% Sink Temperature (K) - Assume a water jacket temperature of 70degC
% average
Tsink = 343;

% Hot Side Gas Temperature (K)
T3_S_exp=922;

% Cold Side Gas Temperature (K)
T1_S_exp = 353;

%Average Temperature of thermodynamic source and sink (K)
Tavg = (T3_S_exp+T1_S_exp)./2;

%% Calculate the e/UA term for the GPU-3 HEX

% Let e/UA = E_UA

% HOT SIDE

E_UA=(Tsource-T3_S_exp)./Qin_S_exp;

% COLD SIDE, e.*UA = E_UA_C

E_UA_C = Qcoolant_S_exp./(T1_S_exp-Tsink);

%% Calculate the New Temperatures for use in the Combined Cycle

Tsource_1 = Tex_avg;

T3_S1 = Tsource_1-(E_UA.*Qin_S_exp);

T3_S=T3_S1(1);

Tsink_1 = Tsink;

T1_S1 = Tsink_1+(Qcoolant_S_exp./E_UA_C);

T1_S=T1_S1(1);

%% Equate the Heat Input to the Otto Engine Exhaust Enthalpy

Qin_S = Qex;

%% Schmidt - Style Isothermal model of Stirling

% this model is used to provide an estimate of Stirling engine work
output
% when losses due to continuous piston movement are accounted for.
The
% model retains the dead volume, temperatures and isothermal
assumptions of
% the ideal case, and so it is a reasonable comparison against the
ideal
% cycle to ascertain the work losses associated with the piston
motion.
```

```
%Specify Dimensionless parameters

% Crank Angle (rads)
phi_S = 0:2*pi();

% Temperature Ratio
TR = T1_S./T3_S;

% Dead Volume Ratio
CHI = Vdead./Vex;

% Swept volume Ratio
KAPPA = Vcomp./Vex;

% Phase Angle;
ALPHA = 1.56;

% Expansion space volume variations
Ve_inst = 0.5.*Vex.*(1+cos(phi_S));

% Compression space volume variations
Vc_inst = 0.5.*KAPPA.*Vex.*(1+cos(phi_S-ALPHA));

% Instantaneous volume of total working space
Vtot_inst = Ve_inst+Vc_inst+Vdead;

% Calculate Substitution terms
SIGMA = 2.*CHI.*TR./(TR+1);

THETA = atan(KAPPA.*sin(ALPHA)./(TR+KAPPA.*cos(ALPHA)));

DEL =
(((TR.^2)+2.*TR.*KAPPA.*cos(ALPHA)+KAPPA.^2).^0.5)./(TR+KAPPA+2.*SIG
MA);

% Calculate the Max Pressure
Pmax = P./(((1-DEL)./(1+DEL)).^0.5);

Pmin = Pmax./((1+DEL)./(1-DEL));

% Calculate the Instantaneous Pressure in the cycle

p_inst = Pmax.*(1-DEL)./(1+DEL.*cos(phi_S-THETA));

% Calculate the cycle work output
VT = Vex+Vcomp;

W = (Pmax.*VT).*pi().*((1-TR)./(KAPPA+1)).*(((1-
DEL)./(1+DEL)).^0.5).*(DEL.*sin(THETA))./(1+(1-DEL.^2).^0.5);

%% Calculate the Cycle Mass

% we calculate the mass of gas in the engine using the ideal gas law
and
% the averaged properties

M_S = (P*Vavg)./(R_S*Tavg);
```

```
%% Determine the ratio of Schmidt cycle work to ideal cycle work

Nw = W./(M_S.*R_S.*log(Rv_S).*(T3_S-T1_S));

% This ratio gives an insight into the work losses inherent in the
use of
% continuous piston motion. The only difference between the two is
the
% accomodation of the volume variations. We can therefore use this
ratio to
% correct the ideal cycle in the FTT method to account for work
losses
% through continuous piston motion

%% Calculate the Mass flowrate of the combustion gases

% Combustion gas mass flowrate at each operating point

Mcomb=Qin_S_exp./(Cp_air.*(Tsource-Tamb));

%% Calculate the Heat that goes to the cycle and the heat lost to
Exhaust

% Cycle Heat Transfer (W)
Qin2 = Mcomb.*Cp_air.*(Tsource-Texh);

% Exhaust Heat (W)
Qex1 = Mcomb.*Cp_air1.*(Texh-Tamb);

% Exhaust Proportion - assumed as 30% in accordance with test data.
It is
% not crucial to know the exhaust heat, as otherwise it would simply
% appear in the cycle waste heat, however it facilitates the
decoupled
% analysis

Qex_S = 0.3.*Qin_S_exp;

%% Specify the Conduction Losses within the engine

% This is calculated from the experimental data given by Thieme (W)

Qcond = 500;

%% Calculate the engine frequency and the thermodynamic cycle
period, t
%% (relevant to calculation of mu term)

f_S = Ns./60;

t_S = 1/f_S;

% We assume that the working spaces (not the heat exchangers!) are
% adiabatic,ie any heat needed to do work is in the system before
the
% piston moves. This is common in Stirling analysis. THis means that
when
% calculating the speed of the piston, the adiabats are considered
```

```
% instantaneous, and the cycle time is divided into two processes
instead
% of four.  Following from Angulo Brown et al, only the piston
movement on
% the power stroke is considered, therefore only half the cycle time
is
% required

tp=t_S/2;

%% Calculate the effective Stroke

% Effective Clearance Displacement
xD = (4*Vdead)./(pi*(d^2));

% Effective Stroke
Se = xD.*(Rv_S-1);

%% Now Calculate the effective Piston Velocity

ve1 = 2.*Se.*f1;

%% Calculate the Regenerator Effectiveness - GPU-3 Engine

% we model the regenerator as a balanced counter flow heat exchanger
(Feidt
% 2002). We use the model for heat transfer coefficienct as
described by
% Petrescu et al (2002). This requires specification of certain
parameters
% to assist calculation. Details of the GPU-3 engine regenerator are
given
% by Martini. There are 8 regenerators in the engine

b=1.5*d_wire;

% WETTED AREA OF REGENERATOR (TOTAL)
Aw = 8*(1/4)*((pi^2)*(Dr^2)*Lr)./(b+d_wire);

% Calculate the gas velocity in the regenerator - we assume
incompressible
% flow in the regenerator, therefore we use the continuity equation
to
% calculate the velocity in the regenerator

%Cross sectional area of regenerator
Ar = 8*(pi*Dr^2)./4;

%Cross sectional area of piston
Ap_S = (pi*Dp^2)./4;

%Velocity of gas in cylinder - assumed equal to piston velocity
Vc = ve1;

% Therefore the velocity of gas in the regenerator
vr=(Ap_S*Vc)./Ar;

% We calculate the temperature ratio, tau. This should technically
be the
```

```
% ratio of gas temperatures not reservoir temperatures, however as
we
% assume isothermal heat exchange, the temperatures are assumed the
same as
% the reservoir temperatures

tau_S = T3_S/T1_S;

% Specific Heat Capacity at constant pressure, Helium
Cp = Cv+R_S;

% CALCULATE CONVECTIVE COEFFICIENT

h_S =
(0.395*((4*P)./(R_S.*T1_S)).*(vr.^0.424).*Cp.*(visc.^0.576))./((1+ta
u_S).*(1-(pi./(4.*((b./d_wire)+1))))).*(Dr.^0.576).*(Pr.^(2/3)));

% CALCULATE THE MASS FLOW THROUGH THE REGENERATOR
% To estimate the mass flow rate through the regenerator, we assume
that only a mass equivalent to that contained in the
% working volumes at any instant is transported through the
regenerator ie only a "live mass" is accounted for, the "dead mass"
% contained in the dead volumes is not accounted for. To estimate
the instantaneous mass
% in each working space, we determine the ratio of instaneous
working space
% volume to the total dead space volume in the system

Nm_1=((Ve_inst./T3_S)+(Vc_inst./T1_S))./((Vh./T3_S)+(Vr./((T3_S+T1_S
)./2))+(Vk./T1_S)+(Ve_inst./T3_S)+(Vc_inst./T1_S));

% this gives a range of values over the full cycle. The mean value
is taken
% to give an approximation of the ratio over one full cycle.

Nm = mean(Nm_1);

% It is assumed that over

Mr = Nm.*2.*Nw.*M_S.*f1;

% CALCULATE THE NTU OF THE REGENERATOR

NTU = (h_S*Aw)./(Cp*Mr);

%% Regenerator Effectiveness

eR = NTU./(2+NTU);

%% CALCULATE THE HOT SIDE HEX EFFECTIVENESS

%% First calculate the convective coefficient on the combustion gas
side

% Free Flow Area (calculated for GPU-3 3/5/2010)
Aff = 0.01912;

%Hydraulic Diameter of Hot Side HEX flow passages
Dh = 0.0115;
```

```
% First Calculate the Mass Velocity
G=((Mcomb)./Aff);

% Reynolds number of gas flow
Re=G.*Dh./mu1;

%Colburn jH value (Formosa 2010)
jH = exp(0.337-0.812.*log(Re));

% Convective Coefficient
h1=(jH.*G.*(Cp_air))./(Pr_air.^(2/3));

%% Second calculate the thermal resistance in the wall of the HEX
tubes

% Calculate the Thermal resistance associated with radial conduction
% through the HEX tube walls
Rt=(log((do./2)./(di./2)))./(2.*pi.*kwH.*LH);

%% Calculate the convective coefficient of the Stirling Working gas
side

% Calculate the Reynolds number of the working fluid flow in the HEX
% (Kanzaka (1992))

p_dash = (1./40).*(P.*Vex)./((Nm.*M).*R.*T3);

Re_St =
(1./40).*(1./(2.*pi().*f1)).*(Mr).*((6.*P.*Vex.*N1)./(p_dash.*R.*T3)
).*(4./(pi.* mu_helium.*di));

%estimate the interior wall temperature and the bulk fluid
temperature for
%the working fluid

Tw_S = T3_S;
Tb = 600;

% Calculate the Nusselt Number
C=0.923+0.75.*(Tw_S./1000);

Nu = 0.021.*(Re_St.^0.8).*(Pr.^0.4).*((Tw_S./Tb).^(-0.5)).*C;

%Conductivity of working Gas (Helium @ 600K)
kf = 252E-3;

h2 = (kf.*Nu)./LH;

%% Calculate U, the overall heat transfer coefficient of the HEX on
the
%% combustion gas side

R1 = 1./(h1.*pi.*do.*LH);

R2 = Rt;

R3 = 1./(h2.*pi.*di.*LH);
```

```
% Calculate the heat transfer area on the working gas side

AH = pi.*di.*LH;

Uh = 1./(AH.*(R1+R2+R3));

% Specify the Cmin term. In this case it is the combustion side gas
Ch

Cmin = (1./Nh).*Mcomb.*Cp_air;

Cmax = (1./Nh).*Mr.*Cp;

Cr = (Cmin./Cmax);

% The NTU then becomes(40 tubes)
NTUh = Nh.*(Uh.*AH)./(Cmin);

% The Effectiveness becomes (Cmin mixed, Cmax unmixed)
eH=1-exp((-Cr.^-1).*(1-exp(-Cr.*NTUh)));

%% CALCULATE THE COLD SIDE HEX EFFECTIVENESS

%% First calculate the convective coefficient on the water coolant
side

% Free Flow Area (calculated for GPU-3 3/5/2010)
Aff_w = 0.016544./2;

%Hydraulic Diameter
Dh_w = 0.00859;

%Average Mass flowrate of cooling water
Mw=0.13;

% First Calculate the Mass Velocity
G_w=(Mw)./Aff_w;

% Reynolds number of gas flow
Re_w=G_w.*Dh_w./mu2;

%jH value (Formosa 2010)
jH_w= exp(-3.575-0.229.*log(Re_w));

% Convective Coefficient
h1_C=(jH_w.*G_w.*(Cp_w))./(Pr_w.^(2/3));

%% Second calculate the thermal resistance in the wall of the HEX
tubes

% Cooler side thermal conductivity resistance
Rt_w=(log((do_w./2)./(di_w./2)))./(2.*pi.*kwC.*LH_w);

%% Calculate the convective coefficient of the Stirling Working gas
side

p_dash_C = (P.*Vcomp)./((Nm.*M).*R.*T1);
```

```
Re_St_C =
(1./(Nc)).*(1./(2.*pi().*f1)).*(Mr).*((6.*P.*Vcomp.*N1)./(p_dash_C.*
R.*T1)).*(4./(pi.* mu_helium_C.*di_w));

% estimate the interior wall temperature and the bulk fluid
temperature for
% the working fluid

Tw_C = T1_S;

% Estimate the fluid temperature
Tb_C = 320;

% Calculate the Nusselt Number
C_w=0.923+0.75.*(Tw_C./1000);

Nu_C = 0.021.*(Re_St_C.^0.8).*(Pr.^0.4).*((Tw_C./Tb_C).^(-
0.5)).*C_w;

%Conductivity of working Gas (Helium @ 300K)
kf_w = 149E-3;

%Convective Coefficient
h2_C = (kf_w.*Nu_C)./LH_w;

%% Calculate U, the overall heat transfer coefficient of the HEX on
the
%% coolant side

R1_w = 1./(h1_C.*pi.*do_w.*LH_w);

R2_w = Rt_w;

R3_w = 1./(h2_C.*pi.*di_w.*LH_w);

% Calculate the heat transfer area on the working gas side

AH_C = pi.*di_w.*LH_w;

Uc = 1./(AH_C.*(R1_w+R2_w+R3_w));

% Specify the Cmin term. In this case it is the combustion side gas
C

Cmin_C = (1./Nc).*Mr.*Cp;

Cmax_C = (1./Nc).*Mw.*Cp_w;

Cr_C = (Cmin./Cmax);

% The NTU then becomes

NTUc = Nc*(Uc.*AH_C)./Cmin_C;

% The Effectiveness becomes (Cmin mixed, Cmax unmixed)
eC=1-exp((-Cr_C.^-1).*(1-exp(-Cr_C.*NTUc)));
```

```
%% Calculate the ideal (reversible) cycle Work

Wrev_S = (Qin_S_exp.*t1_S)-(Nw.*eC.*M_S.*R_S.*T1_S.*log(Rv_S));

%% Calculate the ideal (reversible) cycle Power at the given
frequency

Prev = Wrev_S./t1_S;

%% Calculate the Friction Work

% In this section, we calculate the lost friction work.  We use the
method
% laid out in the document "Development of the FTT Stirling Model".
This
% method introduces the concept of the effective stroke and the
effective
% piston velocity

% To quantify the global friction type losses, we assume that losses
are
% comprised of 1) Pumping losses and 2) Mechanical friction losses.
Walker
% et al (1994) indicate that the indicated power of a well designed
Stirling engine might perform
% to 70% of that of the Schmidt cycle value (Wrev_S here) ie 30%
fluid losses
% in

%Calculate friction Work, Wf_S

Wf_S = 0.15*Wrev_S;

%% Calculate the Friction Power

% we use the same procedure as that used by Angulo Brown et al for
the Otto
% engine, P = mu*(ve)^2

%% Calculate the friction coefficient, mu_S

mu_S = (t*Wf_S)./((pi^2).*(Se^2));

%% Finally calculate the friction power

Pf_S = mu_S.*(ve1.^2);

%% Calculate the Engine Irreversibility Parameter

% Calculate the regenerator exit temperatures
Tx2 = eR.*(T3_S-T1_S)+T1_S;

Tx4 = T3_S - eR.*(T3_S-T1_S);

IR_S =
(eC.*R_S.*log(Rv_S)+Cv.*log(Tx4./T1_S))./(eH.*R_S.*log(Rv_S)+Cv.*log
(T3_S./Tx2));

%% Calculation of Pumping Power Losses
```

```
% First it is necessary to specify the Cf terms for each of the
operating
% spaces. This requires knowledge of the Reynolds Number in each
section.
% Referring to Martini (1983), the Cf values are calculated from:

CfH = exp(-1.34-0.2.*log(Re_St));

CfC = exp(-1.34-0.2.*log(Re_St_C));

% To calculate the Cf in the Regenerator, it is necessary to
calculate the
% Reynolds number of the fluid flow. This is related to the mesh
properties
% through the Hydraulic Radius of the mesh

% Heat transfer area per unit volume of the regenerator
Avol = Aw./(Ar.*Lr);

% Hydraulic Radius
R_H = Por./Avol;

% Frontal area of regenerator mesh
Afr_R = Ar.*(1-Por);

% Freeflow area of regenerator mesh
Aff_R = Ar - Afr_R;

% Mass Velocity of flow through regenerator
G_R = Mr./(Aff_R);

% Reynolds Number
Re_R = (4.*R_H.*G_R)./mu_helium;

% Therefore the Cf value for the regenerator is
CfR = exp(0.015-0.125.*log(Re_R));

% Calculate the density of the gas in each space
rho_H = P./(R_S.*T3_S);
rho_R = P./(R_S.*Tavg);
rho_C = P./(R_S.*T1_S);

% Frontal Area of heater tubes
Ah = Nh.*pi().*(di.^2);

% Frontal Area of cooler tubes
Ac_S = Nc.*pi().*(di_w.^2);

% Pumping Power Loss
sigma2 = Aff_R./Afr_R;
psi = rho_H./rho_C;

Pp = (8.*((1+sigma2.^2).*((1./rho_H).*(psi-1)+(1./rho_C).*((1./psi)-
1)).*((rho_H.^3)./rho_R).*((Ap_S.^3)./(Aff_R.^2))+((rho_R.*CfR.*Lr.*
Aff_R)./R_H))+Nh.*(2.*CfH.*LH.*rho_H.*pi().*di.*(Ap_S./(Ah./Nh)))+1.
*Nc.*(2.*CfC.*LH_w.*rho_R.*pi().*di_w.*(Ap_S./(Ac_S./Nc)))).*ve1.^3;

%% Step 22: Fitted Polynomial for Experimental Power Output
```

```
Pexp = (-5E-8).*(N1.^3)+(2E-05).*(N1.^2)+0.7366.*N1+130.95;

%% Calculate the irreversible cycle work for the series of
%% Operating Speeds - IR varies with eR

Wrev1 = (eH.*Qin_S_exp.*t1_S)-
IR_S.*(Nw.*eC.*M_S.*R_S.*T1_S.*log(Rv_S));

%% Calculate the ideal (reversible) cycle Power at the given
frequency

Prev1 = Wrev1./t1_S;

%% Calculate the Irreversible Power

Pirrev = (Prev1  - Pf_S - Pp-Qcond -Qex_S);

%% Calculate the Stirling Cycle Efficiency

eff_S=Pirrev./Qin_S_exp;

%% Calculate the Total Power Output of the Combined Cycle

P_CC = Potto+Pirrev;

eff_CC = P_CC./Q;
```

APPENDIX D

D.1 Techno-Economic Model

```
%% Economic Analysis of Proposed Combined Cycle Power Plant
%% CHP OTTO CYCLE ENGINE - ALONE

% This is an economic analysis of the Otto Cycle engine acting alone.

%% Input Energy Unit Costs (Gas & Electrical Unit Costs)
%% PRICES AS AT 19/08/2010

% ELECTRICAL TARIFF ASSUMED - ESB GENERAL PURPOSE, SME

% Fuel Gas Cost (FREE)
C_g = 0.0;

% REFIT Electrical Unit Price (€/kWh)
C_REFIT = 0.11;

%% INPUT CAPITAL COST ESTIMATES

% Cost per kW of Otto Engine
Xotto = 1000;

% Cost per kWfuel of Otto Engine
Xotto_f = 283;

%% INPUT ANNUAL MAINTENANCE TARIFF

% Typical Maintenance Tariff for Otto cycle stationary engine (€/kW/year)

C_m = 50;

%% INPUT OPERATING CONDITIONS

% Operating Hours
Nh = 5420;

% Interest Rate (for NPV)
i = 0.08;

% Plant Lifetime(Years)
Ny = 10;

%% Input Engine Specifications
% The analysis is on a per kWe basis. First though we input the specs for
% the engine as used in the thermodynamic analyses

% Fuel energy (kW)
Pfuel = 21.430;

% Brake Power (kW)
Pm = 6.071;

% Brake Efficiency
eff_otto = 0.2833;

% Alternator Efficiency
```

```
eff_alt=0.9;

%% Calculate Electrical Power Output

P_elec = Pm.*eff_alt;

%% CALCULATE THE COST TO RUN THE GENERATOR

% Yearly Fuel Demand (assuming Natural Gas as Fuel)(kWh)
Fd = Pfuel.*Nh;

% Yearly Fuel Cost
C_f = Fd.*C_g;

% Therefore, yearly running cost (excl. maintenance charges)
RCG = C_f;

% Annual maintenance cost
C_Main = C_m.*P_elec;

% Total annual running cost
RCG_T = RCG+C_Main;

%% CALCULATE THE COST TO BUY THE EQUIVALENT POWER FROM UTILITY COMPANIES

%% Calculate Gross Revenue from Electrical Power

EPC = P_elec.*C_REFIT.*Nh;

%% Calculate the total Net revenue from power

ECG = EPC-RCG_T;

%% CALCULATE ANNUAL NET CASH FLOW

A_cash = ECG;

%% Calculate annual savings per kW rated (electrical) power

A_c_kW = A_cash./P_elec;

%% Calculate annual savings per kW rated (Fuel) power

A_c_kW_f = A_cash./Pfuel;

%% SIMPLE PAYBACK PERIOD

% Payback period per (years/kW)
SPP = Xotto./A_c_kW;

%% NET PRESENT VALUE

% Net Present Value per kW
CashFlow = [-Xotto, A_c_kW, A_c_kW, A_c_kW, A_c_kW, A_c_kW, A_c_kW, A_c_kW,
A_c_kW, A_c_kW, A_c_kW];

PresentVal = pvvar(CashFlow, i);

ROR = irr(CashFlow);

%% NET PRESENT VALUE PER kW (FUEL POWER)

% Net Present Value per kW
```

```
CashFlow1 = [-Xotto_f, A_c_kW_f, A_c_kW_f, A_c_kW_f, A_c_kW_f, A_c_kW_f,
A_c_kW_f, A_c_kW_f, A_c_kW_f, A_c_kW_f, A_c_kW_f];

PresentVal1 = pvvar(CashFlow1, i);

ROR1 = irr(CashFlow1);
```